The deformation of carbide cutting tools

Stephen Brooke Bell

THE DEFORMATION OF CARBIDE CUTTING TOOLS

by

Stephen Brooke Bell

A thesis presented for the degree

of

Doctor of Philosophy

The University of Durham

Department of Engineering

May 1988

ABSTRACT

Under certain cutting conditions carbide tools can sustain a significant amount of permanent deformation and this may cause early tool failure.

Tests were devised to investigate the deformation of three different grades of carbide, when machining steel (817M40, EN24) under a wide range of conditions. Each test was carried out on a continuous (60 seconds) and an incremental (5, 5, 10, 20 and 20 seconds) basis. This plan was adopted to investigate transient effects. During each test the cutting forces were measured with a dynamometer, and the boundary temperatures were measured at the tool/chip interface and the tool/shank interface.

The permanent deformation took the form of bulging on the flank face and depression of the rake face. With low metal removal rates the deformation was minimal and the cutting edge was stable. High metal removal rates caused the tool to deform continuously and this gave an unstable cutting edge. It was deduced that within the tool there was a zone of material that had undergone plastic deformation. The rake and flank faces formed two external boundaries of this zone, the remaining boundary being within the tool body. For any particular set of cutting conditions, the amount of deformation for either the continuous test or the total of the incremental tests was essentially the same.

A plane stress Finite Element (F.E.) model was developed to explain the effects of speed and feed in terms of temperature and stress and their variation with time. The F.E. model predicted that the values of both the transient and steady state thermal stresses were very low when compared with the mechanical stresses.

The results from the cutting tests and the F.E. model suggest that the tool material continuously deformed under the applied mechanical stresses (cutting forces). Any contribution to the deformation from the transient thermal stresses was minimal and of a short duration.

∿ they that wait upon the Lord shall renew their strength.

Isaiah, Chap 40, V31.

ACKNOWLEDGEMENTS

The author would like to thank:

Professor P M Braiden for his guidance throughout the course of this work.

Mr J Chan, for permission to use his computer programme for stress smoothing.

Dr G Needham at Newcastle upon Tyne Polytechnic for making the facilities available. Mr B Kimpton for designing and building the electronic amplifier system. Mr J Mason and his workshop personnel for manufacturing the apparatus. Mrs S Nicholson for help with the production of the diagrams and Mrs P Weddell for typing the script.

His mother for her continued interest.

His wife who has encouraged and accompanied him throughout the work with patience and love.

TO FATHER

CONTENTS

ABSTRACT

ACKNOWLEDGEMENTS

CHAPTER 1	LITERATURE SURVEY	1
1.1	Introduction	1
1.2	Wear of Carbide Cutting Tools	2
1.2.1	Diffusion Wear	2
1.2.2	Attrition Wear	3
1.2.3	Abrasive Wear	4
1.3.1	Tungsten - Titanium - Tantalum Carbide Alloys	4
1.3.2	Titanium Carbide Based Tools	5
1.3.3	Coated Carbides	5
1.3.4	Recent Cutting Tool Developments	6
1.3.4.1	Ceramics	7
1.3.4.2	Sialons	7
1.3.4.3	Cubic Boron Nitride (CBN)	8
1.3.4.4	Coated High Speed Steels	10
1.4.1	Stress Distribution on the Tool Rake Face	11
1.4.2	Stresses in Cutting Tools Using Photo-Elasticity	13
1.4.3	Analysis of Stress in Tools with Point Loading	14
1.4.4	Analysis of Stresses in Tools with Distributed Loads	15
1.4.5	Analysis of Tool Stresses Using Finite Element Techniques	16
1.5.1	Temperature Distributions in Cutting Tools	17
1.5.2	Temperature of the Chip/Tool Contact Region	21
1.5.3	Analytical Temperature Distributions in Cutting Tools	23
1.6.1	Thermal Stresses in Cutting Tools	24

1.7.1	Determination of Thermal Stresses Using Finite Element Techniques	26
1.8	Tool Deformation	27
1.8.1	Classifications of Tool Deformation	27
1.8.2	The Influence of Tool Geometry on Deformation	31
1.8.3	The Influence of Cutting Conditions on Deformation	31
1.8.4	The Deformation Mechanism of Cemented Carbide Cutting Tools	33

CHAPTER 2 TOOL TEMPERATURE MEASUREMENT

2.1	Introduction	37
2.1.2	Infra-Red Photography	37
2.1.3	Infra-Red Detectors	37
2.1.4	Thermo-Sensitive Paints	38
2.1.5	Thermocouples	38
2.2.1	Measurement of Tool Insert Temperatures Using Thermocouples	40
2.2.2	Tool/Chip Interface Temperature	40
2.2.3	Temperature Measurement at the Tip-Shank Interface	41
2.2.4	Signal Transfer System for Tool-Work Thermocouple	41
2.3	Selection of Thermocouples for Tip-Shank Interface	42
2.3.1	Manufacture of Thermocouples	43
2.3.2	Thermocouple Output Amplification and Recording System	44
2.3.3	Calibration of the Tip-Shank Thermocouples	45
2.3.5	Calibration of Tool-Work Thermocouples	45
2.3.6	Manufacture of Tool-Work Thermocouples	47
2.3.7	Discussion of Results	49
2.3.8	Influence of Calibration Time	54
2.3.9	Evaluation of Results	56

2.4	Temperature Measurement Using Inserted Thermocouples	58
2.5	Development of Tip-Shank Thermocouples	58
2.6	Evaluation of the Temperature Measurement System	60
2.6.1	Tip-Shank Thermocouples	60
2.6.2	Tool/Work Thermocouples	61
2.6.3	Resolution of Temperature Recording System	62
2.7	Analysis of the Tool/Work Thermocouple	64
2.7.1	Thermocouples in Parallel	64
2.7.2	Model for 'n' Thermocouples in Parallel with Constant Resistance	66
2.7.3	Model for 'n' Thermocouples in Parallel with Temperature Dependant Resistance	67
2.7.4	Determination of Temperature Coefficient of Resistivity	70
2.7.5	Evaluation of Thermocouple Model	72
2.7.6	Conclusions	81
CHAPTER 3	MEASUREMENT OF CUTTING FORCES	83
3.1	Force Dynamometer	83
3.2	Calibration of Force Dynamometer	83
3.3	Charge Amplifiers and Recording System	83
CHAPTER 4	MEASUREMENT OF TOOL DEFORMATION AND WEAR	85
4.1	Introduction	85
4.2	Optical Methods for Measuring Deformation	85
4.2.1	Interferometry	85
4.2.2	Tool Sectioning Techniques	85
4.2.3	Light Sectioning Techniques	86
4.3	Mechanical Methods for Measuring Deformation	86

4.3.1	Stylus Techniques	86
4.3.2	Location of the Tool Tip for Stylus Measurement	87
4.3.3	Interpretation of Stylus Traces	88
4.3.4	Depression of the Cutting Edge	89
4.4	Tool Wear Measurements	90
4.4.1	Introduction	90
4.4.2	Wear on the Clearance Faces	90
4.4.3	Crater Depth	90
4.4.4	Tool/Chip Contact Area	90
CHAPTER 5	SELECTION AND PREPARATION OF TOOLS AND WORKPIECE	94
5.1	Selection of Carbide Grades	94
5.2	Tool Geometry	95
5.2.1	Rake Angle	95
5.2.2	Nose Radius	95
5.3	Preparation of Tool Inserts (Tips)	96
5.4	Choice of Cutting Conditions	97
5.4.1	Cutting Speed	97
5.4.2	Feed Rate	97
5.4.3	Depth of Cut	97
5.5	Workpiece Specification and Preparations	99
5.6	Lathe for Cutting Tests	100
5.7	Duration of Cutting Tests	100
CHAPTER 6	OBSERVATIONS	101
6.1	Introduction	101
6.2	Grade TE	101
6.2.2	Grade TTA	103
6.2.3	Grade TA5	105

6.3	Tool Tip Boundary Temperatures	107
6.3.1	Average Tool/Chip Interface Temperature, Grade TE	107
6.3.2	Average Tool/Chip Interface Temperature, Grade TTA	108
6.3.3	Average Tool/Chip Interface Temperature, Grade TA5	109
6.3.4	Temperature at the Tip-Shank Interface	110
6.4	Deformation (Bulging) of the Flank Face	115
6.4.1	Grade TE	115
6.4.2	Grade TTA	118
6.4.3	Grade TA5	120
6.5	Depression of the Cutting Edge	122
6.5.1	Grade TE	123
6.5.2	Grade TTA	124
6.5.3	Grade TA5	124
6.6	Wear on the Clearance Faces	125
6.6.1	Grade TE	126
6.6.2	Grade TTA	130
6.6.3	Grade TA5	131
6.7	Tool/Chip Contact Length	132
6.7.1	Grade TE	132
6.7.2	Grade TTA	133
6.7.3	Grade TA5	133
6.7.4	Comparison of Contact Lengths for Different Grades	134

CHAPTER 7 FINITE ELEMENT ANALYSIS

7.1	Introduction	135
7.2	Finite Element Model	136
7.3	Selection of Cutting Force Distribution	140
7.4	Selection of Temperature Distribution	140

7.5	Application of Measured Forces	143
7.5.1	Distribution by Chan and Braiden (1981)	144
7.5.2	Distribution by Barrow (1982)	145
7.6	Quantification of Temperature Distribution at the Tool/Chip Interface	145
7.7	Calculation of Temperature Distributions Within the Tool	146
7.8	Calculation of Mechanical and Thermal Elastic Stresses	148
7.9	Choice of Element Size at the Tool/Chip Interface	149
7.10	Evaluation of Mechanical and Thermal Stresses	150
7.11	Stress Smoothing	150
7.12	Prediction of Permanent Plastic Deformation	151

CHAPTER 8 ANALYSIS AND DISCUSSION OF RESULTS

8.1	Introduction	153
8.2	Analysis of Cutting Temperatures	153
8.2.1	Grade TE	154
8.2.2	Grade TTA	155
8.2.3	Grade TA5	155
8.2.4	Discussion	156
8.3	Elastic Analysis to Predict Boundary Stresses	156
8.3.1	Stresses at the Tool/Chip Contact Region	157
8.3.2	Stresses on the Flank Face	158
8.4.	Mechanical and Thermal Elastic Deformations	158
8.5	Stress Distribution Within the Cutting Tool	160
8.6	Permanent Plastic Deformation	162
8.6.1	Introduction	
8.6.1.1	Mechanical Properties of Tool Material Used for the F.E. Model	162

8.6.1.2	Thermal Properties of the Tool Material Used for the F.E. Model	163
8.6.2	The Influence of Cutting Speed on Deformation	163
8.6.2.1	Steady State Temperature Distribution	164
8.6.2.2	Permanently Displaced Shape	164
8.6.3	The Influence of Feed Rate on Deformation	167
8.6.3.1	Steady State Temperature Distribution	167
8.6.3.2	Permanently Displaced Shape	168
8.7	The Influence of Transient Thermal Effects on Deformation	171
8.7.1	Transient Temperature Distribution	172
8.7.2	Transient Thermal Stresses	173
8.8	The Influence of Tool/Chip Stress Distributions	175
8.9	The Influence of Tool/Chip Interface Temperature Distributions	176
8.10	Evaluation of Plane Strain F.E. Models	179
8.11	The Influence of Tool/Chip Contact Length on Predicted Deformation	180
8.12	The Influence of Temperature Variation on Predicted Deformation	182

CHAPTER 9 CONCLUSIONS

9.1	Introduction	185
9.2	The Influence of Speed, Feed and Time	186
9.2.1	Cutting Speed	186
9.2.2	Feed Rate	186
9.2.3	Changes in the Shape of the Plastic Zone	187
9.2.4	Time	188
9.3	Comparison of Experimental Observations with Finite Element Predictions	189
9.3.1	Stress Distribution at the Tool/Chip Interface	189
9.3.2	Plane Strain F.E. Model	189

9.3.3 Temperature Distribution at the Tool/Chip Interface 189

9.3.4 Transient Thermal Effects 190

9.3.4.1 Transient Temperatures 190

9.3.4.2 Transient Thermal Stresses 190

9.4 Deformation Mechanism 191

CHAPTER 10 SUGGESTIONS FOR FURTHER WORK 193

APPENDIX 1 CUTTING FORCE DYNAMOMETER 194

APPENDIX 2 FORCE DISTRIBUTIONS 195

APPENDIX 3 TEMPERATURE DISTRIBUTIONS 201

REFERENCES 212

FIGURES

CHAPTER 1

LITERATURE SURVEY

1.1 Introduction

Modern metal cutting machine tools can subject the cutting tools to very severe conditions. The tools are often required to withstand very high thermal and mechanical stresses, and their performance depends mainly on the following factors:

1) mechanical and thermal properties of the tool material,
2) the strength and hardness of the workpiece material,
3) the severity of the cutting conditions.

During machining the rake face of the tool is subjected to very high normal and tangential loads very close to the cutting edge. Because the tool becomes hot due to the cutting action it is necessary for the tool material to retain its strength at elevated temperatures. Large temperature gradients often occur in the tool and this can lead to very high thermal stresses. It is therefore desirable that cutting tools are made from materials that have good thermal conductivity and low thermal expansion.

Generally speaking the performance or life of a cutting tool is reduced if the workpiece material has high strength or high hardness. If the workpiece material retains its strength at elevated temperatures then the life of the tool is often reduced quite dramatically. Examination of the tool shows that it may have undergone some plastic deformation before failure. If the workpiece is hard and has low ductility then the cutting forces and the highest temperatures are distributed over a very small area close to the cutting edge. Such extreme conditions can lead to early tool failure.

The introduction of Computer Numerically Controlled (CNC) lathes has given the opportunity to increase cutting speeds and the feed rates. Trigger (1966) has shown that the temperatures in cutting are most sensitive to changes in speed. However the cutting forces are largely dependant on the feed rate and depth of cut Kronenberg (1966). Combinations of large feeds and high speeds subjects the tool to high forces which must be supported at high temperatures. Another severe loading condition for carbide tools is intermittent cutting, which subjects the tool to repeated mechanical and thermal shocks which often results in cracking on the tool rake face.

1.2 Wear of Carbide Cutting Tools

The three most common wear mechanisms of carbide cutting tools are generally accepted as diffusion, attrition and abrasion.

1.2.1 Diffusion Wear

When steel is cut at high speeds and feed rates with tungsten cobalt (WC-Co) tools a crater is worn into the tool rake face. The crater starts some distance behind the cutting edge and the wear rate is highest at the position of highest temperature. It was suggested by Trent (1967) that the wear of the tool was caused by atoms from the tool material diffusing into the work material and then being carried away by the chip. The carbide grains were worn smooth with little or no evidence that any particles were broken away from the tool surface. Crater wear by diffusion occurred at relatively high rates of metal removal. Trent (1959) summarized the effects of cutting speed and feed rate by plotting charts with logarithmic scales as shown on Figure 1.1. The dotted lines represent combinations of feed and speed that give a constant metal removal rate. The solid lines give the conditions for transition from built-up edge to

rapid cratering.

Diffusion wear also occurs at the tool flank. The rate of diffusion of tungsten and carbon atoms out of the tool material and into the work is dependant not only on the temperature but also on the rate at which they are swept away. At the tool flank the rate of flow of the work material close to the tool surface is very high and diffusion wear is probably responsible for a high rate of flank wear.

1.2.2 Attrition Wear

When cutting at relatively low speeds the temperature is usually not sufficient to cause diffusion wear. Under these circumstances attrition often becomes the dominant wear process. Wear by attrition is usually associated with build-up of work material at the cutting edge. During cutting the built-up edge (BUE) is continually changing with work material being built onto it and fragments being sheared away. If only the outer layers are sheared while the part of the built-up edge adjacent to the tool remains adherent and unchanged, then the tool will continue to cut for long periods without much wear. WC-Co tools are commonly used for cutting cast iron, and the recommended speeds are often those where a built-up edge is formed. When cutting steel under conditions where a built-up edge is formed, the edge of a WC-Co tool can be rapidly destroyed by attrition. This is because fragments of the tool material are torn from the tool edge when the built-up edge breaks away. This frequently happens during interrupted cutting and it has been suggested by Trent (1967) that fragments of the tool are broken away because localised tensile stresses are imposed by the unevenly flowing metal. Trent (1967) has shown that for WC-Co tools when cutting cast iron the wear rate on

the flank by attrition is reduced if the cutting speed is increased up to a value of 61 m/min. If, however, cutting speeds are raised too high then the diffusion process will start to dominate. Ideally the cutting speed should be chosen such that neither of these two mechanisms is allowed to become excessive.

1.2.3 Abrasive Wear

Abrasion as a wear mechanism is unlikely in carbide based tools, except where large amounts of abrasive material are present such as sand on the surface of castings. The wear of tools used to cut chilled cast iron rolls may be by abrasion. This is because cementite and other carbide particles are present. It is possible that these hard substances may abrade the WC in the cutting tool. However, most of the carbides are not as hard as WC and no detailed studies of this wear mechanism have been reported.

1.3.1 Tungsten-Titanium - Tantalum Carbide Alloys

The WC-Co alloys were successful in raising the economic cutting speed when machining cast iron and non-ferrous metals. However, when machining steel they were found to fail at speeds not much higher than those used for high speed steel tools. This was due to rapid cratering caused by diffusion. After much research alloys containing Tungsten (WC), Titanium (TiC) and Tantalum (TaC) carbide were introduced with cobalt (Co) as the binder. These alloys are often referred to as "steel cutting grades", and the WC-Co alloys as the "straight grades". A typical composition was 9% Co, 9% TiC, 12% TaC and the remainder WC. A typical straight grade has from 6 to 15% Co with the remainder WC. Steel cutting grades have similar hardness values as WC-Co alloys that have the same cobalt content and grain size. However, increasing the Ti and Ta content reduces the toughness

so these elements are usually kept to the minimum satisfactory level. The steel cutting grades retain their hardness and compressive strength at higher temperatures than the WC-Co alloys. They are also more resistant to diffusion wear than WC-Co alloys, consequently they can be used at up to three times the speed of straight grades when cutting steel. At these higher speeds the hot compressive strength becomes important because the tool may fail by deformation at speeds less than that required to give rapid cratering by diffusion. Besides having increasing resistance to cratering, the flank wear is also much reduced with the steel cutting grades. Unfortunately increased resistance to deformation is normally accompanied by a reduction in toughness. The selection of a grade for a particular application is usually a compromise between toughness and resistance to deformation.

1.3.2 Titanium Carbide Based Tools

Alloys based on TiC rather than WC have been developed by some manufacturers. The powder metallurgy process is similar to that used for the production of WC based alloys. Normally 10 to 20% nickel is used as the bonding material and this gives a hardness in the same range as conventional carbides. When cutting steel at high speeds they have lower rates of wear than conventional steel cutting grades. However, TiC based tools do not have the reliability and consistency of performance of the conventional carbides. This is largely due to a lack of toughness in the alloys so far produced. With the relative shortage of tungsten, a substitute for WC based alloys is required and it has been suggested that those based on TiC are likely candidates.

1.3.3 Coated Carbides

The commercial development of chemical vapour deposition (CVD) coatings on cemented carbide tools began in the early 1970s. Very

thin layers, usually 10μm thick were bonded to the surfaces of "throw-away" tool tips. At the present time the coatings that are available are titanium carbide (TiC), titanium nitride (TiN), titanium carbonitride (Ti.(CN)), hafnium carbide (HFN) or alumina (Al_2O_3). Recent developments have produced tools with a number of layers, with the individual layers varying in thickness from one to about ten micrometres. Coates carbide tools are capable of extending tool life by a factor of 2 or 3 when used for high speed machining of steel and cast iron. However, they are not always suitable for operations involving severe interrupted cutting because the coating may fracture and flake away.

It was suggested by Dearnley and Trent (1982) that the improved performance of tools with TiC, TiN and alumina coatings was due to their high resistance to diffusion wear on parts of the surface where seizure occurred. The coating did not prevent seizure when cutting steel at high speed, and the heat source raising the tool temperature was found to be a flow zone with a temperature only slightly lower than that of uncoated tools. For these reasons the rate of metal removal when cutting high strength materials was limited by the ability of the substrate to withstand the stresses and temperatures, and thereby resist plastic deformation of the cutting edge.

1.3.4 Recent Cutting Tool Developments

Introduction

Table 1.1 shows some of the mechanical and physical properties of different tool materials. The trend towards materials with higher values of "hot hardness" has generally been accompanied with a reduction in their fracture toughness and thermal shock resistance. An exception to this trend is a group of materials known as sialons

which are discussed in section 1.3.4.2.

1.3.4.1 Ceramics

Ceramic cutting tools consisting of Al_2O3 (Alumina) have been commercially available for more than 30 years and have been used to cut steel and cast iron. At room temperature they have much the same hardness as cemented carbides, however they retain their hardness and compressive strength at much higher temperatures than carbides. These advantages are offset by the reduction in transverse rupture strength, fracture toughness and thermal conductivity (Table 1.1). Because of these characteristics the number of machining applications are more limited than for cemented carbide tools.

Ceramic tools have been used to cut steels at speeds up to three times that used for carbides, however their common usage has been in the cutting of grey cast iron where a very good surface finish is required. Clutch facings and brake discs are typical components where it has been possible to eliminate a subsequent grinding operation by using ceramic tools. Their unreliable performance under machine shop conditions, however, often more than off-sets the economies gained by their peak performance. Recently manufacturers have made new efforts to improve their performance by modifying the cutting edge. One method is to chamfer the edge at an angle of between 10^{o} and 30^{o} to the tool rake face, and to put a honed radius on the cutting edge.

1.3.4.2 Sialons

Sialons (Si-Al-O-N) are silicon nitride-based materials with aluminium and oxygen additions. Research has shown that these tools inserts can be produced by a process similar to that used for cemented carbide (Lewis 1980). They have a lower thermal expansion and higher

thermal conductivity than ceramics (Table 1.1) so they are more able to withstand thermal shock. The transverse rupture strength is comparable with ceramics, and the fracture toughness is much improved. Up to the present time they have been used to machine grey cast iron at speeds of 1000 m/min with feeds of 0.5 mm/rev (Jack 1982). Steel with a hardness of 700 HV has been cut at 120 m/min with a feed of 0.25 mm/rev. Sialons are normally used with negative rakes and edge modification similar to that for ceramics.

Sialon tools show both flank and crater wear but exact wear mechanisms have not been published. However, deformation of the tool edge followed by fracture has been reported (Jawaid 1983) when cutting a nickel based super alloy. This phenomenon was said to limit the rate of metal removal.

Currently sialon tools are more expensive than cemented carbides and their extra cost has to be justified on the basis of either lower production costs or improved quality of the finished product. However, if the cost can be reduced by producing them in larger quantities their applications may become more widespread.

1.3.4.3 Cubic Boron Nitride (CBN)

Currently there are two main commercially available products, these are BZN and Amborite. BZN is produced as a laminated tool tip with a layer of consolidated boron nitride about 0.5mm thick on a cemented tungsten carbide/cobalt substrate. Amborite is produced as a tool tip consisting entirely of consolidated CBN.

These tools are at early stage of evaluation for industrial use, however there are indications that there will be specific applications

Material	Year	T.R. "Strength GPa	Hardness HV	Fracture Toughness $MN.m^{-\frac{3}{2}}$	Thermal Conductivity $W/m^{o}C$	Thermal Expansion Coefficient $x10^{-6}$
High speed Tool steels	1900	4-5	800-900	15-20	-	-
Cemented Carbides	1940	1-2.5	1100-1600	8-15	40-120	5
Ceramics	1960	0.4-0.9	1550-1800	2	8.5	9
Diamond Compacts	1970		4000			
Sialons	1980	0.8	1800	7	20-25	3.2

TABLE 1.1 SOME PROPERTIES OF TOOL MATERIALS

where their superior performance makes them economic in spite of their high cost. One application (Mullen 1983) was the machining of hardened steel rolls (60-68 Rc) at speeds of 45 to 60 m/min and feeds of 0.2 to 0.4 mm/rev. The tool life was such that the rolls were machined to a tolerance and finish that obviated a subsequent grinding operation. Their ability to cut hard materials at high speeds is due to their strength at high temperatures. It is uncertain how successful they will be in competing with sialons when machining nickel based alloys. They exhibit both crater and flank wear, but no observations of deformation at the tool edge have been reported so far.

1.3.4.4 Coated High Speed Steels

The development of chemical vapour deposition (CVD) processes has resulted in the commercial availability of high speed steel cutting tools coated with thin layers (10 μm) of refractory metal carbide or nitride. Titanium nitride is commonly used for the coating, although not as hard as Titanium carbide it has equal or superior wear resistance (Walker et al, 1981) and (Edwards et al, 1981). Furthermore the bright gold colour allows coated tools to be easily identified when in workshop use. When cutting steel and cast iron the tool life may be extended by up to four times that of uncoated tools for the same cutting conditions. Although the coating can resist wear at high cutting speeds, the strength of the high speed steel substrate is a limitation at higher temperatures. The most promising applications so far have been drills and form tools where only the clearance face is reground. These tools are often used in automatic machines where prolonged tool life may be more important than increases in cutting speed.

1.4.1 Stress Distribution on the Tool Rake Face

Zorev (1963) proposed that when cutting steel the normal and tangential contact stresses on the tool face were distributed as shown in figure 1.2. The normal contact stress was said to vary over the distance x according to the relationship:-

$$\sigma = x^n \qquad (1)$$

having a maximum value at x = c given by

$$\sigma_m = c^n$$

The tangential stress distribution had two distinct regions. In the first region from x = 0 to x = c_1 the tangential stress (τ) varied proportionally with the normal stresses, giving the stress as:-

$$\tau = \mu_\beta . \sigma \qquad (2)$$

where u_β was the co-efficient of sliding friction. Expressed as a function of the normal stress the tangential stress becomes:-

$$\tau = u_\beta . x^n \qquad (3)$$

As the value of x increased the tangential stress τ reached a value equal to the shear yield stress τ_s of the chip material and any further increase became impossible.

In a series of tests that varied the rake angle from 10 to 40 degrees and the cutting speed from 0.02 to 80 m/min the exponent "n" in equation (1) only varied from 3.2 to 3.8. This suggested that for a wide variety of cutting conditions the distribution of stress on the tool face was such that about 90 percent of the load was taken by half

of the chip tool contact region. The length of the tool contact region was a function of the workpiece properties with ductile materials generally giving a larger area of contact.

Barrow et al (1982) have suggested the stress distribution shown on figure 1.3. Unfortunately their technique did not allow a force measurement closer than 0.142 mm to the cutting edge. Consequently the exact form of the distribution at or close to the edge could not be determined. For the range of conditions tested both the normal and the tangential stresses were shown to be constant from the cutting edge to a distance of up to approximately 40% of the tool chip contact length. The ratio of sticking to total contact length was essentially constant for changes in cutting speed, but tended to increase with undeformed chip thickness.

There are some similarities between this model and that proposed by Zorev (1963). In both cases it was suggested that the normal stress decreased exponentially in the sliding region. Barrow et al, however, suggested that the normal stress had a constant value in the sticking region, whereas Zorev proposed that it continued to rise exponentially reaching a maximum at the cutting edge. There is broad agreement in that the model by Zorev allocated about 90% of the normal load to half of the total chip contact area and the distribution suggested by Barrow puts about 70% of the load on to this area. The model by Zorev predicts very high stresses and stress gradients at or close to the cutting edge, and large values of the exponent "n" accentuates the problem.

Kato et al (1972) used a split tool to investigate the stress distribution at the chip/tool interface. A range of non-ferrous

materials were investigated. They included a hard and soft grade of aluminium, a half work hardened copper alloy, a 99.8% zinc with 0.02% aluminium alloy and a 70% lead with 30% tin alloy. These materials were machined using rake angles of 0, 10 and 20 degrees and undeformed chip thickness values of 0.1, 0.2 and 0.3 mm, the cutting speed was 50 m/min. The results showed that with the exception of the zinc alloy the normal and tangential stress distributions were similar to those found by Barrow et al (1982). The results for the zinc alloy gave an approximately similar decreasing normal distribution to that found by Zorev (1963). It was stated that the shape of this distribution was caused by the brittle nature of the zinc alloy.

Usui (1978) determined the stress distributions for a 0.25C tempered steel using a feed of 0.2 mm and wide range of speeds. The results were very similar to those found by Zorev. All the above investigations were carried out using small values of feed. In many cutting operations where deformation is a problem the feed often exceeds 0.5 mm, and these distributions may not apply.

1.4.2 Stresses in Cutting Tools Using Photo-Elasticity

Loladze (1967) and Amini (1968) used photo-elastic techniques to determine the stresses in cutting tools. Because of the limitations of the photo-elastic material as a cutting tool it was only possible to machine lead at low speeds, 3.1 m/min being typical. The photo-elastic models showed two different stress zones. There was a zone of tension and a zone of compression. The border between the zones was shown to meet the rake face near the end of the chip-tool contact region. It was shown that by increasing the wedge angle (or decreasing the rake angle) the size of the tensile zone and the magnitude of the tensile stresses was reduced. Loladze stated that there existed a

maximum undeformed chip thickness (breaking feed) above which the tensile stresses reached a limiting value. It was suggested that if the stress exceeded the ultimate stress in uniaxial tension then the tool would fail by cracking and this would be a brittle failure.

The conditions at the chip/tool interface when maching lead with a photo-elastic material may differ significantly from those found with steel and the difficult to machine alloys. Lead may not exhibit the sticking region that is normally found with steel. Furthermore it is a very ductile material and this gives a relatively large chip/tool contact area. Less ductile materials are likely to give higher loads near the cutting edge and hence a different distribution of contact stresses. When machining lead at such low speeds the temperatures are low so the influence of thermal stresses cannot be investigated. For the above reasons it is unlikely therefore that the stress distributions when machining lead with a photo-elastic material have much similarity with those for machining steel or the difficult alloys. Therefore the results found from using such techniques should be considered with an awareness of their limitations.

1.4.3 Analysis of Stresses in Tools with Point Loading

Early attempts to determine the stresses in cutting tools were based on an analysis produced by Mitchell (1902) and have been summarised by Kronenberg (1966). The analysis gives the stresses that occur in a wedge when it is loaded at its apex with a point load. The radial stress on the rake face (σ_r) is given by

$$\sigma_r = \frac{2P_r}{r}\left[\frac{\cos\ \beta/2.\cos\nu}{\beta+\sin} + \frac{\sin\ \beta/2.\sin\nu}{\beta-\sin}\right] \qquad (4)$$

where, P_r is the resultant cutting force

r is the radial distance from the edge

β is the included angle of the wedge

ν is the direction of the cutting force

Very small values of r give values of stress tending to infinity close to the cutting edge. The use of a point load has limitations, because in practice complex normal and shear loads are known to exist. To understand tool deformation and the various failure mechanisms, a more comprehensive analysis is required.

1.4.4 Analysis of Stresses in Tools with Distributed Loads

Thomason (1974) developed an analysis for load distributions that were similar to those proposed by Zorev (1963) and Barrow (1982). Thomason predicted a stress distribution on the rake face which was similar to that found by Loladze (1967) who used a photo-elastic technique. Loladze suggested that the stress on the rake face became tensile and reached a maximum at a distance of approximately three chip contact lengths from the cutting edge. The analysis by Thomason for a constant linear loading over the entire chip contact region gave a discontinuity in stress at the point of chip separation. Furthermore the stress tended to infinity at this point.

Thomason also analysed the radial stress on the flank face. He predicted a maximum value at a distance of approximately one chip contact length below the cutting edge. This prediction should be compared with the practical results of Trent (1959) and Ekemar (1966) who found that the maximum deformation occurred just beneath the cutting edge. The prediction by Thomason of infinite stresses on the rake face is not confirmed in practice so this analysis must be

considered as having limitations. Regarding the stresses on the tool flank face, it is probable that the reduced yield stress of the tool material at elevated temperatures has a significant influence. Under these conditions the deformation may occur at the points of reduced yield stress and not at the points of maximum stress predicted by an isothermal model.

1.4.5 Analysis of Tool Stresses Using Finite Element Techniques

A number of researchers have applied the techniques of Finite Elements (F.E.) to the problems of cutting tools. It is claimed that more accurate results can be obtained. This is because the complex mechanical and thermal loadings can be more realistically represented than when using analytical methods.

Tlusty and Masood (1978) used F.E. techniques to model a cutting tool tip and the tool shank. The load was applied to the rake face using a distribution very similar to the one suggested by Barrow (1982).

Loads were also applied to the tool flank face on what was assumed to be a wear land. The results presented showed that there were no tensile stresses near the cutting edge. These results agreed well with those obtained by Loladze (1967) who used photo-elastic techniques. A maximum local tensile principal stress was found on the rate face at a distance from the cutting edge of about 3 times the length of chip contact.

The main limitation of this work by Tlusty and Masood was that it did not consider thermal stresses. It has been shown by Braiden (1971) (Section 1.6.1) that the thermal stresses can exceed the mechanical

stresses. Recent work by Chan and Braiden (1981) (section 1.7.1) using Finite Element techniques suggests that the mechanical loads acting alone may not be high enough to cause plastic yielding of the tool material. When the combined thermal and mechanical effects were evaluated they found stresses which exceeded those required to give plastic deformation of the tool material.

1.5.1 Temperature Distributions in Cutting Tools

Two main sources of heat occur in metal cutting: they are the primary or shear zone and the secondary deformation zone. The thickness of the secondary zone varies considerably for different cutting conditions and work materials, typical values ranging from 12 to 100 μm. The heat generated in this thin layer or zone is conducted either into the moving chip or into the tool which acts as a heat sink. The heat flow into the tool depends on its thermal conductivity, shape and any cooling methods that are used.

One of the early successful attempts at showing the temperature distribution in cutting was achieved by Boothroyd (1963) who used infra-red photography. It was shown for both brass and mild steel workpieces that the maximum temperature occurred some distance back from the cutting edge.

Smart and Trent (1975) have investigated the temperature distributions in HSS tools when cutting steel, titanium and nickel. Their experimental technique was based on the phenomenon that changes in metallurgical structure occurred with changes in temperature. By taking sections both parallel and perpendicular to the cutting edge it was possible to obtain a three-dimensional distribution of the temperatures. A series of tests using a constant feed of 0.25 mm and

a range of cutting speeds gave a set of temperature contours shown on figure 1.4.

Smart and Trent argued that the maximum stress at the cutting edge was supported by a part of the tool which was at a lower temperature, thus allowing the tool to continue to cut without collapsing. Tests were also carried out to investigate the effect of changes in feed rate. As the feed rate was increased larger areas of the tool were subjected to higher temperatures. It was noted, however, that the ratio of the undeformed chip thickness to the point of maximum temperature from the cutting edge was not constant.

When machining commercially pure titanium the temperature distribution in the tool differed from that found when machining iron. For the same cutting speeds titanium gave higher temperatures than iron. Also for the same undeformed chip thickness, the maximum temperature was much closer to the cutting edge than for iron. It was suggested that the rake face directly beneath the undeformed chip was at a much higher temperature than when cutting iron, consequently the yield stress of the tool was reduced in the region subjected to the highest normal stress. For this reason the tools used to cut titanium were said to have failed by deformation of the cutting edge.

When machining commercially pure nickel the observed temperature distributions were markedly different than those of iron or titanium. The temperature in the tool contact region was essentially uniform and sometimes it was higher at the cutting edge. It was observed that a wear land quickly developed on the flank face and the temperatures could exceed those on the rake face. This concentration of high temperatures and contact stresses at the cutting edge was said to

cause deformation and failure at relatively low speeds and feeds.

This work by Smart and Trent has yielded some very useful information on three-dimensional temperature distributions in cutting tools. The technique is, however, very specialised and it requires laborious preparation of the samples. Each tool can only be used once because it is necessary to take cross-sections after each test.

Dearnley (1983) has developed a novel technique for determining the temperature distribution in cemented carbide cutting tools. He replaced the usual cobalt binder with iron. A typical tool composition was WC 68%, TiC 12%, TaC 6%, NbC 4% and Fe 10%. The technique depended on the binder transforming to austenite at a characteristic temperature and producing a heat affected zone. Temperature contours were constructed by tracing the boundary of each heat affected zone.

Figure 1.5 shows the contours that were obtained when machining EN24 (817 M40, 326 HV) at 240 m/min for 10 seconds. The exact maximum temperature could not be determined by this technique because of limitations in the method of calibration. The coated tool (TiN) did not reach such a high temperature and the chip contact length was reduced. Consequently the point of the maximum temperature was closer to the cutting edge. Dearnley concluded that TiN coatings reduced the cutting temperatures by reducing the chip/tool contact length. It was suggested that coated tools gave a reduced contact length because the strength of bonding across the chip/tool interface was less than with uncoated tools. It was argued that if the normal contact stress diminished towards the end of the chip/tool contact length in the manner suggested by Zorev (1963) or Barrow (1982), then the position where the chip separated from the rake face would be

sensitive to the interface bond strength. Unfortunately Dearnley did not determine whether the ratio of sticking to sliding remained constant within the reduced chip/tool contact length.

It is generally understood that in the sticking region there is virtually complete contact between the chip and the tool. This condition occurs when the normal stress is equal to or greater than the yield stress of the softer work material. Under these conditions relative motion is caused by shearing in the softer material, and this must represent to a substantial part of the total heat generated in the secondary deformation zone. It is likely that the area of sticking contact was not significantly altered by coating the tool, because it depends on the yield stress of the work material and not the tool coating. Therefore the heat generated in this part of the zone should not alter significantly.

In the sliding region the coefficient of friction is constant and depends on the force required to shear the welded asperities between the chip and tool. The area of welded asperities depends on the normal pressure which decreases to zero at the point of chip separation. It was argued by Dearnley that coated tools gave a reduced bond strength and this led to a reduction in chip contact length.

Dearnley did not completely explain why a reduction in chip contact area gave a reduction in temperature. It could be argued that the possibly less severe friction conditions in the sliding region may have resulted in less heat being generated by sliding between the chip and tool. However, Dearnley quoted a reduction in temperature between the coated and uncoated tools of approximately 200^{o}C. If the

conditions remained substantially constant in the sticking region then it is unlikely that changes in the sliding region had such a significant effect on the temperature. This must be considered as a limitation in the theory proposed by Dearnley.

1.5.2 Temperature of the Chip/Tool Contact Region

One of the earliest attempts to determine the chip/tool contact temperature during the cutting was made by Herbert (1926). He used the phenomenon that the two different materials made a thermocouple junction and the emf could be used as an indication of the contact temperature. This phenomenon has been the basis for systems that control the spindle speed of a lathe to give a constant cutting temperature. Such a system has been reported by Jaeschke (1967), who quoted the following relationship between the cutting variables and temperature:

$$\theta = Kv^{0\cdot237} f^{0\cdot133} d^{0\cdot056} \qquad (5)$$

A paper by Trigger (1966) quoted the following relation for the temperatures as:-

$$\theta = Kv^{0\cdot2} f^{0\cdot14} \qquad (6)$$

Trigger stated that the depth of cut appeared to have little effect provided it was twice the tool nose radius. Both equations (5) and (6) have similar values for the exponents of v and f. The important feature of these relationships was that changes in temperature were most sensitive to changes in cutting speed. This effect was confirmed in practice when it was found that diffusion wear was largely speed-dependant.

Gaylord and Hughes (1957 and 1963) have suggested that the thermocouple emf gives a weighted average of the contact temperatures between the chip and tool. It has also been shown by Braiden (1967) that different tool and workpiece materials have different thermoelectric characteristics, so careful calibration of the system is essential. Although the technique and the results have their limitations, it is useful for determining the trends in temperature when changing the cutting variables or tool materials. The tool/work thermocouple is evaluated in Chapter 2.

Trigger (1961) has also proposed a temperature distribution for a steel workpiece and carbide tool that had the relative shape shown on figure 7.6. The maximum temperature was found to occur some distance from the edge, and to coincide with the position of maximum crater wear. The temperatures were determined indirectly from the tool flank face temperature; the technique is discussed in section 2.1.3.

Usui (1978) and Kitagawa (1975) determined the shape of the tool/chip temperature distribution by using a platinum wire that was in contact with the underside of the chip. A very fine platinum wire 0.01 mm diameter and insulated with a quartz tube was embedded in a carbide tool tip. The end of the wire was exposed and made the hot junction of a thermocouple when it contacted the chip material passing over the tool face. The relative position of the wire in the tool chip contact region was altered by grinding material off the front and end clearance faces. This technique did not allow the temperature to be measured closer than 0.2 mm to the cutting edge. Difficulties were also experienced in determining the temperature at the point of chip departure from the tool rake face. Failure to

determine the temperature at the cutting edge was a serious limitation, because it is known that when cutting many materials the highest normal contact stresses occur at the cutting edge.

Despite these limitations the technique was useful in that it allowed the chip/tool interface temperature to determined perpendicular the direction of chip flow. However, the results showed that the greatest temperature variation was in the direction of chip flow. Although some temperature variation occurred perpendicular to the direction of chip flow, it was not considered to be as significant. The relative shape of the temperature distribution in the direction of chip flow is shown on figure 7.6.

1.5.3 Analytical Temperature Distributions in Cutting Tools

A model to predict the temperature in a cutting tool has been proposed by Thomason (1975), see figure 1.6. It used a technique of conformal mapping and assumed a constant temperature heat source over the rake face for the distance $o < x < 1$, and the same source over the flank face for the distance $o < y < f$. The steady state temperature field was given by the following equation:

$$\theta = \theta_o \left\{ 1 - \frac{1}{n\pi} . \text{arc cosh} \left[\frac{\sqrt{(x^2-y^2+f^2)^2+4x^2y^2} + \sqrt{(x^2-y^2-1)^2)+4x^2y^2)}}{(1+f^2)} \right] \right\} \quad (7)$$

where θ_o was the temperature of the source and θ the temperature at any point given by the x and y co-ordinates. When evaluating the model "f" was assigned a value of 0.2, and "n" was set at 2. The value of "n" was chosen so that the temperature field agreed with the experimental observations. This model used a constant temperature heat source along the rake and flank faces. In practice it has been found that the temperature along the rake and flank faces is not constant, but often has a complex distribution as described by

Trigger (1961), Boothroyd (1963), Smart and Trent (1975), Usui (1978) and Dearnley (1983).

This approach by Thomason is therefore of limited practical value.

1.6.1 Thermal Stresses in Cutting Tools

Cutting tools used under modern conditions of speed and feed rate are subject to severe thermal shock at the start of cutting. It has been shown by Braiden (1971) that during intermittent cutting the temperature at the rake face rises to a maximum in a few micro-seconds.

Thermal stresses are caused by the differential expansion in the cutting tool. Braiden considered the tool as a wedge which was constrained in the normal direction by assuming a plane strain condition (figure 1.6). The stress in the normal direction was given by:

$$\sigma_z = - E\alpha\theta \qquad (8)$$

where E is the Young's modulus of the material

α is the coefficient of thermal expansion

θ is the temperature rise.

It was shown that at the start of intermittent cutting when using a feed of 0.25 mm and depth of cut of 6.35 mm that a compressive stress of 1.8 GN/m^2 could occur. To this stress was added a mechanical stress of 0.41 GN/m^2 giving a total compressive stress of 2.21 GN/m^2. This represented the worst situation; the severity of the thermal stresses was reduced as the bulk of the tool heated up. Woods (1956) showed that for a wide range of cutting conditions the steady state

temperatures beneath the tip were usually reached after about 2 minutes. Further analysis by Braiden (1971) showed that for the same cutting conditions the steady state thermal stress was reduced to a value of 1.4 GN/m^2.

Thomason (1975) used a theory by Musklelishvili (1963) to determine the steady state thermal stress under plane strain conditions. The thermal stress σ_z could be found at any point in the xy plane by using the relationship:-

$$\frac{\theta}{\theta_o} = - \frac{\sigma_z}{E\alpha\theta_o} \qquad (9)$$

where θ and θ_o were discussed in section 1.5.3.

The stress distribution has the same form as the temperature distribution and gives constant values of σ_z along both the flank and rake faces. In practice the temperature varies considerably on the rake face so this analysis has the same limitations as the temperature analysis. Furthermore the assumption of plane strain is only valid if the chip/tool contact area has an aspect ratio of greater than say 6 to 1.

Braiden (1971) proposed that the maximum thermal stress occurred at the point of highest temperature which was at the central portion of the tool/chip contact region. The stresses were such that they caused localised plastic yielding on the hottest part of the rake face. When the tool cooled the material surrounding the locally deformed area contracted and induced tensile stresses. It was postulated that the induced tensile stresses initiated cracks perpendicular to the cutting edge. This analysis by Braiden assumed a condition of plane strain

which may not be justified when the aspect ratio of the tool/chip contact area is reduced to a more typical value of say 2 or 3 to 1.

1.7.1 Determination of Thermal Stresses Using Finite Element Techniques

The use of F.E. techniques for determining the mechanical stresses was discussed in section 1.4.5. Chan and Braiden (1981) have used F.E. techniques to determine the thermal stresses in a cutting tool. The shape of the temperature distribution used on the rake face (XY plane) is shown on figure 7.6 and was based on work published by Trigger et al (1961). The temperature distribution in the Z-direction was considered uniform and plane strain was assumed. The maximum value of σ_z occurred on the rake face at the point of maximum temperature. The authors found it necessary to use Reduced Integration and Local Stress smoothing techniques; this was because large stress discontinuities were found at the element boundaries. It was also stated that a finer element mesh did not necessarily produce better results. The optimum element size was said to depend on the type of problem and its particular boundary conditions.

Chan and Braiden found that they were limited to the use of two-dimensional elements when calculating thermal stresses; this was because three-dimensional elements required an excessive amount of computer time. Plane strain was applied in the z direction in an attempt to simulate the restraint caused by the cooler part of the tool body. The restriction of having to use 2-dimensional elements to solve a 3-dimensional problem was a limitation of this technique. However, their use of the temperature distribution proposed Trigger (1961) was a more realistic approach than that adopted by Thomason (1975) who assumed a uniform temperature distribution on the rake face (section 1.5.3).

1.8 Tool Deformation

Trent (1959) has shown that high metal removal rates or difficult workpiece materials can cause plastic deformation of carbide cutting tools. The rake face of the tool was said to have been forced downwards and this gave a corresponding bulge of the clearance face just below the cutting edge. Trent did not quantify the amount of bulging, but he did classify it as either small or severe. It was stated that when the deformation was small the effect on tool life was negligible. Under conditions of severe deformation the reduction in clearance on the flank face was said to lead to rapid wear which was usually concentrated at the nose. Trent stated that deformation was not easy to observe, but if excessive wear at the nose occurred then deformation was the likely cause. The influence of nose radius is discussed in section 1.8.2.

The main limitation of this work by Trent was that it did not quantify the bulging on the clearance faces or the depression on the rake face. However, this work was very useful because it explored the practical limitations of various combinations of tool and work materials (see figure 1.1). The influence of speed, feed and depth of cut are discussed in section 1.8.3.

1.8.1 Classification of Tool Deformation

Trent (1967) classified four different types of deformation (figure 1.7). Types A and B were said to be caused by the main cutting force. Type A had a bulge on the flank face combined with a depression on the rake face, and was found when cutting steel. The hottest part of the tool was back from the cutting edge, but the whole of the cross-hatched area was at a high temperature. This bulge was said to reduce the clearance angle locally (Trent 1959) and give accelerated

wear on the flank face.

Type B deformation was found when cutting hard cast iron. Under these circumstances the cutting forces and the heat input were restricted to an area adjacent to the cutting edge. It was proposed that these concentrated effects resulted in a more localised deformation mechanism which increased the clearance angle and possibly elongated the rake face. It was also suggested that the increased clearance angle caused the tool to wear rapidly, and that cracks on the rake face perpendicular to the direction of chip flow were caused by the elongation of the tool rake face. The implication by Trent that cracking is a simple tensile failure is doubtful because it has been shown that the stresses on the rake face in the chip contact area are compressive during steady state cutting.

Type C deformation was said to result from a large feed force acting in a direction parallel to the rake face. It was found to occur when feed rates greater than 0.75 mm were used to machine steel railway wheels or high strength alloys. It was suggested by Trent that if a large wear land was formed, or the cutting edge was chipped in such a way as to eliminate the clearance angle locally, then the pressure could become so great in the feed direction to deform the tool as shown. If the deformation was only local to the cutting edge then a small ridge was raised which was broken off, giving a chipped edge which may then lead to rapid tool failure. This type of deformation has only been reported by Trent and it would appear only to occur under certain extreme cutting conditions. In the paper neither the amount of deformation or the cutting conditions were specified, so the exact deformation mechanism must be considered a matter of conjecture.

The final type of deformation (type D) was said by Trent to be rarely encountered. A photo-micrograph of a section of a tool used to rough machine a bar of creep resistant nickel-based alloy was shown. A definite upward deformation of the rake face could be observed and this was combined with the displacement of the flank face close to the cutting edge. Unfortunately neither the magnitudes of the cutting forces or their relative ratios were reported in the paper, so it is difficult to assess their relative importance in causing this type of deformation.

Trent did not report either the cutting forces or temperatures that occurred when investigating the different types of tool deformation. This was probably because some of the effects such as type C occurred as part of industrial practice and could not be observed under strict experimental conditions. Such a lack of information is unfortunate because it does not allow the relative influence of temperature and stress on deformation to be determined.

Ekemar (1966) has reported the plastic deformation of carbide cutting tools. He found that it took the form of bulging at the clearance face and depression of the rake face (figure 1.8). This form of deformation was comparable with type A described by Trent. Ekemar, like Trent, found that the deformation was most pronounced at the nose and it decreased with distance along the cutting edge. Measurements of flank and crater wear and bulging were made at three sections along the cutting edge of the tool/chip contact region. It was found by Ekemar that at any particular cross-section the flank wear and bulging increased proportionally with time and their ratio was almost constant, being largely independant of time. Typical maximum values of bulging were found to be 5 to 20 μm. During

subsequent tests investigations were confined to the area of the nose and its adjacent flank face, because this was found to be the most critical region.

Ekemar used a constant feed rate of 0.7 mm and a depth of cut of 2 mm to investigate the influence of changes in cutting speed on different grades of carbide. Comprehensive data on the wear and bulging was given, but like Trent he did not measure either the forces or the temperatures. However, the relative importance of temperature was inferred by Ekemar because he concluded that increasing the cutting speed had an accelerative effect on plastic deformation. It is well known that tool temperatures are sensitive to changes in cutting speed. Despite the limitations of not directly considering the influence of stress and temperature, this work gave valuable information on tool deformation and is further discussed in section 1.8.3.

Evidence of plastic deformation on the tool rake face was given by Venkatesh et al (1977). When a carbide tool with a 5 μm TiN coating was examined, it was observed that the crater was 25 μm deep and the coating was still intact. It was argued that such a crater could only be formed by a depression of the cutting edge and bulging on the flank face. It was claimed that the flank face coating was worn away at some distance below the cutting edge, and this was the position of maximum bulging. Venkatesh observed the flank surface through a light sectioning microscope (see section 4.3.1), but he did not quote the amount of bulging present.

It is disappointing that neither the tool temperature or the cutting forces were quoted, because the deformation was said to have occurred after 31 minutes when machining low carbon steel (0.22%C) at

200 m/min and a feed rate of 0.1 mm. These values should be compared with the results found by Trent (1959) who stated that with feeds of less than 0.125 mm, failure by deformation was unlikely when machining low carbon steels. This result quoted by Venkatesh should be interpreted with a full awareness of its limitations.

1.8.2 The Influence of Tool Geometry on Deformation

Both Trent (1959) and Ekemar (1966) have stated that deformation of the cutting tool was usually most pronounced in the region of the nose. Ekemar used a constant nose radius of 0.8 mm. Trent stated that the smaller the nose radius the lower the speed and feed values at which deformation will occur. In heavy metal removal operations it was necessary to use a large nose radius to avoid sudden and catastrophic failures. It was proposed that the region near the nose was hotter than elsewhere and that the smaller the nose radius the higher will be the local temperature. This may be explained by the fact that increasing the nose radius increases the length of cutting edge in contact with the chip and work. It therefore may be argued that by increasing the contact length the heat generated is conducted into the tool over a greater area and this reduces the heat flux density. However, it has been shown (see section 1.5.1) when cutting steel that the hottest part of the tool contact region is some distance back from the cutting edge. The proposal that deformation is due solely to local temperature is therefore doubtful, particularly when cutting steel.

1.8.3 The Influence of Cutting Conditions on Deformation

Generally the threshold at which deformation starts for any particular combination of tool and workpiece material is dependant on the cutting conditions. The combinations of feed and speed that

gave severe deformation were plotted by Trent (1959) on graphs with logarithmic axes. It was shown that for a large range of work materials, the combinations of feed and speed gave an approximately straight line relationship. The lines were often at angles of approximately 45^{o} (figure 1.1), so any combination of feed and speed on the line represented a constant metal removal rate. An alternative approach is to consider the line as a performance envelope for the tool material. Under these particular conditions the values of feed and speed must be altered in inverse proportion to each other; if the feed is doubled then the speed must be halved. It should be appreciated, however, that changes in feed rate and cutting speed have very different effects on cutting force and temperature. Changes in feed rate have a very significant influence on the cutting forces but less influence on temperatures (see section 1.5.2). Changes in cutting speed have a dramatic effect on temperature but virtually no effect on the cutting forces.

Trent (1959) stated that deformation was dependant on the depth (or width) of cut, and that increasing the depth of cut would lead to the onset of deformation if the other variables were held constant. This would seem to be an intuitive statement by Trent without any real evidence, because he investigated deformation using a constant depth of cut of 2 mm. Furthermore, it has been shown by Trigger (1966) and Jaeschke (1967) that changes in depth of cut do not significantly alter the temperature (see section 1.5.2). It is also known that the contact stresses between the chip and tool are dependant on the speed and feed rate. The effect of width of cut can probably be considered on a unit width basis in regions that are reasonably remote from the nose and it should not alter the contact pressures.

Ekemar (1966) found that changes in cutting speed had a significant effect on deformation. He used a constant feed rate of 0.7 mm and a depth of cut of 2 mm. The work material was a 0.96%C carbon steel with a hardness of 275 Brinell. Initially three different tool grades were tested; they had the same composition but different sizes of grain. An increase in cutting speed from 80 to 100 m/min caused a drastic increase in the amount of bulging. It was found that the grade with the small grain size was the most resistant to deformation, particularly at the higher speeds. Under these circumstances it would appear that the higher temperatures produced by the higher cutting speeds were responsible for the increased deformation. In a second series of tests three different grades with 15, 20 and 25% TiC were investigated; the change in speed from 80 to 100 m/min gave a large increase in the amount of deformation. However, the grade with the highest TiC content was the most resistant to deformation.

Unfortunately Ekemar did not measure the temperatures or the forces, so it was not possible to determine any correlation with the tool deformation. Ekemar did not investigate the effects of changing the feed, which probably has a significant effect when such large values (0.7 mm) are used on a high strength (0.96%C, 275 BHN) steel. The failure by Ekemar to consider the effect of changes in feed was a limitation of this work. This is because in practice the usual strategy is to maximise the feed rate subject to the restraints of surface finish and total cutting force, and then to select the cutting speed subject to the limitations of power availability or economic tool life.

1.8.4 The Deformation Mechanism of Cemented Carbide Cutting Tools

The precise deformation mechanism of carbide cutting tools is not

fully understood. At room temperatures they behave in a brittle manner when subjected to tensile stresses. When loaded under compression at room temperature they are able to sustain considerable plastic deformation before failure. Above the yield point the stress/strain curve departs gradually from linearity, giving fracture at about 7 to 9 x 10^{-3} strain. Increasing the cobalt content allows a greater amount of strain before fracture.

The hot compressive strength of carbide alloys has been investigated by Trent (1967), who found that at temperatures of 1000°C these alloys could sometimes be deformed by 20 to 40% before complete failure. It was found that the strain was not homogeneous and the specimens were found to barrel. This effect is common to most compression tests and was due to the restraints caused by the anvils. At up to 10% compressive strain no structural change was observed. Between 10 and 15% strain some local disruptions in the structure were found. They usually started at the edges of the end faces and extended progressively towards the centre. At higher magnifications they appeared as localised cracks or voids between the carbide grains. It was proposed by Trent that the plastic deformation at high temperatures was due to either the cobalt bonding failing or the bonds between the carbides and cobalt rupturing. At these higher temperatures no cracking across the grains was observed. This should be compared with room temperature behaviour where the cracks followed a path through some carbide grains and along some boundaries. It was stated that in the high temperature compressive tests, disruptions in the structure of the specimen proceeded gradually and its collapse was the final stage of a prolonged process. Trent (1967) has claimed that it is possible to observe the first stage of disruption on sections of tools that are deformed in service. Because no fracture

of the carbide grains was observed, it was stated that the plastic strain in the initial stages (5 to 10%) was confined to the bonding metal. However, the areas of bonding metal were said to be too small for any evidence of deformation to be observed microscopically.

Jonsson (1972) found that plastic deformation occurred in two separate regions. One region was at the crater remote from the cutting edge, and the other region was on the clearance face. It was observed that porosity was present on that part of the clearance face which suffered the most deformation. Jonsson stated that two kinds of pore were present. The first had a shape and size similar to that of the WC grains (approximately 1.5 μm), and the second type was smaller (1 μm) and was sometimes seen to lie in the binder phase. These observations should be compared with those reported by Trent (1967), who found disruptions in the structure, but claimed that the areas of bonding were too small for deformation to be observed.

Neither Trent (1967) or Jonsson (1972) found evidence of either cracking or deformation in the carbide grains at the elevated temperatures. It was agreed that deformation at high temperatures was due to either the bonding between the grains failing or the bonds between the carbide grains and the binder rupturing. Jonsson, however, suggested that the WC grains appeared to act as nucleating points for the larger pores. It is possible therefore that the interface between the WC grains and the binder is the weakest part of the structure and it is at these points that deformation begins. The tool used by Jonsson contained 56% WC, 20% TiC, 13.5% TaC, 1.5% NbC, and 9% Co. It may be significant that the porosity was said to start at the WC grains and not the TiC or TaC grains, both of which were present in substantial quantities. Ekemar observed fissures at the

bottom of the wear land. Unfortunately he did not give details of their exact nature or the conditions under which they occurred. It would be useful to know if they followed the binder or the carbide grain/binder interface.

Trent (1967) has shown that increasing the TiC content improves the hot compressive strength dramatically. For example, a WC, 23% Tic, 11% Co alloy had a 5% proof stress of 0.855 GN/m^2 at 1125°C, compared with a WC-6% Co alloy that had a 5% proof stress of 0.155 GN/m^2 for the same temperature. The TiC alloy was capable of supporting a stress of 0.155 GN/m^2 at a temperature of 1240°C, which is remarkable because the metallic bond becomes liquid at 1300°C. Ekemar (1966) (section 1.8.3), who used practical cutting tests, has confirmed that increasing the TiC content improves the resistance to deformation.

Deformation of the individual carbide grains was not reported by Trent, Ekemar or Jonsson. As a consequence the research work to improve the hot compressive strength of cemented carbides has concentrated on improving the bonding between the grains and finding better cementing materials. Almond (1981), who used an Electron microscope, has shown an example of deformation in the grain of a WC-11% Co alloy. Unfortunately the load conditions were not specified so the deformation is difficult to relate to a metal cutting application. Furthermore, Almond did not quantify the amount of deformation in the grain relative to the composite structure. If this is not known then it is impossible to decide whether investigations into grain deformation are likely to be worthwhile.

CHAPTER 2

TOOL TEMPERATURE MEASUREMENT

2.1 Introduction

The measurement of cutting tool temperature is a difficult practical problem. It is further complicated because what is normally the hottest part of the tool is usually covered by the chip. The most commonly used measurement techniques for determining tool temperatures are infra-red devices, thermo-sensitive paints, and thermocouples.

2.1.2 Infra-Red Photography

Boothroyd (1963) used infra-red photography to determine the temperatures of the workpiece, chip and tool. From the results it was possible to plot contours of constant temperature and this gave a great deal of detailed information about the distribution of temperature in orthogonal machining. When using this technique it was necessary to pre-heat the workpiece to 600^{o}C before machining, and this was achieved by mounting a furnace on the lathe bed. The observations were made from the side of the tool and not directly on to either the rake or flank face. The limitation of this approach was that the workpiece had to be pre-heated and that the hottest part of the chip was not at the sides but at the central sections.

2.1.3 Infra-Red Detectors

Direct observations of the rake face in the chip contact region can be made by viewing it through a "window" in the chip as it passes over the tool face. The workpiece, which is usually a tube, has a hole drilled axially in its wall. When the hole in the chip passes over the tool, the rake face is exposed and its temperature is measured by using an infra-red detector.

Trigger et al (1961) used a similar technique for measuring the temperatures on the tool flank surfaces. A detector was mounted in the wall of a tubular workpiece. The flank face was observed intermittently through a hole that was drilled axially into the wall of the tube. This technique gave results, but it suffered from several practical limitations; the workpiece required a lot of preparation so that the detectors could be mounted correctly. It was also found that by mounting the detectors in the workpiece, the amount of material available for machining was severely limited. Techniques using infra-red devices have the disadvantage that they can be difficult to use and calibrate and that they are not usually commonly available. It is probably for these reasons that they have not become popular for this type of investigation.

2.1.4 Thermo-Sensitive Paints

Temperature sensitive paints are useful for determining temperatures where access is difficult, but they cannot be used in the tool-chip contact region. They have very limited resolution $\pm 20^{o}C$ being typical. Furthermore, they do not give an output signal which can be processed or stored. In some engineering applications they are useful because of their low cost and ease of use, but have not been used with much success in metal cutting research.

2.1.5 Thermocouples

Despite some limitations, thermocouples in their various different forms continue to be used in metal cutting research. The main reasons for their continued popularity are as follows:-

1) they are relatively inexpensive

2) they are compact and versatile in use

3) they have a wide working temperature range

4) they give an output voltage that can be recorded.

Superficially they appear easy to use, however if consistent results are to be obtained then considerable care and attention to detail is required. Correct selection of the couples is essential and the practical problems of signal conditioning in a machine tool environment should not be minimised.

Thermocouples can be used in two main ways to determine the tool temperature. The first technique is for the chip contact region and uses the dissimilar materials of the tool and work to form the hot junction when cutting is taking place. To form the cold junction a piece of the work material is attached to the tool at some distance from the cutting edge; this is the system in its simplest form. In practice, it is found that a number of practical problems arise and these are discussed in sections 2.2 to 2.4.

Thermocouples can also be used to determine the temperature at other parts of the tool tip body. One approach is to spark-erode holes in the underside of the carbide tool bit and then to insert thermocouples as close as possible to the cutting edge and rake face. There are a number of practical problems and limitations with this technique. It is well-known that very steep temperature gradients occur in the chip contact region, so any holes in this region will distort the temperature field considerably. It is also difficult to get good thermal contact between the thermocouple and the tool tip and the difficulty is compounded when deep holes are used to try and get close to the chip contact region. Because a large amount of preparation is required, the technique cannot be considered viable if

a large number of tips are to be tested. Attempts at using the method are discussed in section 2.4.

An alternative approach is to place thermocouples on the surface of the insert. This method does not give temperatures as close to the chip contact region as do the inserted thermocouples, but there are other advantages. Several thermocouples can be placed at different points on the tool insert and with careful design, good thermal contact can be achieved. Good thermal contact is essential if surface temperatures are to be measured. If the thermocouples are mounted in the tool holder then the need to prepare each tip by spark-erosion and the insertion of thermocouples is obviated. The use of surface mounted thermocouples was finally adopted for this investigation and is discussed in sections 2.2.3 and 2.5.

2.2.1 Measurement of Tool Insert Temperatures Using Thermocouples

In the previous section it was stated that thermocouples were used to determine the temperature of the insert. It was decided to determine the temperature at five different points and these were as follows:-

1) at the tool-chip interface
2) at four points at the tip-toolshank interface

Figures 2.1a to 2.1c show the initial tool tip holder.

2.2.2 Tool-Chip Interface Temperature

The tool-chip temperature was measured by letting the dissimilar materials form the hot junction of the thermocouple. To form the cold junction, one end of a length of steel wire was made to contact the underside of the carbide insert. To ensure good electrical

contact and ease of connection, the steel wire was spring loaded against the underside of the tip (figure 2.1b). The other end of the steel wire was connected to one of the input terminals of the signal amplifier.

2.2.3 Temperature Measurement at the Tip-Shank Interface

A method was required that would ensure good thermal contact between the tool tip and its seating and also good contact between the thermocouple and the tool tip. To achieve this, holes were drilled in the tool shank as shown on figure 2.1c and the thermocouples were placed into the holes. Contact with the tool tip was achieved by seating the thermocouples on small coil springs. The leads for each of the thermocouples were "brought out" along a channel machined in the base of the toolshank, this arrangement giving protection from the hot swarf during the cutting tests. One lead from the hot junction of each couple was taken to an input terminal on the signal amplifier and the other lead to its corresponding cold junction. Similarly, the spare lead from the cold junction was taken to the other input terminal on the signal amplifier.

2.2.4 Signal Transfer System for Tool-Work Thermocouple

In the past a copper disc running in a mercury bath has often been used to transfer the voltage signal from the rotating workpiece. Because of the known dangers of handling mercury, it was decided not to use this technique, but to develop a rotating contact system which was less hazardous. The system is shown diagramatically on figure 2.2. Essentially it consisted of a copper plug which was placed into a steel bar that passed through the spindle of the lathe and was connected to the workpiece. The copper plug had a spherical radius at one end and was plated over its entire surface with "acid hard gold",

this alloy being used for the edge contacts on printed circuit boards. A piece of 16 gauge copper sheet was also gold plated and this made contact with the spherical radius on the plug. The plating was 5 μm thick and did not show signs of any significant wear throughout the series of cutting tests. One end of a steel wire lead was connected to the 16 gauge copper plate and the other end to the input terminal of the signal amplifier. Both the workpiece and transfer system were insulated from the lathe and the leads were shielded to minimise the amount of "pick-up" from stray electrical fields.

2.3 Selection of Thermocouples for the Tip-Shank Interface

When selecting a thermocouple for a particular application, the following points should be considered:

1) temperature range
2) sensitivity
3) response time
4) physical size and shape
5) commercial availability
6) cost

From previous published work (Woods 1956) it was expected that the thermocouples at the tool-shank interface would have to measure temperatures up to a maximum of 250°C. If accuracy and resolution are important then it is essential to choose a thermocouple that has the correct sensitivity. As far as is practicable, the sensitivity should be as high as possible, but not so high as to be outside the range of any signal conditioning or recording equipment when the particular working range of temperatures is being measured. The response time of a thermocouple is largely dependant on its physical

size, since a small weld bead will conduct heat more quickly. It is common practice to remove part of the bead after welding so as to improve its response. Many thermocouples are available in a protective sheath often made from stainless steel, but unfortunately the sheathing has the effect of reducing the response time dramatically. Thermocouples are available commercially from a number of different suppliers but these are usually standard designs. For the standard type the cost is quite modest, however if non-standard types are required in small quantities then they are very expensive.

After consideration of the points above, it was decided to select copper-constantan thermocouples and to manufacture them to a design suitable for this application. Copper constantan thermocouples have a maximum working temperature of 400^{o}C and a sensitivity of approximately 4 mv per 100^{o}C in the range being considered.

2.3.1 Manufacture of Thermocouples

Wires with a diameter of 0.3 mm were selected; they were found to be sufficiently robust and were easily available. The initial arrangement was to separate the conductors close to the bead by using a porcelain insulator as shown on figure 2.3. This arrangement was not very satisfactory because the insulator had the tendency to split the wires off from the bead. A medium was required that would both insulate the conductors and also give them mechanical rigidity. To achieve these requirements it was decided to encapsulate the wires in resin after welding. The mould, which is shown on figure 2.4, consisted of a nylon sleeve and a plug, both of which were held in a steel bar. To locate the bead in the centre of the mould the plug was given an internal taper. Because the resin was very viscous and access to the mould restricted, a hyperdermic needle was used to fill

the mould. After removal from the mould, half the bead was removed by polishing, which ensured good thermal contact with the underside of the tool tip and also improved the response time. Figure 2.5 shows a diagram of an encapsulated thermocouple. A similar technique was used for the corresponding cold junctions, but to ensure thermal stability they were encapsulated in a large block of resin.

2.3.2 Thermocouple Output Amplification and Recording System

In section 2.1.5 it was stated that one of the advantages of using thermocouples was that they gave an output voltage and this voltage could be processed to give a permanent record. It was decided to record the temperatures and forces (Chapter 3) by using two separate ultra-violet (U/V) recorders; these recorders were chosen for the following reasons:-

1) they have 12 recording channels
2) they have a good frequency response
3) a wide range of chart speeds are available
4) they were freely available.

When using a U/V recorder care is needed in selecting the correct galvanometers and also in matching them with the thermocouples. It was decided to use high frequency galvanometers (natural frequency 1000 H_Z) so that the response of the tool-work thermocouple could be recorded. Unfortunately, high frequency galvanometers have low sensitivities and the direct output from the selected thermocouples was not sufficient to "drive" the galvanometers. To overcome this problem an electronic amplifier was built. Initially five channels were required. It was found, however, that four circuits would fit on each printed circuit board, so it was decided to build an eight

channel device, as this would give some spare capacity if needed at a later date. Each channel of the amplifier was designed with five "gain" settings and this was found to be sufficient for the range of temperatures being measured.

2.3.3 Calibration of the Tip-Shank Thermocouples

After the amplifier system had been built and "de-bugged" the tip-shank thermocouples were calibrated. The cold junctions were placed in "iced" water at $0^{o}C$, and the hot junctions were mounted in a special fixture and spring loaded against a carbide tool tip. The complete fixture was then placed in an oil bath and the temperature varied up to a maximum of $200^{o}C$, which was the expected maximum working temperature of the thermocouples. From the calibration chart shown on figure 2.6, it can be seen that the galvanometer deflection was proportional to the temperature for each of the gain positions that were tested. It was not possible to calibrate at the highest gain setting (position 1), because the amplifier was driven into saturation. This was not a problem, because it was found that the other settings gave an adequate deflection of the galvanometer. Similar calibrations were carried out for the other three channels and the results were plotted.

2.3.5 Calibration of Tool-Work Thermocouples

In section 2.2.2 it was stated that the tool-chip interface temperature was measured using the tool-work thermocouple technique. When using this technique it was necessary to calibrate each tool material against the workpiece material being used. The problems of calibrating tool-work thermocuples has been investigated by many different researchers. Braiden (1967), Bus (1971) and Kurimoto (1977) have published their findings for a wide range of temperatures and

combinations of tool and work materials.

The calibration in this investigation was achieved by using carbide bars that were 200 mm long and 6 mm square. Three bars were produced for each of the three grades of carbide being tested. Each of the three bars was produced from the same batch and they were sintered for the same time and at the same temperature as the tools being tested.

The arrangement is shown diagrammatically on figure 2.7. A separate chip of the workpiece material was attached to both ends of the carbide bar. At the hot junction end a Nickel/Chromium versus Nickel/Aluminium thermocouple was attached as close as possible to the chip of workpiece material. The hot junction end of the bar was placed in an electric tube-type muffle furnace. A small water jacket was attached to the carbide bar at a distance of 20 mm from the cold end, the temperature at this end being monitored by a temperature probe that was clamped permanently to the bar. By controlling the flow of cooling water through the jacket, it was possible to maintain the cold junction temperature within a range of 18 to 22^{o}C over a period of two hours. This temperature range was chosen because it corresponded to the initial temperature of the cold junction of a cutting tip before a cutting test was undertaken. The reference junction of the Nickel/Chromium versus Nickel/Aluminium thermocouple was inserted in a bath of "iced water", the temperature of which was monitored with a thermometer that had a resolution of 0.1^{o}C. With careful monitoring it was possible to maintain this water in the range of 0 to 0.3^{o}C, which was achieved by adding additional ice over a two hour calibration period.

The output from the tool-work thermocouple and the reference thermocouple was displayed to two separate digital voltmeters, that had a resolution of 10 microvolts and declared accuracy of ±5 microvolts. The output was also recorded on a two channel pen recorder to give a permanent record. The output from the tool-work couple was recorded for each increase in output of 1 millivolt from the reference thermocouple. This gave increments of approximately 25°C up to a maximum of 1230°C.

In each case the calibration was started with a cold furnace. Argon gas was passed through the furnace throughout the calibration tests at a rate of 2 litres/min, and was used to minimise the effects of oxidation at the elevated temperatures. When the maximum calibration temperature had been achieved, the furnace was switched off and the tool/work thermocouple was allowed to cool in the furnace.

The output emf during cooling was recorded until the temperature reached a value of 600°C. It was not considered necessary to go below this temperature, because it was below the values expected in the cutting tests. The elapsed time during each test was recorded and is shown on the calibration charts (figures 2.8, 2.9 and 2.10).

2.3.6 Manufacture of the Tool-Work Thermocouples

The work material and the reference thermocouple were attached to the carbide bar by using two different techniques, as follows:-

i) oxy-acetylene welding

ii) resistance spot welding.

The practical problems associated with each technique is briefly

discussed below. The oxy-acetylene welding was found to be rather difficult to control, because of the small cross-sectional area of both the work material and the reference thermocouple wires. It was necessary to insert both the work material and the reference thermocouple bead in the same pool of molten metal at the same time. In many cases either the work material or the thermocouple bead were melted before they could be attached. After much practice it was possible to attach both the chip of work material and the thermocouple bead adjacent to each other. However, on some occasions this technique left a relatively large lump of weld material on the bar. It was considered that this might influence the temperature response during calibration.

The technique of resistance spot welding was found to give a better result. The work material and reference thermocouple were attached directly without the need for additional weld metal, however a number of trials were required to find the optimum operating parameters on the spot welding machine. It was found necessary to remove any oxide layer that was present on the carbide bar. This oxide layer had a very significant influence on the strength of the welded joint that was obtained. After some experimentation it was found that good welded joints could be obtained for the carbide grades TTA and TA5. However, the hardest grade (TE) was found to fracture under the combination of mechanical load and thermal shock that was applied by the welding process. To overcome the problem of thermal shock the carbide bar was pre-heated and the oxide layer removed immediately before spot welding. After a number of trials it was possible to obtain a good joint for this particular grade. Generally the spot welding process gave a stronger and neater joint than the oxy-acetylene process.

2.3.7 Discussion of Results

The results that were obtained for each grade are discussed below. In the case of grade TTA a comparison is made with data published by Bus et al (1971). The relationship between temperature and emf is shown on figures 2.8, 2.9 and 2.10 for grades TE, TTA and TA5 respectively. Coincident values of emf are shown adjacent to each other. A more precise comparison can be made by inspecting the data in Tables 2.1, 2.2 and 2.3.

Grade TE

Examination of figure 2.8 shows that in the temperature range from 400 to 800°C the output emf is linearly related to the applied temperature. Also, in the case of the first three tests (resistance spot welded joints), the variation in emf values is approximately 2%; above 800°C a marked departure from linearity occurred. The results for the first test show that for temperatures between 840 and 920°C a much reduced output was produced; above 940°C the relationship became linear again. Tests 2 and 3 show a similar departure from linearity at approximately 840°C, however in these two tests the departure was not as severe as in test 1. The results from tests 2 and 3 show a definite convergence at temperatures greater than 1075°C. The departure from linearity became less severe as the number of tests increased. There would appear to be a settling down effect that occurs after the repetition of each test. In practice it was found that three or four calibration tests were the maximum that could be undertaken with one particular thermocouple. After this the chip material fractured because it was subjected to an elevated temperature for several hours. The results shown for test number 4 were obtained for an oxy-acetylene welded joint, and they show a similar departure from linearity above 840°C. At the lower temperatures this specimen

TEMPERATURE CALIBRATION OF CARBIDE GRADE 'TE'

TEMP DEGR CENT	HEATING CYCLE TEST NO. 1	TEST NO. 2	TEST NO. 3	TEST NO. 4	COOLING CYCLE TEST NO. 1	TEST NO. 2	TEST NO. 3	TEST NO. 4
50	0.51	0.50	0.52	0.48				
74	0.93	0.93	0.94	0.83				
98	1.34	1.34	1.37	1.14				
122	1.75	1.76	1.80	1.52				
147	2.17	2.20	2.23	1.90				
172	2.61	2.64	2.67	2.35				
197	3.06	3.08	3.12	2.79				
222	3.46	3.50	3.53	3.21				
247	3.87	3.94	3.95	3.64				
271	4.30	4.35	4.37	4.07				
295	4.69	4.74	4.77	4.48				
319	5.09	5.16	5.17	4.89				
343	5.48	5.56	5.54	5.29				
367	5.88	5.93	5.91	5.68				
391	6.25	6.30	6.29	6.09				
414	6.64	6.67	6.65	6.45				
438	7.00	7.05	7.04	6.82				
462	7.36	7.40	7.35	7.18				
485	7.71	7.76	7.70	7.54				
508	8.07	8.14	8.07	7.91				
532	8.42	8.49	8.44	8.28				
555	8.76	8.85	8.78	8.65				
579	9.11	9.22	9.15	9.00				
602	9.46	9.58	9.51	9.38				
626	9.81	9.95	9.87	9.75				
649	10.17	10.32	10.24	10.12	9.67	9.76	9.79	9.84
673	10.51	10.70	10.60	10.50	10.00	10.10	10.14	10.19
697	10.89	11.08	10.99	10.87	10.35	10.46	10.51	10.57
721	11.27	11.46	11.38	11.25	10.72	10.84	10.89	10.95
745	11.65	11.86	11.77	11.67	11.04	11.19	11.25	11.33
769	12.06	12.26	12.19	12.08	11.31	11.49	11.58	11.68
793	12.45	12.66	12.59	12.50	11.49	11.75	11.85	11.96
817	12.83	13.13	12.99	12.90	11.64	11.93	12.04	12.17
842	13.11	13.44	13.38	13.30	11.75	12.10	12.22	12.36
866	13.19	13.69	13.65	13.61	11.88	12.29	12.42	12.56
891	13.25	13.88	13.86	13.83	12.03	12.43	12.59	12.75
916	13.38	14.08	14.07	14.04	12.26	12.46	12.72	12.94
941	13.59	14.26	14.28	14.26	12.56	12.61	12.75	13.08
967	13.85	14.38	14.49	14.48	12.87	12.86	12.92	13.13
992	14.13	14.46	14.66	14.69	13.21	13.17	13.19	13.31
1018	14.42	14.58	14.81	14.87	13.54	13.50	13.49	13.58
1043	14.73	14.73	14.89	15.01	13.88	13.85	13.81	13.90
1070	15.02	14.90	14.98	15.09	14.22	14.20	14.21	14.24
1096	15.28	15.11	15.14	15.22	14.59	14.55	14.51	14.61
1122	15.55	15.37	15.36	15.43	14.98	14.95	14.90	15.00
1149	15.84	15.68	15.63	15.72	15.40	15.37	15.33	15.43
1176	16.15	16.00	15.94	16.05	15.85	15.80	15.76	15.88
1203	16.44	16.33	16.28	16.40	16.26	16.23	16.19	16.32
1230	16.70	16.65	16.60	16.72				

TABLE 2.1 TEMPERATURE CALIBRATION OF GRADE 'TE'

EOF..

EOT..

TEMPERATURE CALIBRATION OF CARBIDE GRADE 'TTA'

TEMP DEGR CENT	HEATING CYCLE TEST NO. 1	TEST NO. 2	TEST NO. 3	TEST NO. 4	COOLING CYCLE TEST NO. 1	TEST NO. 2	TEST NO. 3	TEST NO. 4
50	0.63	0.64	0.66	0.66				
74	1.15	1.17	1.16	1.16				
98	1.61	1.70	1.69	1.70				
122	2.08	2.24	2.23	2.19				
147	2.61	2.78	2.77	2.70				
172	3.14	3.33	3.32	3.33				
197	3.67	3.89	3.86	3.76				
222	4.18	4.41	4.40	4.28				
247	4.70	4.94	4.92	4.79				
271	5.20	5.45	5.44	5.32				
295	5.70	5.96	5.94	5.81				
319	6.19	6.44	6.44	6.26				
343	6.68	6.94	6.90	6.75				
367	7.15	7.42	7.37	7.23				
391	7.60	7.90	7.84	7.68				
414	8.05	8.43	8.28	8.14				
438	8.50	8.81	8.73	8.59				
462	8.93	9.24	9.15	9.03				
485	9.37	9.68	9.57	9.47				
508	9.79	10.12	10.00	9.91				
532	10.21	10.53	10.40	10.31				
555	10.62	10.95	10.81	10.76				
579	11.03	11.34	11.22	11.18				
602	11.45	11.75	11.62	11.60	10.98	11.17	11.36	11.15
626	11.86	12.17	12.01	12.03	11.37	11.56	11.75	11.51
649	12.28	12.58	12.42	12.44	11.76	11.96	12.15	11.89
673	12.70	13.00	12.83	12.87	12.12	12.34	12.56	12.27
697	13.14	13.41	13.33	13.31	12.48	12.76	12.97	12.66
721	13.58	13.82	13.74	13.75	12.80	13.16	13.38	13.09
745	14.01	14.26	14.17	14.17	12.97	13.43	13.75	13.40
769	14.34	14.70	14.60	14.51	13.22	13.55	14.00	13.57
793	14.64	15.11	15.01	14.78	13.50	13.75	14.19	13.68
817	14.93	15.46	15.42	15.05	13.80	14.00	14.34	13.89
842	15.16	15.65	15.77	15.31	14.10	14.22	14.57	14.01
866	15.47	15.76	15.91	15.60	14.40	14.47	14.74	14.43
891	15.77	15.95	16.06	15.87	14.71	14.74	14.87	14.55
916	16.03	16.20	16.26	16.15	15.04	15.05	15.09	15.00
941	16.30	16.41	16.50	16.42	15.32	15.38	15.40	15.30
967	16.56	16.62	16.68	16.71	15.65	15.72	15.69	15.60
992	16.82	16.84	16.80	16.99	15.97	16.03	15.95	15.91
1018	17.02	17.10	16.99	17.27	16.32	16.38	16.30	16.23
1043	17.24	17.32	17.20	17.34	16.59	16.76	16.67	16.54
1070	17.48	17.58	17.44	17.80	17.09	17.17	17.07	16.87
1096	17.73	17.83	17.67	18.08	17.52	17.58	17.48	17.20
1122	18.02	18.10	18.02	18.35	17.90	17.96	17.89	17.60
1149	18.12	18.38	18.30	18.61	*	*	*	18.02
1176	*	*	*	18.82	*	*	*	18.46
1203	*	*	*	19.06	*	*	*	18.88
1230	*	*	*	19.38				

TABLE 2.2 TEMPERATURE CALIBRATION OF GRADE 'TTA'

EOF..

EOT..

TEMPERATURE CALIBRATION OF CARBIDE GRADE 'TA5'

TEMP DEGR CENT	HEATING CYCLE TEST NO. 1	TEST NO. 2	TEST NO. 3	TEST NO. 4	COOLING CYCLE TEST NO. 1	TEST NO. 2	TEST NO. 3	TEST NO. 4
50	0.57	0.65	0.62	0.64				
74	1.03	1.13	1.13	1.16				
98	1.54	1.63	1.65	1.67				
122	2.05	2.14	2.15	2.17				
147	2.57	2.65	2.65	2.68				
172	3.09	3.17	3.17	3.18				
197	3.60	3.68	3.69	3.71				
222	4.12	4.18	4.18	4.19				
246	4.60	4.67	4.68	4.70				
271	5.10	5.15	5.15	5.16				
295	5.58	5.61	5.61	5.62				
319	6.03	6.05	6.05	6.05				
343	6.48	6.50	6.48	6.50				
367	6.94	6.95	6.91	6.91				
391	7.32	7.35	7.33	7.31				
414	7.73	7.76	7.73	7.71				
438	8.13	8.15	8.13	8.11				
462	8.53	8.54	8.52	8.51				
485	8.93	8.94	8.90	8.86				
508	9.31	9.33	9.27	9.23				
532	9.70	9.70	9.65	9.61				
555	10.07	10.07	10.03	9.98				
579	10.46	10.46	10.40	10.36				
602	10.83	10.83	10.78	10.76	10.09	10.55	10.54	10.53
626	11.21	11.20	11.16	11.12	10.43	10.91	10.89	10.90
649	11.60	11.60	11.53	11.50	10.79	11.26	11.26	11.26
673	11.99	11.98	11.92	11.88	11.13	11.64	11.62	11.65
697	12.37	12.36	12.31	12.28	11.84	12.02	12.02	12.04
721	12.76	12.77	12.69	12.69	12.22	12.42	12.42	12.45
745	13.16	13.17	13.08	13.09	12.57	12.78	12.78	12.82
769	13.56	13.58	13.50	13.49	12.85	13.07	13.08	13.15
793	13.96	13.99	13.90	13.92	13.07	13.32	13.33	13.43
817	14.36	14.39	14.31	14.33	13.25	13.50	13.51	13.62
842	14.75	14.79	14.70	14.74	13.42	13.70	13.71	13.83
866	15.04	15.05	15.00	15.02	13.52	13.90	13.93	14.03
891	15.20	15.24	15.20	15.22	13.63	14.06	14.10	14.23
916	15.35	15.44	15.40	15.41	13.79	14.18	14.26	14.39
941	15.46	15.61	15.60	15.61	13.93	14.28	14.40	14.54
967	15.50	15.80	15.81	15.82	14.14	14.37	14.48	14.65
992	15.59	15.97	16.02	16.05	14.39	14.55	14.58	14.73
1018	15.77	16.09	16.22	16.27	14.67	14.81	14.79	14.91
1043	15.96	16.22	16.40	16.45	14.96	15.10	15.07	15.15
1070	16.18	16.33	16.51	16.60	15.28	15.40	15.35	15.46
1096	16.40	16.52	16.60	16.70	15.60	15.75	15.69	15.75
1122	16.63	16.71	16.71	16.79	15.97	16.10	16.03	16.12
1149	16.87	16.93	16.93	16.99	16.35	16.52	16.45	16.52
1176	17.18	17.20	17.18	17.22	16.78	16.91	16.87	16.95
1203	17.34	17.46	17.42	17.48	17.20	17.33	17.29	17.35
1230	17.62	17.74	17.70	17.78				

TABLE 2.3 TEMPERATURE CALIBRATION OF GRADE 'TA5'

EOF..

EOT..

gave a lower emf for a given reference thermocouple temperature when compared with the spot welded thermocouple. A possible explanation is that the larger joint, associated with the oxy-acetylene weld, has a greater thermal inertia, therefore the temperature of this joint lags slightly behind the temperature experienced by the reference thermocouple. This effect would be most pronounced during the early part of the test when the rate of heating was most rapid.

On cooling from the maximum temperature the results show an initial linear reduction of emf with temperature. The departure from linearity starts to occur at temperatures below approximately 970°C and is associated with the change of phase that occurs on cooling. Below 750°C the results for each test show a tendency to converge towards a single line.

Grade TTA

The results obtained for this grade are shown on figure 2.9 and in table 2.2. They show an approximate linear relationship in the range 400 to 800°C. For tests 1 to 3 (oxy-acetylene welded joints) the emf values have a spread of approximately 0.3 mv in the temperature range of 450 to 750°C. In the range 800 to 900°C the spread of values increases,however above 975°C these results show a tendency to converge and have less spread than at the lower temperatures. All the tests showed a departure from linearity at a temperature greater than 800°C.

In the temperature range 800 to 950°C the emf for test number 1 was much lower than for tests 2 and 3, and a similar "settling down" phenomena was observed for grade TE. The emf produced in tests 2 and 3 were very similar with a slight divergence occurring in the

temperature range 840 to 890°C. Above this higher temperature the two sets of values could be considered to converge. The results obtained for test number 4 were obtained for the resistance spot welded joint and in general they show close agreement with the results obtained for tests 1 to 3.

Grade TA5

The results obtained are shown on figure 2.10 and in table 2.3, and for this grade the joint for all the tests was resistance spot welded. Up to a temperature of 840°C the results from each test were very consistent, however above this temperature a marked departure from linearity occurred. In the temperature range from 940 to 1070°C the first test gave lower values than the subsequent tests 2, 3 and 4. The "shaking down" effect to a consistent curve occurred at a higher temperature than with the other two grades. At temperatures above 1150°C the results for each test tended to converge to a straight line.

2.3.8 Influence of Calibration Time

The results suggest that the output from the tool/work thermocouples at temperatures greater than 840°C was influenced by the time of exposure to the higher temperatures during both the manufacturing and the calibration processes. Consider, for example, grade TE (figure 2.8) and tests 1 to 3, the joint for this thermocouple was resistance spot welded; the duration of the weld time was probably 0.5 seconds or less. The results from the first calibration test show a large departure from linearity at a temperature greater than 840°C. Between 840°C and 900°C this departure from linearity gave a reduction in the output sensitivity (slope). The results for test 2 show a similar but less pronounced reduction in sensitivity (slope) between approximately 960 and 1040°C. The results for

test 2 were obtained after cumulative total of 3 to to 4 hours of exposure to the high temperatures. The results for test 3 show that the reduction in sensitivity was less than for tests 1 and 2. The results shown as test 4 were obtained from an oxy-acetylene welded thermocouple. The welded joint was difficult to produce, the pool of weld metal was exposed to extremely high temperatures for several minutes until a joint could be produced. The results for this calibration test (4) did not give the same large reduction in sensitivity that was obtained for test 1 (resistance weld joint) when it was calibrated above 840°C for the first time.

The results for tests 1 to 3 for grade TTA (figure 2.9) were obtained from an oxy-acetylene welded thermocouple. The results for test 1 show some reduced sensitivity when compared with the repeated values found for tests 2 and 3. These three sets of results suggest that increasing the exposure time to the elevated temperatures increases the output emf for a given temperature. The results for test 4 were obtained for a resistance spot welded joint and they show a departure from linearity at approximately 800°C. However, the results do not show the pronounced reduction in sensitivity that was clearly identifiable with test 1 of grades TE and TA5 (resistance welded joints).

Figure 2.10 shows the results that were obtained for grade TA5, the four sets of results were obtained from the same thermocouple (resistance spot welded joint). The results from test 1 show a pronounced reduction in sensitivity at 950°C, a similar reduction was observed for grade TE (test 1) at 850°C. Examination of the results for tests 2, 3 and 4 shows that the reduction in sensitivity became progressively less as the exposure time to the higher temperature was increased with each subsequent test.

In the metalcutting tests the contact time between the tool and the workpiece varied from 5 to 60 seconds and in the majority of cases was limited to 20 seconds (section 5.7). When determining tool/chip interface temperatures, it would seem reasonable to use the results obtained from the first calibration test and a resistance spot welded joint.

2.3.9 Evaluation of Results

At this point it is useful to compare the results obtained for grade TTA with those obtained by Bus et al (1971). Bus calibrated a large range of carbide alloys against a steel workpiece (C45N) up to 1000°C, their results being expressed in a relationship of the form:-

$$emf = aT + bT^2 + cT^3 \qquad (2.1)$$

where "a", "b" and "c" were coefficients and T was the temperature. This type of relationship is commonly used to accommodate any non-linearity between the variables of temperature and emf. The results published by Bus et al showed that different grades of carbide gave wide variations in the coefficients a, b and c. A loop in the upper part of the calibration curve was also reported. It was argued that the energy absorbed during the A_c transformation was given up during the A_r transformation and therefore the calibration curve should be in the middle of the loop. They published coefficient that were calculated from the middle values of the loop.

The coefficients for the grade Sandvik S2 (composition 75% WC, 12% TiC, 4% TaC and 8% Co), which was similar to grade TTA (77% WC, 11% TiC, 4% TaC and 8% Co) were given as $a = 0.2239 \times 10^{-1}$, $b = 0.6097 \times 10^{-5}$ and $c = 0.0520 \times 10^{-8}$. The coefficients for the Sandvik grade S2 were substituted into equation (2.1) and the

relationship is shown plotted on figure 2.9 as a comparison. Bus et al (1971) calculated the coefficients using values from the middle of the loop. Consequently it is only possible to compare the mean value published by Bus et al with mean values obtained for grade TTA. It can be observed on figure 2.9 that for temperatures up to 1000°C, the mean line value passes almost exactly through the centre of the calibration loop for grade TTA. The results demonstrate that serious errors can be introduced if the mean value of the calibration loop is used.

For purposes of comparison the coefficients "a", "b" and "c" are given in table 2.4 for each grade and for each test; the table also shows values for Sandvik grade S2 (Bus et al, 1971).

CARBIDE GRADE	COEFFICIENTS		
	"a" x 10^{-1}	"b" x 10^{-5}	"c" x 10^{-8}
TE Test No. 1	0.2096	- 0.5627	- 0.0021
2	0.2058	- 0.3375	- 0.1631
3	0.1935	- 0.1352	- 0.2533
4	0.1828	0.0329	- 0.3134
TTA Test No.1	0.2104	0.1414	- 0.4921
2	0.2439	- 0.3282	- 0.3123
3	0.2289	- 0.0328	- 0.4671
4	0.2277	- 0.2006	- 0.2923
Sandvik S2	0.2239	- 0.6097	0.0520
TA5 Test No.1	0.2400	- 0.5353	- 0.1709
2	0.2252	- 0.2945	- 0.2706
3	0.2161	- 0.1451	- 0.3351
4	0.2047	0.0358	- 0.4105

TABLE 2.4

Temperature coefficients for tool/work thermocouple calibration.

2.4 Temperature Measurement Using Inserted Thermocouples

In an attempt to determine the temperatures in the bulk of the tool it was decided to insert thermocouples into the tool tip. Four holes on a 7 mm square grid were spark-eroded to a depth of 2.5 mm into the underside of a tip which was 19 mm square and 5 mm thick. Copper constantan thermocouples were inserted and held in place with the cynoacrylate adhesive ZIP-GRIP 10. From previous work by Braiden (1971) and Woods (1956) it was shown that the tip/shank temperature reached a maximum of approximately 200^{o}C, so it was felt that this adhesive was suitable.

This technique gave only limited success. It was found to be difficult to get good thermal contact with the thermocouples and on occasions to get adhesion to the tip. Attempts at either welding or brazing the thermocouples to the tip were not successful, largely because of the confined space. When soldering was attempted it was found to be difficult to get a good mechanical joint. For these reasons and those discussed in section 2.1.5 it was decided to discontinue this approach and to concentrate on measuring the surface temperatures of the tip.

2.5 Development of Tip-Shank Thermocouples

After the system had been calibrated for temperature, a number of trial tests were undertaken to determine the temperatures at the tip-shank interface. The cutting conditions were similar to those used by Braiden (1971) and Woods (1956), who quoted temperatures of 90^{o}C and 115^{o}C for intermittent and continuous cutting respectively. It was found that temperatures of approximately 250^{o}C were being recorded. It was concluded that the significant differences in temperature were caused by the arrangement of the thermocouples in

the tool shank. Relatively large holes (3 mm diameter) had been drilled in the seating face of the shank to accommodate the thermocouples (figure 2.1a). As a consequence, the heat transfer from the underside of the tip was much reduced because these areas were in contact with air rather than the better heat conducting steel shank. This effect was giving rise to "hot spots" and therefore higher temperature readings than would normally be expected.

To overcome this problem the arrangement of the thermocouples in the shank was completely modified. The first requirement was to maximise the area of contact between the tip and its seating. This was achieved by drilling holes that were just large enough to allow the bead of the thermocouple to pass through (see fig. 2.11). The thermocouples were then assembled from the underside of the toolshank and secured in place using a small coil spring and a purpose-made adjustment collar. The collar had a hole drilled through the centre to accommodate the thermocouple wires and was screwed into the shank until there was sufficient pre-load on the spring. A photograph of the arrangement is shown on figure 2.12.

When the trial cutting tests were repeated, lower temperatures were recorded with typical steady state values being in the range of 130 to 180^{o}C. From these results it was concluded that increasing the area of contact between the tool tip and its seating had improved the heat conduction and therefore reduced the temperature of the "hot spots" on the underside of the tool tip.

2.6 Evaluation of the Temperature Measurement System

Introduction

Figure 2.13 shows a typical set of traces that were obtained from the temperature measurement system. Traces 1 to 4 were obtained from the thermocouples located at the tool tip/shank interface and trace 5 was obtained from the tool/work thermocouple. The following sections discuss these results in terms of sources of error, response time and accuracy.

2.6.1 Tip-Shank Thermocouples

Figure 2.13 shows the recorded temperatures as a function of time. The horizontal axis has a scale of 10mm/second, or 1mm represents 0.1 seconds. The vertical axis has two scales, traces 1 to 4 which represented the temperatures at the tip/shank interface had a sensitivity of 1.65^{o}C/mm. Trace 5 represented the output from the tool/work thermocouple and this had a sensitivity of 0.36mv/mm. It was necessary to represent trace 5 by this method, because the output from the tool/work thermocouple was non-linear and varied for each grade of carbide between investigated.

The results for traces 1 to 4 show the response of temperature with time. The thermocouple represented by trace 1 was located in the shank directly beneath the tool/chip contact region (see figures 2.1a and 2.12). This thermocouple started to respond within 0.5 seconds from the beginning of the cut. It should be appreciated that the tool tip was 5mm thick. These results therefore indicate that the rate of heat conduction through the tip is very high indeed. Traces 2 and 3 were approximately equidistant from the tool/chip interface and showed a slower response than trace 1. This would be expected because they were further from the heat source at the tool/chip interface. A

similar argument applies to trace 4 which was the furthest away. All the traces show that as the test proceeded the rate of change of temperature was reduced and the traces were approaching a steady state value.

2.6.2 Tool/Work Thermocouples

The output for the tool/work thermocouple (trace 5) shows a very rapid rise with time and reached its maximum value after approximately 0.2 seconds. After this maximum value had been attained, there was a reduction in the output emf as time proceeded. It should be noted that the reduction in emf was coincident with the rise in temperature at the tool tip-shank interface.

The problems of using the tool/work thermocouple have been reviewed by many researchers. Nakayama (1963) has highlighted the possibility of spurious emf's being generated at the interface between the steel shank and the carbide tool tip. These emf's are generated when the temperature at the base of the tip increases as the cutting process proceeds. Such emf's may cause inaccuracies in the measured output emf from the tool/work thermocouple. This problem may be overcome by either:-

i) Electrically insulating the tool tip from the shank and ensuring electrical contact between the tool tip and the steel wire at the cold junction only (see figure 2.16). However, many electrical insulating materials are also good thermal insulators. The installation of thermal insulation between the tip and the shank would cause a rise in temperature at the base of the tip. Such a rise in temperature would not represent the normal situation that occurs in practice, because the shank acts as a high capacity heat sink that keeps the bulk of the tool cool. Typical tip/shank interface temperatures are 120 to 140^{o}C

(Braiden, 1971 and Woods, 1956). The increase in temperature would also raise the temperature of the cold junction between the carbide tip and the steel wire. This would lead to a reduction in output emf.

ii) The problem can be overcome by considering the tool/chip interface temperature during the early part of the cutting process. This approach was adopted by Takayama (1963) and is also discussed by Kurimoto (1977). This approach can be justified for this investigation as follows:

The tool/chip interface temperature is known to be achieved very quickly, trace 5 on figure 2.13 shows that the maximum temperature was achieved within 0.2 to 0.3 seconds from the start of cutting. Braiden (1971) found a similar result for intermittent cutting. When only 0.2 to 0.3 seconds have elapsed the tip/shank interface temperature is still effectively zero; this is because insufficient heat has been conducted through the tip to the shank. Traces 1 to 4 show that no rise in temperature could be detected. It is therefore not possible for any spurious emf's to be produced during this early part of the cutting test. Similar reasoning may be applied to the cold junction that is formed by the tool and the steel wire on the remote underside of the tip (figure 2.16). This approach can be further justified by considering the duration of the cutting tests (section 5.7) which had values of 5, 5, 10, 20 and 20 seconds. Any rise in temperature during a particular test was detected at the start of the next test (see section 6.3).

2.6.3 Resolution of Temperature Recording System

Trace 5 on figure 2.13 was not as smooth or "clean" as the other traces. The reason for this was due to the system picking up stray

50 hertz signals from other electrical equipment in the laboratory and a certain amount of "noise" from the slip-ring system. Also on occasions there was some "shorting out" between the tool shank and the workpiece material. This was caused by stray chips of workpiece material making contact with the bar and tool shank at the same time.

When determining the temperature from the U/V trace it was necessary to take the mean value to represent the output emf from the tool/work thermocouple. Generally it was possible to consistently measure the position of the trace to within half a millimetre. This represented 0.18mv because the recorder had a sensitivity of 0.36 mv/mm. If a typical temperature of 1000^{o}C is considered, then the output emf at this temperature can be found by differentiating equation 2.1 and substituting the constants a, b and c from the calibration curve (see section 2.3.9).

Differentiating equation 2.1 and substituting the coefficients for grade TTA (a = 0.02104, b = 1.414 x 10^{6}, c = -4.921 x 10^{-9}) gave the output sensitivity at T = 1000^{o}C as 9.1 μvolts/^{o}C. This can be represented in terms of temperature resolution as follows:-

$$\text{Temperature resolution} = \frac{0.18\text{mV}}{9.1\mu\text{V}} .{}^{o}\text{C} = 19.78^{o}\text{C}$$

At a temperature of 1000^{o}C this represented a resolution of less than 1.98%.

The voltmeter used in the tool/work thermocouple calibration had a resolution of 10 μvolts. If this value is considered in terms of the output sensitivity calculated above (i.e. 9.1 μV/^{o}C), then the resolution of calibration voltmeter was given by:-

$$\frac{10\mu V}{9.1\mu V}.\,^{o}C = 1.1\,^{o}C$$

It can be seen that the temperature calibration system had a resolution that was almost twenty times less than the U/V recording systems.

2.7 Analysis of the Tool/Work Thermocouple

Introduction

The tool/work thermocouple has been used for many years as an aid to metalcutting research. Although this measurement technique is generally accepted, questions still arise (Trent 1983) with regard to precisely which temperature is measured with this technique. The problem is complicated by the following factors:-

i) the contact area between the two materials is subjected to a wide variation in temperature,

ii) the output emf from the temperature calibration is non-linear,

iii) the resistivity of the tool and work materials changes with temperature.

To analyse this problem a number of practical and theoretical investigations have been undertaken. The outcome of this work is a model which incorporates the three factors considered above.

2.7.1 Thermocouples in Parallel

The tool/chip contact area can be considered as a large number of thermocouples at different temperatures all connected in parallel.

Doebelin (1966) states that:- "Several thermocouples may be

connected together in series or parallel to achieve useful functions. The parallel combination generates the same voltage as a single couple if all measuring and reference junctions are at the same temperatures. If the measuring junctions are at different temperatures and the thermocouples are all the same resistance, the voltage measured is the average of the individual voltages. The temperature corresponding to this voltage is the average temperature only if the thermocouples are linear over the temperature range being measured."

To confirm this statement by Doebelin it was decided to connect 1, 2 and 3 thermocouple junctions in parallel with a reference junction at $0^{o}C$. The three junctions were immersed in water which varied in temperature from 0 to $100^{o}C$. The results are shown on figure 2.14. The results for the first test shows the output emf when the temperature of one junction was raised from 0 to $100^{o}C$. This gave an output of approximately 4.2 mv for $100^{o}C$. The results for test 2 were obtained by keeping one junction at $100^{o}C$ and varying the temperature of the second junction from 0 to $100^{o}C$. If the output at the extremes is considered, then it can be seen that the output emf was the average output from the two individual couples, i.e. (4.2 + 0)/2=2.1mv. at $0^{o}C$ and (4.2 + 4.2)/2 = 4.2 mv at $100^{o}C$. A similar result was obtained for test 3 in which 3 thermocouple junctions were connected in parallel. At $0^{o}C$ the output was (0 + 4.2 + 0)/3 = 1.4 mv and at $100^{o}C$ the output was (0 + 4.2 + 4.2)/3 = 2.8 mv.

These results were taken to confirm the statement by Deobelin regarding thermocouples connected in parallel.

2.7.2 Model for 'n' Thermocouples in Parallel with Constant Resistance

The tool/work thermocouple can be considered as 'n' thermocouples connected in parallel as shown on figure 2.15. Each thermocouple can be considered as having its own emf e_1, e_2 to e_n or e_i for i = 1 to n. The emf for each individual thermocouple will depend on its temperature T_1, T_2 to T_i etc.

The temperature T_i will depend upon the position being considered along the tool chip contact length ℓ_c, and also on the shape of the temperature distribution (figure 7.6). The value of T_i at any point x_i along the contact length is given by the polynomial:-

$$T_i = a_o + a_1 x_i + a_2 x_i^2 + \text{------} a_n x_i^n \qquad (2.2)$$

The coefficients a_o and a_i to a_n where obtained from the Chebychev polynomials given in Appendix 3.

The emf e_i for any particular point along the tool/chip contact length will be a function of the temperature T_i at that point. The emf e_i is found by using equation 2.1 (section 2.3.9) and can be written in the form shown below:-

$$e_i = aT_i + bT_i^2 + cT_i^3 \qquad (2.3)$$

The output emf for all the thermocouples in parallel is given by:-

$$E = \frac{1}{n} \sum_{i=T}^{i=n} e_i \qquad (2.4)$$

This relationship will accommodate any non-linearity that may

occur between the applied temperature and the output emf, when calibrating tool/work thermocouple materials. It does not, however, accommodate any changes in resistance of the tool or work materials with changes in temperature.

The output emf can be considered as the weighted average emf of all the thermocouples being considered. The amount of weighting will depend on the emf produced by each individual thermocouple being considered. This is because the relationship between emf and temperature is non-linear (see calibration curves, i.e. figures 2.8 to 2.10).

2.7.3 Model for 'n' Thermocouples in Parallel with Temperature Dependant Resistance

Figure 2.16 shows 'n' thermocouples connected in parallel each with its own emf e_i. In series with each emf is the resistance of the steel member (R_{si}) and also the resistance of the carbide member (R_{ci}). The emf and resistance for each individual thermocouple will depend upon the temperature T_i.

The change in resistance with temperature is given by the following relationships:-

$$R_{si} = R_{os} (1 + \alpha_{1s} T_i + \alpha_{2s} T_i^2 + \text{---} \alpha_{ns} T_i^n) \qquad (2.5)$$

$$R_{ci} = R_{oc} (1 + \alpha_{1c} T_i + \alpha_{2c} T_i^2 + \text{---} \alpha_{nc} T_i^n) \qquad (2.6)$$

where R_{os} and R_{oc} are the resistivities of steel and carbide at 0^oC. The coefficients α_{1s}, α_{2s}, α_{1c} and α_{2c} etc are the coefficients for change in resistivity with temperature. Usually sufficient accuracy can be obtained by using the first and or second order terms of these

relationships.

By using these relationships it was possible to incorporate changes in resistance with temperature into the model.

To determine total output E from all the thermocouples it was necessary to consider the system as a number of separate loops and then combine the output to give the total (figure 2.17a). For the first loop the source emf is e_1 and it is connected in series with R_{s1} and R_{c1}. The remaining resistors are connected in parallel with e_1 and their equivalent resistance is given by R_{p1}. Where R_{p1} is the combination of all other resistors in parallel with e_1, it does not include the resistors R_{s1} and R_{c1} associated with source e_1 (figure 2.17a).

By using superposition theory the contribution to the final current produced by each separate source acting alone can be found as follows. Assume that all sources other than e_1 are suppressed, and that the resistances of these sources are in parallel eith e_1. Then the contribution i_{e1} produced by e_1 is given by:-

$$i_{e1} = \frac{e_1}{(R_{s1} + R_{c1}) + R_{p1}} \qquad (2.7)$$

The partial contribution by e_1 to the total output E is given by:-

$$E_{e1} = i_{e1} . R_{p1}$$

and is shown on figure 2.17b.

Substituting equation (2.7) for i_{e1} gives the partial contribution by e_1 to the total output as:-

$$E_{e1} = \frac{e_1 . R_{p1}}{(R_{s1} + R_{c1}) + R_{p1}}$$

A similar argument can be applied to source e_2 acting alone as follows:-

$$i_{e2} = \frac{e_2}{(R_{s2} + R_{c2}) + R_{p2}}$$

The resistance R_{p2} is the combined resistance of all values in parallel with e_2 but excluding R_{s2} and R_{c2}, see figure 2.17c.

The partial contribution by e_2 to the total output E is given by:-

$$E_{e2} = i_{e2} . R_{p2}$$

By analogy the partial contribution by e_3 is given by:-

$$E_{e3} = i_{e3} . R_{p3}$$

The total output E is given by:- $E = \sum_{i=1}^{n} E_{ei}$ giving:-

$$E = \frac{e_1 . R_{p1}}{(R_{s1} + R_{c1}) + R_{p1}} + \frac{e_2 . R_{p2}}{(R_{s2} + R_{c2}) + R_{p2}} + \text{-------}$$

$$\frac{e_n . R_{pn}}{(R_{pn} + R_{pn}) + R_{pn}} \qquad (2.8)$$

By using this relationship and equations 2.5 and 2.6 it was possible to calculate the output emf for any number of thermocouples in parallel along the tool/chip contact length.

The constants R_{os}, α_{1s} and α_{2s} in equation 2.5 were obtained from data published by Kaye (1986). The values for R_{oc}, α_{1c} and α_{2c} were not available, so it was decided to measure them. The method used is described in the next section.

2.7.4 Determination of Temperature Coefficient of Resistivity

The resistivity of the carbide tool material (TTA) was measured by using bars of material that were 200mm long and 6mm square. The arrangement is shown diagrammatically on figure 2.18. Essentially the technique consisted of passing a constant current through the bar and measuring the drop in voltage over a given distance of 170mm. If the current and drop in voltage were known then it was possible to determine the resistance of the bar over a given length. If the cross-sectional area is uniform then the resistivity can be determined.

A number of practical problems arise when operating at elevated temperatures; they are as follows:-

1) to select suitable materials to act as electrical conductors and leads;

2) overcoming spurious thermocouple effects caused by joining together different materials and subjecting them to temperature.

The problem of the lead material was overcome by using alumel wire. Two lengths of wire were resistance spot welded onto the ends of the bar, these two leads were used to carry the constant current. Two additional leads were also welded to the bar at a distance of 15mm from the ends (170mm apart). This was done to minimise any end effects which could cause a non-uniform current density. These two leads were connected to a high impedance (10MΩ) volt meter with the

consequences that no current would flow through this part of the circuit. Any change in resistance of these leads due to changes in temperature would not influence the measured volt drop across the bar. Provided the bar was at a uniform temperature no emf should be produced between the carbide material and the alumel leads used for measuring the drop in voltage. During the tests the polarity of the voltmeter was reversed to check for any spurious effects, but none could be detected.

Two chromel/alumel thermocouples were also attached to the bar to determine its temperature during the tests. The complete assembly was placed in the central section of a muffle furnace and argon was passed through to minimise the effects of oxidation. The temperature of the bar was increased in increments of 100^{o}C and the bar was allowed to soak for approximately five minutes before the voltage reading was taken. The test was carried out three times up to a maximum temperature of 1200^{o}C, the results are shown on figure 2.19.

The results on figure 2.19 show that between 20 and 500^{o}C the resistance increased approximately linearly with temperature. Above 500^{o}C the slope was much reduced and for practical purposes the resistance could be considered to be constant. This phenomenon of almost constant resistance at elevated temperature would appear to be similar to that observed by Metcalfe (1947) and was reported by Schwarzkopf and Kieffer (1960). Metcalfe found that the resistance of certain carbide alloys with 25% titanium carbide did not increase above 700^{o}C. The resistivity at room temperature of the grade being tested (TTA) was found to be 38.0 x $10^{-6}\Omega$.CM. This value was very close to the resistivity for Sandvik grade S2 (38.4 x 10^{-6} Ω.CM) which has an almost identical composition (Brookes, 1982).

2.7.5 Evaluation of Thermocouple Model

It was decided to evaluate equations 2.4 and 2.8 to compare the effect of incorporating changes in resistance with temperature into the model. The above equations were evaluated in three different ways, as follows:-

i) Determine the number of parallel thermocouples required to give sufficient accuracy. An alternative approach was to consider the number of steps or the step size required to cover the tool/chip contact length.

ii) Compare the difference in calculated emf for different tool/chip temperature distributions, with the emf obtained for a uniform temperature distribution.

iii) Compare the above differences (ii) on a percentage basis.

The results shown in tables 2.5 to 2.7 were obtained from evaluating equation 2.4, and do not consider changes in resistance with temperature.

Table 2.5 allows a comparison between the nominal calibration emf (EO) mv and the output emf for decreasing step sizes S = 0.1, S = 0.01 and S = 0.001 obtained from equation 2.4. The results show that for a particular temperature such as 1000^{o}C the difference in emf between S = 0.1 and S = 0.01 was 0.15 mv or 15 μv. This represented a difference of 0.08 percent. A step size of S = 0.001 represented 1001 thermocouples in parallel. If the tool chip contact length was 1 mm then this represented a spacing of 1 μm. It was considered that a step size of 0.001 gave sufficient accuracy and was adopted in subsequent calculations.

The results in table 2.6 show the output emf for three different distributions, they are Trigger (ET), Usui (EU) and Dearnley (ED). Their particular values can be compared with the emf (EO) obtained for the calibration. The output emf from the distributions proposed by Usui and Dearnley give very similar values that were also close to the nominal emf EO. These results would be expected because the two distributions are essentially the same shape and they can be considered to be quite flat when compared with the relative 'peaky' distribution proposed by Trigger. In section 2.7.2 it was stated that the output emf given by equation 2.4 was a weighted average of the individual contributions from all the thermocouples. The amount of weighting will depend on the emf associated with the temperature of the particular thermocouple being considered. The calibration curves (figures 2.8 to 2.10) show that a non-linear relationship existed between temperature and emf, the output emf being proportionally less at higher temperatures. If the data in columns one and two of table 2.5 are compared, it can be seen that at 100°C the output is 2.11 mv/100°C, whereas at 1000°C the output was 1.75 mv/100°C. For any given average temperature, the distribution proposed by Trigger has a much higher peak value than the distributions proposed by either Usui or Dearnley. Consequently the emf contribution to the total output will be reduced because the emf is proportionally less at the higher temperatures. This has the effect of reducing the average output from the combined thermocouples.

The results in Table 2.7 show the percentage differences between nominal emf (EO) and the output from the three distributions considered. It can be seen that within the normal temperature range that occurs in metalcutting (900 to 1200°C) the difference between EO and EU or ED is less than 1%. The difference between EO and ET was found to be 3.6 to 10.5%.

MODEL OF THERMOCOUPLE USING CARBIDE GRADE TTA AND STEEL 817M40.

THE TEMPERATURE CALIBRATION COEFFICIENTS ARE :-
A= .02104 B= .000001414 C=-4.921E-09

RESISTIVITY OF STEEL 'ROS' = 0
RESISTIVITY OF CARBIDE RELATIVE TO STEEL 'ROC' = 0

TEMPERATURE COEFFICIENT OF RESISTIVITY FOR STEEL A1S = 0
TEMPERATURE COEFFICIENT OF RESISTIVITY FOR CARBIDE A1C = 0

TOOL/CHIP TEMPERATURE DISTRIBUTION PROPOSED BY USUI(1984)

THE DATA SHOWS THE CONVERGENCE OF MODELLED EMF WITH DECREASING STEP SIZES , 'S'= 0.1, 'S'= 0.01, 'S'= 0.001

AVERAGE NOMINAL TEMPERATURE (TO)	EMF FOR AVERAGE TEMPERATURE (EO)	EMF FOR DISTRIBUTED TEMPERATURE STEP=0.1	EMF FOR DISTRIBUTED TEMPERATURE STEP=0.01	EMF FOR DISTRIBUTED TEMPERATURE STEP=0.001
100	2.113	2.113	2.143	2.146
150	3.171	3.171	3.215	3.220
200	4.225	4.225	4.283	4.289
250	5.271	5.270	5.343	5.350
300	6.306	6.304	6.390	6.399
350	7.326	7.322	7.422	7.432
400	8.327	8.322	8.433	8.444
450	9.306	9.297	9.420	9.433
500	10.258	10.246	10.379	10.393
550	11.181	11.165	11.307	11.321
600	12.070	12.049	12.199	12.214
650	12.922	12.895	13.051	13.067
700	13.733	13.698	13.860	13.876
750	14.499	14.456	14.621	14.637
800	15.217	15.165	15.331	15.347
850	15.884	15.820	15.985	16.002
900	16.494	16.418	16.580	16.597
950	17.045	16.955	17.113	17.128
1000	17.533	17.428	17.578	17.593
1050	17.954	17.832	17.972	17.986
1100	18.305	18.163	18.292	18.304
1150	18.582	18.419	18.532	18.543
1200	18.781	18.595	18.690	18.699
1250	18.898	18.688	18.762	18.769

TABLE 2.5

EOT..

COMPARISON OF THE NOMINAL EMF (EO) WITH THE MODELLED EMF FOR THE TOOL/CHIP TEMPERATURE DISTRIBUTIONS PROPOSED BY TRIGGER(1961), USUI(1984) AND DEARNLEY(1983).

TOOL :~ CARBIDE GRADE TTA, WORKPIECE :~ STEEL 817M40 (EN24)
RESISTIVITY OF STEEL 'ROS' = 0
RESISTIVITY OF CARBIDE RELATIVE TO STEEL 'ROC' = 0

TEMPERATURE COEFFICIENT OF RESISTIVITY FOR STEEL 'A1S' = 0
TEMPERATURE COEFFICIENT OF RESISTIVITY FOR CARBIDE 'A1C' = 0

STEP SIZE 'S' = 0.001

NOMINAL AVERAGE TEMPERATURE (TO)	EMF FOR AVERAGE TEMPERATURE (EO)	EMF FOR DISTRIBUTION TRIGGER (ET)	EMF FOR DISTRIBUTION USUI (EU)	EMF FOR DISTRIBUTION DEARNLEY (ED)
100	2.113	2.161	2.146	2.154
150	3.171	3.241	3.220	3.232
200	4.225	4.314	4.289	4.306
250	5.271	5.376	5.350	5.371
300	6.306	6.421	6.399	6.424
350	7.326	7.445	7.432	7.460
400	8.327	8.442	8.444	8.476
450	9.306	9.408	9.433	9.468
500	10.258	10.338	10.393	10.432
550	11.181	11.227	11.321	11.363
600	12.070	12.070	12.214	12.258
650	12.922	12.862	13.067	13.113
700	13.733	13.598	13.876	13.924
750	14.499	14.274	14.637	14.687
800	15.217	14.884	15.347	15.398
850	15.884	15.423	16.002	16.052
900	16.494	15.887	16.597	16.647
950	17.045	16.271	17.128	17.178
1000	17.533	16.569	17.593	17.642
1050	17.954	16.777	17.986	18.033
1100	18.305	16.890	18.304	18.349
1150	18.582	16.903	18.543	18.585
1200	18.781	16.812	18.699	18.737
1250	18.898	16.610	18.769	18.801

TABLE 2.6

EOT..

COMPARISON OF PERCENTAGE DIFFERENCE BETWEEN NOMINAL EMF (EO) AND MODELLED EMF FOR THE TOOL/CHIP TEMPERATURE DISTRIBUTIONS PROPOSED BY TRIGGER(1961), USUI(1984) AND DEARNLEY(1983)

TOOL :~ CARBIDE GRADE T1A , WORKPIECE :~ STEEL 817M40(EN24)
RESISTIVITY OF STEEL 'ROS' = 0
RESISTIVITY OF CARBIDE RELATIVE TO STEEL 'ROC' = 0

TEMPERATURE COEFFICIENT OF RESISTIVITY FOR STEEL 'A1S' = 0
TEMPERATURE COEFFICIENT OF RESISTIVITY FOR CARBIDE 'A1C' = 0

STEP SIZE 'S' = 0.001

NOMINAL AVERAGE TEMPERATURE (TO)	EMF FOR AVERAGE TEMPERATURE (EO)	PERCENTAGE DIFFERENCE DISTRIBUTION TRIGGER (EO-ET)/(EO)	PERCENTAGE DIFFERENCE DISTRIBUTION USUI (EO-EU)/(EO)	PERCENTAGE DIFFERENCE DISTRIBUTION DEARNLEY (EO-ED)/(EO)
100	2.113	-2.237	-1.532	-1.929
150	3.171	-2.186	-1.525	-1.921
200	4.225	-2.098	-1.512	-1.908
250	5.271	-1.974	-1.494	-1.888
300	6.306	-1.813	-1.470	-1.861
350	7.326	-1.615	-1.440	-1.828
400	8.327	-1.377	-1.403	-1.789
450	9.306	-1.098	-1.361	-1.742
500	10.258	-.777	-1.312	-1.688
550	11.181	-.412	-1.256	-1.626
600	12.070	.001	-1.192	-1.556
650	12.922	.464	-1.121	-1.478
700	13.733	.980	-1.041	-1.390
750	14.499	1.555	-.952	-1.292
800	15.217	2.192	-.854	-1.184
850	15.884	2.898	-.745	-1.064
900	16.494	3.679	-.624	-.930
950	17.045	4.542	-.490	-.783
1000	17.533	5.498	-.342	-.620
1050	17.954	6.556	-.178	-.439
1100	18.305	7.729	.005	-.238
1150	18.582	9.032	.207	-.015
1200	18.781	10.484	.433	.233
1250	18.898	12.107	.685	.511

TABLE 2.7

EOT. .

MODEL OF THERMOCOUPLE USING CARBIDE GRADE TTA AND STEEL 817M40.

TOOL/CHIP TEMPERATURE DISTRIBUTION PROPOSED BY USUI(1984)

THE TEMPERATURE CALIBRATION COEFFICIENTS ARE :-
A= .02104 B= .000001414 C=-4.921E-09

RESISTIVITY OF STEEL 'ROS' = 1
RESISTIVITY OF CARBIDE RELATIVE TO STEEL 'ROC' = 2.222

TEMPERATURE COEFFICIENT OF RESISTIVITY FOR STEEL 'A1S' = 0.12474
TEMPERATURE COEFFICIENT OF RESISTIVITY FOR STEEL 'A2S' = .000025
TEMPERATURE COEFFICIENT OF RESISTIVITY FOR CARBIDE 'A1C' = 0.003

THE DATA SHOWS THE CONVERGENCE OF MODELLED EMF WITH DECREASING STEP SIZES , 'S'= 0.1, 'S'= 0.01, 'S'= 0.001

AVERAGE NOMINAL TEMPERATURE (TO)	EMF FOR AVERAGE TEMPERATURE (EO)	EMF FOR DISTRIBUTED TEMPERATURE STEP=0.1	EMF FOR DISTRIBUTED TEMPERATURE STEP=0.01	EMF FOR DISTRIBUTED TEMPERATURE STEP=0.001
100	2.113	2.098	2.132	2.135
150	3.171	3.147	3.198	3.203
200	4.225	4.192	4.260	4.267
250	5.271	5.230	5.314	5.322
300	6.306	6.256	6.356	6.366
350	7.326	7.267	7.382	7.393
400	8.327	8.259	8.388	8.401
450	9.306	9.229	9.371	9.386
500	10.258	10.177	10.331	10.346
550	11.181	11.093	11.256	11.272
600	12.070	11.974	12.145	12.163
650	12.922	12.815	12.995	13.013
700	13.733	13.618	13.803	13.821
750	14.499	14.375	14.564	14.583
800	15.217	15.084	15.274	15.293
850	15.884	15.741	15.930	15.949
900	16.494	16.342	16.528	16.547
950	17.045	16.883	17.063	17.081
1000	17.533	17.361	17.532	17.550
1050	17.954	17.771	17.931	17.947
1100	18.305	18.110	18.256	18.271
1150	18.582	18.374	18.503	18.516
1200	18.781	18.559	18.668	18.678
1250	18.898	18.662	18.747	18.755

TABLE 2.8

EOT..

COMPARISON OF THE NOMINAL EMF (EO) WITH THE MODELLED EMF FOR THE TOOL/CHIP TEMPERATURE DISTRIBUTIONS PROPOSED BY TRIGGER(1961), USUI(1984) AND DEARNLEY(1983).

TOOL :~ CARBIDE GRADE TTA, WORKPIECE :~ STEEL 817M40 (EN24)

RESISTIVITY OF STEEL 'ROS' = 1
RESISTIVITY OF CARBIDE RELATIVE TO STEEL 'ROC' = 2.222

TEMPERATURE COEFFICIENT OF RESISTIVITY OF STEEL 'AS1' = 0.12474
TEMPERATURE COEFFICIENT OF RESISTIVITY OF STEEL 'A2S' = -.0000257
TEMPERATURE COEFFICIENT OF RESISTIVITY OF CARBIDE 'A1C' = 0.003

STEP SIZE 'S' = 0.001

NOMINAL AVERAGE TEMPERATURE (TO)	EMF FOR AVERAGE TEMPERATURE (EO)	EMF FOR DISTRIBUTION TRIGGER (ET)	EMF FOR DISTRIBUTION USUI (EU)	EMF FOR DISTRIBUTION DEARNLEY (ED)
100	2.113	1.984	2.135	2.146
150	3.171	2.956	3.203	3.219
200	4.225	3.923	4.267	4.288
250	5.271	4.882	5.322	5.349
300	6.306	5.831	6.366	6.398
350	7.326	6.764	7.393	7.430
400	8.327	7.686	8.401	8.443
450	9.306	8.589	9.386	9.431
500	10.258	9.463	10.346	10.396
550	11.181	10.305	11.272	11.325
600	12.070	11.111	12.163	12.217
650	12.922	11.877	13.013	13.071
700	13.733	12.599	13.821	13.882
750	14.499	13.271	14.983	14.645
800	15.217	13.890	15.293	15.356
850	15.884	14.450	15.949	16.012
900	16.494	14.946	16.547	16.609
950	17.045	15.365	17.081	17.143
1000	17.533	15.721	17.550	17.609
1050	17.954	16.000	17.947	18.004
1100	18.305	16.198	18.271	18.324
1150	18.582	16.308	18.516	18.565
1200	18.781	16.326	18.678	18.722
1250	18.898	16.247	18.755	18.793

TABLE 2.9

EOT. .

COMPARISON OF PERCENTAGE DIFFERENCE BETWEEN NOMINAL EMF (EO)
AND MODELLED EMF FOR THE TOOL/CHIP TEMPERATURE DISTRIBUTIONS
PROPOSED BY TRIGGER(1961),USUI(1984) AND DEARNLEY(1983)

TOOL :~ CARBIDE GRADE TTA , WORKPIECE :~ STEEL 817M40(EN24)
RESISTIVITY OF STEEL 'ROS' = 1
RESISTIVITY OF CARBIDE RELATIVE TO STEEL 'ROC' = 2.222

TEMPERATURE COEFFICIENT OF RESISTIVITY FOR STEEL 'A1S' = 0.12474
TEMPERATURE COEFFICIENT OF RESISTIVITY FOR STEEL 'A2S' = -.0000259
TEMPERATURE COEFFICIENT OF RESISTIVITY FOR CARBIDE 'A1C' = 0.003

STEP SIZE 'S' = 0.001

NOMINAL AVERAGE TEMPERATURE (TO)	EMF FOR AVERAGE TEMPERATURE (EO)	PERCENTAGE DIFFERENCE DISTRIBUTION TRIGGER (EO-ET)/(EO)	PERCENTAGE DIFFERENCE DISTRIBUTION USUI (EO-EU)/(EO)	PERCENTAGE DIFFERENCE DISTRIBUTION DEARNLEY (EO-ED)/(EO)
100	2.113	6.136	-1.045	-1.546
150	3.171	6.795	-1.008	-1.516
200	4.225	7.154	-.984	-1.493
250	5.271	7.381	-.962	-1.471
300	6.306	7.542	-.940	-1.447
350	7.326	7.672	-.916	-1.419
400	8.327	7.699	-.889	-1.387
450	9.306	7.703	-.858	-1.349
500	10.258	7.758	-.858	-1.338
550	11.181	7.839	-.817	-1.288
600	12.070	7.948	-.766	-1.221
650	12.922	8.087	-.705	-1.155
700	13.733	8.261	-.644	-1.083
750	14.499	8.472	-.576	-1.002
800	15.217	8.726	-.500	-.911
850	15.884	9.028	-.415	-.810
900	16.494	9.385	-.319	-.698
950	17.045	9.859	-.213	-.573
1000	17.533	10.337	-.094	-.433
1050	17.954	10.885	.039	-.277
1100	18.305	11.513	.188	-.103
1150	18.582	12.236	.356	.092
1200	18.781	13.069	.544	.311
1250	18.898	14.030	.757	.557

TABLE 2.10

EOT..

Table 2.8 shows the results that were obtained when equation 2.8 was evaluated for different step sizes. The values of resistivity and their temperature coefficients are shown at the top of the table. These results show a convergence with reducing step size similar to that found in table 2.5. It was decided that a step size of 0.001 gave sufficient accuracy and was adopted in all subsequent calculations.

Table 2.9 shows the calculated output emf for the three different distributions when changes in resistivity with temperature are taken into account. The results show that for the temperature distributions proposed by Usui and Dearnley, the difference from the nominal emf EO is very small. At 1000°C the difference ranges from 0.02 to 0.06 mv. The temperature distribution proposed by Trigger gives a much larger difference, at 1000°C this amounts to 3.2 mv. There are two reasons for the reduction in output from the distribution proposed by Trigger.

The first reason is the reduced output emf produced by the higher peak temperatures associated with this distribution. This was discussed when considering the results in table 2.5.

The second reason can be explained by considering the influence of changes in resistance with temperature on equation 2.8 shown below:-

$$E = \sum_{i=1}^{i=n} \frac{e_i . R_{pi}}{(R_{si} + R_{ci}) + R_{pi}}$$

Increases in temperature will increase the resistance of all the elements such as R_{si}, R_{ci} and all the remaining combined values in parallel given by R_{pi}. The effect of the higher peak temperatures associated with distribution proposed by Trigger is to increase the value of R_{si}. This has the effect of increasing the denominator and thereby reducing the output E. It should be noted that the change in resistivity for steel with temperature contained a second order term and was given as follows:-

$$R_s = R_{os}(1 + 0.0242T + 0.000214T^2)$$

The high peak temperatures associated with this distribution (Trigger) cause the second order term to make a significant contribution to R_s.

The results in table 2.10 show the percentage differences between the nominal emf (EO) and the output from the three distributions considered. These results show that for a wide range of temperature (400 to 1250^{o}C), introducing changes in resistance with temperature does not cause a significant difference when considering the distributions proposed by Usui or Dearnley. The distribution by Trigger causes large differences and the reasons for this have been discussed above. The data given in columns one and three of table 2.9 could be used to determine the average temperature if the shape of the distribution was known to conform to that proposed by Trigger.

2.7.6 Conclusions

1. The output emf from the tool/work thermocouple is dependant on the following factors:-

   i) the shape of the emf versus temperature calibration curve

for the tool and work materials,

ii) the shape of the temperature distribution at the chip/tool interface,

iii) the change in electrical resistivity with temperature of the tool and work materials.

2. The three factors above can be incorporated into a model that considers the chip/tool contact region as a large number of thermocouples connected in parallel.

3. For the tool and work materials considered, the output emf for the temperature distributions proposed by either Usui or Dearnley gave a difference of less than 1% from the nominal output.

4. When the distributions by either Dearnley or Usui were considered, it was found that changes in resistivity with temperature had very little influence on the output emf.

5. When operating at temperatures of 1000^{o}C, the relatively peaky distribution proposed by Trigger caused differences of typically 10% between the nominal calibration emf and that given by the model.

CHAPTER 3

MEASUREMENT OF CUTTING FORCES

3.1 Force Dynamometer

The forces on the cutting tool were measured using a Kistler (type 9257A) three force component dynamometer. This type of dynamometer uses the piezo-electric principle and has a very high level of performance; the specification is given in Appendix 1. The dynamometer was mounted on the cross-slide of the lathe and the tool holder that had a 25 mm square shank was clamped onto the platform. Because the total length of the shank was in contact with the dynamometer, the arrangement was very rigid and the thermocouple wires were protected from the hot swarf. Figure 3.1 shows the dynamometer mounted on the lathe.

3.2 Calibration of Force Dynamometer

The dynamometer manufacturers did not supply a direct calibration chart, but they gave values of sensitivity for each axis. These values were checked by applying weights to the dynamometer and checking the voltage output from the charge amplifier. It was found that sensitivities quoted gave the expected values of output. Further calibration tests were carried out on the dynamometer at intervals during the cutting test programme, but no detectable variations were found.

3.3 Charge Amplifiers and Recording System

When using a piezo-electric transducer it is necessary to connect it to a charge amplifier. This is a device that converts the variation in charge on the transducer to an output voltage that is suitable for either a display unit or a recorder. Three charge

amplifiers were used, one being necessary for each channel. They were Kistler type 5001 and they gave a wide range of output.

It was decided to record the force measurements on an ultra-violet (U/V) recorder. The reasons for choosing a U/V recorder for the force measurement were largely the same as those given in section 2.5.1. Although seven channels were still available on the temperature recorder, it was felt that there was not sufficient room on the paper trace for the three force measurement traces. Fortunately, a second recorder was available and this had an identical range of paper speeds to the first. Galvanometers with a natural frequency of 1000 hz (type A.1000) were selected, and a 1.5 kΩ resistor was placed in series with the galvanometers to protect them from any accidental overload. A calibration of applied voltage against galvanometer deflection was carried out and is shown on figure 3.2. A general view of the instrumentation is shown on figure 3.3.

CHAPTER 4

MEASUREMENT OF TOOL DEFORMATION AND WEAR

4.1 Introduction

The measurement of tool deformation and wear has usually been achieved by either optical or mechanical techniques. Each particular technique has its advantages and limitations and these are briefly discussed in the following sections, together with the methods that were adopted for this particular investigation.

4.2 Optical Methods for Measuring Deformation

4.2.1 Interferometry

Trent (1959) used interferometry to determine the deformation or bulging on the flank face of carbide cutting tools. The flank face was lapped as flat as possible and after each cutting test it was placed in contact with an "optical flat". Any deformation appeared as a contour map formed by the interference pattern. This technique was useful in that it did not require a large amount of specialist equipment; provided lapping facilities were available it could be used quite easily. It suffered from the disadvantages that the interference patterns were both difficult to interpret and to quantify and also a permanent record of the deformation was not produced by this technique.

4.2.2 Tool Sectioning Techniques

The deformed shape of a cross-section of the cutting tool can be observed using a microscope. After a cutting test, a section is taken perpendicular to the cutting edge of the tool and it is observed under a microscope. This type of observation reveals the amount of flank

bulging and also any cratering or depression on the rake face. The facility of being able to observe a profile of the rake and flank faces at the same time is very useful and is the main advantage of this method. This technique has also been used with success to investigate the flow of the workpiece material over the rake face and around the cutting edge when a built up edge was present. Under these conditions both the tool and the adhering chip are sectioned together.

The main limitation of this technique is the necessity to remove part of the cutting edge to provide a cross-section of the tool. Because of this the tool cannot be used in subsequent cutting tests.

4.2.3 Light Sectioning Techniques

Venkatesh et al (1977) used a light sectioning microscope to determine the bulging on the flank face of a coated carbide cutting cool. A narrow slit of light was shone on to the surface under investigation and the reflected image was projected on to the eyepiece of a microscope. Any deformation present on the flank face of the tool caused the light beam to distort, and this was measured using the calibrated eyepiece on the microscope. The main advantage of this technique was that the cutting tool could be measured without the need for any elaborate preparation. Against this advantage must be set the following limitations. The technique did not give a permanent record of the deformation and the equipment was expensive and not commonly available.

4.3 Mechanical Methods for Measuring Deformation

4.3.1 Stylus Techniques

Over recent years surface measuring instruments that use a stylus to detect irregularities in engineering surfaces have been developed.

Any movement of the stylus as it is traversed across the surface is amplified electronically and the profile of the surface is recorded on a permanent paper chart. The stylus is mounted in an arm which is supported by a pivot at one end and a skid at the end which rests on the surface of the workpiece. The stylus is mounted in the arm adjacent to the skid and arranged in such a manner that irregularities on the surface are "picked-up" by the stylus. When access to the surface is difficult or the length of surface to be measured is short then it is necessary to remove the skid. Under these circumstances the arm is supported by a "straight line" unit. This unit is essentially a precision glass block which has its top surface ground flat; the angle and height of the block can be adjusted so that is is parallel to the surface being measured.

4.3.2 Location of the Tool Tip for Stylus Measurement

A feature of the stylus instruments discussed above is that they are capable of large vertical magnifications, values ranging from 1000 to 50,000 being usual. To take the maximum advantage of this feature it is necessary to be able to relocate the tool tip consistently. The usual way to precisely relocate an engineering component is to use a fixture which is designed using kinematic principles. These principles ensure that the six degrees of freedom of the body are constrained with no redundant restraints. Point contact between the workpiece and fixture is made at six positions and the closing force is normally gravity. Such a fixture was designed and manufactured for this particular investigation and is shown on figure 4.1 along with the straight line unit and the stylus instrument. To test the repeatability of the feature the tool tip was removed from the fixture and relocated several times. On every occasion it was found that the position was repeated to within less than 1 μm.

Because of the advantages of large magnifications and the production of a permanent record combined with the ease of availability, it was decided to adopt the stylus technique to determine the deformation on the flank face of the cutting tool.

4.3.3 Interpretation of Stylus Traces

A feature of stylus instruments is that the record produced on the paper trace often has a much higher vertical than horizontal magnification. The vertical magnification usually has a range from 1000 to 50,000X, whereas the horizontal magnification usually has a range from 20 to 100X. It was necessary therefore to correct the results from the trace to obtain the true shape of the profile.

It was decided to evaluate the results of the stylus technique by recording the profile of the flank face of a tool tip. The tool had zero rake angle and the flank face was ground to give a clearance angle of 6 degrees. Figure 4.2 shows a typical trace with both flank wear and deformation (bulging) present. The flank wear was represented by the inclined linear region and had a true angle of approximately 6 degrees to the undeformed flank face. During cutting this surface was parallel and in contact with the newly machined work surface. The deformation or bulging was represented by the curved region on the trace and its maximum value occurred at the bottom of the wear land.

To confirm the above interpretation of the trace it was decided to grind a small wear land onto the flank face of an unused tool tip. This gave a flank face with a wear land but with no deformation. A trace of the flank face before and after grinding the land is shown on figures 4.3 and 4.4 respectively. Figure 4.4 shows the wear land as a linear region which was at a true angle of 6^{o} to the flank face when

corrected values of magnification were considered. To obtain an independant measurement of the length of the land, a toolmakers microscope was used and the results were found to confirm those obtained from the trace.

A series of cutting tests using the same tip was then undertaken and typical traces of the flank face are shown on figures 4.5 to 4.7. The continued bulging on the flank face with increasing cutting time can be clearly identified. The bulging was measured at a cross-section of the cutting that corresponded to the central part of the chip width.

From the results of these investigations it was considered that this was a satisfactory technique for determining deformation on the flank face, and it was used in all subsequent investigations.

4.3.4 Depression of the Cutting Edge

It was decided to measure the depression of the cutting edge with a stylus instrument which was similar to the one described in section 4.3.1. It had equal magnifications of 100X in both the vertical and horizontal directions. The tool tip was located in a special fixture that was capable of rotation about the centre of the nose radius (see figure 4.8). This arrangement allowed traces to be taken at various angular positions around the tool nose radius as well as perpendicular to the cutting edge. Figures 4.9 and 4.10 show two typical types of rake face profiles; figure 4.9 shows parallel edge deparession, and figure 4.10 shows tapered edge depression.

4.4 Tool Wear Measurement

4.4.1 Introduction

It was considered necessary to determine the size of the wear lands on the clearance faces, the depth of the crater, and the area of tool/chip contact. These measurements gave a comprehensive record of tool performance during the cutting tests being taken using a toolmakers microscope that had a resolution of 2 μm.

4.4.2 Wear on the Clearance Faces

The results of preliminary tests revealed that the tool suffered considerable wear on the clearance faces of the cutting edge and the nose radius. To facilitate measurement of the wear an indexing fixture was used which made it possible to measure the wear at a number of points around the nose radius. The results were recorded on the chart shown as figure 4.11.

4.4.3 Crater Depth

The depth of crater on the rake face was determined from the trace that gave the depression of the cutting edge and is described in section 4.3.4 and shown on figures 4.9 and 4.10.

4.4.4 Tool/chip Contact Area

The area of contact between the chip and the cutting tool has much significance when determining the temperature and stress distributions, both on the rake face and within the body of the tool.

One common method of determining the area of contact is to observe the rubbing marks made by the chip with an optical microscope. The problem exists to accurately determine the point of chip departure the tool rake face. At the point of chip departure the contact

stresses are considered to be very low and approaching zero. In non-orthogonal cutting the tool nose radius, rake angle and plan approach angle influence the direction of chip flow across the tool rake face. Figures 6.55 to 6.60 show typical views of the tool chip contact area. In some cases a clearly defined crater can be observed and beyond the crater a region of chip contact and wear. Unfortunately, the region of wear beyond the crater was not always clearly defined, which caused some difficulty in exactly determining the extent of the tool/chip contact area. Figures 6.55 to 6.60 also show that the area of contact had a complex shape, due to a number of factors, such as the direction of chip flow and the temperature and stress distribution perpendicular to the direction of chip flow. Figures 4.12 to 4.14 show typical chip cross-sections for different feeds. The variation of temperature and stress across the chip is discussed in section 7.2. Any measurements obtained must be considered as an estimate of the precise contact area.

In an attempt to confirm the results obtained for the contact area, it was decided to coat a number of tools. The coating was to be sufficiently durable to withstand any stray contact with hot chips outside the contact area, but sufficiently thin and soft to wear away in the region of contact. A number of coatings were considered, including varnish, paint, copper, gold and titanium nitride.

The varnish and paint coatings were easy to apply but did not perform very well. They were easily removed and did not give a very clearly defined contact area. The copper was applied using a sulphate solution; this coating was better than the varnish or paint but was still vulnerable to the action of the stray chips. On occasions it was found that the coating could be easily chipped. To apply the gold

coating the sputtering process was used. This process is used to apply coatings for specimens that are to be examined using the scanning electron microscope. This coating was found to be very soft and did not perform as well as the copper or the varnish.

Titanium nitride coatings are used extensively on cutting tools to minimise wear, and they have typical thickness of 10 μm. A coating of approximately 0.20 to 0.30 μm was applied to the rake face of the tool. The thickness of the coating was estimated from the coating time and current, in conjunction with the known deposition rate for the coating material. It was decided to check the thickness of the coating by using the Scanning Electron Microscope. Figure 4.15 shows a view of the tool and the coating. To achieve the necessary contrast between the coating and the substrate it was necessary to fracture an unused coated tool. Figure 4.15 clearly shows the fractured carbide grains and the thin titanium nitride coating. This figure confirmed that the average grain size for the tools was approximately 2 μm (section 5.1). From figure 4.15 it was estimated that the coating was less than 0.5 μm thick and this value was in reasonable agreement with the value calculated from the coating time and current.

The tool/chip contact area was determined from the area of coating that was removed during a series of cutting tests. The tests were carried out in increments of 20 seconds up to a maximum 60 seconds. The area of the exposed carbide on the rake face was recorded on the charts shown as figure 4.11. These tests were organised in increments of 20 seconds to determine whether the exposed area was approaching a steady state value. If continuous

tests of 60 seconds had been undertaken, then it would not have been possible to determine the rate at which the exposed area was increasing. The results on figures 4.16 to 4.18 show that an exposed area on the tool was established very rapidly. In most of the cases there was very little increase in the exposed area after 40 seconds of machining. These results suggest that the coating was sufficiently thin to allow its rapid removal and it did not significantly influence the tool chip interface conditions. It was appreciated that the exposed area of carbide on the rake face was probably slightly less than the total chip/tool contact area. This was due to the generally accepted assumption that the contact stresses at the chip departure point are effectively zero. Consequently the conditions of temperature and stress may not have been sufficient to remove the coating just within the contact area. Despite this possible limitation it was felt that this technique was sufficient to allow a comparison with the results obtained for uncoated tools.

When the tool/chip contact length in the direction of chip flow was compared for the lightly coated and uncoated tools, there was a typical variation of 0.1 to 0.15 mm. This variation occurred over a distance of 1 to 1.3 mm and can be considered as approximately 10%. The implications of variations in contact length are considered in section 8.11.

CHAPTER 5

SELECTION AND PREPARATION OF TOOLS AND WORKPIECE

5.1 Selection of Carbide Grades

The deformation of carbide cutting tools when cutting high strength steels was discussed in sections 1.8 to 1.8.4. Both Trent (1967) and Ekemar (1966) have shown that increasing the TiC content increases the resistance to deformation. However, the increase in resistance to deformation is usually accompanied by a reduction in toughness. It was therefore decided to investigate three different steel cutting grades. Their composition and some physical properties are shown in table 5.1 below.

Grade	% Composition by Weight WC	TiC	TaC	Co	Transverse Rupture Stress N/mm^2	Hardness (Vickers) Scale	I.S.O. Code
TA5	80	7	4	9	1850	1550	P25-P35
TTA	77	11	4	8	1700	1575	P15-P25
TE	70	18	4	8	1450	1600	P05-P10

Table 5.1 Composition and Properties of the Tool Materials

All the grades had an average grain size of 2 μm. The TaC and Co content was essentially constant for all three grades. The influence of TiC on the Hardness and Transverse rupture stress is clearly shown in Table 5.1; the table also shows the different ISO classification codes which ranged from P35 to P05.

Grade TA5 was a heavy duty grade suitable for machining at relatively low speeds and heavy feeds. Grade TTA was a general purpose

grade for machining steel from a range of heavy duty machining to high peripheral speed finishing. Grade TE was suitable for the finish turning of steel using high speeds and fine feeds.

5.2 Tool Geometry

5.2.1 Rake Angle

In practice a variety of rake angles are used in cutting tools. The choice of rake angle is governed by the type of work material and the tool material. Generally speaking, tools with positive rake angles give lower cutting forces, however these tools are usually considered to be less durable in service when compared with zero or negative rake angles. In recent years there have been many developments in rake face geometry. These developments are intended to give chip control when machining at high metal removal rates. In many cases these tools have a secondary positive rake angle, known as a chip breaker groove. This is situated behind a short land which is often set at a negative rake angle. This configuration gives a chip/tool contact region which is inclined at a combination of different rake angles. Such a situation is difficult to analyse because the stress distributions on the tool rake face are likely to be very complex.

After considering these factors it was decided to adopt a constant rake angle of zero degrees for the cutting tests being undertaken.

5.2.2 Nose Radius

It was stated by Trent (1959) that the nose radius of the tool has an influence on deformation. However, neither Trent (1959) reported, or Ekemar (1966) investigated, the effect of changing the

nose radius. The choice of nose radius is usually a compromise between obtaining a satisfactory surface finish and minimising the radial cutting force component. For a given feed rate a large nose radius will give a low value of surface roughness, but will usually result in a large radial force component which can often cause the onset of chatter.

A nose radii of 0.8 mm was selected for this investigation for two reasons. Firstly it was the recommended value in the ISO standard (3685) for tool life testing, and secondly it would allow some direct comparison with the results report by Trent and also Ekemar.

5.3 Preparation of Tool Inserts (Tips)

The tool inserts were supplied in the as sintered condition and had a nominal size of 19 x 19 x 5 mm. A special fixture was designed and manufactured to hold the inserts so that they could be ground on the top, bottom and flank faces. The flank faces were ground to an angle of 6^{o} to the rake face. Grinding was carried out on a surface grinding machine using a diamond wheel. The nose radius was ground on to the inserts using the radius grinding attachment shown on figure 5.1. This attachment was designed and manufactured to fit on to an Abwood tool grinding machine. With careful use it was possible to grind a radius of any value and to blend it with the flank faces on the insert.

The final stage of insert preparation was to lap the flank faces flat. This was achieved by mounting three tips in a fixture such that the faces protruded by 2 mm. This arrangement of mounting the tips ensured that the fixture was stable when rotating in the lapping machine, thus ensuring that flat surfaces were produced. After

lapping it was possible to "wring" the surfaces together.

5.4 Choice of Cutting Conditions

5.4.1 Cutting Speed

The recommended cutting conditions for the three carbide grades chosen are shown in Table 5.2. It can be seen that the grades TA5 and TE are recommended for rough and finish machining respectively. The workpiece material was 817M40(EN24) and was supplied with a hardness of 295 to 320 VPN, which was equivalent to a UTS value of 850 MN/m^2 (55 tons/sq in). For each grade it was decided to run a range of cutting tests and to use the tool manufacturer's recommended values as a starting point. The cutting speed was increased by increments of 0.5 m/s (100 ft/min) to a value that gave rapid failure. The duration of the tests is discussed in section 5.7.

5.4.2 Feed Rate

Starting values for the feed rates for each grade were taken from Table 5.2. However, in the case of grade TA5 the maximum feed rate was limited to 0.80 mm/rev (0.032 ins/rev). It was considered that feed rates in excess of this would not be advisable for the lathe being used or for the size of the workpiece specimens.

5.4.3 Depth of Cut

The depth of cut was kept constant at 2 mm for all the tests. This value was chosen for three reasons: first it would allow some comparison with the results obtained by Trent and Ekemar; secondly it was felt to be the minimum acceptable for a nose radius of 0.8 mm. The ISO standard (3685) recommends a 2.5 mm depth of cut for a nose radius of 0.8 mm. However, when this value is not possible or the feed is a test variable then a minimum depth of cut of twice the nose

U.T.S.	ROUGH TURNING				FINISH TURNING			
MN/m^2	GRADE	I.S.O. Code	Speed M/S	Feed mm/rev	GRADE	I.S.O. Code	Speed M/S	Feed mm/rev
				Up to				Up to
Up to 540	TA5 TTA	P25/P35 P15/P25	0.75-1.0 1.25-1.75	3.0 0.6	TE TTA	P05/P10 P15/P25	2.0-4.0 1.5-2.25	0.25 0.25
540 to 850	TA5 TTA	P25/P35 P15/P25	0.75-1.0 1.00-1.25	1.5 0.6	TE TTA	P05/P10 P15/P25	1.5-2.0 1.0-1.5	0.25 0.25
850 to 1000	TA5 TTA	P25/P35 P15/P25	0.4-0.5 0.9-1.0	2.0 0.6	TE TTA	P05/P10 P15/P25	2.25-1.75 1.0-1.25	0.25 0.25
1000-1150	TA5 TTA	P25/P35 P15/P25	0.35-0.45 0.7-0.9	2.0 0.5	TE TTA	P05/P10 P15/P25	1.0-2.35 0.85-1.0	0.25 0.25
1235-1545	TA5 TTA	P25/P35 P15/P25	0.25-0.35 0.5-0.6	0.5 0.25	TE TTA	P05/P10 P15/P25	0.75-0.9 0.6-0.75	0.13 0.25

TABLE 5.2 RECOMMENDED SPEEDS AND FEEDS FOR MACHINING STEEL

radius is recommended. The third reason for selecting 2 mm was the possibility of a restriction in power available when operating with a combination of high speeds and feeds.

5.5 Workpiece Specification and Preparation

A steel workpiece (817M40, EN24) was used for the investigations. This particular steel contained nickel, chromium and molybdenum and is commonly used for high duty engineering applications. It was supplied as black bar in 4 metre (13 ft) lengths and was 100 mm (4 ins) dia., the bar was cut into one metre lengths. To check the uniformity the hardness was measured across the diameter and at several positions along the length. The results of the hardness (VPN) measurements, given in Table 5.3, were obtained from the Vickers Hardness Machine using the 30 kg load.

Bar dia mm	30	40	50	60	70	80	90	100
Position No. 1	302	304	295	299	310	308	315	320
Position No. 2	298	299	301	302	304	307	312	315
Position No. 3	298	308	305	307	299	303	314	319
Position No. 4	297	305	308	305	301	308	311	317

Table 5.3 Hardness (VPN) of Workpiece Material

The results show that the hardness of the bar was essentially uniform across the diameter and along the length. There was a slight increase in hardness towards the outside diameter, however most of this material was machined away when the scale was removed and the bars were "trued-up" before the cutting tests began. The workpiece was insulated from the lathe by fitting a split Tufnol ring at the chuck end and a Tufnol plug at the tailstock end.

5.6 Lathe for Cutting Tests

The lathe selected for the cutting tests was a Colchester 2000, with a range of speeds varying from 25 to 2000 rpm, and a range of feeds 0.05 to 1.0 mm per revolution. The speeds were arranged in a geometric progression with a ratio of approximately 1.3. Ideally, a lathe should have a steplessly variable speed range when being used for cutting tests. This allows a particular surface speed to be selected for any diameter of the workpiece. Although the steplessly variable speed range was not available on the lathe selected, it was felt that the problem could be overcome with careful planning of the cutting tests. During the tests the surface speed of the workpiece was checked using a tachometer.

5.7 Duration of Cutting Tests

In the work reported by Trent (1959) the cutting tests had a duration of 1 minute, which was said to be sufficient to determine whether the tool would sustain permanent plastic deformation. It was decided to organise the cutting tests in two different ways. For each combination of cutting conditions a continuous test of 60 seconds (1 minute) was carried out. The same set of cutting conditions were then repeated with increments of 5, 5, 10, 20 and 20 seconds, giving a cumulative total of 60 seconds. This test procedure was adopted to try and determine the influence of the transient thermal effects that occurred at the start of each cut.

CHAPTER 6

OBSERVATIONS

6.1 Introduction

The following chapter contains details of the observations that were made during the cutting tests. For each grade and set of cutting conditions the following data were recorded:-

1) cutting forces
2) tool tip boundary temperatures
3) deformation (bulging) of the flank face
4) depression of the cutting edge (rake face)
5) wear on the clearance faces
6) tool/chip contact length

The results are discussed by considering the influence of cutting speed and feed rate on the above dependant variables for each of the three grades. Where it is appropriate, comparisons are also made between the grades.

6.2 Cutting Forces

The vertical and axial cutting forces are shown on figures 6.1 to 6.12, each figure is plotted for a constant feed rate and shows the variations of force with time and cutting speed.

6.2.1 Grade TE

Figure 6.1 shows the cutting forces for a feed rate of 0.25 mm/rev. The vertical forces appear to be largely independent of cutting speed. There was a general trend of the vertical cutting force increasing

slightly during the first 10 seconds of machining, after which it remained essentially constant.

The axial forces for the lower speeds followed a similar trend to the vertical forces, and were independent of speed and time after the first 10 seconds. However, the 3.71 and 4.00 m/s cutting speeds gave axial force components that started to rise with time. In the case of the 3.71 m/s speed, it was necessary to suspend the test after 20 seconds duration. Figures 6.13 and 6.25 show the corresponding temperatures and deformations which are discussed in sections 6.3.1 and 6.4.1.

Figure 6.2 shows the cutting forces for the feed rate of 0.3 mm/rev. The vertical forces were independent of time but they appeared to be approximately inversely related to the cutting speed. When compared with the 0.25 mm feed rate the vertical and axial forces levels for the 2.5, 2.85 and 3.25 m/s cutting speeds were slightly higher. Generally the axial forces gave a steady increase with machining time, however in the case of the 4.0 m/s speed, a rapid increase in axial force was observed between 10 and 40 seconds of machining. This was accompanied by an increase in temperature and a large amount of deformation (see figures 6.14 and 6.26).

Figure 6.3 shows the cutting forces for a feed rate of 0.35 mm/rev and they are similar to those found for the 0.25 and 0.3 mm/rev feed rates. Because of the reasons discussed previously, the test using the 4.0 m/s cutting speed was stopped after 40 seconds (see figures 6.15 and 6.27).

Figure 6.4 shows the cutting forces for a feed rate of 0.4 mm/rev. The speeds of 2.50 m/s and 2.85 m/s gave a steady increase in both vertical and axial force over the 60 second machining test. The lower speed of 2.13 m/s gave a slight increase in axial force.

Examination of figures 6.1 to 6.4 indicates that the axial forces varied much less than the vertical forces for the range of feeds and speeds that were tested. The axial force values were found to lie in a band from 400 to 700 newtons.

The vertical forces were more sensitive to changes in feed rate than changes in cutting speed. Increasing the feed rate caused an increase in the vertical force. For the feed rate of 0.25 mm/rev the steady state vertical force values were in the range from 1060 to 1180 newtons.

The 0.3 mm feed rate gave steady state vertical force values from 1100 to 1280 newtons. For the 0.35 mm and 0.4 mm feeds a region of constant vertical force could not be clearly identified. In both of these cases the vertical forces increased with increasing feed rate and also machining time. The 0.35 mm feed gave vertical forces in the range of 1440 to 1680 newtons and the 0.4 mm feed 1420 to 1860 newtons.

6.2.2 Grade TTA

Figure 6.5 shows the force values for the feed rate of 0.35 mm/rev. The two higher speeds (V = 2.13 and V = 2.50 m/s) gave a small but definite increase in vertical force as the tests proceeded. In the case of the 2.5 m/s speed, this was accompanied by an almost continuous rise in the axial force. The axial force for the two lower speeds was essentially constant for the duration of the tests.

Figure 6.6 shows the force values for the feed rate of 0.4 mm/rev. With the exception of the 1.75 m/s speed, the vertical values were largely independent of cutting speed and time. Examination of the axial forces show there to be a variation not only with cutting speed but also as the test proceeded. The 1.75 and 2.13 m/s cutting speeds also gave a steady increase in axial force as the cutting test proceeded. This increase in force correlated with an increase in temperature (figure 6.18) and also in the rate of bulging (figure 6.31).

If the force values are compared with the feed rate of 0.4 mm for Grade TE (figure 6.4) then it can be observed that the vertical force values were essentially similar. However, the axial values were significantly higher than those found for grade TE.

Figure 6.7 shows that the vertical forces were not dependent on either time or cutting speed when the 0.5 mm/rev feed rate was used. The axial forces were found to increase with time and the initial rate of change was found to be speed dependant. This is illustrated when the 2.13 m/s and 1.25 m/s cutting speeds are compared. In the first case the force started to increase immediately; this should be compared with the 1.25 m/s speed where the force only started to increase after 40 seconds of machining. The corresponding temperatures and deformations are given on figures 6.19 and 6.32 respectively.

Figure 6.8 shows the forces for a feed rate of 0.65 mm/rev. The vertical forces were essentially constant for the duration of the tests and the vertical forces were directly related to the cutting speeds.

It can be seen that the highest speed of 1.75 m/s gave a

continuous rise in axial force from the beginning of the test. This corresponded with continuous bulging on the flank face of the tool (see figure 6.33 and an erratic variation in temperature (figure 6.20).

6.2.3 Grade TA5

The forces shown in figure 6.9 were obtained when using a feed rate of 0.4 mm/rev. It can be observed that the vertical forces increased slightly during the test, but they did not show any clear relationship with cutting speed. When the axial forces are examined it can be seen that a steady increase occurred with time and the lowest speed (1.25 m/s) gave the highest axial force.

When the force values are compared for grades TE (figure 6.4) and TTA (figure 6.6) it can be seen that there was little variation in the vertical forces for the range of cutting speeds that were tested.

However, it can be seen that there was a considerable variation in the initial axial forces. Grade TE gave values lying in the range from 440 to 540 newtons, grade TTA gave values in the range from 670 to 930 newtons, and grade TA5 from 480 to 650 newtons. Thus grade TTA gave higher values of axial force.

Figure 6.10 shows the cutting forces for a feed rate of 0.5 mm/rev. With the exception of the 2.5 and 1.0 m/s cutting speeds, the vertical forces were neither speed or time dependant. The axial forces, however, did increase with time, but the 1.25 m/s cutting speed remained essentially constant after an initial increase. In the other cases the influence of cutting speed on the rate of change of force is clearly demonstrated. Higher cutting speeds gave higher rates of change of force earlier in the test. When testing the 2.5

m/s speed, it was necessary to stop the test after 40 seconds; the corresponding temperatures and deformation are given on figures 6.22 and 6.36 respectively. Figure 6.7 shows the corresponding force values for grade TTA. It can be seen that the vertical force values are approximately the same in both cases, however the axial forces are generally lower with grade TA5.

The results shown on 6.11 were obtained for a feed rate of 0.65 mm/rev, and show that the vertical forces were essentially constant with the exception of the 1.75 m/s cutting speed. For the first 20 seconds of the test the results suggest an inverse relationship between the force and cutting speed. With the exception of the 1.75 m/s speed the relationship is maintained for the duration of the tests. It can be seen that the axial forces were essentially constant if the 1.75 m/s speed is excepted. In the case of the 1.75 m/s speed the forces started to rise significantly after 20 seconds of testing and this corresponded with the rise in temperature shown on figure 6.23.

Comparison with the results shown on figure 6.8 shows that the axial cutting forces for grade TTA were generally higher than those found for grade TA5.

Figure 6.12 shows the cutting forces for a feed rate of 0.80 mm/rev. It can be seen that the vertical forces were found to be essentially constant throughout the cutting tests. The higher speeds (1.25 and 1.00 m/s) were found to give the highest vertical cutting forces. This result contrasts with that found for the 0.65 mm feed rate where the opposite trend was found. Examination of the axial forces shows a slight but steady increase for the 1.25 m/s speed and

this was accompanied by continuous bulging on the flank face of the cutting tool (figure 6.38).

6.3 Tool Tip Boundary Temperatures

The average tool/chip interface temperatures are shown on figures 6.13 to 6.24. Each figure represents a constant feed rate and shows the variation of temperature with time and cutting speed. It should be noted that the values shown were those recorded immediately after the engagement of the cut. They represent the maximum temperature recorded by the tool/work thermocouple system and were not influenced by any spurious emf's that might occur at the tip-shank interface. This problem was discussed in section 2.6.2. The values shown for 60 seconds of cutting were obtained by taking an additional cut of approximately 3 seconds duration. This allowed a comparison to be made for any increase in temperature from the start of the previous cut, i.e. the value of temperature shown at 40 secs.

The temperatures on the underside of the tool, at the tip-shank interface, were also recorded any they are discussed in section 6.3.4.

6.3.1 Average Tool/Chip Interface Temperature, Grade TE

Figure 6.13 shows the variation of average temperature with cutting speed for the 0.25 mm feed rate. With the exception of the 3.71 m/s speed all the results show the same trend. An initial rise in temperature was found to occur in the first 10 seconds. This was followed by cutting at a steady temperature or a slight rise at the end of the test. The 3.71 m/s speed caused the temperature to rise rapidly and this was accompanied by a rapid breakdown of the cutting edge.

Figure 6.14 shows a similar trend to figure 6.13; it can be seen that increasing the speed caused an increase in temperature. The highest speed of 4.00 m/s gave a rapid temperature increase after 10 seconds duration and this correlated with the increase in axial force shown on figure 6.2 and a condition of continuous bulging shown on figure 6.26.

Similar trends were observed for the feed rates of 0.35 and 0.4 mm/rev, and are shown on figures 6.15 and 6.16. It can be seen from figure 6.15 that the 4.0 m/s speed gave an increase in temperature as the test proceeded, the increase in temperature being accompanied by a rise in axial force (figure 6.3) and also in the rate of deformation (figure 6.27).

The results shown on figure 6.13 to 6.16 show the influence of feed rate as well as speed on the average cutting temperature. It can be seen that increasing the feed rate for a given cutting speed gave an increase in temperature.

6.3.2 Average Tool/Chip Interface Temperature, Grade TTA

Figure 6.17 shows the influence of cutting speed on temperature for a constant feed rate of 0.35 mm/rev. Each of the speeds gave a similar trend. This consisted of an initial temperature rise in the first 5 seconds, followed by a steady state temperature and finally a further slight rise during the final 20 seconds of the test. It is interesting to note that a 43% increase in cutting speed from 1.75 to 2.50 m/s only increased the average temperature by approximately 80°C. This was, however, sufficient to cause a substantial increase in bulging on the flank face of the tool (figure 6.30).

The results shown on figure 6.18 were obtained for a constant feed rate of 0.4 mm/rev, and the influence of cutting speed on temperature is clearly demonstrated. It can be observed that the two lowest speeds (1.25 and 1.50 m/s) gave only a slight increase in temperature for the duration of their tests. The three highest speeds, however, gave a continuous rise in temperature after 20 seconds of machining, and this was accompanied by a condition of continuous bulging on the flank face of the tool (figure 6.31).

Figure 6.19 displays the results that were obtained for a constant feed rate of 0.5 mm/rev. The general trend of increasing temperature with increasing speed can be observed. The three highest speeds showed a continuous rise in temperature throughout the tests and this was accompanied by a state of continuous bulging on the flank face of the tool (figure 6.32).

The temperatures obtained for the 0.65 mm feed rate are shown on figure 6.20. It can be seen that the highest speed of 1.75 m/s gave an increase in temperature as the test proceeded, and this was accompanied by a state of continuous bulging on the flank face of the tool (figure 6.33). In the case of the three lower speeds, no significant increase in temperature occurred during the tests.

The results shown on figures 6.17 to 6.20 show the influence of feed rate as well as speed on the average cutting temperatures, it can be seen that for a given speed an increase in the feed rate gave an increase in temperature.

6.3.3 Average Tool/Chip Interface Temperature, Grade TA5

Figure 6.21 shows the temperatures that were obtained for a

constant feed rate of 0.4 mm/rev. Each particular speed gave a slight increase in temperature as the tests proceeded and it can be observed that the temperature was found to increase with speed.

Examination of the results shown on figure 6.22 for the 0.5 mm feed rate reveals a similar trend to that found for the 0.4 mm feed rate. In the case of the 2.5 m/s speed it was necessary to stop the test after 40 seconds. It was observed that the tool edge was breaking down catastrophically and the rise in temperature was accompanied by a continuous rise in axial force (figure 6.10).

The results given on figure 6.23 were obtained when testing the 0.65 mm/rev feed rate, with the exception of the highest speed (1.75 m/s) the temperatures were essentially constant throughout the tests.

Figure 6.24 shows the temperatures that were obtained for the 0.80 mm feed rate. In all three cases it can be seen that the temperature remained essentially constant throughout the tests. The higher speeds were observed to give the higher temperatures and this correlated with the amount of bulging on the flank face (figure 6.38).

The relationship between temperature, cutting speed, feed rate and tool grade is shown on figure 8.1. In Chapter 8 a number of empirical relationships between temperature, cutting speed and feed rate are established, and these relationships allow a comparison with data published by other researchers.

6.3.4 Temperatures at the Tip-Shank Interface

The temperature of the tool tip was measured on the underside at the interface with the tool shank. Four thermocouples were inserted

into the tool shank and the arrangement is shown on figure 2.12. The development and evaluation of the measuring system was discussed in section 2.5 and 2.6.1.

Figure 2.13 shows a typical response of the four thermocouples with time. The hottest area on the underside of the tool (trace 1) was found to be below the tool/chip contact region. This result would be expected, because this particular area was located on the shortest path between the heat source on the rake face and the large heat sink represented by the body of the tool shank. The results in table 6.1 show the highest measured temperature ^{o}C (trace 1, figure 2.13) and the elapsed cutting time for a wide range of cutting conditions.

The amount of heat conducted into the cutting tool depends on a number of factors as follows:-

i) the temperature at the tool/chip interface
ii) the area of the tool/chip interface
iii) the thermal conductivity of the tool material.

The previous experimental results showed that the temperature at tool/chip interface was dependant on the cutting speed and the feed rate. Increases in either of these variables caused an increase in average temperature at the tool/chip interface. These increases in temperature at tool/chip interface increased the temperature gradient across the tool and caused more heat to be conducted into the tool. The increased heat conduction raised the temperature at the tip-shank interface.

The total amount of heat conducted into the tool at the tool/chip

Speed m/s	Feed mm	Grade	Average Tool/Chip Contact Temperature °C	Tool/Chip Contact length (mm)	Temperature (°C) at the Tip-Shank Interface for elapsed machining times of 1 to 60 secs								
					1	2	5	10	15	20	30	40	60
4.00	0.25	TE	1175	0.79	25	41	63	94	104	112	129	139	151
2.85	0.25	TE	1050	0.67	26	38	56	84	96	104	119	126	132
2.13	0.35	TE	1020	0.81	27	38	57	86	99	109	126	132	146
2.13	0.35	TTA	995	0.84	38	63	96	107	132	144	158	168	183
1.75	0.50	TTA	1010	1.09	38	64	101	126	140	153	169	181	196
1.75	0.50	TA5	1050	1.17	40	65	103	129	145	157	175	187	203
1.00	0.80	TA5	1000	1.37	38	64	100	127	141	152	172	183	195

Table 6.1 Typical Temperatures at the Tip-Shank Interface

interface was dependant upon the area of contact across which conduction could occur. Increasing the feed rate increased the tool/chip contact area and this allowed an increase in the total amount of heat conducted into the tool.

The rate of heat conduction into the tool is directly related to the thermal conductivity of the tool material. Unfortunately the precise thermal conductivity of the tool materials under investigation was not known. However, by considering their composition (table 5.1) and data published by Brookes (1982, pages 122, 168 and 169), it was possible to deduce the relative thermal conductivity of the three grades that were being investigated. The results in table 5.1 show that the tantalum carbide and the cobalt content for the three grades was essentially constant. The main variation was between the relative proportions of tungsten and titanium carbide. Examination of the data published by Brookes (pages 168 and 169) shows that alloys with a high tungsten carbide content (80 to 90%) have a thermal conductivity of 115 to 120 W/mK. This value can be compared with alloys that have a 60% titanium carbide content and a thermal conductivity of 20 W/mK. The data published by Brookes clearly shows that increasing the ratio of titanium carbide to tungsten carbide greatly reduces the thermal conductivity of the alloy. The data in table 5.1 shows that grade TE had the highest ratio of titanium to tungsten carbide. It may therefore be deduced that this grade had the lowest value of thermal conductivity, and by the same reasoning grade TA5 had the highest value of thermal conductivity.

Examination of the data in table 6.1 shows that grade TE had substantially lower tip-shank interface temperatures than the other two grades. In the case of the 2.13 m/s speed the average tool/chip

interface temperatures and tool/chip contact areas were essentially the same for both grades TE and TTA. There was, however, a significant difference in temperature at the tip-shank interface. This lower temperature associated with grade TE was caused by the lower thermal conductivity of this tool material.

It is possible to determine the influence of tool/chip contact area on the tip-shank interface temperature. Consider grade TE for example, and the results for the combination of a 2.85 m/s speed and a 0.25 mm feed, with the 2.13 m/s speed and a 0.35 mm feed (table 6.1). The average tool/chip interface temperatures were approximately 1050 and 1020°C respectively, and the tool/chip contact lengths were 0.67 and 0.81 mm respectively. Comparison of the data in table 6.1 shows that the higher tip-shank interface temperature occurred for the conditions that had the lowest average tool/chip interface temperature but the highest contact length. It may be concluded that the 21 percent increase in contact length from 0.67 to 0.81 mm, more than compensated for the slight reduction (30°C) in the average tool/chip interface temperature.

The data in table 6.1 shows that for a wide range of conditions at the tool/chip interface the temperature at the tip-shank interface only varied by 70°C. Most of this variation was due to the grade TE which had a lower thermal conductivity. If grade TE is excepted then the variation in temperature at the tip-shank interface for the other two grades was approximately 20°C. If the variation in temperature for grade TE alone is considered then a similar difference of approximately 20° can be observed. This small variation was surprising because the cutting conditions gave a variation of approximately 155°C at the tool/chip interface. Such a small variation

in the tip-shank interface temperature is further evidence of the low thermal conductivity of this particular grade (TE).

The results in table 6.1 suggest that an increase in temperature at the tool/chip interface increased the temperature gradient across the tool, because the temperature at the underside remained essentially constant. If the tool material has a low thermal conductivity then the temperature gradients will be higher. The effect of the increased temperature gradients was to raise the temperature of the tool in the regions immediately below the tool/chip interface, and also on the flank face immediately below the cutting edge.

6.4 Deformation (Bulging) of the Flank Face

The deformation on the flank face below the cutting edge was measured and recorded using a Talysurf surface measuring instrument. The technique and the method of interpreting the results was discussed in section 4.3.3. The maximum deformation or bulging on the flank face was found to occur at the bottom of the wear land.

The bulging is represented by two different methods. The first method shows the deformation as a function of time for different values of speed and feed. The second method gives the deformation after 60 seconds and is shown as a function of feed and speed. This latter technique was similar to a method used by Trent (1959). Trent, However, did not quantify the deformation, he expressed it as either small or severe.

6.4.1 Grade TE

Figures 6.25 to 6.28 show the flank face bulging for the various

combinations of speed and feed. In the case of the 0.25 mm feed rate (figure 6.25) the cutting speeds of 3.25 m/s or less had little or no influence on the amount of deformation during the first 40 seconds of the test. During the last 20 seconds a small increase was observed for all of these speeds. The results suggest that there exists a critical speed greater than 3.25 m/s at which the cutting edge becomes unstable. This is confirmed by the large amount of deformation which occurred at 3.71 and 4.0 m/s. In the former case it was necessary to stop the test after 20 seconds due to a rapid rise in axial force, which was accompanied by a rapid increase in temperature. Examination of the tool revealed a large amount of wear at the tool nose. The tool used at 4.0 m/s sustained a similar amount of deformation but did not experience the dramatic rise in temperature or force, so it was possible to complete the test.

Figure 6.26 shows the deformation for the 0.3 mm feed rate. The two lower speeds did not give any significant deformation even though the feed rate had been increased. The 3.25 m/s speed was sufficient to cause continuous steady deformation of the tool, with the rate increasing slightly during the last 20 seconds. Examination of the 4.0 m/s speed reveals a result similar to that found for the 3.71 m/s speed when the feed rate was 0.25 mm/rev.

The results shown on figure 6.27 have a distinctive pattern for the speeds of 2.5, 2.85 and 3.25 m/s. They were characterised by a high rate of deformation for the first 5 seconds, which was then followed by a reduced rate for the next 35 seconds. The final 20 seconds gave an increase in the rate of deformation. When the 4.0 m/s speed was investigated the results were similar to those for the 0.25 and 0.3 mm feeds, and the test was suspended after 40 seconds.

The results shown on figure 6.28 were obtained using the 0.4 mm feed rate. Because the 4.0 m/s cutting speed caused an unstable cutting edge in the previous tests, it was decided to use a lower range of speeds for this particular feed rate. The results had a pattern similar to that found for the 0.35 mm feed. The 2.85 m/s and 2.5 m/s speeds gave identical deformation patterns for the first 20 seconds, however during the remaining part of the test the 2.85 m/s speed gave a higher rate of deformation. This was accompanied by a small but definite rise in both axial and vertical force (figure 6.4).

Figure 6.29 shows the combined influence of speed and feed rate on bulging at the flank face and depression of the cutting edge (shown in brackets, see section 6.5). The upper values represent the results that were obtained with the periodic incremental tests of 5, 5, 10, 20 and 20 seconds, and the lower values are the results that were obtained by a continuous test of 60 seconds (see section 5.7).

If a constant value of feed is chosen then an increase in deformation with speed can be clearly identified. Similarly, an increase in feed rate for a constant speed caused increased deformation. The lines shown on figure 6.29 represent combinations of feed and speed that give a constant metal removal rate. The amount of deformation (bulging) can be put into three classes as follows:

i) Class 1 where the total deformation was equal to or less than 2 μm, this class had limiting values of 3.25 m/s for speed and 0.4 mm for feed.

ii) Class 2 was bounded by the constant metal removal rate lines

and corresponded to deformation of 2 to 9 μm. It was found that the speed was again limited to 3.25 m/s and the feed to 0.4 mm/rev. When these conditions were used, the cutting edge was considered to be at the limit of its stability.

iii) Class 3 deformation occurred when the cutting edge was completely unstable and was caused by speeds in excess of 3.71 and 4.0 m/s. Under these conditions it was often necessary to stop the test prematurely because the cutting edge had completely failed. The influence of feed rate was investigated up to a value of 0.44 mm, which far exceeded the manufacturer's recommended value of 0.25 mm for this particular grade of carbide (see section 5.4.2 and table 5.2).

Comparisons of the results for the continuous and periodic incremental tests showed that in most cases there was no substantial difference in the amount of bulging.

6.4.2 Grade TTA

Figure 6.30 shows the bulging on the flank face for the speeds of 1.75, 2.13 and 2.50 m/s. The two highest speeds gave a similar trend. This consisted of an initial rapid deformation rate followed by a reduced rate of bulging,and in the case of the highest speed, a further increase in the deformation rate.

The results shown on figure 6.31 are for a constant feed and a wide range of speeds; the influence of speed on deformation is clearly demonstrated. In the case of the 2.5 m/s speed, the tool was found to bulge at a very rapid rate, which was coincidental with a rise in axial force and average temperature (figures 6.6 and 6.18).

Examination of the results for the 0.5 mm feed rate (figure 6.32) clearly shows the influence of cutting speed on deformation. In the case of the three highest speeds, 1.75, 2.13 and 2.5 m/s, it can be seen that the tool was beyond the limit of its stability. In each of these cases the flank face was bulging at a very high rate. The three lower speeds of 1.00, 1.25 and 1.5 m/s exhibited much more stability.

Figure 6.33 displays the results that were obtained for a constant feed rate of 0.65 mm/rev. The highest cutting speed (1.75 m/s) gave an almost continuous breakdown of the cutting edge and this was accompanied by a rapid rise in the axial cutting force. The deformation at the two lower speeds occurred in a more controlled manner. However, a 25% increase in speed from 1.00 m/s to 1.25 m/s was sufficient to cause a substantial increase in both the amount and the rate of bulging.

Figure 6.34 shows the influence of feed and speed on flank bulging and edge depression for the incremental and continuous tests. If a constant value of feed is chosen then the influence of cutting speed on flank face deformation can be clearly identified. Similarly, if a constant speed is chosen then an increase in feed can be seen to increase the amount of deformation. The lines shown on figure 6.34 represent lines of constant metal removal rate for particular combinations of feed and speed. The amount of bulging can be classified as follows:-

i) Class 1 deformation occurred when the bulging was generally equal to or less than 3 μm.

ii) Class 2 was bounded by the two lines shown and the deformation was found to be within the range of 5 to 13 μm. Under these circumstances the cutting edge was operating within the limit of its stability.

iii) Class 3 deformation represented a continuous breakdown of the tool and was nearly always accompanied by a rise in temperature and axial force. It should be appreciated, however, that the highest speeds (2.13 and 2.5 m/s) far exceeded the values recommended by the manufacturers for this grade when rough turning (see table 5.2 and section 5.4.1).

Generally it was found that the continuous and incremental tests gave approximately the same amount of deformation and edge depression when identical values of feed and speed were tested.

6.4.3 Grade TA5

The deformations shown on figure 6.35 were obtained for a feed rate of 0.4 mm/rev, and the influence of cutting speed on the deformation is clearly shown.

Figure 6.36 shows the results for a wide range of speeds and a constant feed of 0.5 mm/rev. It can be observed that the two highest speeds of 1.75 and 2.5 m/s caused the tool to deform at an almost constant rate. The limiting cutting speed for the tool to remain stable was 1.25 m/s.

Examination of the results for the 0.65 mm feed (figure 6.37) suggests that there was a critical speed between 1.0 and 1.25 m/s that caused the tool to deform plastically. The highest speed of

1.75 m/s was sufficient to cause a continuous breakdown of the tool and this was accompanied by a continuous rise in both axial force and temperature (figures 6.11 and 6.23).

The results shown on figure 6.38 were obtained for a feed rate of 0.80 mm. As in the previous case (0.65 mm feed), the influence of cutting speed can be clearly identified. It would appear that there is a critical speed greater than 1.00 m/s which is sufficient to cause the tool to become unstable. It should be noted that although the highest speed of 1.25 m/s caused a continuous breakdown of the tool, there was not an increase in either the axial force or the temperature. In the case of the lowest speed (0.75 m/s) the deformation was imperceptable even though the cutting forces were essentially the same (figure 6.12). There was, however, a lower temperature (figure 6.24) and this may have been sufficient to allow the tool to resist any significant deformation.

Figure 6.39 summarizes the results in a similar manner to that shown on figures 6.31 and 6.36 for grades TE and TTA. The same general observations can be made regarding the influence of increasing either the speed or the feed rate. However, there was a minimum limiting speed of 0.75 m/s below which very little deformation (2 μm) occurred. This condition occurred even though the feed (0.95 mm/rev), and therefore the forces, were very high and is represented by speeds of 0.5 and 0.75 m/s with a feed 0.95 mm/rev (figure 6.39).

The amount of bulging can be classified in a manner similar to that for the other two grades as follows;-

i) Class 1 deformation which occurred when the bulging was equal to or less than 3 μm.

ii) Class 2 deformation was in the range from 3 to 10 μm.

iii) Class 3 deformation occurred when the cutting conditions vave a total amount of bulging greater than about 10 μm.

It should be observed that when cutting with stable conditions there was not a significant difference between the amount of bulging obtained by either continuous or incremental cutting.

The constant metal removal rate lines shown on figures 6.29, 6.34 and 6.39 were obtained for a 2 mm depth of cut, which was constant for the three grades that were tested. It can be observed that the threshold point for deformation was dependant on the grade and its hardness. Grades TA5, TTA and TE had hardness values of 1550, 1575 and 1600 (VPN) respectively, and the corresponding threshold values were 1000, 1250 and 1700 mm^3/sec. The upper limits were found to be 1625, 1750 and 2280 mm^3/sec respectively.

6.5 Depression of the Cutting Edge

The technique used for measuring the depression of the cutting edge was discussed in section 4.3.4. Figures 6.40 and 6.41 show typical traces taken on the rake face of a tool tip. The traces show both cutting edge depression and crater wear. It was found that the cutting edge was displaced relative to the original rake surface in either a parallel (P) or tapered (T) manner. Figures 6.40 and 6.41 show parallel and tapered displacements respectively. The amount of displacement was measured from the original rake face, and in the tapering case the maximum amount was determined at the cutting edge.

Because the cutting tests were of a short duration, little or no wear was found to occur immediately adjacent to the cutting edge. The amount of displacement was therefore regarded as representing the true depression of the cutting edge.

The data given in brackets on figures 6.29, 6.34 and 6.39 shows the amount of edge depression (μm) for the combinations of speed, feed and grade that were tested. The upper and lower values were obtained for the incremental and continuous tests respectively.

6.5.1 Grade TE

The results shown on figure 6.29 indicate that the amount of edge depression was not as sensitive to changes in cutting conditions as was the amount of bulging. A certain amount of edge depression occurred even when the bulging was either zero or minimal. The tapering type of edge depression was found to occur with the combinations of cutting conditions that gave the highest metal removal rates.

Figures 6.42 to 6.45 show the edge depression plotted against time for grade TE. Generally the amount of depression was found to fall into three categories. Usually there was a high rate of depression during the first 5 to 10 seconds. This was then followed either by zero depression for the remainder of the test, or an increase during the final 20 seconds of machining. When the higher speeds were used (4.0 and 3.71 m/s), it was found that the cutting edge was being depressed continuously and it was necessary to stop the test prematurely (see section 6.2.1, and figures 6.1 and 6.2).

6.5.2 Grade TTA

Figure 6.34 shows the amount of edge depression for grade TTA. Tapering type of edge depression was found to occur more frequently than the parallel type. With the exception of the 1.25 m/s speed, tapering type of depression occurred for all the 0.5 and 0.65 mm feed rates that were tested.

Figures 6.46 to 6.49 show the edge depression plotted against time for grade TTA. The results show a similar trend to grade TE, consequently it was possible to put the depression into 3 distinct categories. It was found that the feeds of 0.4 and 0.5 mm/rev and their associated speeds gave the largest amount of edge depression. The highest speeds of 2.13 and 2.5 m/s were sufficient to cause a condition of continuous edge depression when they were used in combination with the 0.4 and 0.5 mm feed rates.

6.5.3 Grade TA5

The results shown on figure 6.39 were obtained for grade TA5. With the exception of the 1.25 and 1.5 m/s speeds at the 0.4 mm/rev feed rate, all the edge depression was of the tapering mode. If a constant feed rate was considered then the influence of speed on edge depression was clearly demonstrated. Consider the 0.5 mm/rev feed rate for example, the 1.0 m/s speed gave an edge depression of 15 μm whereas the 1.75 m/s speed gave 35 μm edge depression. This trend was sustained for all the feed rates that were tested. A similar trend was observed for constant speed and increasing feed rate, However the lowest speed of 1.0 m/s was not found to be as sensitive to increases in feed rate.

Figures 6.50 to 6.53 show the edge depression as a function of

time and speed for the different feed rates. These results show the same general trend as the other two grades. However, the region of zero depression rate during the central part of the test was much reduced for many of the speeds and feeds that were tested. This condition was particularly illustrated when the 0.5 and 0.65 mm feed rates were tested.

6.6 Wear on the Clearance Faces

The wear on the clearance faces beneath the tool nose radius and the side cutting edge was measured using a special fixture and a tool-makers microscope (see section 4.4.2). Generally it was found that the conical surface beneath the nose radius sustained more wear than tha flank face beneath the side cutting edge. The extent of the wear marks were recorded on a special chart (figure 4.11) which incorporated the wear on both the conical and flank surfaces.

A number of different wear patterns were observed and they are shown diagrammatically on figure 6.54 as follows:-

A) Conical Surface

(i) Even wear below the tool nose radius which extended from the flank face around the conical face towards the end clearance face. Designated by the symbol "E".

(ii) Variable wear on the conical surface usually with the maximum at 45^{o}. Designated by the symbol "45".

(iii) Very heavy wear with a maximum at 45^{o} but showing two distinct wear surfaces. This condition was usually associated with the total breakdown of the tool. Designated by the symbol "2".

B) Flank Surface

(i) Even wear along the flank face with the wear mark parallel to the cutting edge. Designated by the symbol "E".

(ii) Even wear in the region of the chip outer edge, but also having a transition region which connected with the longer wear scar on the conical surface. Designated by the symbols "ET".

(iii) Tapered wear on the flank face which connected very little wear at the chip outer edge to the very heavy wear at 45^{o} on the conical clearance face. Designated by the symbols "TR".

Different combinations of wear were found to occur on the conical (No) and flank (Fl) surfaces. When stable cutting conditions existed the most common combination was of even (E) wear on the conical surface with transition to even (ET), but less wear on the flank surface. The most common wear combinations are shown on figures 6.55 to 6.60. The amount and type of wear that was sustained during the various tests is given in tables 6.1, 6.2 and 6.3 for grades of TE, TTA and TA5 respectively, and is discussed in the following sections.

6.6.1 Grade TE

The data shown in table 6.2 represents the results after 60 seconds of machining for both the incremental and continuous test procedures. The influence of high cutting speeds (4.00 and 3.71 m/s) on nose (No) and flank (Fl) wear is clearly shown. Under these conditions the cutting edge was unstable and the maximum wear occurred at 45^{o}. In the case of 4.00 m/s speed and 0.30 mm/rev feed, two distinct wear patterns could be observed on the nose, see figure 6.55.

FEED RATE				CUTTING SPEED m/s											
				4.00		3.71		3.25		2.85		2.50		2.13	
	0.25 mm/rev	INCREMENTAL	fl No lc Kt	50 200 0.79 40	E 45 3.16 20P	- 400 0.71 0	TR 2 2.84 5P	70 220 0.70 35	ET E 2.80 10P	80 180 0.67 15	E E 2.68 10P	0 120 0.68 0	- E 2.72 10P		
		CONTINUOUS	fl No lc Kt	70 300 0.80 40	E E 3.20 15P	- 510 0.96 0	TR 2 3.84 20P	0 230 0.62 30	- E 2.48 10P	80 80 0.60 15	E E 2.40 10P				
	0.30 mm/rev	INCREMENTAL	fl No lc Kt	60 512 0.80 30	TR 2 2.67 20P			60 240 0.60 25	ET E 2.00 20P	20 190 0.68 20	ET E 2.27 10P	50 150 0.71 15	ET E 2.37 10P		
		CONTINUOUS	fl No lc Kt					60 270 0.80 70	ET E 2.67 25P	30 210 0.66 30	E E 2.20 15P	60 150 0.76 15	ET E 2.53 10P		
	0.35 mm/rev	INCREMENTAL	fl No lc Kt	- 580 0.97 40	TR 45 2.77 25T			0 300 1.01 35	- E 2.88 15T	80 240 0.92 15	TR E 2.63 15T	50 170 0.87 30	E E 2.49 10P	30 140 0.81 10	E E 2.31 5P
		CONTINUOUS	fl No lc Kt	- 530 1.06 37	TR 45 3.03 15P			60 150 1.05 70	ET E 3.00 30T	0 240 0.90 20	- E 2.57 10P	60 220 0.88 22	ET 45 2.51 10P	50 140 0.83 10	ET E 2.37 5P
	0.40 mm/rev	INCREMENTAL	fl No lc Kt							40 240 1.02 40	ET E 2.55 20P	30 270 0.95 20	TR E 2.38 2ST	40 40 0.98 20	E E 2.45 10P
		CONTINUOUS	fl No lc Kt							60 280 1.06 40	ET E 2.65 20P	40 300 0.96 25	E E 2.40 10T	20 80 0.90 20	E E 2.25 10P

TABLE 6.2, WEAR PATTERNS FOR GRADE - TE

FEED RATE				CUTTING SPEED, m/s											
				2.50		2.13		1.75		1.50		1.25		1.00	
	0.35 mm/rev	INCREMENTAL	fl	-	TR	90	ET	80	ET						
			No	360	E	300	E	170	E						
			lc	0.89	2.54	0.84	2.40	0.74	2.11						
			Kt	30	10P	25	12T	15	10P						
		CONTINUOUS	fl	-	TR	340	E	90	ET						
			No	400	E	340	E	180	E						
			lc	0.90	2.57	0.87	2.49	0.83	2.37						
			Kt	50	25T	40	20P	30	10P						
	0.40 mm/rev	INCREMENTAL	fl	-	TR	-	TR	20	ET	200	E				
			No	300	45	500	45	210	45	200	E	210	E		
			lc	1.04	2.60	1.03	2.57	0.83	2.07	0.77	1.93	0.95	2.37		
			Kt	45	50T	35	30T	5	25P	0	10P	0	30T		
		CONTINUOUS	fl	-	TR	8D	ET	20	E	20	E	30	ET		
			No	32D	45	320	E	280	E	70	E	110	E		
			lc	1.07	2.67	1.01	2.53	0.82	2.05	0.81	2.02	0.90	2.25		
			Kt	50	45T	35	25T	5	20P	10	15P	0	30T		
	0.50 mm/rev	INCREMENTAL	fl	-	TR	-	TR	100	ET	80	ET	50	ET	ET	
			No	750	45	570	45	500	45	330	E	260	E	E	
			lc	1.52	3.04	1.02	2.04	1.09	2.18	0.97	1.94	0.92	1.98	1.08	2.16
			Kt	45	30T	40	50T	0	15T	10	15T	0	10T	0	10T
		CONTINUOUS	fl	-	TR	-	TR	30	ET	90	ET	60	ET	ET	
			No	710	45	500	45	270	E	300	E	250	E	E	
			lc	1.56	3.12	1.22	2.44	1.08	2.16	0.84	1.68	1.03	2.06	1.05	2.10
			Kt	60	40T	50	65T	25	25T	0	15T	0	10T	0	15T
	0.65 mm/rev	INCREMENTAL	fl					50	ET	50	ET	0	-	50	ET
			No					270	E	220	E	200	E	240	E
			lc					1.40	2.15	1.25	1.92	1.21	1.86	1.19	1.83
			Kt					25	20T	30	30T	0	5P	20	
		CONTINUOUS	fl					-	TR	60	ET	0	-	60	ET
			No					820	45	210	E	150	E	300	E
			lc					1.28	1.97	1.43	2.20	1.47	2.26	1.20	1.85
			Kt					30	25T	30	25T	0	5P	0	

TABLE 6.3, WEAR PATTERNS FOR GRADE - TTA

FEED RATE				CUTTING SPEED, m/s									
				1.75		1.50		1.25		1.00		0.75	
	0.40 mm/rev	INCREMENTAL	fl	50	ET	50	ET	30	E				
			No	150	E	100	E	80	E				
			lc	1.04	2.65	0.99	2.48	0.97	2.43				
			Kt	25	20T	15	10P	0	10P				
		CONTINUOUS	fl	110	E	50	ET	30	E				
			No	160	E	130	E	70	E				
			lc	1.08	2.70	1.06	2.65	1.01	2.52				
			Kt	25	20T	25	12P	0	15P				
	0.50 mm/rev	INCREMENTAL	fl	50	ET	50	ET	50	ET	50	ET		
			No	300	E	170	E	190	E	90	E		
			lc	1.17	2.34	1.13	2.26	1.05	2.10	1.06	2.12		
			Kt	50	35T	30	30T	10	20T	0	15T		
		CONTINUOUS	fl	30	ET	60	ET	80	ET	70	E		
			No	340	E	120	E	200	E	70	E		
			lc	1.26	2.52	1.20	2.40	1.31	2.62	1.23	2.46		
			Kt	40	40T	40	35T	12	10T	0	15T		
	0.65 mm/rev	INCREMENTAL	fl	-	TR	50	ET	60	ET	0	-		
			No	470	45	210	E	160	E	170	E		
			lc	1.31	2.01	1.12	1.72	1.20	1.85	1.22	1.88		
			Kt	75	120T	30	30T	0	30T	0	20T		
		CONTINUOUS	fl		TR	70	ET	80	ET	0	-		
			No	500	45	230	E	120	E	160	E		
			lc	1.33	2.05	1.28	1.97	1.35	2.08	1.21	1.86		
			Kt	80	100T	30	40T	0	30T	0	15T		
	0.80 mm/rev	INCREMENTAL	fl					70	ET	50	ET	0	-
			No					150	E	140	E	60	E
			lc					1.47	1.84	1.37	1.71	1.31	1.63
			Kt					0	55T	0	20T	0	10T
		CONTINUOUS	fl						TR	80	ET	0	-
			No					300	45	170	E	70	E
			lc					1.39	1.74	1.38	1.73	1.35	1.69
			Kt					0	35T	0	45	0	10T

TABLE 6.4, WEAR PATTERNS FOR GRADE - TA5

A reduction in speed to 3.25 m/s allowed a transition to more stable cutting and the wear pattern in the nose region to become even. Although there was some anomalies in the results, certain general trends could be observed as follows. By decreasing the speed it was found that the nose wear was reduced when the feed rate was constant. Similarly, if the speed was held constant then an increase in nose wear occurred with increases in feed rate. The 2.13 m/s speed and 0.40 mm/rev feed combination was, however, an exception. In many cases, even wear on the nose was accompanied by even wear on the flank which was usually one sixth to one third of that on the nose (figure 6.56). There were occasions, however, when no flank wear occurred; consider for example 2.50 m/s speed and 0.25 mm feed combinations (figure 6.57) and also the 3.25 m/s speed and 0.35 mm feed. Comparison of the results for the incremental and continuous tests did not reveal any consistent difference in the amount of wear.

6.6.2 Grade TTA

Table 6.3 gives the results for grade TTA. The three highest speeds of 1.75, 2.13 and 2.50 m/s when combined with the 0.5 mm feed rate were sufficient to cause excessive nose wear. They gave values of 500, 570 and 750 μm respectively, with the maximum value occurring at 45^{o} (see figure 6.58). The wear was such that it extended into the flank face and tapered to a minimum at the outer edge of the chip. Similar high rates of wear were found for the continuous tests when using the conditions given above. The 1.75 m/s cutting speed combined with the 0.35 and 0.4 mm feeds gave a reduction in nose wear and a more even wear pattern on the flank face (figure 6.59). However, at this particular speed the nose wear was observed as being feed rate dependant. Increases in cutting speed generally gave an increase in nose wear; a variation from the general trend was observed when the

0.65 mm feed was tested incrementally. The three lower speeds of 1.0, 1.25 and 1.5 m/s were found to give values of nose wear between 200 and 260 μm for the majority of the tests. With one exception (V = 1.50, f = 0.4) the corresponding flank wear values were between 0 and 90 μm. A condition of zero flank wear occurred for the 1.25 m/s speed and 0.65 mm feed in both the incremental and continuous tests (see figure 6.60). Where a comparison with grade TE was possible, it was found that grade TTA sustained more wear than grade TE.

6.6.3 Grade TA5

The data in table 6.4 was obtained for grade TA5. The results show that for a constant feed rate, reductions in cutting speed generally gave a reduction in nose and flank wear. The exceptions to this were the 1.50 m/s speed at a feed rate of 0.5 mm and the 1.25 m/s speed at a feed rate of 0.65 mm. When the 1.00 m/s speed was tested, it was found that increasing the feed rate from 0.65 to 0.8 mm did not cause a significant change in the nose wear. Similar observations were made for the 1.25 m/s speed and the above feed rates of 0.65 and 0.80 mm. The continuous test using the latter feed rate caused a tool nose wear value of 300 μm, which was exceptional for the speeds and feeds being used.

When compared with the other two grades the wear marks on the flank and conical surfaces were found to be more evenly distributed. Excessive wear on the nose at 45^{o} was only observed in two tests, they were 1.75 m/s at a feed rate of 0.65 mm and 1.25 m/s at a feed rate of 0.8 mm; the latter case may have been exceptional. Comparisons of wear patterns for the incremental and continuous tests showed that the flank faces tended to sustain slightly more wear in continuous testing. When the nose wear was examined, such a tendency was not

found. A comparison between grades TTA and TA5 for similar cutting conditions shows that neither grade consistently sustained a larger amount of wear.

6.7 Tool/Chip Contact Length

The tool/chip contact length (l_c) was measured using a toolmakers microscope. It was taken as the most extreme point of chip departure from the cutting edge and is discussed in section 7.2. In some cases it was quite difficult to determine the exact point of chip departure from the rake face. This was particularly the case when low speeds were used and a definite crater or rubbing mark could not be easily identified. A method of checking these results was discussed in section 4.4.4.

The results are shown in tables 6.2, 6.3 and 6.4 for the three grades TE, TTA and TA5 respectively. The measured tool/chip contact length (l_c) is expressed in mm. Also shown adjacent to l_c is the contact length expressed as a ratio of the respective feed rate.

A number of general trends can be observed when the contact length is considered as a function of speed, feed and the type of grade.

6.7.1 Grade TE

The results given in table 6.2 show that for a constant feed there was generally a reduction in contact length with a reduction in cutting speed. With one or two exceptions, this trend was found to apply for all the feeds that were tested. When the 4.0 and 3.71 m/s speeds were tested it was found that the contact length to feed ratio exceeded the value of 3:1 for the 0.25 mm feed rate. These values

should be compared with the ratios found for the lower speeds (2.5 and 2.13 m/s) and higher feeds (0.35 and 0.4 mm) where ratios in the range 2.25 to 2.51:1 were typical. If the two highest speeds are excepted the ratio of contact length to feed rate was in the range of 2.20 - 3.00:1.

6.7.2 Grade TTA

Table 6.3 contains the results that were obtained for grade TTA. It can be seen that for the constant feed, the contact ratio generally decreased with the cutting speed. The 1.50 and 1.25 m/s speeds gave a slight reduction in the contact ratio with increases in feed from 0.4 to 0.5 mm/rev. The combined influence of speed and feed is clearly indicated if a combination of high speed and low feed (2.5 m/s, 0.35 mm), is compared with a combination of low speed and high feed (1.25 m/s, 0.5 mm). Under these conditions the contact ratio changed from approximately 2.5 to 2.0:1 respectively.

6.7.3 Grade TA5

Table 6.4 shows the results that were obtained for grade TA5. It can be observed that a decrease in cutting speed gave a decrease in contact ratio for the two lower feed rates of 0.4 and 0.5 mm. These results for the two highest feeds did not indicate a clear trend that could be related to the cutting speed. If a constant speed was considered, then a definite reduction in the contact length to feed ratio could be identified for increases in feed rate. Take for example the 1.75 m/s speed and the 0.4 mm feed; the contact ratio was 2.65 and 2.70 respectively for the incremental and continuous tests. These values should be compared with the 0.65 mm feed rate that gave values 2.01 and 2.05. This same general trend was found to occur for the five values of speed that were tested.

6.7.4 Comparison of Chip Contact Lengths for Different Grades

The tool/chip contact length (l_c) and its ratio to the feed rate is shown on figure 6.61 for the different grades and cutting conditions.

The results show that grade TTA gave longer contact lengths than grade TE and grade TA5 gave longer contact lengths than TTA. If grades TE and TTA are compared for say the 0.35 mm feed and the 2.50 and 2.13 m/s speeds, then a small but definite increase in contact length was found for grade TTA. A similar effect was found for the 0.4 mm feed rate when the speeds of 2.5 and 2.13 m/s were compared. When grades TTA and TA5 were compared for feed rates of 0.4 and 0.5 mm with speeds of 1.75, 1.50 and 1.25 m/s, then the contact length was higher for grade TA5. It should be noted that the increase in contact length was not sustained for the 0.65 mm feed rate.

CHAPTER 7

FINITE ELEMENT MODEL

7.1 Introduction

Finite Element (F.E.) techniques are used in situations that are too complex for analytical solutions to be applied. These techniques can be used for both the thermal analysis and the stress analysis of engineering problems. A cutting tool is subject to complex thermal and mechanical loads and cannot be adequately analysed using the standard techniques.

The F.E. package used for this work was supplied by PAFEC (Programme for Automatic Finite Element Calculations), and was available for use on NUMAC (Northern Universities Multiple Access Computer). This computer was an AMDAHL Model 5860 and was extremely powerful (approximately 5 times faster than an IBM Model 370). The package had been substantially modified and developed by Mr J Chan (1983), who has produced a stress smoothing routine (see sections 1.7.1 and 7.11). Some of these modifications have now been adopted by the suppliers. The package consisted of a collection of modules, each of which was capable of performing certain functions. Modules existed for calculating transient and steady state temperature distributions and also for performing both linear (elastic) and non-linear (plastic) stress analysis. It was also possible to vary the properties of a material with temperature. This was an essential feature when analysing the cutting tool, because it was subjected to large variations in both temperature and stress.

7.2 Finite Element Model

Figure 7.1 shows a 3D view of the carbide cutting tool with its co-ordinate axes. The tool was 19 mm x 19 mm x 5 mm, and a 0.8 mm nose radius was ground on each corner. To produce a F.E. model of the cutting tool it was necessary to make a number of assumptions about the cutting process. By making these assumptions it was possible to reduce the complex 3D cutting process to a 2D process and thereby keep the model within the computing capacity of NUMAC.

The most significant assumptions are given below:-

(i) the chip/tool temperature distribution was uniform in the z direction;

(ii) the stress distribution was uniform in the z direction;

(iii) the radial cutting force was small compared with the other forces.

(iv) the nose radius was small in relation to the depth of cut.

These assumptions may be justified as follows:-

(i) Usui (1984) has investigated the chip/tool temperature distribution. It was found that the variation in temperature was much greater in the direction of chip flow than across the chip.

(ii) With regard to the stress distribution, it was found that the chips had a reasonably rectangular cross-sectional area. There was some tapering on the inner most edge of the chip, caused by the tool nose radius. If the chip cross-section was reasonably rectangular

then it can be assumed that the forces across the section were essentially uniform.

(iii) With regard to the radial force, it was found that for a sharp tool (used at the beginning of each test), the radial force was approximately half the axial (or horizontal) force. The radial forces were measured during the tests, but the results have not been presented.

(iv) The influence of nose radius on tool deformation has not been investigated. The effect of increasing the nose radius is to reduce the undeformed chip thickness, a similar effect being created by increasing the plan approach angle (Taylor 1906). Figure 7.2 shows the change in cross-section of the undeformed chip when the plan approach angle is varied and a nose radius is added to the tool. The bulging and edge depression were measured at a cross-section on the cutting tool which corresponded to the central part of the chip width. This section was some distance from the nose radius, which was constant throughout the cutting tests. It was considered that its influence was constant throughout the cutting tests. Although it was felt to be desirable to incorporate the nose radius into the model, for the reasons given above it was not considered to be essential.

The model was given a thickness of 2 mm in the z direction, which was equal to the nominal depth of cut used in the cutting tests. It was expected that width of the chip would be greater than the nominal depth of cut for the following two reasons. Changing the plan approach angle decreases the thickness of the undeformed chip but

correspondingly increases its width. Some spreading of the undeformed chip in the direction of its width occurs during machining, however the results shown on figures 4.16 to 4.18 show that the maximum width of the tool/chip contact area was essentially constant at 2 mm. It would appear that any differences between the maximum width of the tool/chip contact area and the nominal depth of cut were minimal.

The results represented on figures 4.16 to 4.18 show that the measured tool/chip contact area had a complex shape. The boundary that represented the point of chip departure was not parallel with the cutting edge. This effect was caused by a combination of effects, as follows. The temperature and stress distributions were not perfectly uniform in the direction perpendicular to the chip flow. The direction of chip flow was not perfectly perpendicular to the cutting edge, caused by the influence of the nose radius. These effects acting together influenced the distance of the boundary from the cutting edge.

To apply the tool/chip contact length to the F.E. model it was necessary to apply a consistent criterion to the recorded data. The choice existed between using some mean or average value from the cutting edge or the point that was furthest from the cutting edge. The choice of an average value seemed attractive because it would allow some accommodation of variations that might naturally occur in the cutting process. This option was rejected because the boundaries were found to taper continuously towards the cutting edge. To determine the position of the chip departure would require a subjective judgement.

It was decided to take the chip departure point (l_c) as the most

extreme point from the cutting edge, as shown on figure 4.16. It was appreciated that on occasions this may have caused an underestimate in the calculated applied stress at the tool/chip contact region, because it overestimated the contact area. The principal advantage of using this criterion was that the extreme point could be more easily defined. If this value was always used then the results would be calculated on a consistent basis, thus allowing different cutting conditions to be compared.

As a result of these assumptions and simplifications it was possible to produce a 2D model of the cutting tool. The F.E. package had the facility to carry out either a plane stress or a plane strain analysis, which was achieved by allowing σ_z and ϵ_z to equal zero respectively (figure 7.1).

The F.E. technique essentially consists of dividing the component to be analysed into a mesh of discrete elements that have suitable properties for the analysis being attempted. For example, a different type of element was required for a thermal analysis than for a stress analysis. To obtain the necessary accuracy the mesh was made finer at points of high stress concentration or of high thermal gradients. In the case of a cutting tool this was at the chip/tool interface region. Care was taken to avoid an excessively fine mesh in the regions of low stress, because this gave a large number elements and lead to an excessive amount of computer time being required for the solutions. Two-Dimensional (2D) type elements were used in the model with a thickness of 2 mm, which was equal to the depth of cut. Although it was desirable to use 3D type elements, it was found to be impracticable, because 3D elements required an excessive amount of computing time. In most cases it was necessary to use up to 1800

seconds of cpu (central processing unit) time to carry out a 2D plastic analysis of the cutting tool (see section 7.12).

A diagram of the initial F.E. model is shown on figure 7.3, the overall dimensions being 19 mm long by 5 mm high. PAFEC had a facility for the automatic generation of the mesh, called Pafblocks, which allowed the sides of the model to be automatically divided into the proportions shown on figure 7.3. The flank and rake face regions close to the cutting edge were covered with a fine mesh (see sections 7.9 and 7.10).

7.3 Selection of Cutting Force Distribution

Chan and Braiden (1981) simplified the distribution proposed by Zorev (1963) and Kato (1972); they used a linearly decreasing force distribution for the normal force. The shear force was applied by using a combination of linear loading for the chip sticking region and linearly decreasing load for the sliding region. Tlusty and Masood (1978) applied loads using a distribution similar to the one suggested by Barrow (1982). As a starting point for this particular work the measured cutting forces were applied to the F.E. model by using two different force distributions; they were the simplified linearly decreasing distribution (Chan and Braiden, 1981) and the distribution by Barrow (1982).

7.4 Selection of Temperature Distribution at the chip/tool interface

The shape of the temperature distribution at the chip/tool interface has been investigated by Trigger (1961), Usui (1984) and Dearnley (1983). The merits and limitations of the techniques used by these researchers is discussed in sections 1.5.1, 2.1.3 and Appendix 3.

Before any of these distributions could be used in a F.E. model, it was necessary to quantify their particular shape and to express it as a function of the tool/chip contact length. Trigger investigated a range of 3 cutting speeds and 3 feed rates and proposed that the general shape of the distribution was essentially constant. The maximum temperature was found to occur at a distance of approximately 60% of the chip contact length from the cutting edge. Usui has published a distribution for a speed of 1.67 m/s and a feed rate of 0.25 mm/rev. This distribution was much flatter than the distribution proposed by Trigger. From the limited data it was possible to compare the maximum temperatures at the chip/tool interface when using a feed rate of 0.25 mm/rev. Trigger gave a value of 833^{o}C for a speed of 1.33 m/s and Usui a value of 827^{o}C for a speed of 1.67 m/s. These speeds represent a difference of 25% for the same maximum temperature. It would appear that the distribution proposed by Trigger, which has a much higher peak value, has the effect of over estimating the maximum temperature. The maximum temperature given by Usui was determined by direct measurement using a platinum wire. The maximum temperature quoted by Trigger was found by an indirect technique. This involved measuring the flank face temperature and then using electric analogue techniques to determine the rake face temperature. The shape of this temperature distribution is a result of conjecture, because it was not possible to measure the rake face temperatures and thereby check the accuracy of the electrical analogue.

Research work by Dearnley (1983), who used carbide tools and a steel work material (817M40,EN24), suggests that the temperature distribution along the tool rake face (figure 1.5) is more uniform than that proposed by Trigger. Unfortunately, the data given by Dearnley was limited in that only two values of speed and one value

of feed were published. Dearnley estimated that the maximum temperature occurred at a distance of 0.64 along the chip/tool contact region, which was very similar to values given by Trigger and Usui. The method of quantifying the shape of these three distributions is discussed in section 7.6 and Appendix 3.

The data in Table 7.1 below gives the relative temperature (T) expressed as a fraction of the mean temperature for the interval x = 0 to 1 for the three distributions that were considered. These values are given to 2 decimal places.

interval-x	0.0	0.1	0.2	0.3	0.4	0.5	0.6	0.7	0.8	0.9	1.0
T(Trigger)	0.54	0.54	0.60	0.77	1.12	1.27	1.31	1.30	1.26	1.19	1.08
T(Usui)	0.78	0.90	1.00	1.05	1.09	1.09	1.08	1.06	1.03	0.98	0.93
T(Dearnley)	0.83	0.91	1.00	1.02	1.04	1.06	1.07	1.08	1.09	1.05	0.85

Table 7.1 Relative temperatures of tool/chip temperature distributions

The shape of the different distributions is shown on figure 7.6. It can be observed that the distributions proposed by Usui and Dearnley have a very similar general shape. In the region close to the cutting edge they have very similar values. This was surprising considering the assumptions (Appendix 3) that had to be made to quantify the shape of the distributions in this region.

It was decided to select the distribution proposed by Usui for inforporation into the F.E. models. This distribution was chosen for the following reasons: Firstly, it was obtained by direct measurement at the tool/chip interface. Secondly it had a shape similar to that obtained by Dearnley and was therefore likely to be more

applicable than the distribution proposed by Trigger. The distribution by Trigger gave much lower values at the cutting edge and much higher values at the central part of the chip contact length. The third reason for choosing the distribution proposed by Usui was that the maximum value occurred within the central part of the tool/chip contact length. This should be compared with the distribution proposed by Dearnley, who estimated that the maximum value occurred at the central part of the tool/chip contact. However, the detailed calculations in Appendix 3 suggest that maximum was closer to the point of chip departure.

Although it was decided to select the distribution proposed by Usui and use it to model a wide range of cutting conditions, the other two distributions were also modelled for a limited set of conditions. It should be appreciated that the three distributions considered were all obtained for a feed rate of 0.25 mm, whereas the cutting tests investigated feed rates ranging from 0.25 to 0.80 mm. It may well be that these distributions do not apply when the higher feed rates are used. The different shapes of these distributions can, however, be used for the purposes of F.E. modelling. These F.E. models can be used to predict the influence of the different distributions on tool deformation.

7.5 Application of Measured Forces

The measured forces from the cutting tests were applied to the elements on the tool rake face in accordance with the requirements of F.E. theory (PAFEC 1977).

7.5.1 Linearly decreasing distribution by Chan and Braiden (1981)

Figure 7.4a shows the linearly decreasing normal force distribution acting on the chip contact length l_c, and the contact length divided into T_c elements. The total force on each element was subdivided into a rectangular region and a triangular region as shown on figure 7.4b. This allowed the forces to be applied to the corner and midside nodes in the proportions shown on figure 7.4c and was in accordance with requirements of F.E. theory. A general relationship was developed so that the total normal force could be distributed in the correct proportions to the corner and midside nodes for any number of elements T_c. The relationship is shown in Appendix 2.1.

Figure 7.5 shows the axial force distribution. The horizontal part of the distribution was allocated to T1 elements and the linearly decreasing region to T2 elements. The relationship between T_c, T1 and T2 was given by:-

$$T1 = \text{Integer}\ (T_c/2 + 0.5) \qquad (7.1)$$

and

$$T2 = T_c - T1 \qquad (7.2)$$

These relationships were used after considering the relative lengths of the sticking regions (l_s) and contact lengths (l_c) given by Barrow (1982). The corner and midside nodes in the sloping region (figure 7.5) were allocated the necessary forces in a manner similar to that used for the normal force (figure 7.4c).

To facilitate the allocation of the two forces to the corner and midside nodes for different numbers of elements (or contact lengths), it was decided to write a computer programme. The programme gave the node numbers, forces and their respective directions; a sample run is shown in Table A2.1. By formatting the output in the manner shown

it was possible to use it directly in the PAFEC F.E. computer package.

7.5.2 Distribution by Barrow (1982)

Both the normal and axial forces were treated in a similar manner to the axial force in the section above. The length of the sticking region (l_s) was allocated T1 elements and the sliding region was allocated T2 elements. The relationship between T_c, T1 and T2 is given by equations 7.1 and 7.2. The allocation of the forces to each corner and midside is shown in Appendix 2.3.

7.6 Quantification of Temperature Distribution at Chip/Tool Interface

In order to quantify the shape of the temperature distributions discussed in section 7.4, it was necessary to fit a polynomial such that the temperature (T) at any point could be expressed as a function of its position (x) along the tool chip contact length. The different distributions were normalized by giving the contact length the interval x = 0 to 1, and dividing the interval into 10 equal divisions. The temperature was also normalized by expressing it as a fraction of the mean value at each interval. The method of normalizing the temperature for each distribution is discussed in detail in Appendix 3.

The normalized distributions are shown on figure 7.6. A Chebychev polynomial was fitted to each distribution by using a curve fitting routine available on the Polytechnic Computer.

The direct application of the Chebychev polynomial to the tool/chip interface was not possible other than for the interval for x = 0 to 1. It was therefore necessary to express the polynomial in the form given by:-

$$T = a_o + a_1 x + a_2 x^2 + \text{----------} a_n x^n \qquad (7.3)$$

The tool/chip contact length (l_c) was allocated the distance x = 0 to 1, and the number of elements (T_c) in the contact region was given by:-

$$T_c = l_c / e \qquad (7.4)$$

where l_c was the tool/chip contact length

e was the element size (0.1 mm, see section 7.9).

The required step size (S) necessary to cover the distance x = 0 to 1 and to incorporate the midside nodes was given by:-

$$S = \frac{1}{2T_c} \qquad (7.5)$$

This arrangement allowed the relative temperature (T) to be determined at the corner and midside nodes for any tool/chip contact length that was required.

The temperature at each node (x, value) was calculated by multiplying the relative temperature value (T), given by equation 7.3, by the mean temperature obtained from the tool/work thermocouple. An example of the temperature allocation for the distributions by Usui and Dearnley is shown in Appendix 3. When used in this form it was possible to incorporate it directly into the F.E. package.

7.7 Calculation of Temperature Distribution in the Tool

When using the PAFEC finite element package it was necessary to calculate the temperature distribution in the tool before attempting to determine the thermal stresses. The package had the facility to

calculate both transient and steady state stresses. A steady state condition of 60 seconds was chosen because the thermocouples at the tip-shank interface were approaching a steady temperature after 60 seconds of machining. The boundary temperatures and times were determined directly from the traces produced by the ultraviolet recorder (sections 2.6 and figure 2.13). They were applied to the model during both the transient and steady state calculations.

In order to determine the steady state and transient temperatures it was necessary to determine the thermal properties of the tool materials that were being modelled. These properties were obtained from Brookes (1982) and also Schwarzkopf and Kieffer (1960), see section 8.6.1.2.

The F.E. package calculated the transient temperatures by using a series of time steps. It was found that the size of the step was very critical. If the steps were too large then it was found that oscillations could arise in the calculated temperatures. Alternatively if the steps were too small this could lead to temperatures changing in the wrong direction. These effects are dependant on a non-dimensional number known as the Fourier Number (F). The Fourier Number relates the thermal properties of the tool material and mesh size of the model as follows:-

$$F = \frac{k.\delta t}{C_p \rho e^2}$$

where δt = time step

k = thermal conductivity

C_p = specific heat

ρ = density

e = distance between closest nodes.

If the transient temperature calculations were to converge and not oscillate, it was essential that the Fourier number had a value equal to or close to unity. Because the thermal properties of the material were fixed, it was only possible to alter either the time step δt or the distance e between the nodes. The distance between the nodes was fixed at 0.1 mm to achieve sufficient accuracy in the stress calculations (see section 7.9). As a consequence of these restrictions it was necessary to use a very small step of $\delta t = 0.625 \times 10^{-3}$ seconds to achieve a Fourier Number of F = 1. To determine the temperature distribution in the tool after 0.1 seconds of elapsed cutting time it was necessary to take 160 steps each having a duration of 0.625×10^{-3} seconds. Similarly, 1.5 seconds required 2400 steps and this required approximately 3900 seconds of computing time. These long runs were very expensive on computing time and special permission was required before they could be executed at the weekends. Fortunately, it was found that the transient temperature distributions were such that 1.5 seconds of elapsed time was sufficient (see section 8.7.1).

The steady state temperature distributions were not dependant on the Fourier Number, so it was not necessary to calculate the temperatures in a series of discrete steps; these calculations required approximately 30 seconds of cpu time.

7.8 Calculation of Mechanical and Thermal Elastic Stresses

The F.E. package had the capability of calculating mechanical and thermal stresses both separately and also as a combined quantity. The procedure for calculating the stresses was as follows:-

Mechanical:

1) Apply the force distributions (figures 7.4 and 7.5) and restraints (figure 7.3) and calculate the mechanical stresses.

Thermal:

1) Apply mechanical restraints to the tool as shown on figure 7.3, read the previously calculated temperature distribution (section 7.7) from the file and calculate the thermal stresses.

Combined Mechanical and Thermal:

1) Apply the force distributions and restraints and read the temperature distribution from the file to calculate the combined mechanical and thermal stresses.

7.9 Choice of element size at the tool/chip interface

A number of different models were investigated to obtain a balance between the required accuracy of results and the limitations of available computer processing time. It was essential that the vertical and horizontal forces were spread over several elements if full advantage was to be taken of the shape of the different distributions. An initial mesh size of 0.2 mm was chosen in the region of the tool chip contact area. However, this was found to be rather unsatisfactory when the fine feeds and short contact lengths were being analysed. In some cases the contact length was only 0.6 mm, which resulted in the forces being distributed over three elements only. It was decided to reduce the mesh size to 0.1 mm in this region so that the forces could be spread over a minimum of six elements. A value of 0.1 mm was also chosen along the flank face in the region immediately below the cutting edge. It was in this region that the bulging was found to occur, so a fine mesh was considered to be

essential. The two main restrictions on reducing the size of the mesh were as follows. A fine mesh increased the number of elements in the model and this increased the computer time for the solutions. If the length to width ratio of the elements exceeded a value of 15:1 then grossly distorted elements would occur. In regions of high stress concentration it was recommended that the length to width ratio should not exceed a value of 5:1.

7.10 Evaluation of Mechanical and Thermal Elastic Stresses

Figures 7.7 and 7.8 show typical mechanical and thermal stresses on the rake face of the tool. They were obtained by using a mesh size of 0.1 mm in the tool chip contact region. The results show very large discontinuities at the corner nodes of each element and a parabolic distribution of stress within each element. This problem arises when the rate of mechanical or thermal loading changes rapidly over relatively small distances as in the case of a metal cutting tool.

7.11 Stress Smoothing

The problem of stress discontinuities at the element nodes has been investigated by Chan and Braiden (1981), who found it necessary to develop a stress smoothing technique which sampled the values of stress within each element. The technique was developed in such a manner that it could be interfaced with the existing Finite Element package; this technique was applied to the existing model. The results shown on figures 7.9 and 7.10 were obtained for 0.1 mm mesh size. When compared with figures 7.7 and 7.8 it can be seen that there was a large reduction in the stress discontinuities at the corner nodes. It was decided to incorporate this technique in the future work when calculating the stresses.

Figure 7.10 shows that the thermal stresses were very small. This result was expected because the tool was free to expand in both the x and y directions. Because the thermal stresses were small in comparison with the mechanical stresses, it was decided to combine the two stress systems in future calculations.

7.12 Prediction of Permanent Plastic Deformation

To predict permanent tool deformation it was necessary to consider the non-linear behaviour of the tool material. The F.E. package had the facility to carry out a non-linear analysis and to vary the stress /strain properties of the material with temperature. The capability of being able to vary the stress/strain relationship with temperature was most important for two reasons. Firstly, the stress/strain relationship of the tool material is sensitive to the elevated temperatures that occur in a cutting tool. Secondly, wide variations in temperature are known to occur in a cutting tool, consequently there will be wide variations in the mechanical properties through the tool.

To incorporate the stress/strain data into the F.E. model it was necessary to specify a number of points on the curve. This was undertaken by considering the elastic modulus (E) followed by a series of points on the curve, each point giving a stress and the subsequent slope. The stress at the first point was considered to be the yield stress or the point of departure from linearity. A number of stress/ strain curves for different temperatures were incorporated into the model; the F.E. package had the facility to interpolate for values of temperature not supplied. Figure 8.8 shows the variation of stress/ strain data with temperature for two different tool materials (see section 8.6.1.1).

When the stress/strain relationship is non-linear, it is necessary to apply the load in a series of increments. The first increment was sufficient to just exceed the yield stress of the material. The size of subsequent increments was dependant on the slope of the stress/strain curve. As the slope of the stress/strain curve decreased, it was necessary to apply progressively smaller increments of load. A typical sequence of percentage load increments was 49 + (11 x 3) + (4 x 2) + (10 x 1) - 100. After the load had been applied it was removed by using an increment of -100%. The removal of the load gave the permanent plastic deformation of the tool. A large number of computer runs were required to determine the optimum sequence of load increments. If the increments were too large, the numerical routine would fail to converge. If the increments were too small, the routine would converge but the computing time became excessive. It was found that a typical load sequence to give convergence could be achieved in a minimum of 1800 seconds of cpu time.

CHAPTER 8

ANALYSIS AND DISCUSSION OF RESULTS

8.1 Introduction

In the following chapter the results from the cutting tests and the F.E. models are analysed and discussed.

To compare the cutting temperatures with previously published results the exponents for speed and feed were determined. A preliminary analysis of the stresses using a linear elastic model of the cutting tool was undertaken. This model was of limited value because it could not predict permanent deformation of the tool. It did, however, give an initial estimate of the stresses that can occur in a cutting tool. Furthermore, it represented the current position of research in this particular area. To model the permanent deformation of the cutting tool a non-linear analysis was used. It was possible to incorporate into the model changes in the properties of the tool material with temperature, and also to investigate transient effects due to thermal shock.

8.2 Analysis of Cutting Temperatures

The average tool/chip interface temperatures obtained from the cutting tests are compared on figure 8.1. Each symbol represents the range of the first three values of temperature that were obtained for each test. The first three values were chosen because the cutting edge was considered to be stable if the temperature and forces were not rising too rapidly. By choosing the first three values it was possible to give some significance to the results when attempting to analyse them.

A number of empirical relationships that relate average temperature to the variables of speed, feed and depth of cut have been published. For the purposes of comparison, it was decided to determine the empirical relationships between the variables for the data obtained in this investigation.

The expected form of the relationship was given by:-

$$\theta = k\, v^{a} f^{b}$$

It was decided to initially only investigate the effect of changes in cutting speed and to keep the feed rate f constant. After the constant k and the exponent "a" had been determined for each feed, the data was analysed to determine the exponent "b" and a new constant k. The results for each grade are given below:-

8.2.1 Grade TE

Feed = 0.25 mm

$$\theta = 825\, v^{0.228}$$

Feed = 0.30 mm

$$\theta = 812\, v^{0.267}$$

Feed = 0.35 mm

$$\theta = 838\, v^{0.262}$$

Feed = 0.40 mm

$$\theta = 875\, v^{0.243}$$

Relationship for combined cutting speed and feed rate:-

$$\theta = 1009\, v^{0.253}\, f^{0.167}$$

8.2.2 Grade TTA

Feed = 0.35 mm

$$\theta = 884\ v^{0.162}$$

Feed = 0.40 mm

$$\theta = 860\ v^{0.258}$$

Feed = 0.50 mm

$$\theta = 923\ v^{0.191}$$

Feed = 0.65 mm

$$\theta = 937\ v^{0.240}$$

Relationship for combined cutting speed and feed rate:-

$$\theta = 1019\ v^{0.212}\ f^{0.161}$$

8.2.3 Grade TA5

Feed = 0.40 mm

$$\theta = 913\ v^{0.213}$$

Feed = 0.50 mm

$$\theta = 938\ v^{0.213}$$

Feed = 0.65 mm

$$\theta = 971\ v^{0.210}$$

Feed = 0.80 mm

$$\theta = 1001\ v^{0.231}$$

Relationship for combined cutting speed and feed;-

$$\theta = 1028\ v^{0.214}\ f^{0.132}$$

8.2.4 Discussion

The exponents "a" had values ranging from 0.162 to 0.267; with the exception of the lowest and the highest values the remainder are quite closely grouped together. These values were similar to those found by Kurimoto (1977), who quoted values of 0.242, 0.231 and 0.232 for feed rates of 0.1, 0.2 and 0.32 mm respectively. Jaesche (1967) and Trigger (1966) quoted values of 0.237 and 0.20 respectively for the exponent "a". When the influence of feed rate was considered, the grades TE, TTA and TA5 gave values of the exponent "b" as 0.167, 0.161 and 0.132. These values compare favourably with values of 0.133 and 0.14 quoted by Jaesche and Trigger respectively (see section 1.5.2.).

The values of the exponents "a" and "b" found from the cutting tests, confirm the generally accepted conclusion that changes in temperature are more sensitive to changes in cutting speed than feed rate. The significance of increases in temperature with cutting speed and feed rate is considered in sections 8.6.2 and 8.6.3.

8.3 Elastic Analysis to Predict Boundary Stresses

In the following section the mechanical and thermal stresses are calculated for the rake and flank faces of the cutting tool. For purposes of comparison the elastic stresses in the tool are compared with the 5% proof stress of different tool materials. A plane stress model was used for the calculations. The uniaxial equivalent stress was taken as twice the maximum shear stress. The value of the elastic modulus (E) was taken as 510 GN/m^2 and Poisson's ratio as 0.22.

8.3.1 Stresses at the Tool/Chip Contact Region

Figure 8.2 shows the combined mechanical and thermal stresses on the rake face for the linearly decreasing force distribution used by Chan and Braiden (1981). The forces and temperatures were obtained by using a cutting speed of 1.25 m/s and a feed rate of 0.40 mm/rev with carbide grade TA5. The normal stress σ_y was a maximum at the cutting edge and decreased almost linearly to zero at the end of the chip contact region. This stress distribution was expected because it was a direct consequence of the normal loading in the tool/chip contact region. Similarly, the shear stress distribution σ_{xy} had a shape that followed the axial force distribution used in the model. The stress σ_x was found to increase with distance from the cutting edge and reached its maximum at a distance of 0.6 mm from the edge.

Figure 8.3 shows the combined mechanical and thermal stresses for the force distribution proposed by Barrow (1982). The normal stress σ_y and the shear stress σ_{xy} were a direct consequence of the normal and axial force distributions that were applied to the rake face. The stress σ_x was found to rise rapidly and to reach its maximum at a distance of 0.5 mm from the cutting edge.

When the stresses were compared for both models it was found that the model used by Chan and Braiden gave values of σ_y at the cutting edge, which were 40% higher than the model proposed by Barrow. In the region close to the cutting edge the stress σ_y was dominant. When the relative values of σ_x and σ_y were compared on figure 8.3, it was observed that there was not such a large difference in values in the region close to the cutting edge. The maximum shear stress had a maximum value close to the cutting edge in the model used by Chan and Braiden, due to the dominant influence of σ_y in this region. In

the model proposed by Barrow, the maximum shear stress was more uniformly distributed.

8.3.2 Stresses on the Flank Face

The stresses on the flank face immediately below the cutting edge are shown on figure 8.4 for the linearly decreasing force distribution. The stress σ_x was found to decrease rapidly to a value of almost zero in a distance of 0.1 mm. This result was expected because the model treated the flank face as a free surface. It was observed that the stress σ_y decreased rapidly in the region immediately below the cutting edge, after which the rate of decrease was reduced. The shear stress σ_{xy} was observed to obtain a constant value after a distance of 0.1 mm from the cutting edge. The maximum shear stress was dominated by the stress σ_y with some contribution from the shear stress σ_{xy}.

Figure 8.5 shows the stress in the flank face for the model proposed by Barrow. The stress σ_x decreased rapidly to a practical value of zero in a manner similar to the model used by Chan and Braiden. It was found that the stress σ_y decreased initially and reached a minimum value at a distance of between 0.1 and 0.2 mm from the cutting edge. Beyond this minimum the stress began to increase and it reached a value of 0.78 GN/m^2 at a distance of 0.5 mm below the cutting edge. The shear stress σ_{xy} was observed to fall to a value of zero in a distance of 0.3 mm. As expected, the maximum shear stress was largely dominated by the value of σ_y in the regions away from the cutting edge.

8.4 Mechanical and Thermal Elastic Deformations

Figure 8.6 shows the shape of the tool after being subjected to

the following loading conditions;-

i) thermal

ii) mechanical

iii) combined thermal and mechanical.

(i) Thermal Loading

The tool was free to expand in both the x and y directions, when using an average temperature of 980°C and the distribution by Dearnley. Typical displacements were -28 and 13 μm in the x and y directions respectively, and because the tool was free to expand, the thermal stresses were very small. Figures 7.9 and 7.10 show typical values of smoothed thermal and mechanical stresses. It can be observed that in a plane stress system, the thermal stresses were two orders of magnitude less than the mechanical stresses.

(ii) Mechanical Loading

The displaced shape due to mechanical loading is shown on figure 8.6. Typical values on both the flank and rake faces were found to be 3 and -6 μm in the x and y directions respectively. It should be noted that these typical values applied to all the surface nodes in the region of the cutting edge.

(iii) Combined thermal and Mechanical Loading

Figure 8.6 shows the displaced shape for combined thermal and mechanical loading. Displacements in the x and y directions were found to be -2 and 8 μm respectively.

A feature of the predicted elastic displaced shapes was that the loading conditions did not cause any significant change in the geometry of the tool. The forces applied in the x direction did not

cause a loss of clearance immediately below the cutting edge. Similarly, the forces in the y direction did not cause excessive clearance at the cutting edge. It was therefore necessary to investigate the stresses to find an explanation for the permanent plastic deformation at the rake and flank faces.

8.5 Stress Distribution Within the Cutting Tool

The flank face bulging and edge depression recorded in Chapter 6 was a result of permanent plastic deformation. There was no evidence of cracking either on the rake face or on the flank face of the tool. It is therefore suggested that the deformation was caused by the tool material deforming by a process of shear along planes of maximum shear stress. A mechanism of shear at elevated temperatures has been reported by Trent (1967), who conducted hot uniaxial compressive tests on various grades of carbide.

It was decided to calculate the maximum shear stress at each node in the region of the tool chip contact area. This stress was calculated by using the values σ_x, σ_y and σ_{xy}, obtained from the finite element analysis. Figure 8.7 shows the magnitude and direction of the uniaxial equivalent (σ_{eq}) of the maximum shear stress at each node. Also shown on each node is the 5% uniaxial proof stress (Trent 1967) for the three grades of carbide used in the cutting tests. It should be appreciated that published stress/strain data for carbide tool materials at elevated temperatures is extremely limited. The best approximation that could be achieved was to compare the composition of the grades being investigated with the composition of the grades that were tested by Trent (1967).

By using figure 8.7 it was possible to compare the stresses acting at each node with the 5% hot proof stress of the tool material. It can be observed that in the central portion of the chip contact region the uniaxial equivalent of stress was greater than the hot compressive stress of the three carbide grades. The results show that at the cutting edge the uniaxial equivalent stress was greater than the 5% hot proof stress of grade TA5. It is therefore suggested that plastic deformation will occur at this point. At the node immediately below the cutting edge, the uniaxial equivalent stress due to the temperatures and cutting forces decreased and was less than the load carrying capacity of the tool material. It is further suggested that a point exists somewhere between the nodes beyond which yielding will not occur.

The advantage of using this type of model was that it allowed a comparison between the hot compressive stress of different tool materials. It was possible to determine if the 5% proof stress would be exceeded for a given applied stress and temperature distribution. However, the model did not accommodate any non-linear behaviour that would occur when the elastic limit was exceeded. As a consequence, it does not predict permanent deformation. Despite these limitations it was an advance on any previously published model. Chan and Braiden (1981) took no account of the change of the tool material properties with temperature. Tlusty and Masood (1978) stated that in some cases the stresses they calculated exceeded the hot strength of the tool material. They did not make any attempt to relate the hot strength of the material to the temperature and stress distributions in the cutting tool.

8.6 Permanent Plastic Deformation

8.6.1 Introduction

The following section is concerned with using the F.E. model to explain the effects of speed and feed in terms of the concepts of temperature stress and time. The model incorporates the properties of a tool material and their variation with temperature.

8.6.1.1 Mechanical Properties of Tool Material Used for the F.E. Model

Very little data exists that gives a true relationship between stress and strain at the elevated temperatures which occur in a cutting tool. Of the data that has been published, it almost exclusively applies to the WC-Co alloys and it was usually obtained by using the transverse rupture test. Trent (1967) published values of applied stress against a given percentage of permanent deformation for a range of temperatures. These values were obtained for compressive loading when using a WC-6%Co alloy. Ueda (1977) has published continuous stress/strain data for a WC-16%Co alloy that was tested in tension. The two sets of data are shown for comparison on figure 8.8. If temperatures up to 1000^{o}C are considered in conjunction with strains of up to 1%, then the stress/strain relationships are broadly similar. This similarity is rather surprising considering the differences in compositions and the methods of testing. Above temperatures of 1000^{o}C the data published by Trent shows a large increase in strain for a given applied stress. This effect was particularly pronounced at the very high temperatures of 1117 and 1220^{o}C.

Because true stress/strain data did not exist for the grades of carbide being tested, it was decided to use the data published (by

Ueda) for the WC-16%Co alloy. This data was chosen because it was obtained from a continuous stress/strain test.

8.6.1.2 Thermal Properties of the Tool Material Used for the F.E. Model

The thermal properties of thermal conductivity (k) and specific heat (Cp) were not available for the grades being investigated. It was therefore necessary to use data for a grade of similar composition. Sandvik grade S2 was found to have a very similar composition to grade TTA (Brookes, 1982). The following data was given: density (ρ) 11700 kg/m^3, thermal conductivity (k) 40 W/mK and specific heat (C_p) 210 J/kg.K. This value of specific heat was confirmed by Schwarzkopf and Kieffer (1960), who gave values of 0.05 to 0.08 cal/g/^oC for a range of carbide alloys.

The corresponding thermal properties for the WC-16%Co alloy that was used in the F.E. model were found by using the data published for Sandvik grade CG60 (Brookes, 1982). The published properties were as follows: density (ρ) 13,900 kg/m^2, thermal conductivity (k) 115 W/mk, and specific heat (Cp) 210 J/kg.K. The influence of these different thermal properties on the transient temperature distributions within the tool is discussed in section 8.7.

8.6.2 The Influence of Cutting Speed on Deformation

To investigate the influence of changes in cutting speed it was necessary to select a range of cutting conditions. It was decided to consider the forces and temperatures that were obtained for grade TTA when used at a constant feed rate of 0.50 mm. For this particular feed rate it was found that the measured forces and the tool/chip contact length (ℓ_c) were essentially constant for the speeds of 1.00 m/s and 1.75 m/s.

8.6.2.1 Steady State Temperature Distribution

Figure 8.9 shows the predicted temperature contours within the tool for average temperatures of 937 and 1022°C at the tool/chip interface, when using the distribution proposed by Usui. The average temperatures corresponded to cutting speeds of 1.00 and 1.75 m/s respectively.

The influence of the higher temperature at the chip/tool interface is immediately apparent. For example, when the highest speed (1.75 m/s) is considered then it can be observed that 1000°C contour encompasses much more tool material than the 1000°C contour produced by the lower speed of 1.00 m/s. A similar observation may be made for any pair of contours that have the same temperature. The influence of increasing the speed is to raise the temperature of an element of tool material that is close to the chip/tool interface. The data on figure 8.8 indicates that raising the temperature of the tool material will give an increase in strain for a constant applied stress.

8.6.2.2 Permanently Displaced Shape

Figure 8.10 shows the predicted permanently displaced shape of the elements. They were subjected to the boundary conditions of temperature and force (linearly decreasing normal distribution) measured in the cutting tests.

The rake face was depressed and the flank face was displaced forward. The model predicted maximum bulging at about 0.5 mm below the cutting edge. The highest speed which gave the highest temperature shows the most edge depression and bulging.

The influence of differences in temperature at given points in the tool is shown on figure 8.11. It gives the temperature, stresses and strains for four different elements. If the results for element 1 are considered then it may be observed that σ_y was the dominant stress. The values of σ_y are similar for both the cutting speeds considered. There is, however, a difference in average temperature of 74°C for this element. This higher temperature gives a much higher strain ε_y for essentially the same applied stress. The results show a similar trend if the Von-Mises equivalent stress σ_{eq} is considered. This result would be expected because the equivalent stress σ_{eq} was dominated by σ_y.

Element 5 was located at approximately half way along the tool/chip contact region, the value of σ_y was reduced and the value of σ_x was increased. This result was similar to that shown on figure 8.2. The value of σ_y was still dominant and was approximately equal to the equivalent stress σ_{eq}. The slight increase in equivalent stress and higher temperature, associated with the 1.75 m/s cutting speed, did not cause a very large increase in equivalent strain. The reason for this can be explained by examining the stress/strain data shown on figure 8.8.

Element 61 was located on the flank face and covered a distance of 0.3 to 0.4 mm from the cutting edge. There was a difference in average temperature of the elements of 76°C for the two cutting speeds of 1.00 and 1.75 m/s. A consequence of the higher tool/chip interface temperature was to cause an increase in the temperature of this element located at the flank face. The stress σ_y was found to be dominant in both cases. Examination of the results shows that the

higher temperature gave higher values of strain.

Element 65 gave generally similar results to those obtained for the other elements that were considered. There was a difference in temperature of 72°C. The effect of the higher temperature associated with the 1.75 m/s cutting speed was to cause an increase in the amount of strain sustained by the element.

These results show that as the distance of any particular element from the chip/tool interface increased, its temperature decreased. This reduction in temperature reduced the amount of permanent strain for any given applied stress system. A boundary will exist within the tool, beyond which the combination of temperature and stress are such that plastic deformation does not occur. Figure 8.10 shows the reduction in displacement of the elements as the distance from the tool/chip interface increases. If the applied forces and the contact length are constant, then the size of the zone of material contained by the proposed boundary will be temperature dependant. Increases in cutting speed gave an increase in temperature and this caused the zone of plastic material to penetrate further into the tool. The results shown on figure 8.10 suggest that the penetration was predominantly downwards. This result would be expected because the dominant stress σ_y acted in a downward direction.

Figure 8.12 shows a comparison between the calculated displaced shape and the measured shape for three different speeds of 1.00, 1.25 and 1.75 m/s. With the exception of the highest speed, they compare very well indeed. It should be appreciated, however, that the observed bulging and edge depression appeared to be time dependant

(figures 6.32 and 6.48). In the case of the highest speed (1.75 m/s) the flank face was observed to bulge continuously. The F.E. model was not time dependant and therefore cannot be used to predict the continuous deformation of the cutting tool. The model can, however, be used to predict the influence of increases in cutting speed on the extent of the plastic zone.

8.6.3 The Influence of Feed Rate on Deformation

To investigate the influence of feed rate on deformation, a range of feeds and a constant cutting speed were selected. It was decided to consider the forces and temperatures that were obtained for grade TTA when using a constant speed of 1.25 m/s. For the purposes of analysis two feed rates were considered, they were 0.40 and 0.65 mm. The results from the cutting tests showed that increasing the feed rate increased the average temperature, the tool/chip contact length and the forces. It should be noted that the vertical force increased by a greater proportion than the horizontal force.

8.6.3.1 Steady State Temperature Distribution

Figure 8.13 shows the calculated temperature distributions for the feed rates of 0.40 and 0.65 mm; the average tool/chip interface temperatures were 914 and 988^{o}C respectively. The tool/chip contact lengths were 0.95 and 1.21 mm respectively.

The influence of the higher average temperature at the chip/tool interface was immediately apparent. For example, the 950^{o}C contour associated with the higher feed rate encompassed much more tool material than the same contour associated with the lower feed rate of 0.40 mm. It should be noted that these contours are offset relative to each other. In the case of the 0.65 mm feed rate, the lowest point

in the contour was further from the cutting edge and flank face. This result would be expected because the tool chip contact length was increased for the higher feed rate. As a consequence, the position of the highest temperature at the tool/chip interface was moved further from the cutting edge. This offset of temperature contours did not occur when changes in speed were considered for a constant feed rate (see figure 8.9). This was because the tool/chip contact length was essentially the same for both cutting speeds. The effect of increasing the feed rate was to raise the temperature of an element of tool material that was beneath the tool/chip interface. Increasing the feed rate extended the tool/chip interface, which had the effect of increasing the temperature of some tool material that was not previously covered when the 0.4 mm feed was used.

8.6.3.2 Permanently Displaced Shape

Figure 8.14 shows the predicted permanently displaced shape of the elements when subjected to the boundary conditions of temperature, force and contact length that were measured in the cutting tests.

In both cases the rake face was depressed and the flank face was displaced forward with a prediction of maximum bulging occurring at about 0.5 mm below the cutting edge. The highest feed rate gave the highest temperature and greatest contact length, and was found to sustain the largest amount of edge depression and bulging. The results from the model show that the edge depression extends much further along the rake face for the higher feed rate. This result would be expected because the mechanical and thermal loads were applied over a greater region of the rake face. When the 0.4 mm feed rate was modelled the depression of the rake face close to the cutting edge was

found to be parallel with its original position. When the 0.65 mm feed rate was modelled the rake face was found to taper downwards. These predictions by the F.E. model largely agreed with the results obtained from the cutting tests. In the cutting tests it was generally observed that feed rates greater than 0.4 mm gave tapered edge depression, whereas feed rates less than 0.4 mm gave parallel edge depression (see figures 4.10, 6.29, 6.34 and 6.39).

The influence of differences in applied temperature and stress at the tool/chip interface can be evaluated by considering the temperature, stress and strain for four different elements within the tool (see figure 8.15). The results show that for element 1 there was a difference in temperature of $47^{o}C$ for the two different feed rates. In both cases the stress σ_y was found to be dominant when compared with the other stresses. It was also found that σ_y had a higher value for the case of the higher feed rate. This higher value of σ_y, combined with the higher temperature, was sufficient to cause larger values of strain. The values of strain associated with the higher feed rate were approximately twice those obtained for the lower feed rate.

Examination of the results for element 8 for the lower feed rate reveals that the stress σ_y and the strain ε_y were much reduced when they were compared with element 1. This result would be expected because this element was close to the chip departure point and the value of applied stress σ_y was much reduced. The strain ε_y was found to be -0.0013, which compares with -0.0102 found for element 1. A comparison of the results found for element 8 reveals the influence of the higher temperature associated with the higher feed rate. It is useful to compare the values of equivalent stress and equivalent

strain. The values of equivalent stress were 0.74 and 0.81 GN/m^2 for temperatures of 897 and 1034°C respectively, and gave the corresponding values of equivalent strain as 0.0039 and 0.0153. These results clearly demonstrate that for an approximately constant stress, the strain was very sensitive to increases in temperature when operating at these elevated temperatures.

Element 61 was located on the flank face and covered a distance of 0.3 to 0.4 mm from the cutting edge. There was a temperature difference of 72°C for the two different feed rates. In both cases the stress σ_y was dominant. The higher stresses and higher temperatures associated with the 0.65 mm feed rate were sufficient to cause strain values that were approximately three times those found for the 0.40 mm feed rate. This large difference in strains can be compared by examining the shape of element 61 which is shown on figure 8.14.

The results shown for element 68 on figure 8.15 reveal that the permanent strain caused by the 0.40 mm feed rate was very small when compared with the other elements. Examination of this element on figure 8.14 shows that it suffered very little distortion or displacement. The average temperature of this element was quite low when compared with the regions close to the tool/chip interface. Because these permanent strains for this element were low, it must be considered to be close to the boundary of the plastic zone that was proposed in section 8.6.2.2. The results for the 0.65 mm feed rate show that the strains for this element (68) were mugh higher than for the 0.4 mm feed rate. The results (not given) showed that the strains for elements either to the right of, or below this element were also higher than those for 0.4 mm feed rate. It may be concluded that when

the 0.65 mm feed rate was considered, this element (68) was well within the plastic zone, whereas with the 0.4 mm feed rate, it was close to the boundary.

It can be seen (figure 8.14) that increasing the feed rate for a constant cutting speed caused an extension of the plastic zone within the tool material. The zone was found to extend both downwards from the rake face and horizontally sideways from the flank face. This result should be compared with that found for a variable speed and constant feed rate (figure 8.10 and section 8.6.2.2.). It was found that increasing the cutting speed caused the plastic zone to extend predominantly downwards, any sideways movement was minimal.

Figure 8.16 shows a comparison between the calculated displaced shape and the measured shape for three different feed rates of 0.40, 0.50 and 0.65 mm/rev. With the exception of the highest feed rate, the calculated and measured values were found to compare favourably. It should be appreciated that the F.E. model was not time dependant, but it could be used to predict the influences of changes in feed rate on the size and shape of the plastic zone.

8.7 The Influence of Transient Thermal Effects on Deformation

The metal cutting process can subject a cutting tool to very high temperatures and very high rates of thermal shock. Under certain circumstances these two conditions can cause both high steady state thermal stresses and high transient stresses. Braiden (1971) has shown that if a plane strain model is used then the thermal stresses can exceed the mechanical stresses. Thermal stresses are caused by the existence of temperature gradients within the cutting tool.

8.7.1 Transient Temperature Distribution

During intermittent turning the tool is subjected to the maximum undeformed chip thickness at the instant the workpiece becomes engaged with the cut. The rise in temperature can be considered as a step function. With normal continuous turning the undeformed chip thickness increases from zero to a maximum during the first revolution of the workpiece. Under these circumstances the rise in temperature can be approximated to a ramp function. The duration of the ramp input can be calculated from the surface speed of the workpiece and its diameter. A typical speed of 2.13 m/s and workpiece diameter of 70 mm gives a ramp duration of 0.1 seconds (equivalent to 600 rpm).

Figure 8.17 shows the calculated transient temperature distribution within the cutting tool for an average chip/tool temperature of 1022^{o}C and a chip contact length of 1.22 mm. The temperatures were applied at the tool/chip interface boundary using a ramp function over a time interval of 0.1 seconds. Temperatures were applied at the tip-shank interface over a period of 60 seconds. These temperatures were obtained from results similar to those shown on figure 2.13. For practical purposes it was decided to consider that steady state temperatures had been achieved after 60 seconds of machining (see section 7.7). Two values of thermal conductivity were used for the calculations, they were 40 W/mk (TTA) and 115 W/mk (WC-16%Co), see section 8.6.1.2. The higher value was used for purposes of comparison only.

Each contour is labelled with its temperature and the elapsed time (figure 8.17). The contours representing 1000^{o}C for different periods of elapsed time were very close together. This indicates that initially the steady state temperature was approached very rapidly.

A similar observation can be made regarding the 900°C contour. If the position of the contour is considered as a function of time then the rate of advancement through the tool was much reduced after 1 second had elapsed. The steady state 850°C contour encompassed a large part of the tool material, and a large part of this material was encompassed after only 1 second had elapsed. The contours approached their final positions asymptotically. To represent this behaviour of the contours it was decided to plot the position of the 840°C contour after 1.5 seconds. A similar technique was used for the 790, 1.5 contour. There were two advantages to using this technique. Firstly, it indicated the proportion of material that was within a contour that was only 10°C less than a desired steady state value. Secondly, it allowed the transient temperature calculations to be terminated after only 1.5 seconds had elapsed. This was important because the transient temperature calculations required 3850 seconds of cpu time for 1.5 seconds of elapsed cutting time on the F.E. model.

Figure 8.17 also shows a number of contours that were calculated for a thermal conductivity of k = 115 W/mk. The results show the expected higher rate of heat conduction. It can be observed that any contour at a particular temperature has advanced further into the tool for a given elapsed time. If the 900°C temperature contours are examined for the two different values of thermal conductivity, then it may be observed that their positions are almost coincident for the elapsed times of 0.2 and 0.5 seconds. A similar observation may be made for the 850°C contour.

8.7.2 Transient Thermal Stresses

Figure 8.18 shows the equivalent stresses and strains for a number of elements in the tool at different periods of elapsed time.

(These results were calculated from the transient temperature distributions shown on figure 8.17, for the two values of thermal conductivity.) The values shown for 0.2, 0.5 and 1.0 seconds were due to thermal effects only, the values shown for 60 seconds included the stress caused by the application of the mechanical loads.

A column of elements was considered that were approximately half way along the tool/chip contact region. These elements were exposed to some of the highest temperatures. If the stresses for 0.2 seconds of elapsed time are considered then the equivalent stress can be seen to increase with penetration into the cutting tool. The results show that for both values of thermal conductivity there was a reduction in equivalent stress with the passage of time. This reduction in the thermal stresses with time was expected, because the temperature gradients in the tool were reduced as the steady state temperatures were approached. The results show that close to the rake face, the stresses for a combination of 40 W/mk thermal conductivity and 0.5 seconds of elapsed time were approximately equal to those calculated for the 115 W/mk thermal conductivity and 0.2 seconds of elapsed time. These results can be explained by considering the transient temperature distributions (figure 8.17). The results show that for these two sets of conditions, the transient temperature distributions are almost identical. The results suggest that close to the rake face the transient thermal stresses had a decay time of approximately 1 to 1.5 seconds.

The results shown for 60 seconds include the mechanical stresses caused by the application of the cutting forces. It can be observed that these combined stresses and their associated strains were very much greater than the thermal stresses and their associated strains.

It would appear therefore that the thermal stresses have a minimal influence on the amount of deformation when they are compared with the influence of the mechanical stresses.

Figure 8.18 shows the maximum amount of bulging predicted by the model for different periods of elapsed time. It should be appreciated that the amount of bulging shown for each time period was not cumulative; it did not include any previous strain history. It was the predicted bulging that would occur if each respective temperature distribution was considered to be a steady state distribution. Despite this limitation, the results show that the predicted bulging caused by the thermal stresses was very small when compared with the predicted bulging caused by the mechanical stresses.

8.8 The Influence of Tool/Chip Stress Distributions

To determine the influence on permanent deformation of the stress distribution at the tool/chip interface, it was decided to model two different distributions. They were the distribution proposed by Barrow (1982) and the linearly decreasing distribution used by Braiden and Chan (1981).

The boundary conditions of force and temperature were obtained from two different cutting tests as follows. A cutting speed of 1.25 m/s with a feed rate of 0.40 mm, and a cutting speed of 1.25 m/s with feed rate of 0.65 mm/rev. Figure 8.19 shows the permanently displaced shape predicted by the F.E. model for the 0.40 mm feed rate. The linearly decreasing distribution (Braiden and Chan), which is similar to the distributions proposed by Zorev (1963) and Kato (1972), gave parallel depression of the rake face. The force distribution

suggested by Barrow, caused the rake face to sustain more depression at the central part of the tool/chip contact region than at the cutting edge. Figure 8.20 shows the predicted shapes for the 0.65 mm feed rate. The linearly decreasing distribution predicted that the tool would sustain tapered depression on the rake face. This deformation should be compared with that predicted for the distribution proposed by Barrow. In this case the maximum depression occurred away from the cutting edge in a manner similar to that predicted for the 0.40 mm feed rate (figure 8.19).

If the deformation observed in practice is compared with the predicted deformation, then it may be deduced that the linearly decreasing force distribution or a similar version must apply. This deduction may be justified as follows. The cutting tests gave a transition from parallel to tapered rake face depression at feed rates equal to and greater than 0.4 mm. When the linearly decreasing force distribution was used in the F.E. models, they predicted a transition from parallel to tapered edge depression at feed rates greater than 0.4 mm. The force distribution proposed by Barrow did not predict this transition. Furthermore, it did not fit the shape observed in practice for either of the feed rates that were considered. It is therefore suggested that when machining steel of the type 817M40 (En24), that a stress distribution similar to that used by Braiden and Chan (1981) and proposed by Zorev (1963) and Kato (1972) must apply.

8.9 The Influence of Tool/Chip Interface Temperature Distributions

A number of different tool/chip interface distributions have been proposed by various researchers. The relative shape of these different distributions is shown on figure 7.6. The F.E. models in

the previous sections have used the distribution proposed by Usui (1984); this section compares the influence of the different temperature distributions on tool deformation.

Figure 8.21 shows temperature contours for the tool/chip interface distributions proposed by Usui (1984) and Dearnley (1983 for an average tool/chip contact temperature of 969^{o}C. Examination of figure 8.21 shows that for temperatures of 900^{o}C or less, the contours for both distributions have similar locations. If the 900, 950 or 1000^{o}C contours are considered, then it can be observed that the contours for the distribution proposed by Dearnley are further from the cutting edge. This would be expected because the maximum value at the interface was found to be further from the cutting edge (see Table 7.1 and Appendix 3). Examination of the upper 850 and 875^{o}C contours shows that the distribution by Dearnley produced slightly higher temperatures at the cutting edge. This result would be expected because the value of relative temperature at the tool/chip interface was higher. The results show that the lower 850 and 875^{o}C contours for the two distributions were almost coincident in the region of the flank face.

Figure 8.22 shows the calculated contours for the temperature distribution proposed by Trigger (1961) for an average tool/chip temperature of 969^{o}C. The general shape of the distribution within the tool was sifnificantly different from that obtained from the other two distributions. The temperatures at the cutting edge were much lower and a larger amount of tool material was encompassed by the 700^{o}C contour. In the region away from the cutting edge the contours penetrated deeper into the tool body. This deeper penetration was caused by the much higher peak temperatures that occurred at the

central part of the tool/chip contact region.

It is useful to compare the general shape of the calculated distributions with the general shape of the distribution determined experimentally by Dearnley (figure A3.1). Although Dearnley only determined three contours, it can be seen that their general shape and location are similar to those calculated for the distributions proposed by either Usui or Dearnley. Exact comparison on a temperature basis was not possible because different average temperatures were used at the tool/chip interface. The general shape of the contours produced from the distribution proposed by Trigger did not compare favourably with the experimental results determined by Dearnley. It would seem reasonable to assume that the distribution proposed by Trigger does not apply for steel of the type 817M40(En24).

Figure 8.23 shows the predicted permanently displaced shape for the three temperature distributions that were considered. The model used the stress distribution at the rake face proposed by Braiden and Chan. The predicted deformation associated with the temperature distributions proposed by Usui and Dearnley was found to be almost identical, the differences being so small they could not be shown on figure 8.23. This result would be expected, because figure 8.21 shows that the temperature distributions close to the cutting edge were very similar. The stresses and temperatures in this region should be compared with those towards the point of chip departure. The distribution by Dearnley predicted higher temperatures in this region. If the same stress was applied then a larger amount of deformation would be expected. The applied stresses, however, are much lower in this region when compared with the stresses at the cutting edge. Therefore, the increase in strain due to the higher temperatures was

negligible compared with the strains at the cutting edge and the flank face.

The predicted permanently displaced shape associated with the temperature distribution proposed by Trigger, shows that the position of maximum depression was away from the cutting edge. The maximum depression was found to occur approximately at the point of maximum temperature. The region close to the cutting edge was subjected to higher applied stresses, but lower temperatures. The reduction in temperature was sufficient to compensate for the increase in applied stress, because several of the elements showed no evidence of permanent deformation. This region should be compared to the central part of the tool/chip contact region. The applied stresses were lower but the temperatures were sufficient to allow substantial permanent deformation of the tool material.

The type of rake face depression predicted for the temperature distribution by Trigger was not observed in practice. This difference between the predicted and observed deformation, combined with the differences in the predicted and observed temperature distributions, suggests that the temperature distribution proposed by Trigger did not apply to the conditions being investigated.

8.10 Evaluation of Plane Strain F.E. Models for Permanent Deformation

It was decided to model some of the cutting conditions using a plane strain model of the cutting tool. Figure 1.6 shows that for a plane strain model the strain in the z direction is zero.

Figure 8.24 shows a comparison between the predicted

permanently displaced shape for a plane stress and a plane strain model. The results were calculated by using the measured boundary conditions obtained for a speed of 1.25 m/s and a feed rate of 0.4 mm. It can be observed that the plane strain model predicted a rise or bulge on the rake face. The cutting edge was displaced both forwards and downwards; a bulge on the flank face was not predicted. Similar results were obtained for the 1.00 m/s speed and 0.5 mm feed and are shown on figure 8.25. The predicted shape from the plane strain model was significantly different from the shape predicted by the plane stress model.

The bulging on the rake face predicted by the plane strain model was not observed in practice. If a plane strain model is to be justified, then the width to length ratio of the tool/chip contact area must have a minimum value of 6:1 and preferably a value of 10:1. In these investigations the ratio was approximately 2 to 3:1. The predictions from the plane stress model were found to give good agreement with the observed deformation. It can therefore be concluded that for the conditions being investigated, a plane strain stress system did not exist within the tool.

8.11 The Influence of Tool/Chip Contact Length on Predicted Deformation

It was decided to use the F.E. model of the cutting tool to investigate the influence of possible errors in the measurement of the tool/chip contact length. The measured forces were held constant and the measured contact length (ℓ_c) was varied by ±10%. This had the effect of decreasing and increasing the applied stress at the rake face by approximately 9 and 11 percent respectively. Two sets of cutting conditions were considered, consisting of a constand speed (1.25 m/s) and two values of feed rate (0.40 mm and 0.65 mm). It was

decided to use the measured values of temperature and force obtained for grade TTA.

Figure 8.26 shows the values that were obtained for the speed of 1.25 m/s and a feed rate of 0.4 mm. The figure shows the predicted permanent deformation for the measured contact length. The values in the table give the predicted deformation for a 10% variation in the contact length. If the depression of the rake face is considered, then it may be observed that by decreasing the applied stress by 9% the depression of the rake face was reduced by approximately 18%. An opposite effect can be observed if the applied stress is increased (by decreasing the contact length). In this case an 11% increase in applied stress caused an increase in predicted deformation of approximately 19%. These two sets of results show the non-linearity of the absolute values of stress and strain when referred to zero. However, the results show that over the range of stress being considered, the incremental stress/strain relationship was essentially linear.

The results for bulging on the flank face show a similar trend to those found for the depression of the rake face. The predicted permanent displacement was found to be quite small. In practice it was found that when such small amounts of bulging occurred, say typically 1 μm after 60 seconds, then the cutting tool was found to be stable. Under these conditions deformation was not found to be a problem.

Figure 8.27 shows the values that were obtained for the cutting speed of 1.25 m/s and a feed rate of 0.65 mm. The results show that

for the nodes 1 to 5 on the rake face a decrease in applied stress of 9% gave a reduction in predicted depression of approximately 7 to 9%. These values can be compared with the effect of increasing the applied stress by 11%. Under these circumstances this increase in stress caused the predicted depression to increase by 15 to 20%. These results show the non-linearity of the stress/strain relationship within the tool.

The results for the bulging on the flank face show a similar trend to those found on the rake face. A reduction in the applied stress of 9% gave reduction in the amount of predicted bulging of approximately 8 to 11%; increasing the applied stress by 11% gave a predicted increase in bulging of approximately 17 to 19%. In actual practice it was found that if a tool had sustained more than about 4 μm of bulging, then it was approaching the limit of its stability.

8.12 The Influence of Temperature Variation on Predicted Deformation

It was decided to use the F.E. model to evaluate the sensitivity of predicted deformation to changes in temperature. The temperature at the tool/chip interface was varied by ±2% and ±10%, for the two sets of cutting conditions considered in section 8.11 above. (In section 2.6.3 it was estimated that the tool/chip interface temperature could be measured to a value better than 2%). It was decided to use a value of ±10% so that the results could be compared with those obtained for a ±10% variation in the measured contact length (section 8.11).

Figure 8.28 shows the predicted deformation for a cutting speed of 1.25 m/s combined with a feed rate of 0.4 mm, while the data in the table shows the predicted deformation when the average tool/chip

interface temperature was varied by ±10%. A 10% reduction in temperature was sufficient to allow a reduction in depression of the rake face of approximately 50 to 55%. These results should be compared with those obtained for 9% reduction in applied stress (figure 8.26), which predicted reduction in deformation of 18%. The effect of increasing the average temperature by 10% was very substantial; the predicted depression of the rake face was increased by approximately 70 to 100%. When the applied stress was increased by 11% (figure 8.26) the predicted depression was increased by 19%. The values predicted for bulging show similar percentage variations to those found for edge depression when the temperature was varied by ±10%.

Figure 8.29 shows the results obtained for a speed of 1.25 m/s and a feed rate of 0.65 mm. When the average tool/chip interface temperature was reduced by 10%, the predicted depression of the rake face was reduced by approximately 50%. An increase in average temperature of 10% gave an increase in predicted depression of the rake face that varied from approximately 40 to 60%. To a first approximation the variation of predicted depression with temperature was found to be linear over the range of temperature considered. These results should be compared with those obtained for the 0.40 mm feed rate (figure 8.28). In this case equal decreases and increases in temperature gave reductions and increases in predicted depression of 50 to 55% and 70 to 100% respectively. For the 0.40 mm feed rate the average tool/chip interface temperature varied from 823 to 1005^{o}C and for the 0.65 mm feed rate the corresponding temperatures varied from 889 to 1087^{o}C. These results show the sensitivity of the stress/strain relationships to changes in temperature, which may be explained as follows. In the case of the 0.65 mm feed rate, varying the

temperature by ±10% caused a variation in predicted deformation of approximately ±50%. In the case of the 0.40 mm feed rate, the predicted depression varied by 50 to 55% and 70 to 100% respectively for average tool/chip temperatures of 823 and 1005°C (±10%). These results reflect the decreasing slope of the stress/strain relationship of the tool material with increasing temperature (see figure 8.8).

Examination of the results for the two sets of cutting conditions (feed = 0.40 and 0.65 mm), shows that within the range of temperatures and stresses used, the predicted deformation was much more sensitive to ±10% variation in average temperature than to a similar variation in applied stress.

The results given on figures 8.28 and 8.29 show that a ±2% variation in temperature gave less variation in predicted deformation than a ±10% variation in temperature. These results were expected because a variation of ±2% represented a smaller perturbation from the nominal values. The results show that a ±10% variation in contact length and a ±2% variation in temperature gave approximately the same variation in predicted deformation. Although the estimated accuracy of the measuring techniques differed by a factor of five times (±10% and ±2%), their influence on the variation of predicted deformation was essentially the same.

CHAPTER 9

CONCLUSIONS

9.1 Introduction

A series of experimental investigations have shown that under certain combinations of cutting conditions, the tool will suffer an amount of permanent deformation. This deformation takes the form of depression of the rake face and bulging of the flank face. The amount of deformation has been found to be dependent on cutting speed, feed rate and time.

It may be deduced that within the cutting tool there exists a zone of material that has undergone plastic deformation. The rake face and flank face form two clearly defined external boundaries of this zone; the remaining boundary is within the tool body.

A Finite Element (F.E.) model has been developed to explain the specific effects of speed and feed in terms of temperature and stress and their variation with time. The model uses the properties of the tool material and permits their variation with temperature.

The results from the model predict that plastic deformation occurs within the tool material when the measured values of mechanical force are applied at the appropriate temperatures. This plastic deformation is further increased by the thermal stresses which arise due to temperature gradients. Changes in the shape and extent of the plastic zone are also predicted by the model.

9.2 The Influence of Speed, Feed and Time

The extent of the plastic zone and the behaviour of the material in the zone may be considered as a function of cutting speed, feed rate and time.

9.2.1 Cutting Speed

It was found that, at the rake face boundary, changes in cutting speed did not significantly change the measured cutting forces or the measured tool/chip contact length. Consequently the applied mechanical stresses were essentially constant. Increasing the speed, however, increased the measured temperature at the tool/chip interface, but the temperatures at the underside of the tool remained essentially constant. Thus the higher tool/chip interface temperatures caused a higher temperature gradient across the tool. This had the effect of raising the temperature of the tool in the regions immediately below the tool/chip interface, and on the flank face immediately below the cutting edge.

For a given point in the (existing) plastic zone at a given thermal and mechanical stress, an increase in temperature will allow an increase in strain to occur. In addition, the size of the plastic zone will increase since increases in temperature will reduce the yield stress of the surrounding material. Both of these effects will result in an increase in bulging at the flank face and depression of the rake face. These proposals are confirmed by the predictions obtained from the F.E. models (see section 9.3).

9.2.2 Feed Rate

The effect of changing the feed rate was complex. Increasing the

feed was found to increase the measured tool/chip contact temperature, the measured tool/chip contact length (over which the heat is conducted into the tool), and the measured mechanical forces. However, the vertical mechanical force was found to increase by a larger proportion than the horizontal mechanical force.

The increased temperature at the tool/chip interface increased the temperature gradient within the tool (since the temperature at the underside of the tool remained essentially constant). Combined with the increased temperature gradient was an increased contact length. These two factors increased the size of the plastic zone.

An increase in feed rate was found to give an increase in vertical force (F_v). However the contact length (ℓ_c) did not increase in the same proportion. The differential increases in F_v relative to ℓ_c caused an increase in the applied mechanical stress σ_y at the rake face boundary.

It is concluded that the combined effects of increased temperature within the tool, together with a greater applied stress (σ_y) over a longer contact length, cause the size of the plastic zone to increase with increases in the feed rate. These proposals are confirmed by the results obtained from the F.E. Models (see section 9.3).

9.2.3 Changes in the Shape of the Plastic Zone

The mechanism given above suggests that increases in speed cause an extension of the plastic zone mainly in the vertical direction. Changes in the feed rate cause an extension in both the vertical and horizontal directions.

9.2.4 Time

The experimental results show that in many cases the measured bulging and rate of bulging was time dependent. However, the relationship between deformation rate and time was found to be complex.

When examining the results of measured bulging against time, it was possible to identify three characteristic stages as follows:

(i) initial bulging or edge depression,
(ii) bulging or depression at a reduced or zero rate,
(iii) accelerated bulging often followed by rapid tool failure.

Under some conditions these separate stages cannot be clearly identified. For example, stages (i) and (ii) may not be observed under circumstances of rapid failure. Alternatively, under less severe conditions, stage (i) may only be identified after 20 to 40 seconds of cutting.

For similar cutting conditions the total amount of bulging and edge depression observed in both the incremental and continuous tests was essentially the same.

From a practical view-point for the range of conditions investigated, subjecting the tool to additional transient thermal stress cycles does not cause a measurable increase in the amount of bulging.

9.3 Comparison of Experimental Observations with Finite Element Predictions

9.3.1 Stress Distribution at the Tool/Chip Interface

When a linearly decreasing normal stress distribution was applied to the rake face of a plane stress F.E. model, a transition from parallel to tapered edge depression of the rake face was predicted for feed rates equal to or greater than 0.4 mm. The cutting tests were found to give a similar transition at feed rates equal to or greater than 0.4 mm.

When the normal stress distribution proposed by Barrow (1982) was applied to the rake face of the plane stress F.E. model, the predicted deformation did not fit the deformation observed in practice.

It may be concluded that a linearly decreasing normal stress distribution (or a similar exponential version) applied to the conditions under investigation.

9.3.2 Plane Strain F.E. Model

The plane strain F.E. models predicted a bulge on the rake face of the cutting tool. Bulging was not observed on the rake face for any of the conditions that were investigated. It may therefore be concluded that for the conditions being investigated a plane strain stress system did not apply within the tool.

9.3.3 Temperature Distribution at the Tool/Chip Interface

The tool/chip interface temperature distributions proposed by Dearnley (1983) and Usui (1984) were very similar. When they were applied to the rake face, the model predicted temperature contours in

the tool that had the same general shape as those determined experimentally by Dearnley. When either of these temperature distributions were used to predict permanent deformation, the results were found to be in good agreement with the deformation observed in practice.

When the temperature distribution proposed by Trigger (1961) was applied at the tool/chip interface, the F.E. model predicted temperature contours that had a substantially different shape from those determined experimentally by Dearnley (1983). Furthermore, when this calculated temperature distribution (Trigger) was used to predict the permanent deformation, the results did not conform with the deformation observed in practice.

It may be concluded that the tool/chip interface temperature distribution proposed by Trigger did not apply to the cutting conditions being investigated.

9.3.4 Transient Thermal Effects

9.3.4.1 Transient Temperatures

The results from the transient temperature calculations show that close to the cutting edge the steady state temperatures are approached very quickly. It is therefore suggested that the tool achieved its operating temperature in a relatively small fraction of the total cutting time.

9.3.4.2 Transient Thermal Stresses

The maximum calculated transient thermal stresses (plane stress model) were 0.25 GN/m^2 and these were restricted to a region below the central part of tool/chip contact length. For thermal stresses

acting alone the model predicted bulging of 0.15 μm. When the measured mechanical loads were applied to the thermal model, a value for bulging of 2 μm was predicted. These mechanical loads gave typical equivalent stresses of 1 to 2 GN/m^2 distributed over a large part of the cutting tool. (It should be noted that it was not sensible to apply mechanical loads acting alone because the thermal conditions were required to give changes in the mechanical properties of the tool material).

9.4 Deformation Mechanism

After considering the experimental observations and the results from the model, it is suggested that measured deformation is a consequence of material in the plastic zone undergoing a process of continuous straining. The amount of strain will vary throughout the plastic zone. For a given point in the tool material it will be dependent on the local value of temperature and stress.

The thermal conductivity of the tool material was such that the tool approached its steady state temperature very quickly. As a consequence the transient thermal stresses were low when compared with the mechanical stresses due to the applied loads (cutting forces).

It is proposed that the measured deformation was a result of the tool material at or close to its steady state temperature deforming under the applied mechanical loads. Any contribution due to the transient thermal stresses was both minimal and of a short duration.

The proposal above explains why subjecting the tool to additional

thermal transient conditions (the incremental tests) did not have any significant influence on the amount of measured deformation.

CHAPTER 10

SUGGESTIONS FOR FURTHER WORK

1) These investigations were carried out using uncoated carbide tools. It is now common to use tools that have wear resistant coatings. These coatings are also claimed to reduce the temperature of the tool. Coated tools should be investigated, because the lower temperatures should give less deformation.

2) Recent developments in tooling have incorporated complex geometry on the rake face. These developments were introduced to improve the chip breaking performance of the tools. It would be useful to compare the deformation of these tools with the deformation found for a plain rake face with zero angle.

3) A three dimensional F.E. analysis of the temperatures and stresses would probably help to explain the influence of nose radius on deformation and wear. However such an analysis would require a more detailed knowledge of the force and temperature distributions.

4) The effect of large depths of cut should be investigated, along with its incorporation into a F.E. model.

5) There is a need for data on the time dependant characteristics of the carbide alloys used in these investigations. The method of loading, temperatures and stresses investigated should be similar to those that occur in a cutting tool.

APPENDIX 1

CUTTING FORCE DYNAMOMETER

KISTLER

9257A 6. 3.72 1
9257de

3-KOMPONENTEN-MESSPLATTFORM
3-COMPONENT MEASURING PLATFORM

VORLAEUFIGE DATEN

Quarzkristall 3-Komponenten-Messplattform zur Messung einer Kraft in drei orthogonalen Komponenten. Höchste Auflösung, grosse Steifheit, minimale Messwege, kompakte Konstruktion.

TENTATIVE DATA

Piezo-electric 3-component measuring platform for measuring a force in three orthogonal components. Highest resolution, high rigidity, minimal deflection, compact design.

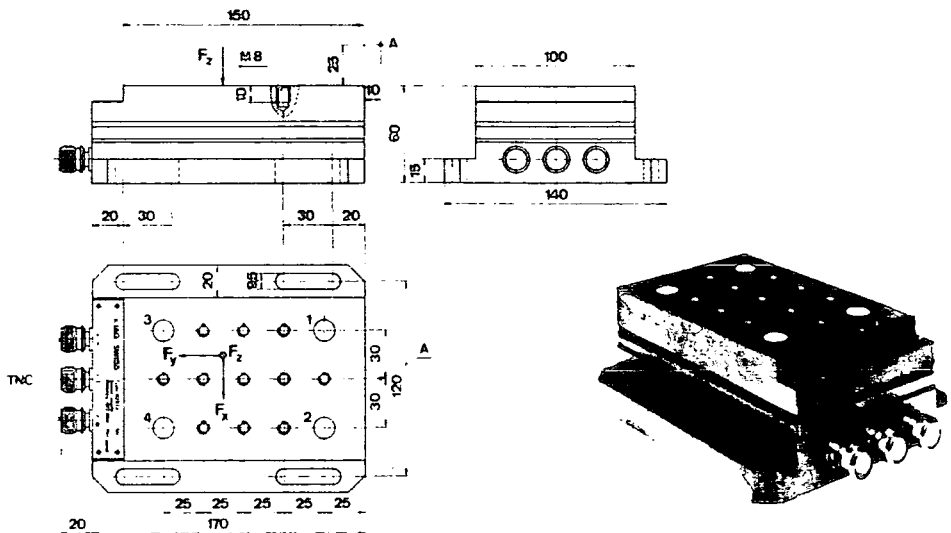

TECHNISCHE DATEN / TECHNICAL DATA

max. Messbereich, Fx = Fy = Fz: Kraftangriff innerhalb und max. 25 mm oberhalb der Deckfläche	max. measuring range Fx = Fy = Fz: application of force inside and max. 25 mm above top plate area	N	±5'000
max. Messbereich beim Drehen, Fz: (Fx = Fy = 0,5 Fz) Kraftangriff bei A	max. measuring range for turning Fz: (Fx = Fy = 0,5 Fz) appl. of force at A	N	10'000
Ansprechschwelle	resolution	N	0,01
Ueberlastbarkeit	overload capacity	%	50
Empfindlichkeit: Fz	sensitivity: Fz	pC/N	- 3,5
Fx, Fy	Fx, Fy	pC/N	- 7,5
Steifheit in z-Richtung	rigidity (z-direction)	N/µm	2000
Steifheit in x- und y-Richtung	rigidity (x- and y-direction)	N/µm	1'000
Eigenfrequenz (für jede Achse)	resonant frequency (for each axis)	kHz	ca. 4,0
Linearität	linearity	%	<±1
Uebersprechen	crosstalk	%	<2
Isolationswiderstand (jeder Kanal)	insulation resistance (each channel)	Ω	$>10^{13}$
Kapazität (jeder Kanal)	capacity (each channel)	pF	140
Temperatur-Koeffizient	temperatur coefficient	%/°C	- 0,02
Betriebstemperatur-Bereich	working temperature range	°C	0...70
Gewicht	weight	kg	6,9

1 N (Newton) = 1kg·m·s^{-2} = 0,1019..kp = 0,2248..lbf; 1kg = 2,204 ... lb; 1 in = 25,4 mm

APPENDIX 2

FORCE DISTRIBUTIONS

A2.1 Allocation of Vertical Forces (Chan and Braiden)

Figure A2.1 shows the vertical force distribution sub-divided into a number of portions T_c. Each portion was further divided into a triangular and rectangular region as shown. The corner nodes were given the numbers $N1_i$ for i = 1 to T_c and the mid-side nodes $N2_i$ for i = 1 to T_c. The corresponding total vertical forces at each corner node was $V1_i$ and $V2_i$ at the mid-side nodes.

The total area of figure A2.1 was made equal to the vertical force F1, each element was given unit length, and this gave:-

$$H = \frac{2.F1}{T_c}$$

Figure A2.2a shows the dimensions and areas of the triangular and rectangular regions for any particular portion of the distribu tion. Figures A2.2b and A2.2c show how the areas of each portion were allocated to each corner and mid-side node for the triangular and rectangular regions.

The vertical force at the first corner node $V1_{i=1}$ was given by

$$V1_{i=1} = \frac{2}{3} A_t + \frac{1}{6} A_r$$

$$= \frac{2}{3} \cdot \frac{1}{2} \cdot \frac{H}{T_c} + \frac{1}{6} \cdot \frac{H}{T_c} (T_c - N1_i)$$

$$= \frac{H}{6T} (2 + T_c - N1_i)$$

For subsequent corner nodes $V1_{i>1}$ was given by:-

$$V1_{i>1} = \frac{2}{3} \cdot \frac{1}{2} \cdot \frac{H}{T_c} + \frac{1}{6} \frac{H}{T_c} (T_c - n1_i) + \frac{1}{6} \frac{H}{T_c} (T_c - N1_i + 1)$$

$$= \frac{H}{3T} (T_c + 1.5 - N1_i)$$

The vertical force on the mid-side nodes was given by:-

$$V2_i = \frac{1}{3} A_t + \frac{2}{3} A_r$$

$$= \frac{1}{3} \cdot \frac{1}{2} \cdot \frac{H}{T_c} + \frac{2}{3} \frac{H}{T_c} (T_c - N1_i)$$

$$= \frac{H}{6T_c} (1 + 4 (T_c - N1_i))$$

A2.2 Allocation of Horizontal Forces (Chan and Braiden)

Figure A2.3 shows the shape of the horizontal force distribution. The linear region was allocated T1 portions and the sloping region T2 portions. If T_c was an even number then T1 = T2; if T was an odd number then:

$$T1 = \text{Integer } (T_c/2 + 0.5)$$

$$\text{and } T2 = T_c - T1$$

The corner and mid-side nodes were allocated the forces $H1_i$ and $H2_i$ and the total area of the figure A2.3 was allowed to equal the horizontal force F2. The height of the distribution was given by:-

$$H = \frac{F2}{T1 + 0.5\ T2}$$

A2.2.1 Linear Region

Figure A2.4a shows a rectangular area for the linear region. The

horizontal force on the first corner node was given by:-

$$Hl_{i=1} = \frac{A}{6}$$

$$= \frac{H}{6}$$

For subsequent corner nodes in the linear region, but excluding the start of the sloping region then:-

$$Hl_{i=1} = \frac{A}{6} + \frac{A}{6} = \frac{H}{3}$$

The horizontal force at the mid-side node in the linear region was given by:-

$$H2_i = \frac{2}{3} A$$

$$= \frac{2}{3} H$$

A2.2.2 Sloping Region

Figures A2.4b and A2.4c show the areas for the sloping region of the axial force distribution. The total horizontal force on the corner node at the start of the sloping region had three components and was given as:-

$$Hl_{i=T1+1} = \frac{A_r}{6} + \frac{A_{rs}}{6} + \frac{2A_t}{3}$$

$$= \frac{H}{6} + \frac{1}{6}\frac{H}{T2}(T2-(N1_i - T1)) + \frac{2}{3} \cdot \frac{1}{2} \cdot \frac{H}{T2}$$

$$= \frac{H}{6.T2} \cdot (T2 + 2 + (T_c - N1_i))$$

For subsequent corner nodes in sloping region then:-

$$H1_{i>T1+1} = \frac{H}{6T2}(T-N1_i) + \frac{H}{6T2}(T_c - N1_{i-1}) + \frac{2}{3} \cdot \frac{1}{2} \cdot \frac{H}{T2}$$

$$= \frac{H}{3T2}(T_c + 1.5 - N1_i)$$

The horizontal force on the mid-side nodes was given by:-

$$H2_{i>T1+1} = \frac{2}{3}\frac{H}{T2}(T2-(N1_i - T1)) + \frac{1}{3} \cdot \frac{1}{2} \cdot \frac{H}{T2}$$

$$= \frac{H}{6T2}(1 + 4(T_c - N1_i))$$

A2.3 Force Distribution by Barrow (1982)

Both the vertical and horizontal force distributions proposed by Barrow were treated in a similar manner as the horizontal distribution described above. Table A2.1 shows some typical output that was obtained for the two different force distributions. Also shown is the direction of the forces with their appropriate corner and mid-side node numbers.

TABLE A2.1

```
976      C GRADE/TEST NO.=1.5/(41-45)I
977      C VERTICAL FORCE (BARROW) 2160 NEWTONS
978      C SPEED,V=1 M/S= -FEED,F= .5 MM/REV
979      C CONTACT LENGTH1.06 MM
980      1        1     2     -45
981      1      101     2    -180
982      1        2     2     -90
983      1      102     2    -180
984      1        3     2     -90
985      1      103     2    -180
986      1        4     2     -90

LISTING OF TASLOADS AT 10:34:33 ON DEC  2, 1986

987      1      104     2    -180
988      1        5     2     -90
989      1      105     2    -180
990      1        6     2     -98
991      1      106     2    -158
992      1        7     2     -83
993      1      107     2    -128
994      1        8     2     -68
995      1      108     2     -98
996      1        9     2     -53
997      1      109     2     -68
998      1       10     2     -38
999      1      110     2     -38
1000     1       11     2     -23
1001     1      111     2      -7
1002     C AXIAL FORCE (BARROW) 748 NEWTONS
1003     1        1     1     16
1004     1      101     1     62
1005     1        2     1     31
1006     1      102     1     62
1007     1        3     1     31
1008     1      103     1     62
1009     1        4     1     31
1010     1      104     1     62
1011     1        5     1     31
1012     1      105     1     62
1013     1        6     1     34
1014     1      106     1     55
1015     1        7     1     29
1016     1      107     1     44
1017     1        8     1     23
1018     1      108     1     34
1019     1        9     1     18
1020     1      109     1     23
1021     1       10     1     13
1022     1      110     1     13
1023     1       11     1      8
1024     1      111     1      3
1025     C
```

TABLE A2.1 continued

```
926      C GRADE/TEST NO.=TA5/(41-45)1
927      C VERTICAL FORCES (BRAIDEN AND CHAN) 2160 NEWTONS
928      C SPEED.=1 M/S= -FEED.= .5 MM/REV

LISTING OF TA5LOADS AT 10:34:33 ON DEC  2, 1986 FOR CCID=ME04

929      C CONTACT LENGTH1.06 MM
930      1        1     2    -71
931      1      101     2   -244
932      1        2     2   -125
933      1      102     2   -220
934      1        3     2   -113
935      1      103     2   -196
936      1        4     2   -101
937      1      104     2   -173
938      1        5     2    -89
939      1      105     2   -149
940      1        6     2    -77
941      1      106     2   -125
942      1        7     2    -65
943      1      107     2   -101
944      1        8     2    -54
945      1      108     2    -77
946      1        9     2    -42
947      1      109     2    -54
948      1       10     2    -30
949      1      110     2    -30
950      1       11     2    -18
951      1      111     2     -6
952      C AXIAL FORCES (BRAIDEN AND CHAN) 748 NEWTONS
953      1        1     1     16
954      1      101     1     62
955      1        2     1     31
956      1      102     1     62
957      1        3     1     31
958      1      103     1     62
959      1        4     1     31
960      1      104     1     62
961      1        5     1     31
962      1      105     1     62
963      1        6     1     34
964      1      106     1     55
965      1        7     1     29
966      1      107     1     44
967      1        8     1     23
968      1      108     1     34
969      1        9     1     18
970      1      109     1     23
971      1       10     1     13
972      1      110     1     13
973      1       11     1      8
974      1      111     1      3
975      C
```

APPENDIX 3

TEMPERATURE DISTRIBUTIONS

A3.1 Introduction

The general shape of the temperature distributions at the tool/chip interface was discussed in section 7.4 and they are shown on figure 7.6. The following sections explain how these distributions were quantified so that they could be generally applied to the F.E. model. The tool/chip contact length was given the distance x = 0 to 1 and was divided into 10 equal divisions having a step length of 0.1. The temperature at each point was determined either directly from the published results or by a combination of interpolation and extrapolation. It was decided to normalise the temperature at each point by expressing it as a ratio of the average temperature. This was undertaken to allow a comparison between the different distributions for a standard contact length of unity.

A Chebychev polynomial was fitted to the standardised data that was found for each distribution. The form of the polynomial is shown below:-

$$f(x) = \tfrac{1}{2} C_o T_o^{\,1}(x) + C_1 T_1^{\,1}(x) + C_2 T_2^{\,1}(x) + C_3 T_3^{\,1}(x) + \ldots C_n T_n^{\,1}(x) \quad (A.1)$$

where C_o to C_n were the Chebychev coefficients, and:-

$$T_o^{\,1}(x) = 1$$

$$T_1^{\,1}(x) = (2x - 1)$$

$$T_2^{\,1}(x) = (8x^2 - 8x + 1)$$

$$T_3^1(x) = (3x^3 - 48x^2 + 18x - 1)$$

$$T_4^1(x) = (128x^4 - 256x^3 + 160x^2 - 32x + 1)$$

$$T_5^1(x) = (512x^5 - 1280x^4 + 1120x^3 - 400x^2 + 50x - 1)$$

$$T_6^1(x) = (2048x^6 - 6144x^5 + 6912x^4 - 3584x^3 - 840x^2 - 72x + 1)$$

By using a special computer programme it was possible to determine the coefficients C_o to C_n. The value of C_{n-1} gave the degree of the polynomial and this was increased until a sufficiently good fit was achieved for the data. A measure of the fit is given by the Root Mean Square (R.M.S.) residual. A number of runs were required for each temperature distribution to determine the degree of polynomial that gave the minimum R.M.S. residual.

A3.2 Temperature Distribution by Trigger (1961)

The temperatures for this distribution were obtained directly from the figure published by Trigger. The position along the contact length and normalised temperature are shown as the values of abscissa(x) and ordinate(θ) respectively in Table A3.1. Also shown in the table are the Chebychev coefficients, the R.M.S. residual and the approximation to the ordinate(θ) value calculated from the coefficients. It was found that an adequate fit was obtained by using a polynomial of degree 6.

A3.3 Temperature Distribution by Usui (1984)

The distribution published by Usui gave variations in temperature both parallel and perpendicular to the direction of chip flow. A distribution was published that gave the variation in temperature

R	ABSCISSA (X)	ORDINATE (Θ)
1	0.00000E+01	0.53400E+00
2	0.10000E+00	0.54300E+00
3	0.20000E+00	0.60300E+00
4	0.30000E+00	0.77900E+00
5	0.40000E+00	0.11200E+01
6	0.50000E+00	0.12750E+01
7	0.60000E+00	0.13180E+01
8	0.70000E+00	0.13090E+01
9	0.80000E+00	0.12570E+01
10	0.90000E+00	0.11690E+01
11	0.10000E+01	0.10770E+01

RESULTS

DEGREE 6

J	CHEBYCHEV COEFF A(J)/
1	0.19231E+01
2	0.37161E+00
3	-0.19545E+00
4	-0.10342E+00
5	0.79614E-01
6	0.84510E-03
7	-0.40941E-01

R.M.S RESIDUAL = 0.33141E-01

POLYNOMIAL APPROXIMATION AND RESIDUALS FOR DEGREE 6

R	ABSCISSA	APPROXIMATION	RESIDUAL
1	0.00000E+01	0.53577E+00	0.17672E-02
	0.50000E-01	0.54754E+00	
2	0.10000E+00	0.53766E+00	-0.53354E-02
	0.15000E+00	0.54863E+00	
3	0.20000E+00	0.57867E+00	-0.43324E-02
	0.25000E+00	0.68890E+00	
4	0.30000E+00	0.80944E+00	0.34441E-01
	0.35000E+00	0.94463E+00	
5	0.40000E+00	0.10773E+01	-0.42716E-01
	0.45000E+00	0.11920E+01	
6	0.50000E+00	0.12776E+01	0.25742E-02
	0.55000E+00	0.13284E+01	
7	0.60000E+00	0.13448E+01	0.26844E-01
	0.65000E+00	0.13331E+01	
8	0.70000E+00	0.13035E+01	-0.55168E-02
	0.75000E+00	0.12682E+01	
9	0.80000E+00	0.12381E+01	-0.18923E-01
	0.85000E+00	0.12183E+01	
10	0.90000E+00	0.12034E+01	0.14364E-01
	0.95000E+00	0.11707E+01	
11	0.10000E+01	0.10738E+01	-0.31664E-02

TABLE A3.1 CHEBYCHEV COEFFICIENTS ::: TRIGGER (1961)

EOT..

R	ABSCISSA (X)	ORDINATE (8)
1	0.00000E+01	0.78600E+00
2	0.10000E+00	0.90200E+00
3	0.20000E+00	0.10010E+01
4	0.30000E+00	0.10520E+01
5	0.40000E+00	0.10870E+01
6	0.50000E+00	0.10870E+01
7	0.60000E+00	0.10800E+01
8	0.70000E+00	0.10650E+01
9	0.80000E+00	0.10300E+01
10	0.90000E+00	0.98000E+00
11	0.10000E+01	0.93000E+00

RESULTS

DEGREE 6

J	CHEBYCHEV COEFF A(J)/
1	0.19513E+01
2	0.54917E-01
3	-0.11921E+00
4	0.18375E-01
5	-0.26308E-02
6	-0.12833E-02
7	0.41129E-02

R.M.S RESIDUAL = 0.36498E-02

POLYNOMIAL APPROXIMATION AND RESIDUALS FOR DEGREE 6

R	ABSCISSA	APPROXIMATION	RESIDUAL
1	0.00000E+01	0.78593E+00	-0.70958E-04
	0.50000E-01	0.84443E+00	
2	0.10000E+00	0.90267E+00	0.66972E-03
	0.15000E+00	0.95500E+00	
3	0.20000E+00	0.99851E+00	-0.24861E-02
	0.25000E+00	0.10323E+01	
4	0.30000E+00	0.10567E+01	0.46647E-02
	0.35000E+00	0.10729E+01	
5	0.40000E+00	0.10826E+01	-0.43964E-02
	0.45000E+00	0.10872E+01	
6	0.50000E+00	0.10881E+01	0.11403E-02
	0.55000E+00	0.10861E+01	
7	0.60000E+00	0.10815E+01	0.15267E-02
	0.65000E+00	0.10742E+01	
8	0.70000E+00	0.10636E+01	-0.13633E-02
	0.75000E+00	0.10491E+01	
9	0.80000E+00	0.10302E+01	0.20967E-03
	0.85000E+00	0.10069E+01	
10	0.90000E+00	0.98016E+00	0.15923E-03
	0.95000E+00	0.95284E+00	
11	0.10000E+01	0.92995E+00	-0.53476E-04

TABLE A3.2 CHEBYCHEV COEFFICIENTS ::: USUI (1984)

EOT..

R	ABSCISSA (X)	ORDINATE (Θ)
1	0.00000E+01	0.82900E+00
2	0.10000E+00	0.91300E+00
3	0.20000E+00	0.99700E+00
4	0.30000E+00	0.10150E+01
5	0.40000E+00	0.10420E+01
6	0.50000E+00	0.10620E+01
7	0.60000E+00	0.10710E+01
8	0.70000E+00	0.10830E+01
9	0.80000E+00	0.10860E+01
10	0.90000E+00	0.10480E+01
11	0.10000E+01	0.85500E+00

RESULTS

DEGREE 6

J	CHEBYCHEV COEFF A(J)/
1	0.19644E+01
2	0.50761E-01
3	-0.10491E+00
4	-0.23123E-01
5	-0.32532E-01
6	-0.13553E-01
7	-0.30677E-02

R.M.S RESIDUAL = 0.95776E-02

POLYNOMIAL APPROXIMATION AND RESIDUALS FOR DEGREE 6

R	ABSCISSA	APPROXIMATION	RESIDUAL
1	0.00000E+01	0.82759E+00	-0.14144E-02
	0.50000E-01	0.87818E+00	
2	0.10000E+00	0.92028E+00	0.72794E-02
	0.15000E+00	0.95514E+00	
3	0.20000E+00	0.98355E+00	-0.13453E-01
	0.25000E+00	0.10061E+01	
4	0.30000E+00	0.10234E+01	0.84067E-02
	0.35000E+00	0.10362E+01	
5	0.40000E+00	0.10454E+01	0.34099E-02
	0.45000E+00	0.10521E+01	
6	0.50000E+00	0.10576E+01	-0.43797E-02
	0.55000E+00	0.10630E+01	
7	0.60000E+00	0.10691E+01	-0.19258E-02
	0.65000E+00	0.10762E+01	
8	0.70000E+00	0.10837E+01	0.71444E-03
	0.75000E+00	0.10896E+01	
9	0.80000E+00	0.10898E+01	0.38020E-02
	0.85000E+00	0.10781E+01	
10	0.90000E+00	0.10448E+01	-0.31962E-02
	0.95000E+00	0.97670E+00	
11	0.10000E+01	0.85576E+00	0.75689E-03

TABLE A3.3 CHEBYCHEV COEFFICIENT ::: DEARNLEY (1983)

EOT..

along a section of the chip that was parallel with the direction of flow. The section considered was slightly away from the centre of the chip and may not have represented the maximum temperature that occurred at the tool/chip interface. However, any error was likely to be minimal, because the temperature variation across the direction of chip flow was much less than the variation in the direction of chip flow.

The data for this distribution was obtained in similar manner to that obtained for the distribution proposed by Trigger. It was, however, necessary to determine the temperatures at the cutting edge and chip departure point by a process of extrapolation. The values were extrapolated by fitting a linearly decreasing line tangentially to the measured part of the distribution. The Chebychev coefficients and the R.M.S. residual are shown in Table A3.2.

A3.4 Distribution by Dearnley (1983)

This distribution was obtained when using a cutting speed of 4 m/s and a feed rate of 0.25 mm/rev with a depth of cut of 1.3 mm. The tool had suffered a large amount of deformation after only 10 seconds machining. There was 140 μm of edge depression and 30 μm of bulging on the flank face (figure A3.1). The bulging caused a loss of clearance and this would allow rubbing to take place with the newly machined work surface. This rubbing action must be considered as an additional heat source.

The temperature distribution along the rake face was determined from the 762, 900 and 1210^{o}C contours by using a combination of interpolation and extrapolation. The tool/chip contact length was divided into 10 equal divisions, which produced 11 positions shown as

0 to 10 on figure A3.1. Figure A3.2 shows how the temperature at each point was determined. The positions numbered 3 to 8 on the rake face were obtained by extrapolating from the 900°C and 1210°C temperature contours. The perpendicular distance from the rake face to these two contours was measured, and the ratio of these two values was used to determine the temperature on the rake face. Consider, for example, point number 3; the perpendicular distance from the rake face to the 900 and 1210°C contours was 50 and 48 mm respectively. The temperature on the rake was extrapolated as:

$$\frac{50}{48}\ (1210 - 900) + 900 = 1223^{\circ}C.$$

The temperature at point number 10, which was the point of chip departure from the tool, was determined by linearly interpolating between the 900° and 1210°C contour. It was decided to determine the temperature at this point by interpolation rather than by extrapolation from the 762 and 900°C contours. It was considered that determining the temperature at this point by extrapolation would give an erroneous result, because a line drawn perpendicular to the rake face was found to make a very acute angle with the 762 and 900°C contours. To extrapolate a value along such a line would not give a correct result. Ideally, the extrapolation line should be perpendicular to all the contour lines it crosses, because a temperature gradient has its maximum value perpendicular to the contour line.

The temperature at point number 9 was obtained by both horizontal extrapolation and perpendicular extrapolation from the 1210°C contour. The horizontal method gave 1273°C and the perpendicular method 1256°C; these two results were considered to give agreement when the

limitations of the technique are considered. It was decided to use the average value of 1264°C.

It was found to be very difficult to determine the temperature at the points 0, 1 and 2. It was decided to calculate the temperature at point number 2 by extrapolating from the temperature previously determined at point 2 and the known contour of 1210°C, this method gave a value of 1202°C. Extrapolation of the temperature from the 900 and 762 contours gave a temperature of 1134°C. It was considered that this value was unlikely to be correct, because it represented an extremely rapid rise in temperature over the relatively short distance to the known position of the 1210 contour. It was therefore decided to use the value of 1202°C.

The temperature at the cutting edge (position 0) was found by perpendicular extrapolation from the 900 and 762 contours and gave a value of 999°C. Horizontal extrapolation for this point from the temperature at position number 3 and the 1210 contour gave a temperature at the cutting edge of 1157°C. It was considered that this value was extremely high, and may not occur if a sharp undeformed tool was used for the tests. Such a value may have occurred in this tool because it was subjected to rubbing at the flank face and this caused an increase in temperature at the flank region. For this reason it was decided to use the lower temperature of 999°C.

A similar situation occurred when trying to determine the temperature at position number 1. Extrapolation from the 762 and 900 contours gave a value of 1000°C, which was effectively the same temperature as that found at the cutting edge. It was considered that this value was not correct for two reasons, as follows. Firstly, it

would be expected that some rise in temperature would occur along the tool/chip contact length. Secondly, if the temperature at position number 1 was 1000°C, then an extremely high rise in temperature would be required over the short distance between position number 1 and the 1210°contour; such a high rise in temperature was unlikely. It was decided to use a value of 1100°C, which was the average found from positions 0 and 2.

It should be appreciated that the calculated shape of the temperature distribution along the rake face was entirely dependant on the relative positions of the temperature contours. Examination of the data on figure A3.1 shows that the maximum temperature occurred close to position 6, and was approximately half way between the two points where the 1210°C contour intersected the rake face. Such an estimate would seem to be reasonable and was probably correct. If the position of the maximum temperature was correct then there must be some doubt as to the correct position of the 900°C contour. The calculated position of the maximum temperature can only be made coincident with the estimated position by moving the right hand side of the 900°C contour closer to the cutting edge.

A more realistic estimate of the shape of the distribution could have been made if additional contours had been available, such as 1000 and 1100°C. It is interesting to note that there was a difference of 310°C between the contours; this occurred at the hottest part of the tool where the high temperatures have the most significant effect on the hot compressive stress of the tool material. The temperature in the region immediately below the cutting edge was not defined, however it is well-known that when cutting steel this region is subjected to the highest stresses.

Figure A3.1 shows that extremely high temperature gradients can occur in a cutting tool, a value of approximately 2500°C/mm having been estimated in certain regions. The severity of the temperature gradients was dependant on the location of the temperature contours. There would appear to be two main causes of error that can occur when attempting to locate the temperature contours, as follows:-

(i) the boundary of transformed material was not clearly defined;

(ii) a reference point on the tool for locating the different contours was not defined.

With regard to the first cause of error, Dearnley showed metallographic sections of two tools used to cut the steel. In both cases a change in colour density across the sections could be observed, however the change was not clearly defined and at many positions on the tools it occurred over a distance of 50 to 100 μm. If these distances are translated into temperature using the gradient calculated above (2500°C/mm), then they represent values of 125 and 250°C respectively. This error can be considered as follows, either a contour of known value cannot be located more accurately than ±50 μm; alternatively, if the location of a contour is considered to be correct, then the value of the contour may be considered to vary by as much as ±125°C.

The second cause of error is concerned with relating the known contours to a reference point on the tool. It was necessary to use a different tool for each cutting test to determine the temperature contours. At the speed used (4 m/s) the tool was observed to be

unstable; it suffered a large amount of edge depression, crater wear and flank face bulging, which caused a lack of definition of a fixed reference point on the tool. The absence of a clearly defined and fixed reference point is a source of error when attempting to locate the temperature contours from different tools.

This technique by Dearnley is useful in that it confirms that certain known temperatures occur in a cutting tool. It is, however, subject to the limitations discussed above when determining the temperature gradients. Under certain circumstances temperature gradients can be very significant because they cause thermal stresses.

Table A3.3 shows the data obtained for this distribution and the calculated Chebychev coefficients along with the R.M.S. residual and the approximation to the ordinate value (θ).

REFERENCES

ALMOND, E A	Joint NPL and Metals Society Conf. Teddington, 28-29 April 1981, p161-90.
ALVELID, B	Annals of the C.I.R.P. Vol XVIII pp547-554.
AMINI, E	Journal of Strain Analysis, Vol.3, No.3, (1968), p206-213.
BARROW, G	Int. Jnl. Mach. Tool Design and Research, Vol.22, No.1, (1982), p75-85.
BOOTHROYD, G	Proc. I.Mech.E., Vol.177, (1963), p789.
BRAIDEN, P M	M.T.D. R. Conf. Vol.8, (1967), p653-666.
BRAIDEN, P M	Society of Manufacturing Engineers, MR71-916, (1971).
BROOKES, A J	World Directory and Handbook of Hard Metals, 3rd Ed. 1982. Published Jointly by Engineers Digest Ltd and International Carbide Data.
BUS, C and VEENSTRA, D C	Proc. 12th Int. MTDR Conf. 1971.
CHAN, J F L and BRAIDEN, P M	Proc. Second Int. Conf. on Numerical Methods in Thermal and Mechanical Problems, Venice, (1981).
CHAN, J F L	Private Communication, May 1983.
DAWIHL, W and ALTMEYER, G	Z. Metallk.; 54(2): 66, (1963).
DEARNLEY, P A and TRENT, E M	Metals Technology, Vol.9, (1982), p60-75.
DEARNLEY, P A	Metals Technology, Vol.10, (1983), p205-214.
DOEBELIN, E O	Measurement Science, Application and Design, McGraw-Hill, 1966.
EDWARDS, R	Joint NPL and Metals Society Conf. Teddington, 28-29 April 81, p93-95.
EKEMAR, S	M.T.D.R. Conf. Birmingham Sept. (1966). (Paper read but not published.)
GAYLORD, E W and HUGHES, W F	A.S.M.E. Paper No.56-A-86, (1957)
GAYLORD, E W and HUGHES, W F	A.S.M.E. Paper No.63 - Lub. - 6, (1963)

HERBERT, E G	Proc. I.Mech.E., Vol.1, (1926), p289-329.
I.S.O. 3685-1977(E)	Tool life testing with single-point tools.
JACK, K H	Metals Technology, Vol.9, (1982), p297.
JAESCHKE, J R	Int. Jnl. Mach. Tool Design and Research, Vol.7, (1967), p465-475.
JAWAID, A	Metals Technology, Vol.10, (1983), p482-489.
JONSSON, H	Planseeberichte Fur Pulvermetallurgie, Bd20, (1972), p39-62.
KATO, S and YAMAGUCHI, K	Jnl. Eng. Ind. 94(2) (1972), pp683-689.
KAYE, G W C and LABY, T H	Tables of Physical and Chemical Constants, 15th Ed. 1986. Published by Longman - London and New York
KITAGAWA, T	Bull. Japan Soc. of Prec., Vol.9, No.3, (Sept. 1975), pp83-84.
KRONENBERG, M	Machining Science and Application. Pergamon Press, (1966).
KURIMOTO, T	PhD Thesis. The University of Manchester Institute of Science and Technology, May 1977.
LEWIS, M H	Journal Materials Science, 15, 103, (1980).
LOLADZE, T N	M.T.D.R. Conf. Vol.8, (1967), p821-843.
METCALFE, A G	Intern. Powder Met. Congress Graz (1947) (Unpublished).
MITCHELL, J H	Proc. London Mathematics Society, 34, (1902).
MULLEN, H	Industrial Diamond Review, Vol.43, 494, (1983), p30-33.
MUSKLELISHVILI, N I	Mathematical Theory of Elasticity, P. Nordshoff, Groningen, (1963).
PAFEC	Theory, Results and Data Preparation Manual.
SCHWARZKOPF, P and KIEFFER, R	Cemented Carbides, Published by The Macmillan Company, 1960.
SMART, E F and TRENT, E M	Int. Jnl. Prod. Res., Vol.13, No.3, (1975), pp265-290
TAKEYAMA, H and MURATA, R	Jnl. Eng. Ind., 85, Feb. 1963, pp33-37.
TAYLOR, F W	Trans. A.S.M.E., 28, 31 (1907).

THOMASON, P F	Jnl. Mech. Eng. Science, Vol.16, No.6,(1974), p418-424.
THOMASON, P F	Jnl. Eng. for Ind. Trans. ASME.97, (1975), p1060-1075.
TLUSTY, J and MASOOD, Z	Jnl. Eng. for Ind. Trans. ASME.100, (1978), p403-412.
TRENT, E M	Inst. Prod. Eng. Jnl., 38, 105, (1959).
TRENT, E M	Iron and Steel Inst., Special Report, Conf. on Machinability, Vol.94, (1967), pp77-87.
TRENT, E M	M.T.D.R. Conf. Vol.8, (1967), p629-642.
TRENT, E M	Metalcutting (2nd Edition), Butterworths, (1983).
TRIGGER, K J	Jnl. Eng. for Ind. Trans. ASME.83, (1961), p496-501.
TRIGGER, K J	American Machinist, Vol.110, No.15 (1966), p.101.
UEDA, F and DOI, H	Trans. J.I.M. Vol.18,(1977), pp247-256.
USUI, E and HIROTA, A	Trans. A.S.M.E., Vol.100 (1978), pp 222-243.
USUI, E and SHIRAKASHI, T	Wear, Vol.100 (1984), pp129-151.
VENKATESH, V C	Tribology International, Dec. 1977, p313-318.
WALKER, P I and DICKINSON, E A	Joint N.P.L. and Metals Society Conf. Teddington, 28-29 April 81, p89-92.
WOODS, W O	Rodman Process Lab. U.S.A. Interim Reports, No. RPL 42/2 and 42/3, (1956).
ZOREV, N N	Int. Res. in Prod. Eng., ASME 85, (1963), p42-49.

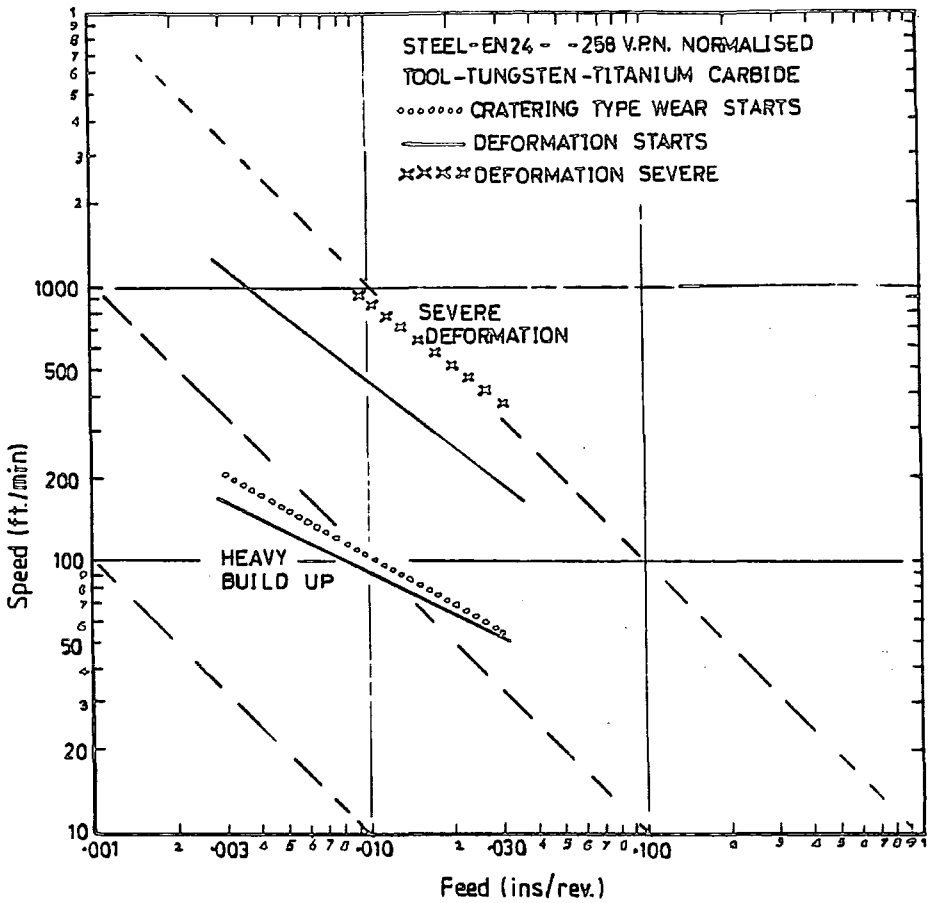

Fig. 1·1 THE INFLUENCE OF FEED & SPEED ON TOOL DEFORMATION & WEAR (TRENT 1959)

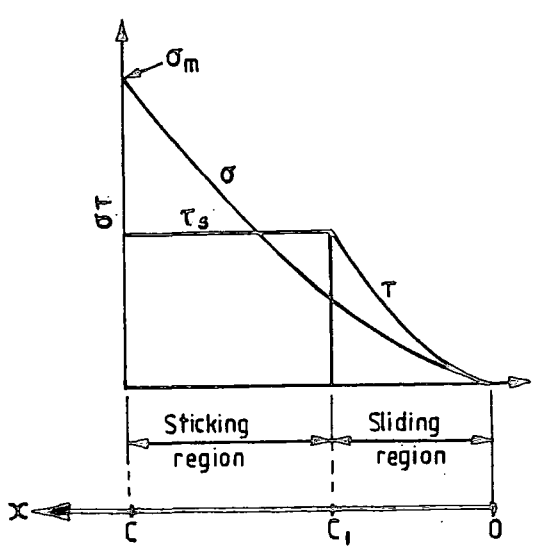

Fig. 1·2 STRESS DISTRIBUTION ZOREV (1963)

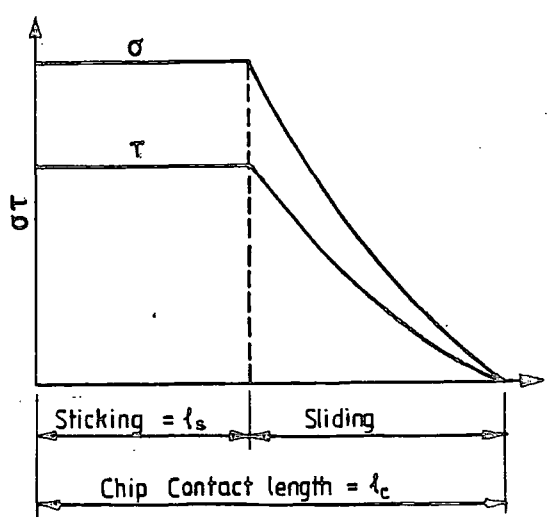

Fig. 1·3 STRESS DISTRIBUTION BARROW (1982)

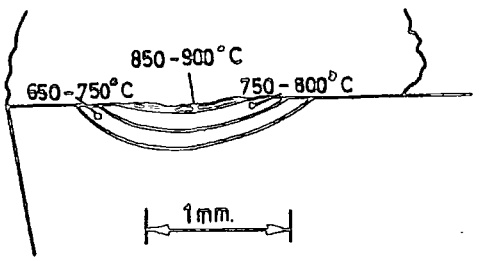

(a) Speed = 152 m/min., feed = 0·25 mm./rev.

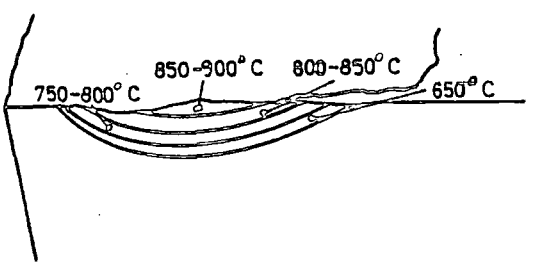

(b) Speed = 183 m/min.. feed = 0·25 mm./rev.

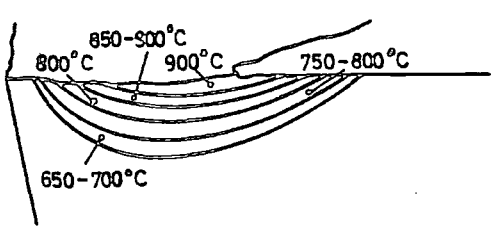

(c) Speed = 213 m/min. feed = 0·25 mm./rev.

Fig. 1·4 TEMPERATURES IN HSS TOOLS WHEN MACHINING LOW CARBON STEEL (SMART & TRENT (1975)

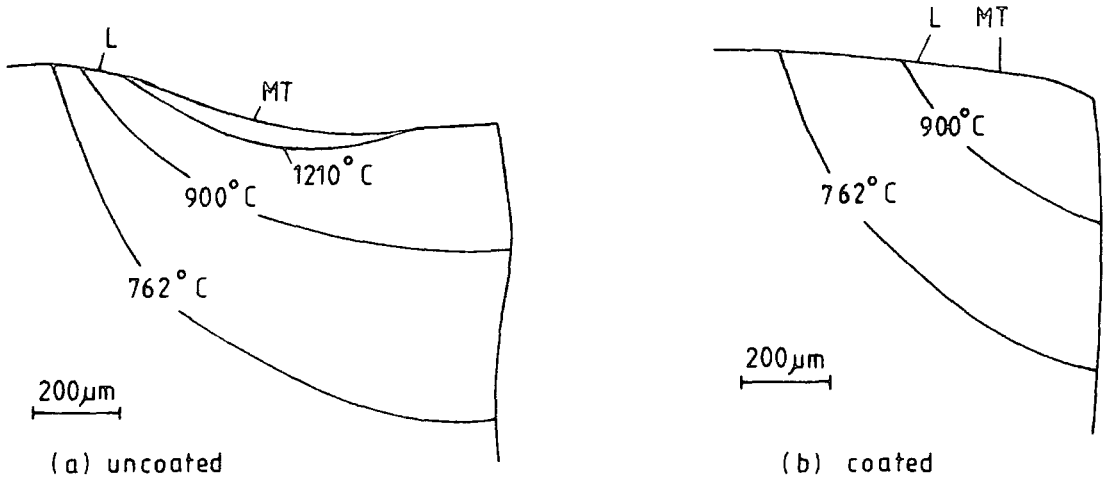

FIGURE 1·5 TEMPERATURES IN CARBIDE TOOLS AFTER MACHINING STEEL (817 M40. EN 24) FOR 10 secs.
Speed = 240m/min., feed = 0·25mm./rev., depth = 1·3mm.
(DEARNLEY 1983)
Note :- L = Chip/tool departure point
MT = Position of maximum temperature

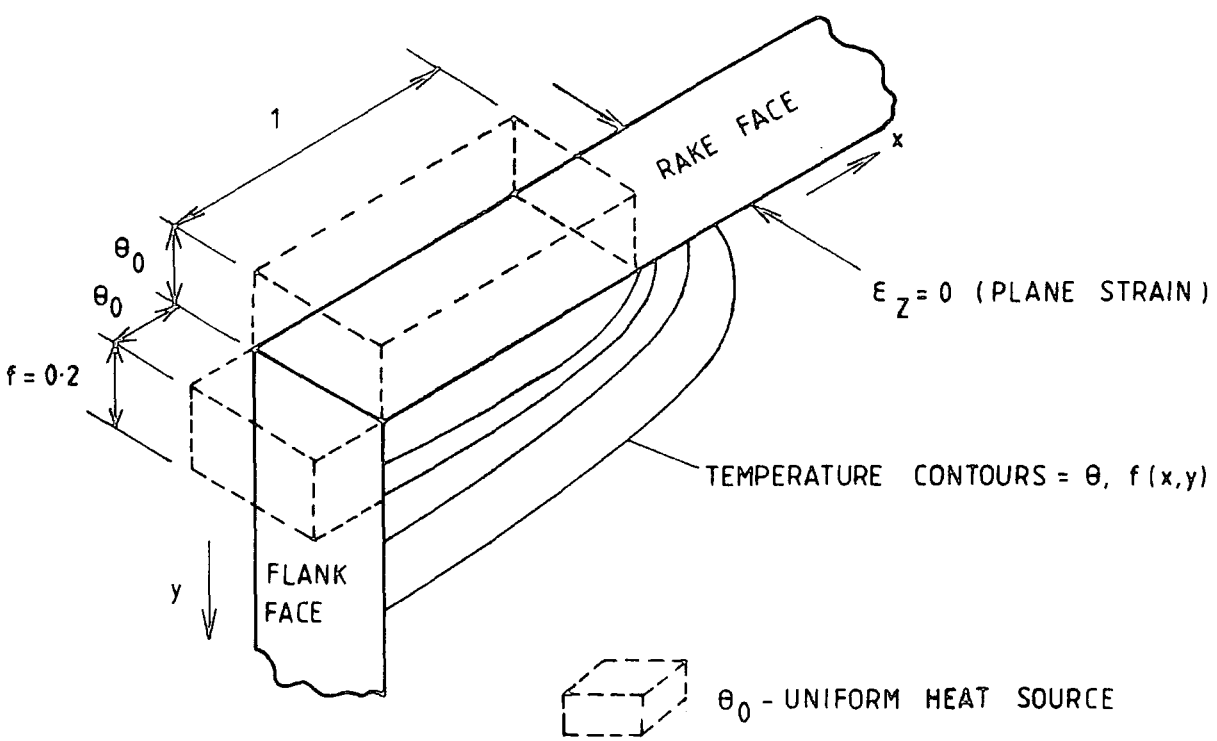

FIGURE 1·6 TOOL TEMPERATURE MODEL (THOMASON, 1975)

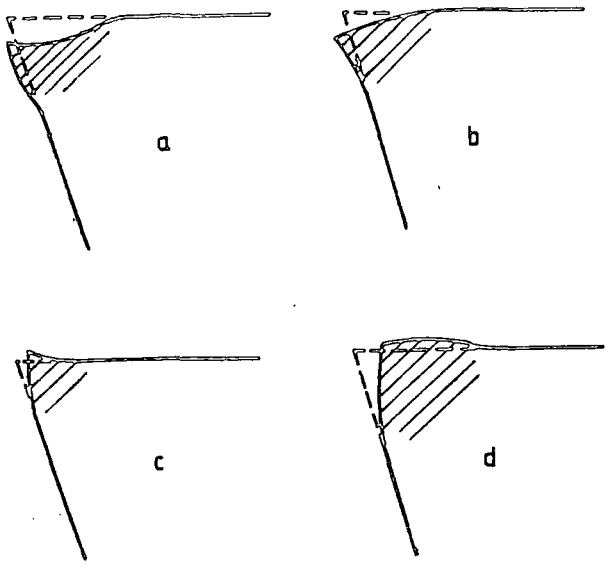

Fig. 1·7 CLASSIFICATION OF TOOL DEFORMATION BY TRENT (1967)

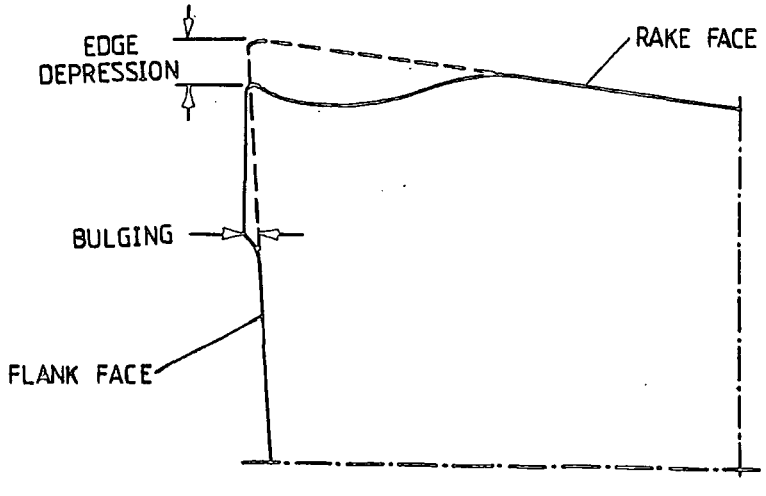

Fig. 1·8 FLANK BULGING & EDGE DEPRESSION (EKEMAR 1966)

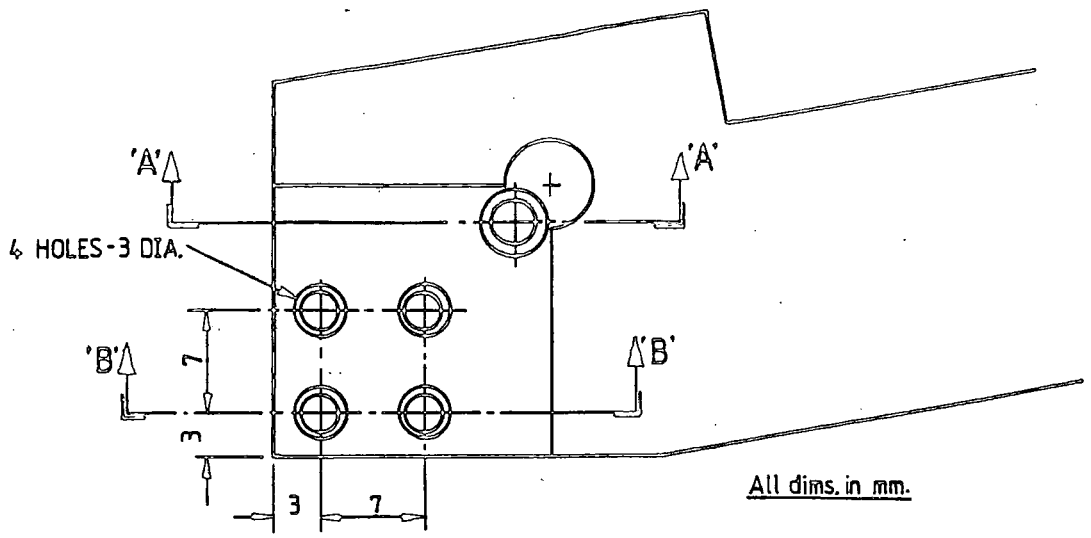

Fig. 2·1a PLAN VIEW OF TOOL TIP HOLDER

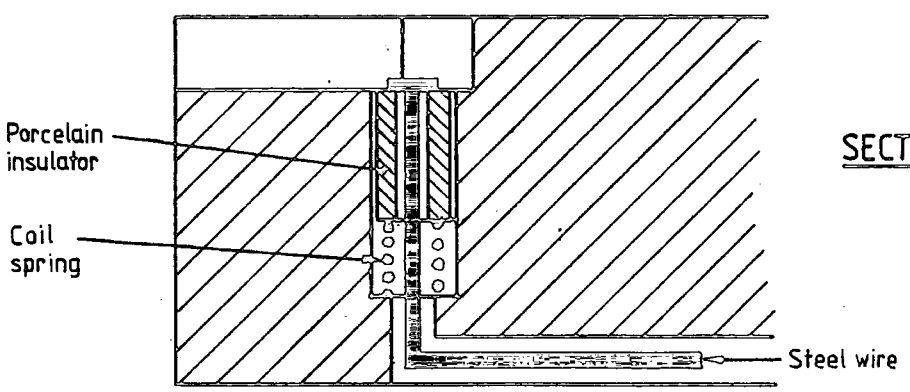

SECTION 'A-A'

Fig. 2·1b ARRANGEMENT OF TOOL/WORK COLD JUNCTION

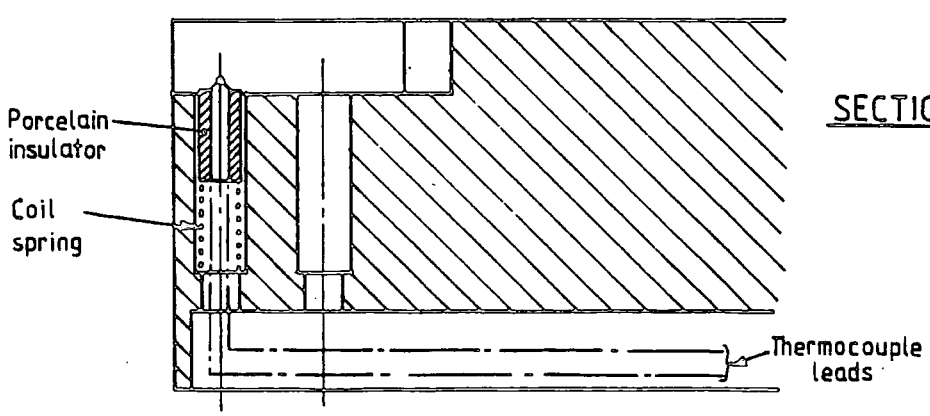

SECTION 'B-B'

Fig. 2·1c ARRANGEMENT OF TIP-SHANK THERMOCOUPLES

SCALE:- 2:1

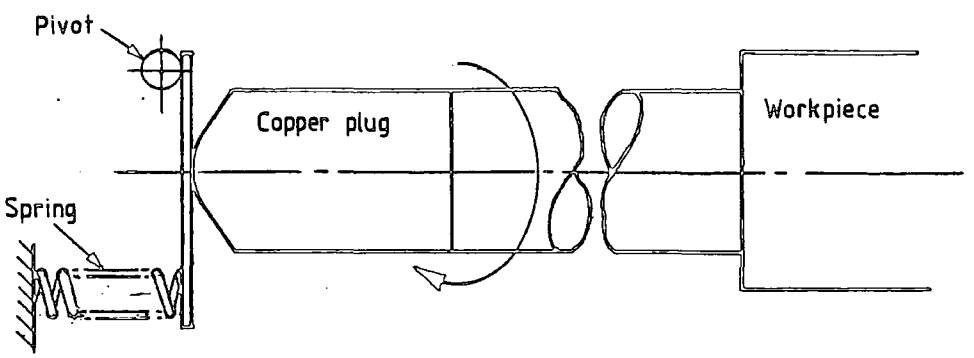

Fig. 2·2 SIGNAL TRANSFER SYSTEM FOR TOOL-WORK THERMOCOUPLE

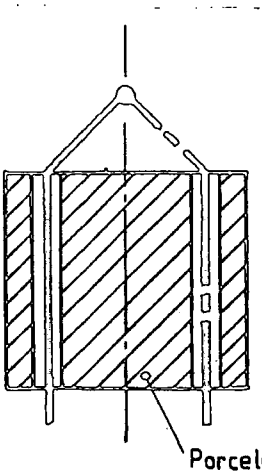

Fig. 2·3

Fig. 2·3 THERMOCOUPLE MOUNTED IN PORCELAIN INSULATOR

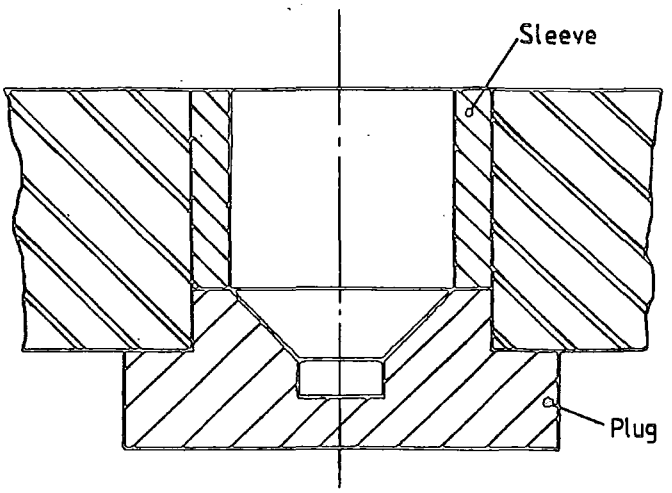

Fig. 2·4

Fig. 2·4 MOULD FOR ENCAPSULATING THERMOCOUPLES

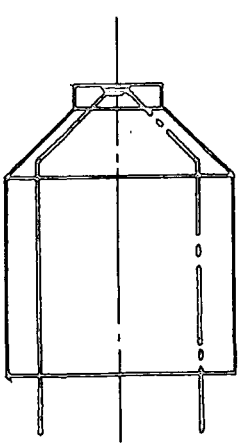

Fig. 2·5

Fig. 2·5 ENCAPSULATED THERMOCOUPLE

SCALE:- 10:1 (approx.)

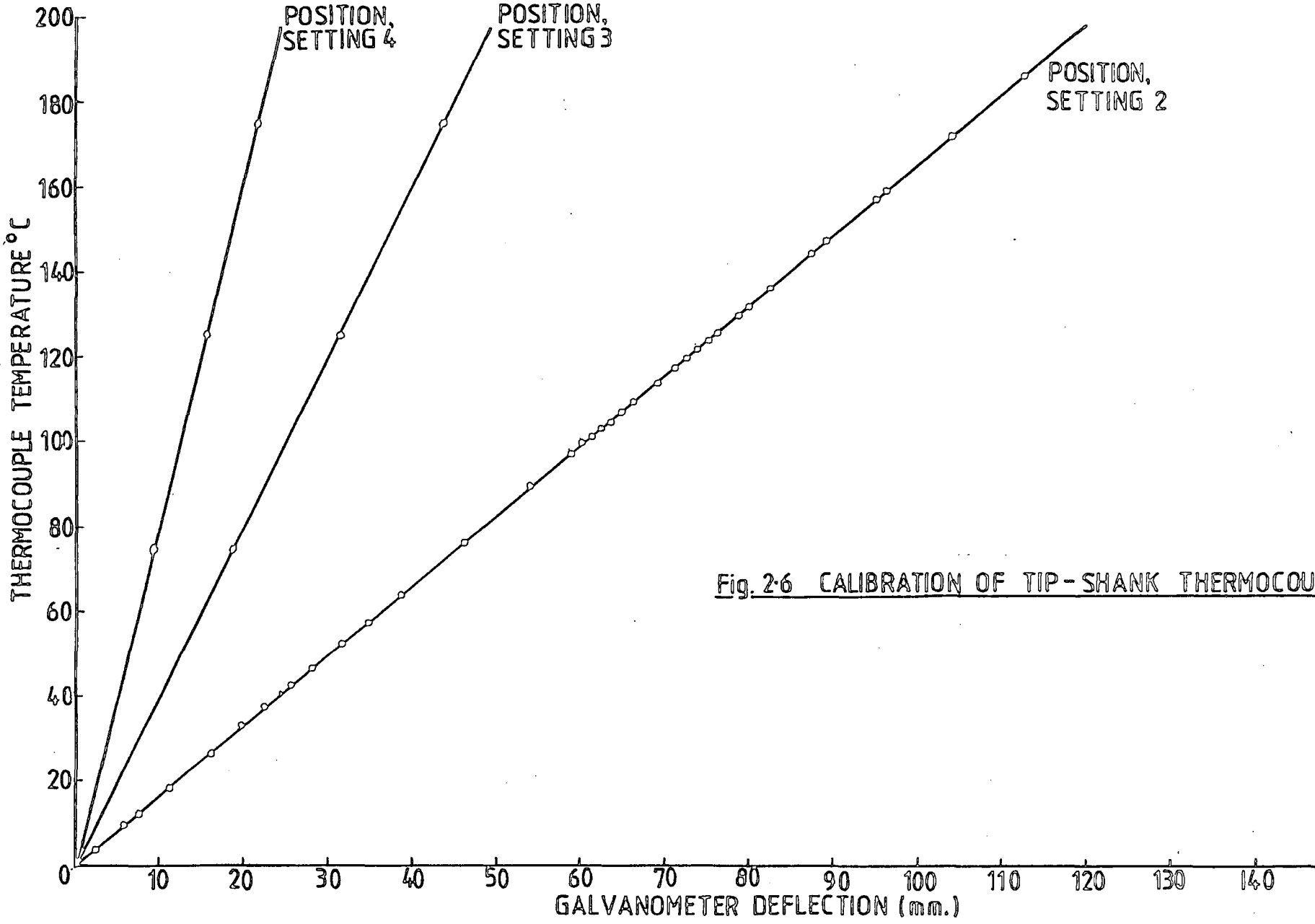

Fig. 2·6 CALIBRATION OF TIP-SHANK THERMOCOUPLES

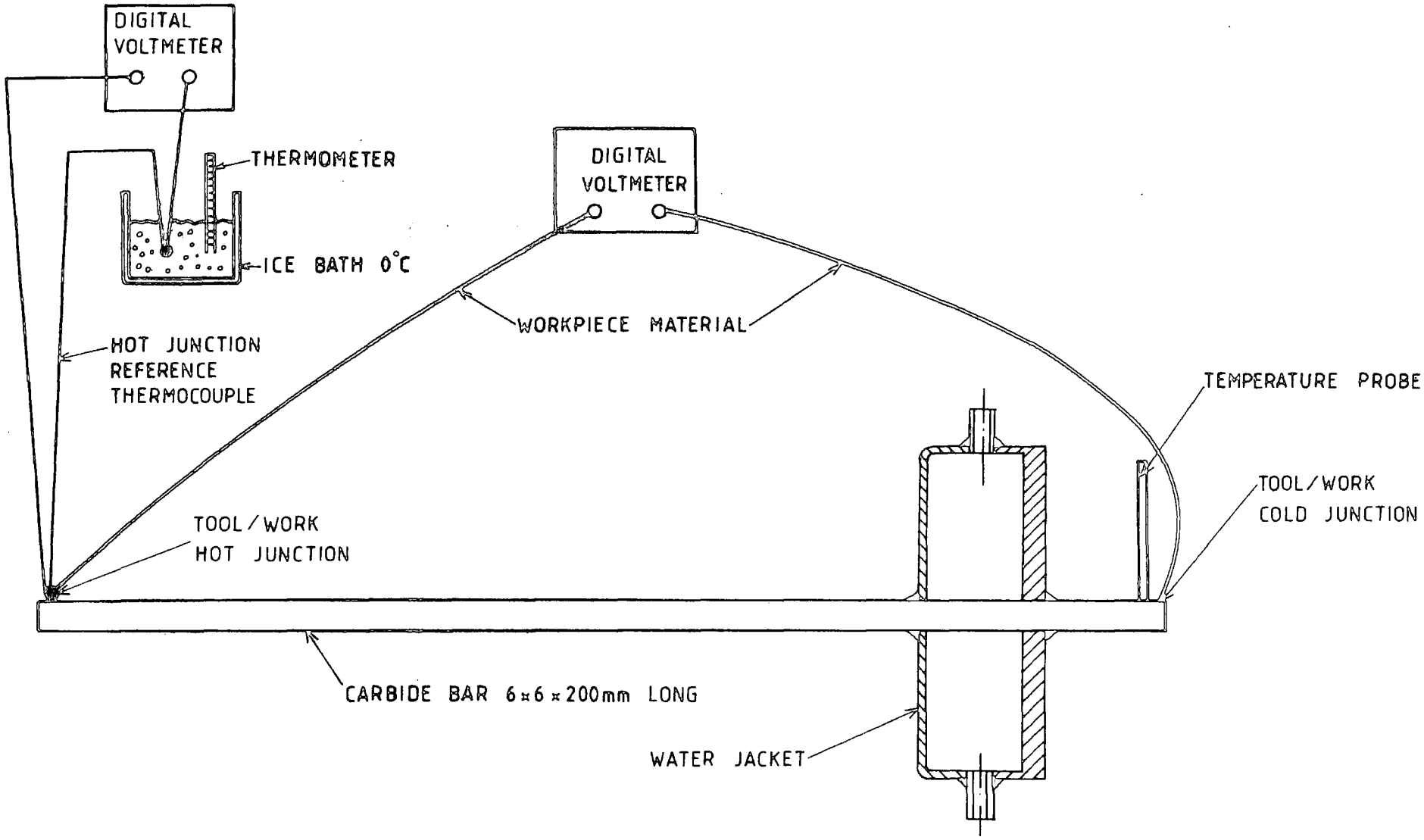

FIGURE 2·7 ARRANGEMENT FOR CALIBRATING TOOL/WORK THERMOCOUPLES

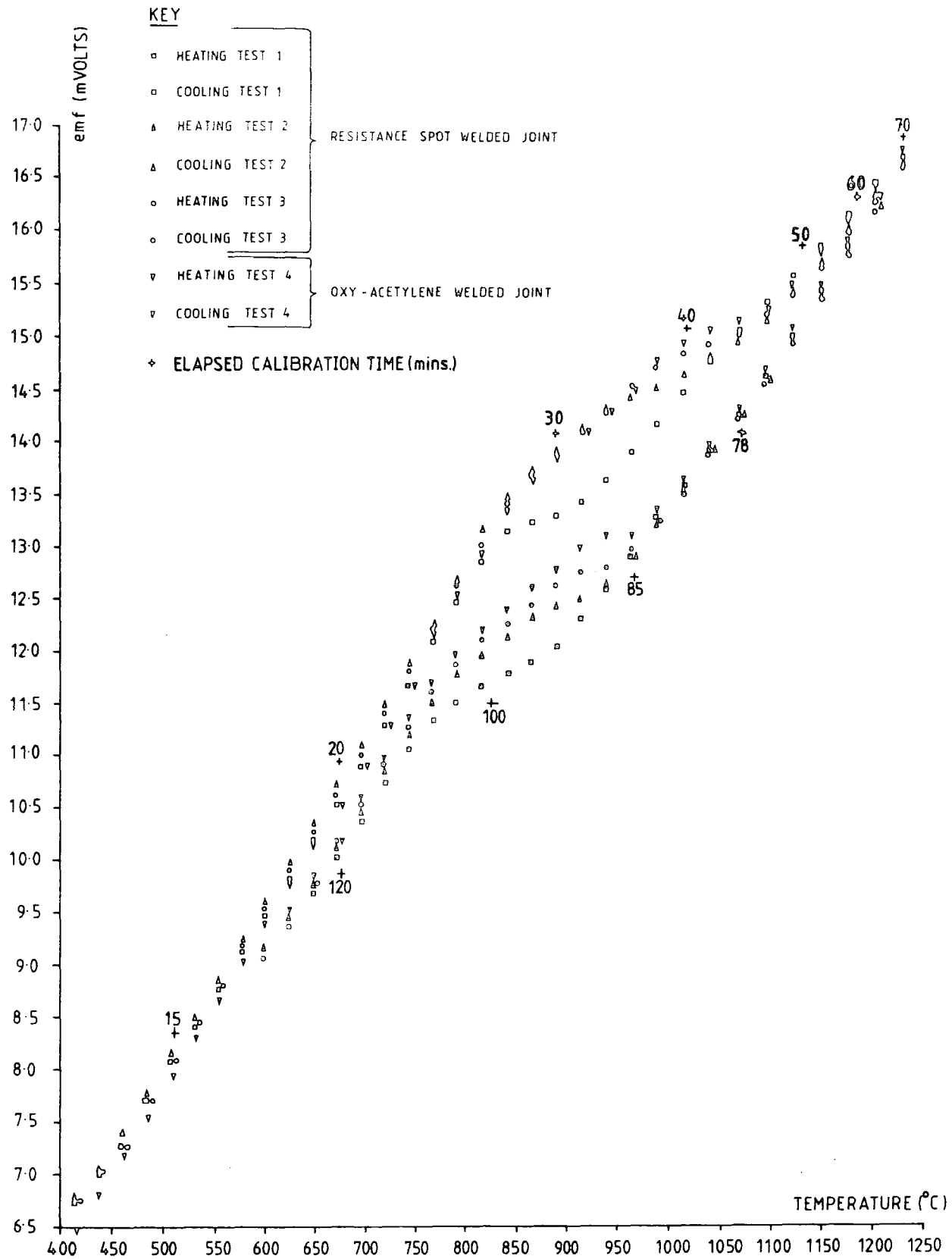

FIGURE 2·8 TEMPERATURE CALIBRATION OF CARBIDE GRADE 'TE'

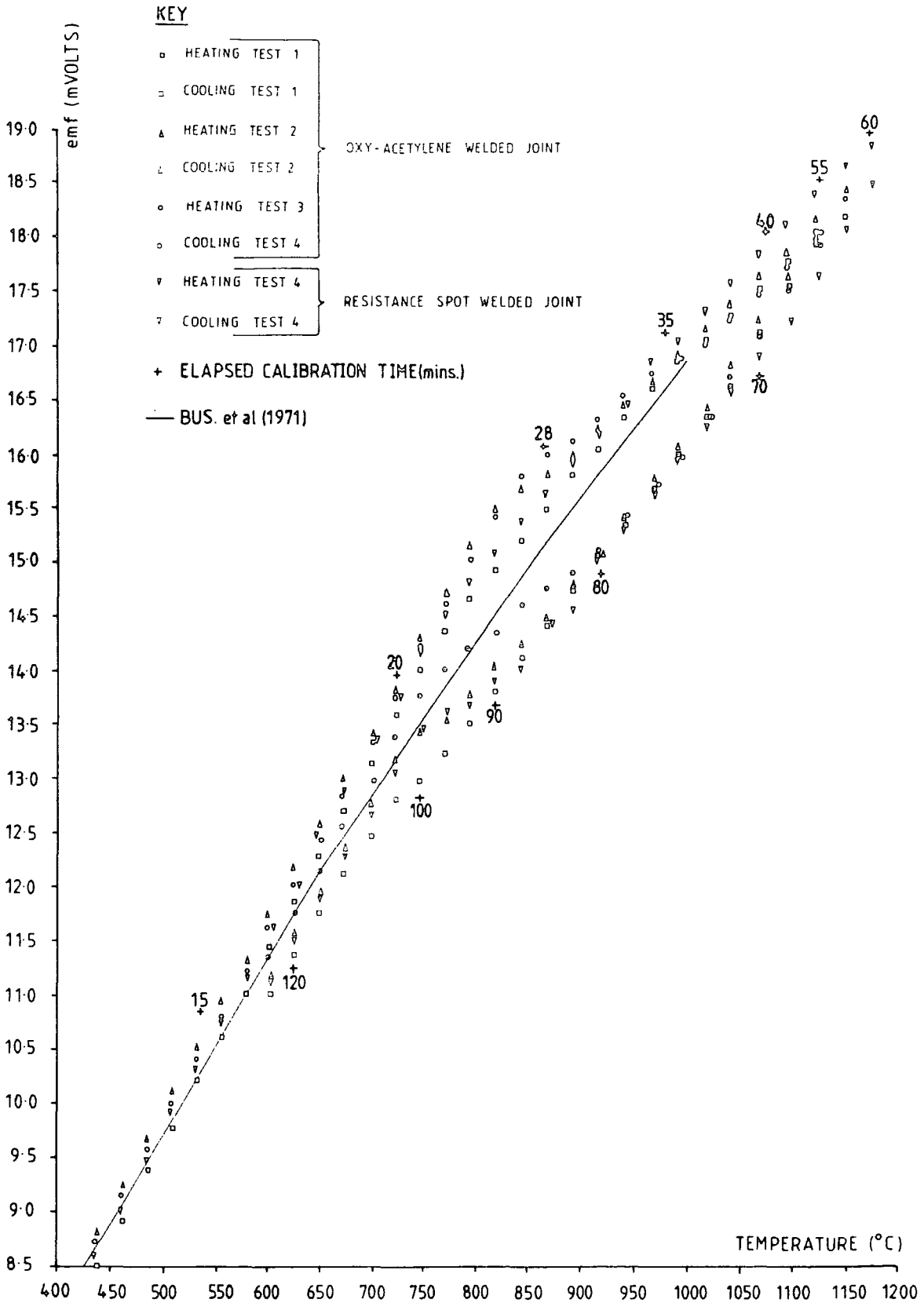

FIGURE 2·9 TEMPERATURE CALIBRATION OF CARBIDE GRADE 'TTA'

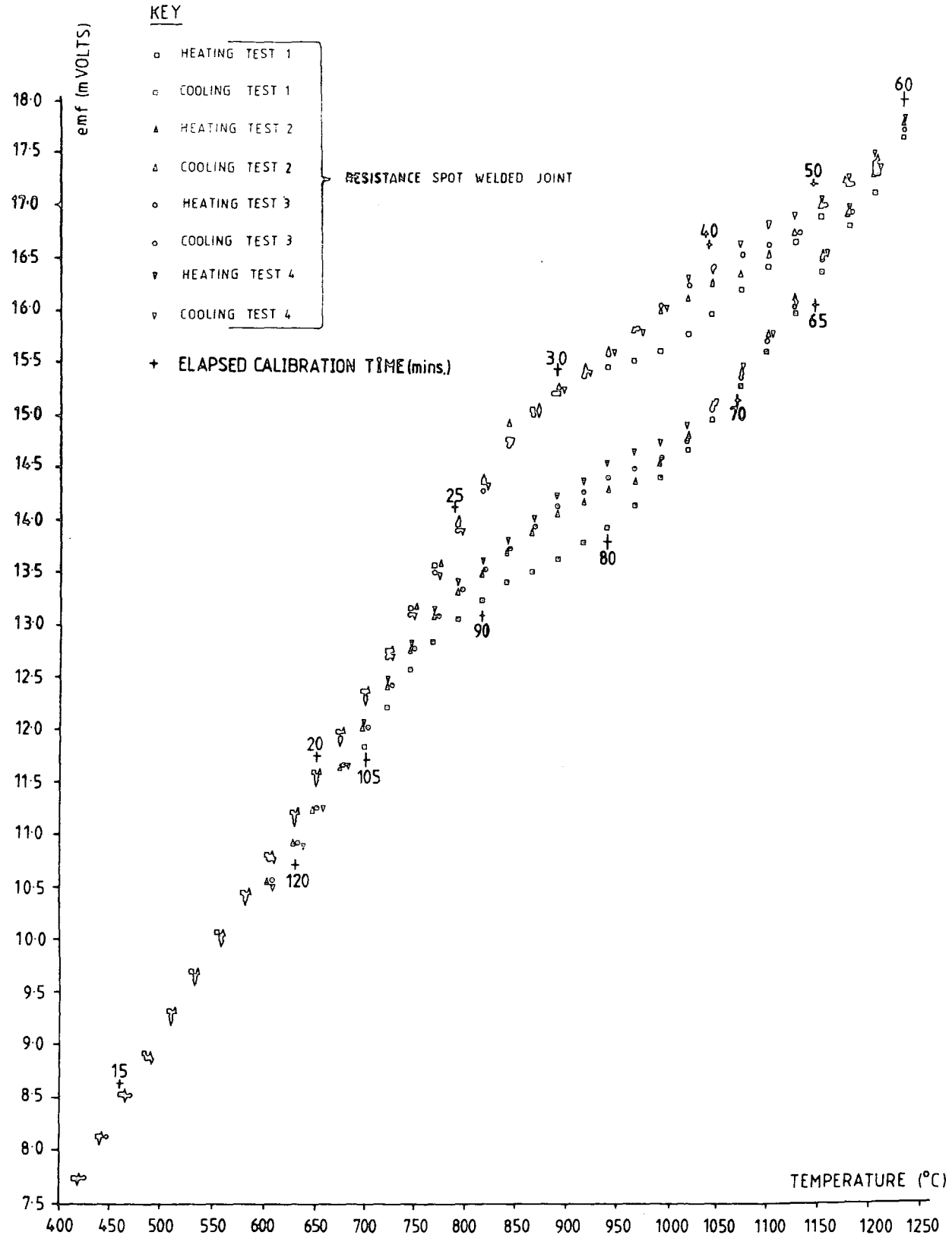

FIGURE 2·10 TEMPERATURE CALIBRATION OF CARBIDE GRADE 'TA5'

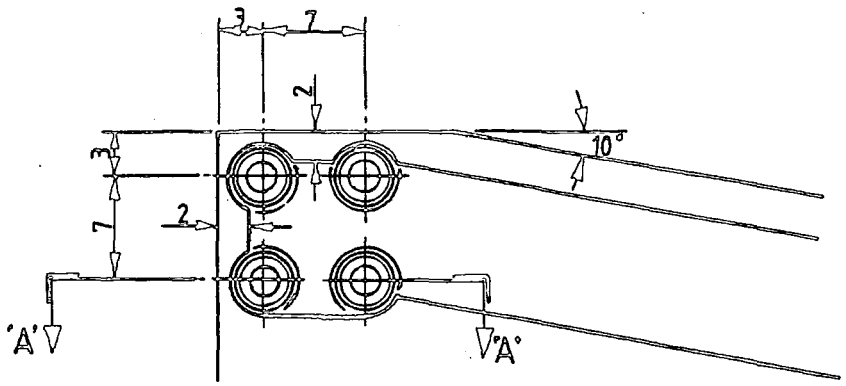

VIEW ON UNDERSIDE OF TOOL TIP HOLDER

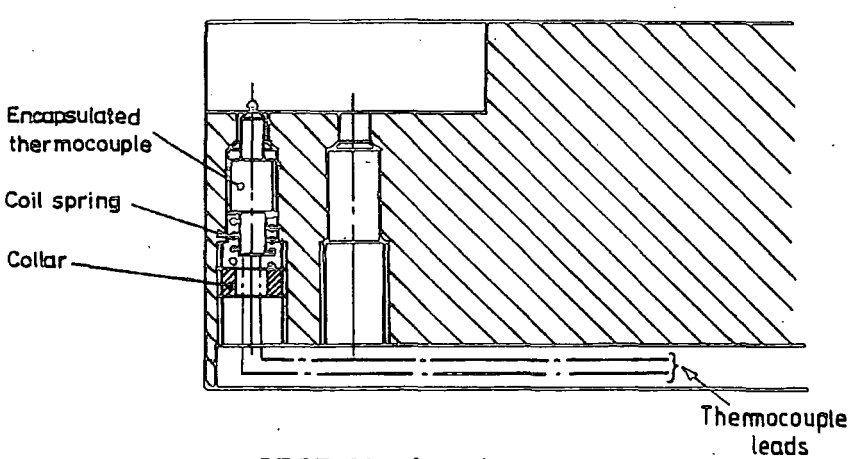

SECTION 'A-A'

Fig. 2-11 MODIFIED ARRANGEMENT OF TIP SHANK THERMOCOUPLES

SCALE :- 2 :1

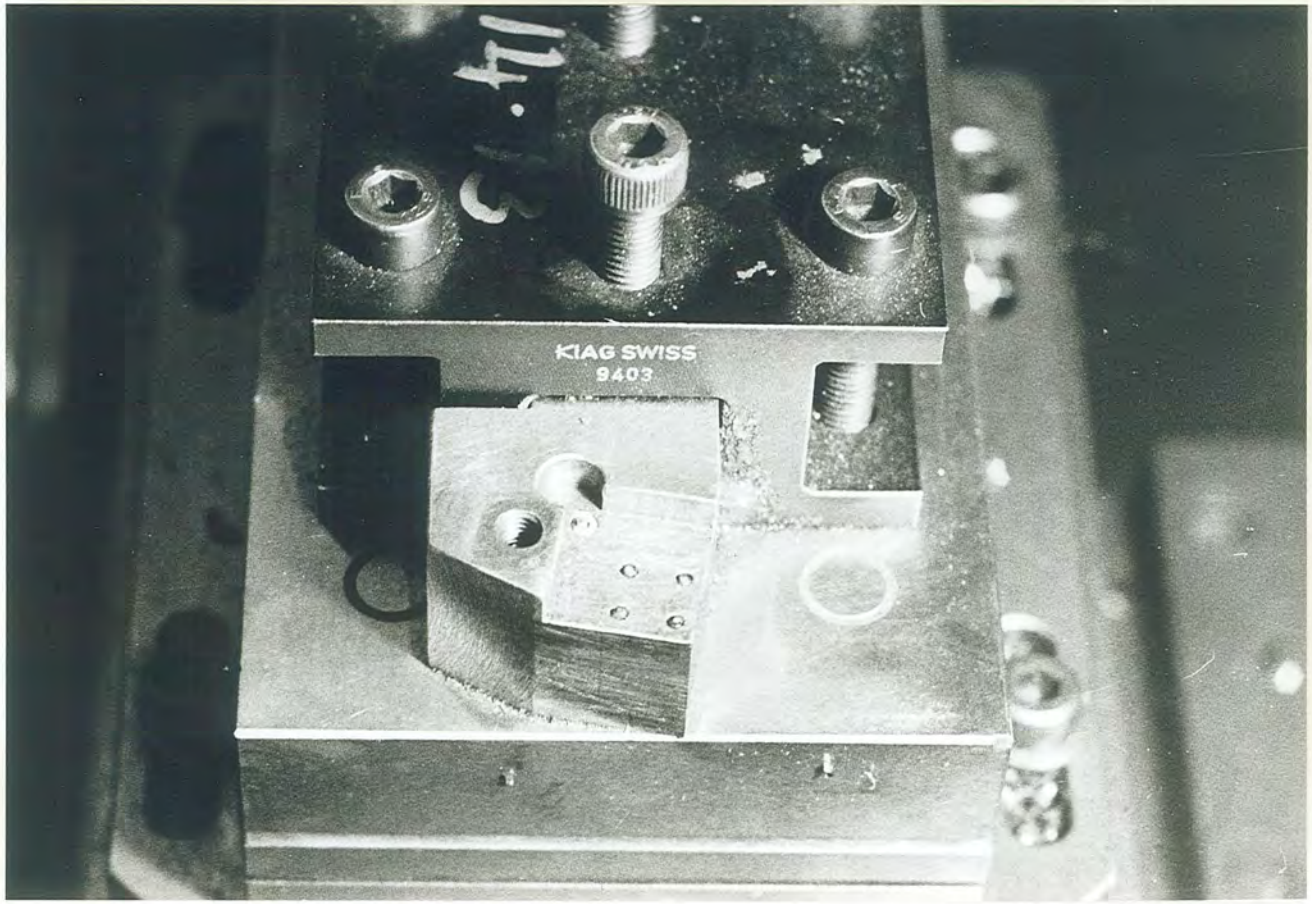

FIGURE 2.12, ARRANGEMENT OF THERMOCOUPLES IN TOOL SHANK.

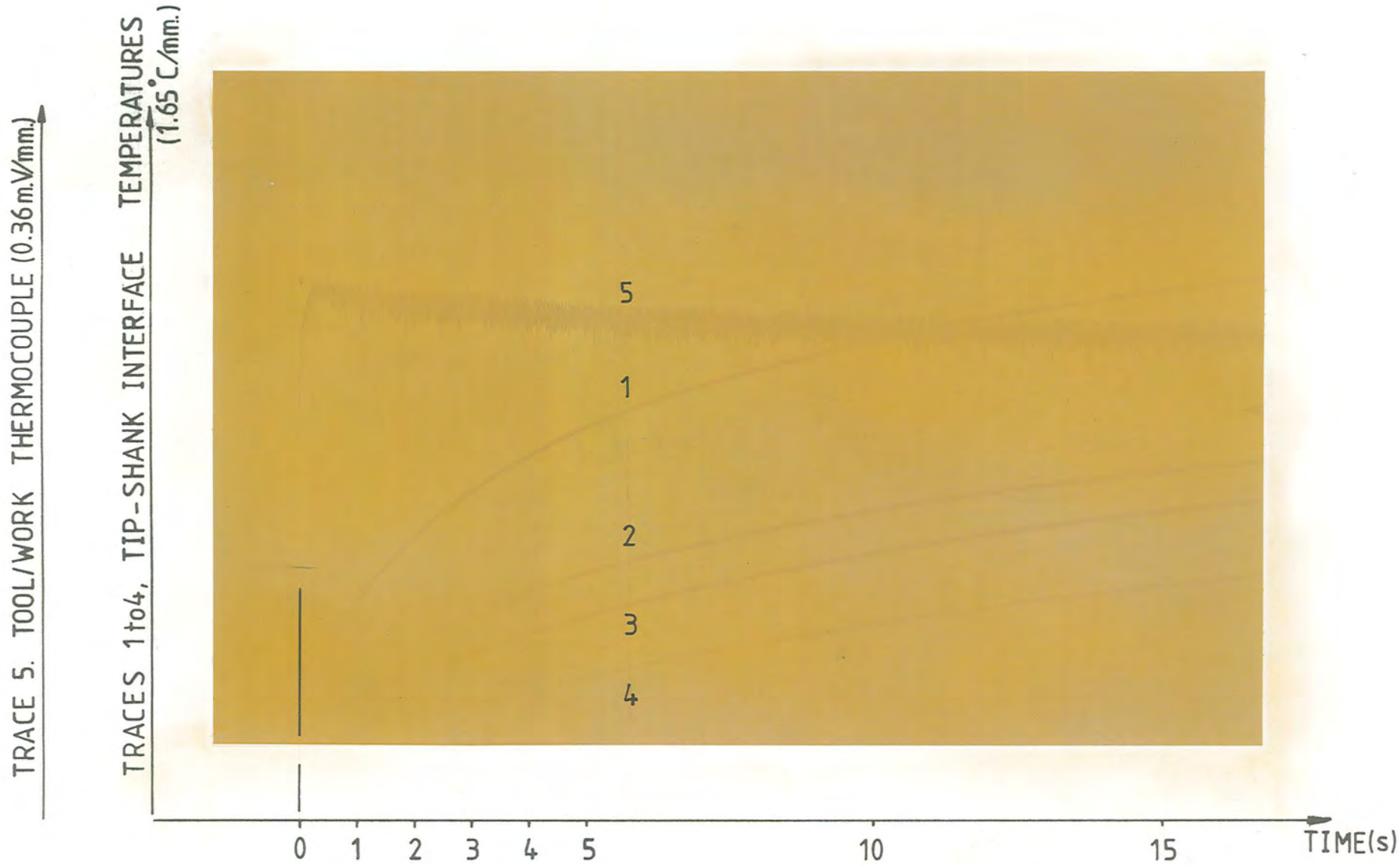

FIGURE 2.13, TYPICAL TOOL/WORK AND TIP/SHANK INTERFACE TEMPERATURES Vs TIME.

FIGURE 2·14 RESPONSE OF 1, 2 AND 3 THERMOCOUPLES IN PARALLEL.

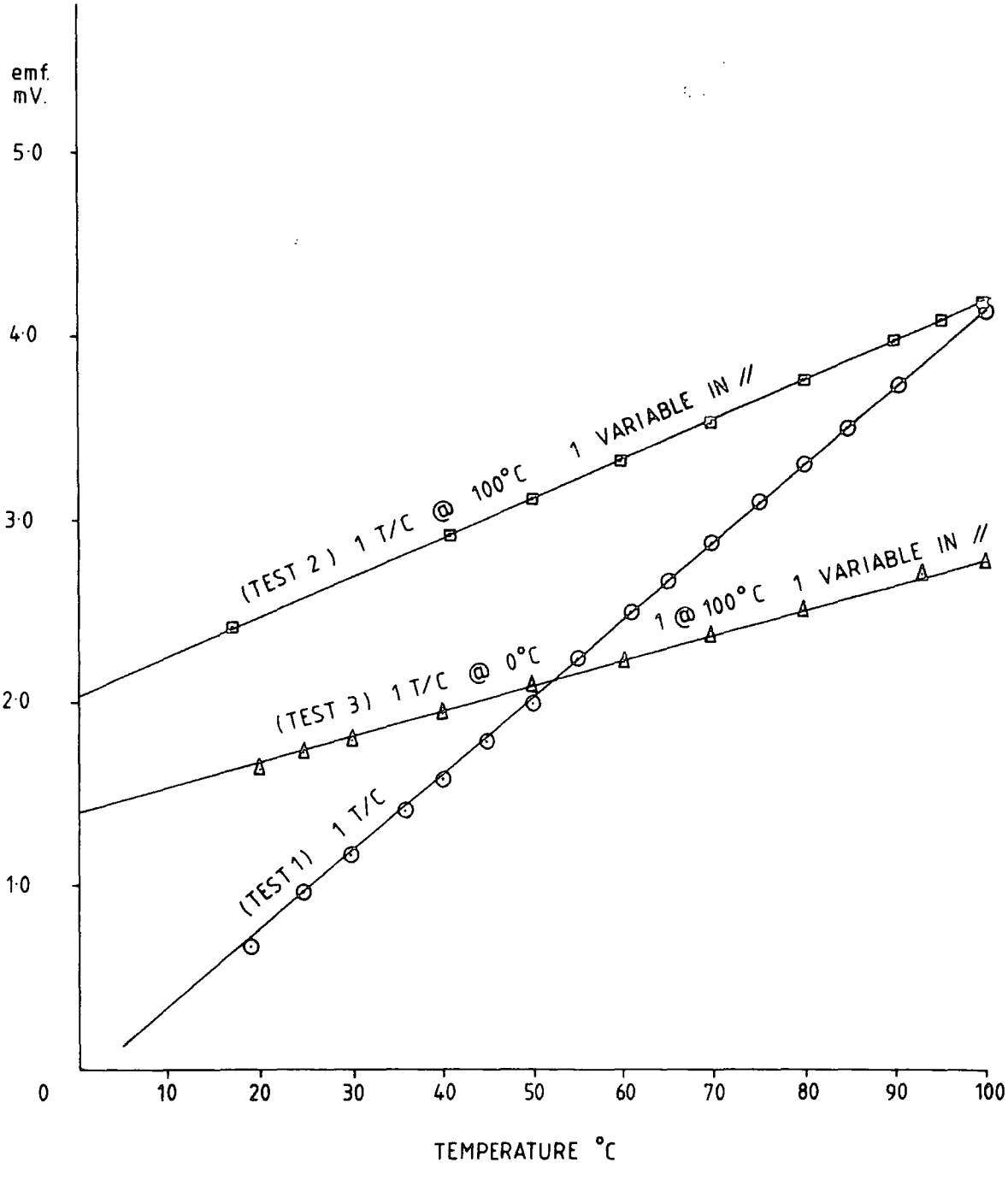

FIGURE 2·14 RESPONSE OF 1, 2 AND 3 THERMOCOUPLES IN PARALLEL

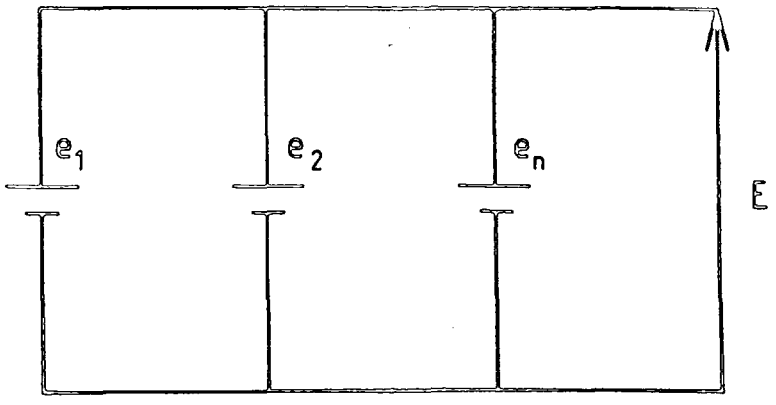

FIGURE 2·15 MODEL FOR 'n' THERMOCOUPLES IN PARALLEL

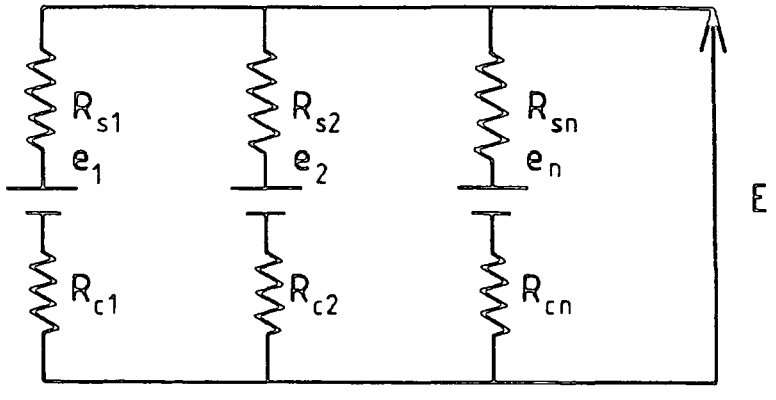

FIGURE 2·16 'n' THERMOCOUPLES WITH VARIABLE RESISTANCE

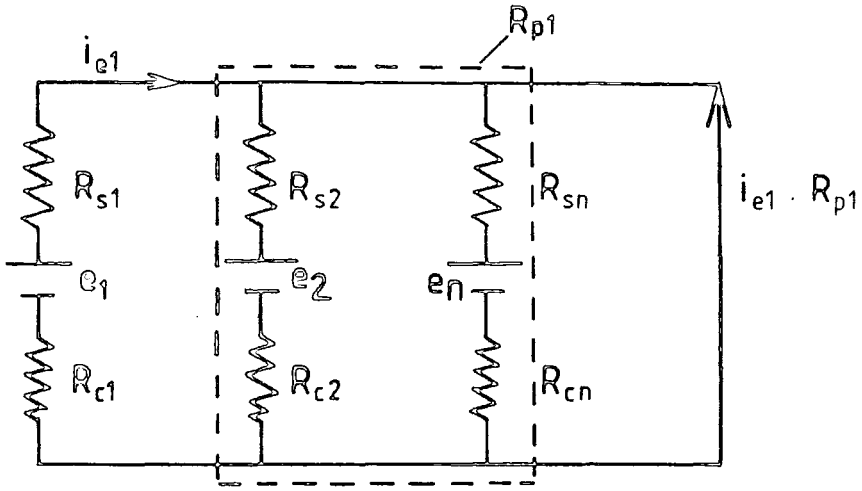

(a)

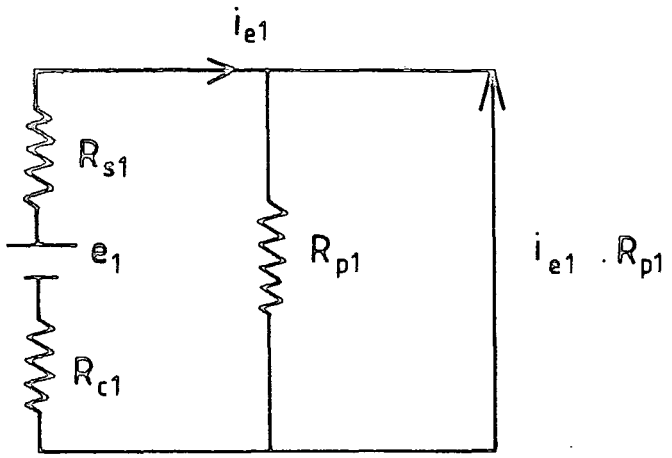

(b)

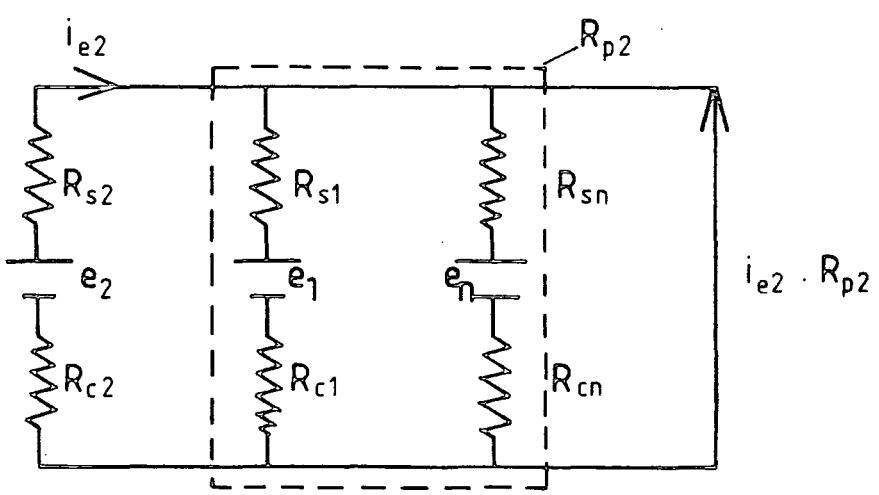

(c)

FIGURE 2·17 EQUIVALENT CIRCUIT FOR THERMOCOUPLE MODEL

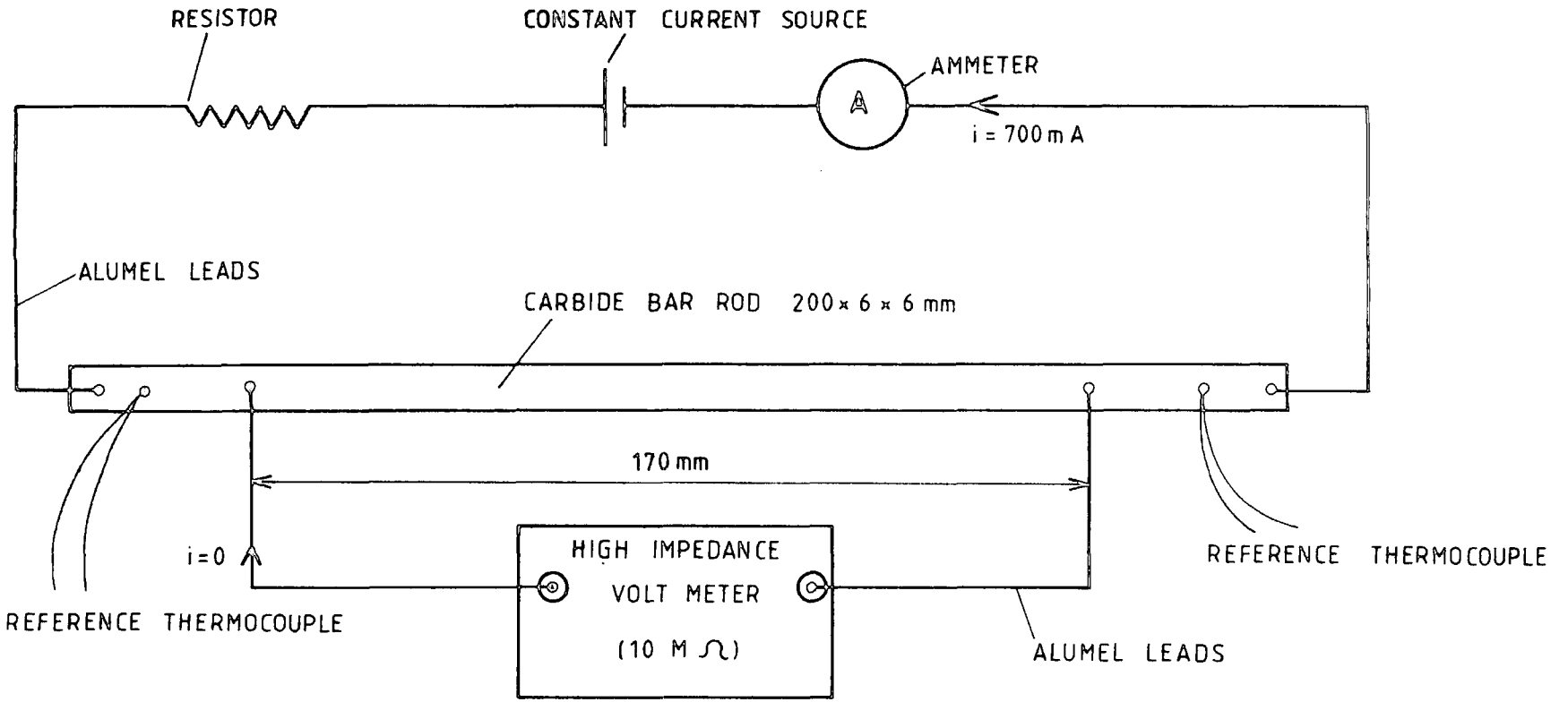

FIGURE 2·18 TECHNIQUE FOR MEASURING CHANGE OF RESISTIVITY WITH TEMPERATURE

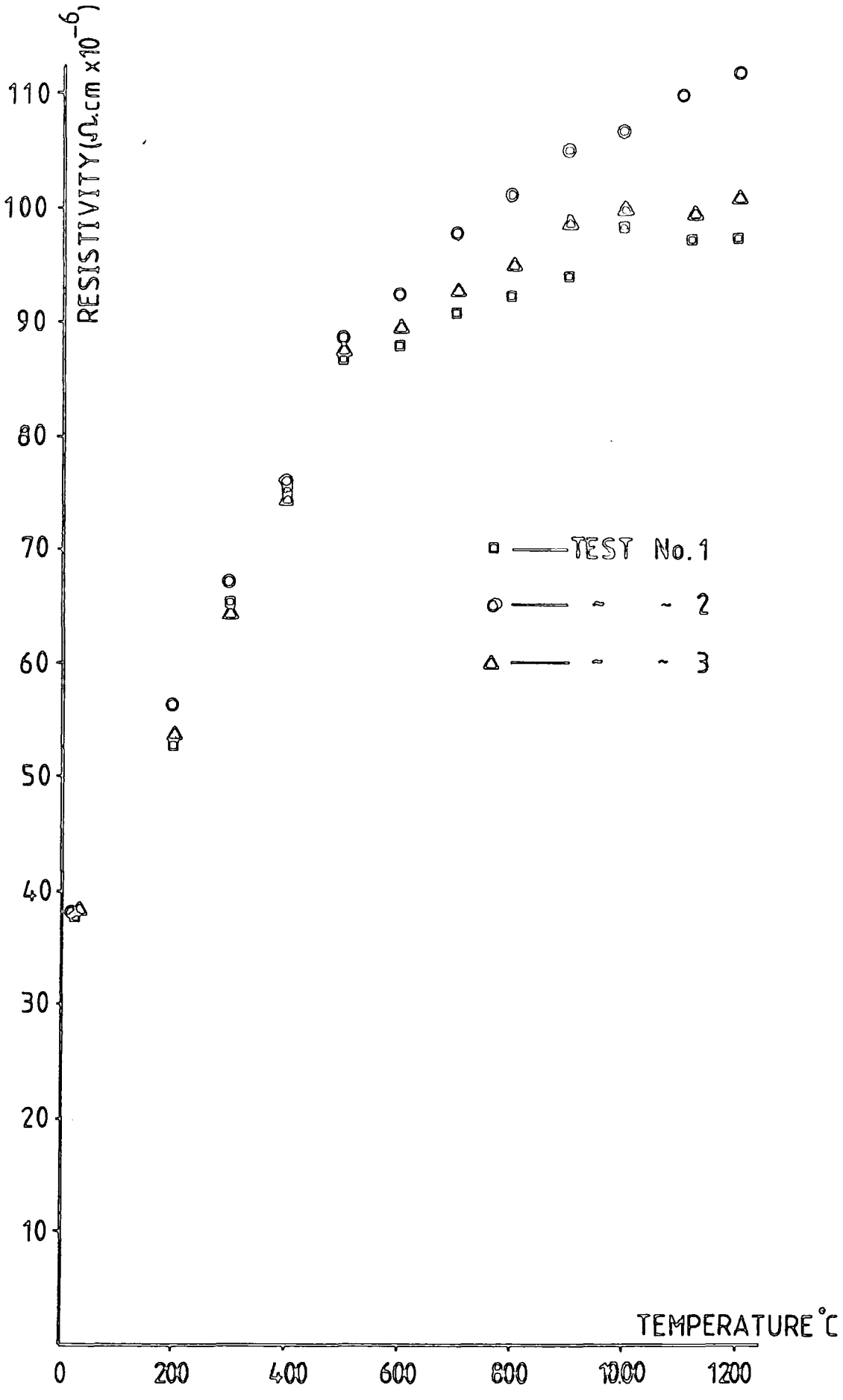

FIGURE 2.19, CHANGE IN RESISTIVITY OF GRADE TTA.

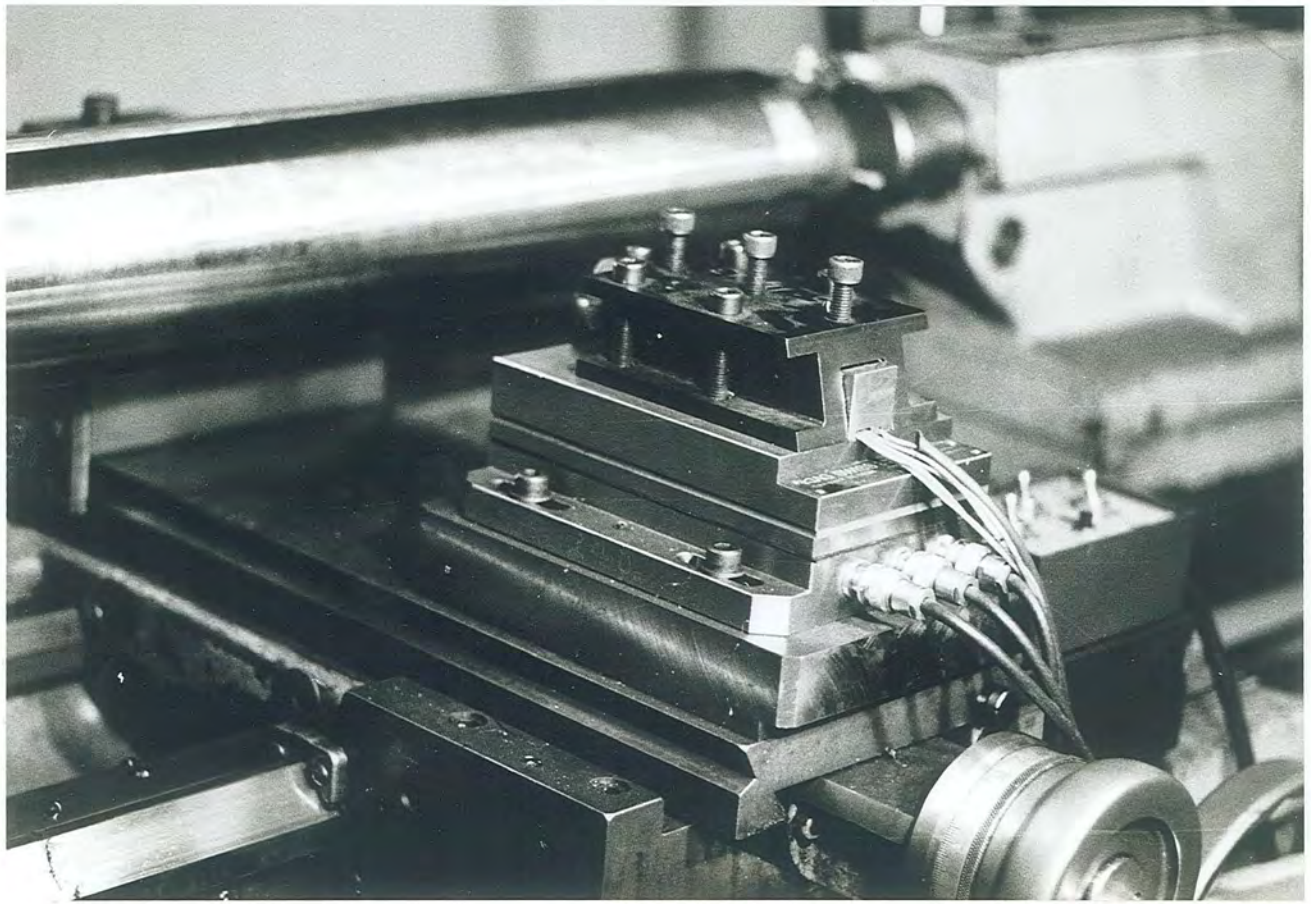

FIGURE 3.1, CUTTING FORCE DYNAMOMETER

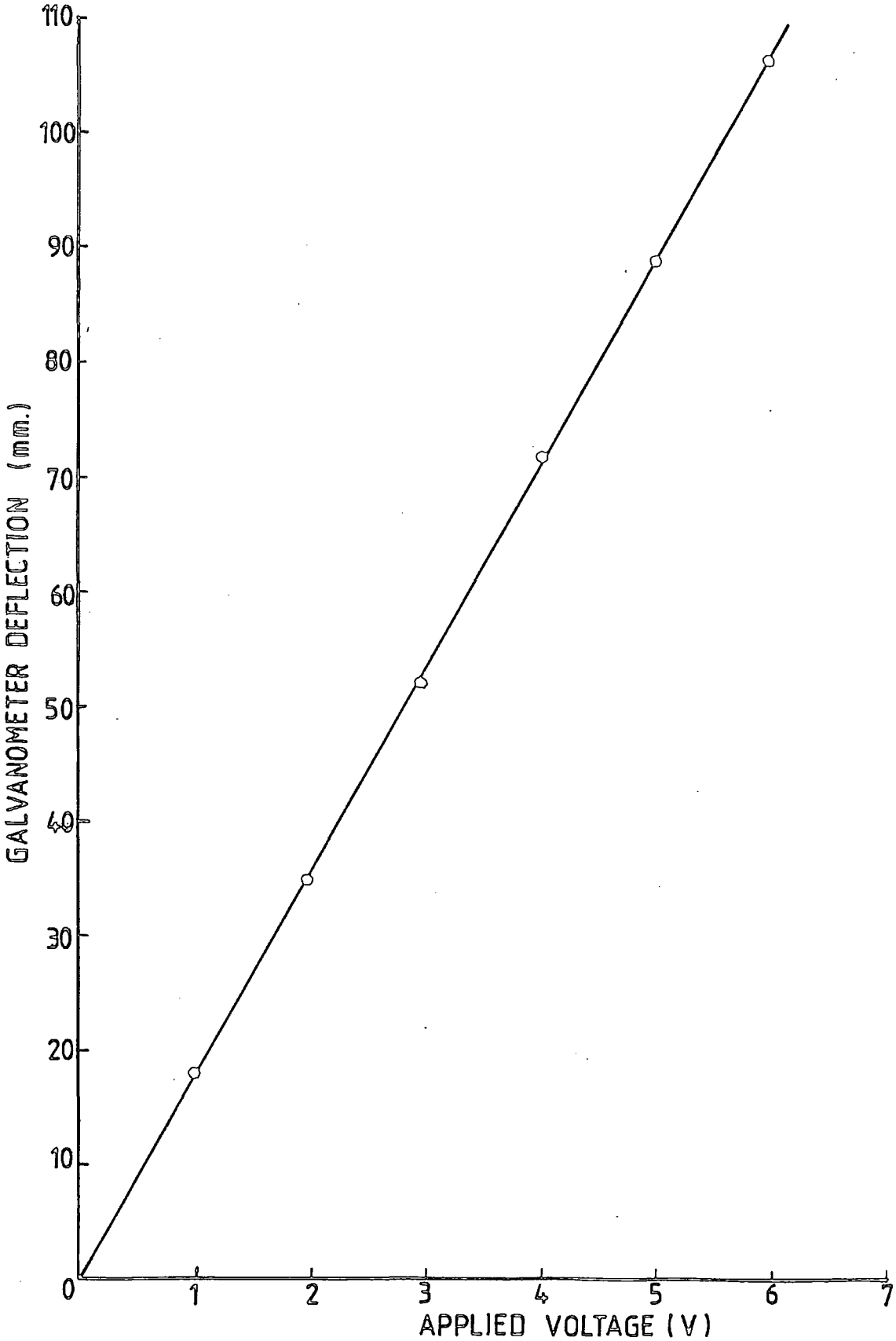

Fig. 3-2 CALIBRATION OF RECORDER GALVANOMETER DEFLECTION

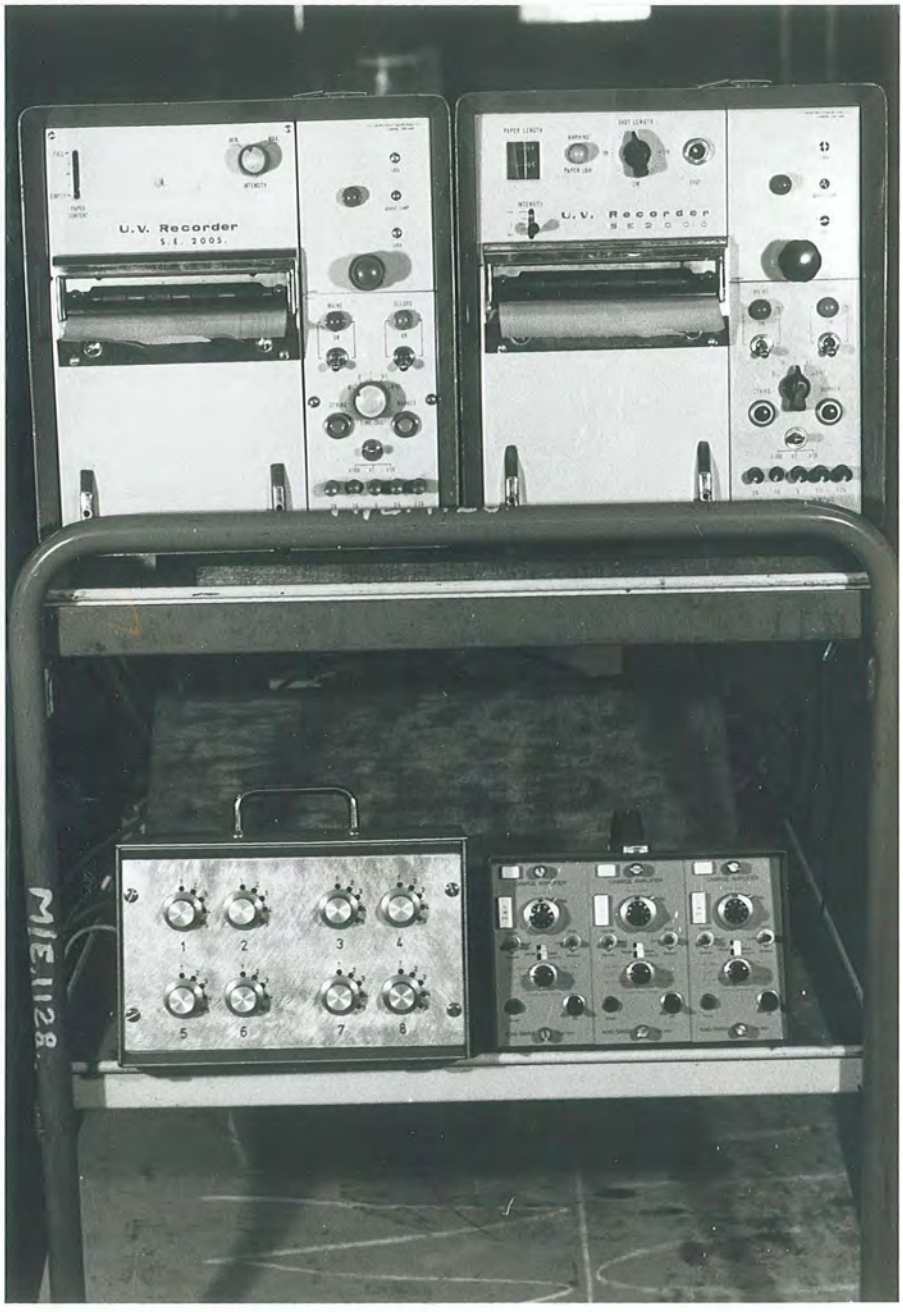

FIGURE 3.3, AMPLIFIERS AND RECORDING EQUIPMENT.

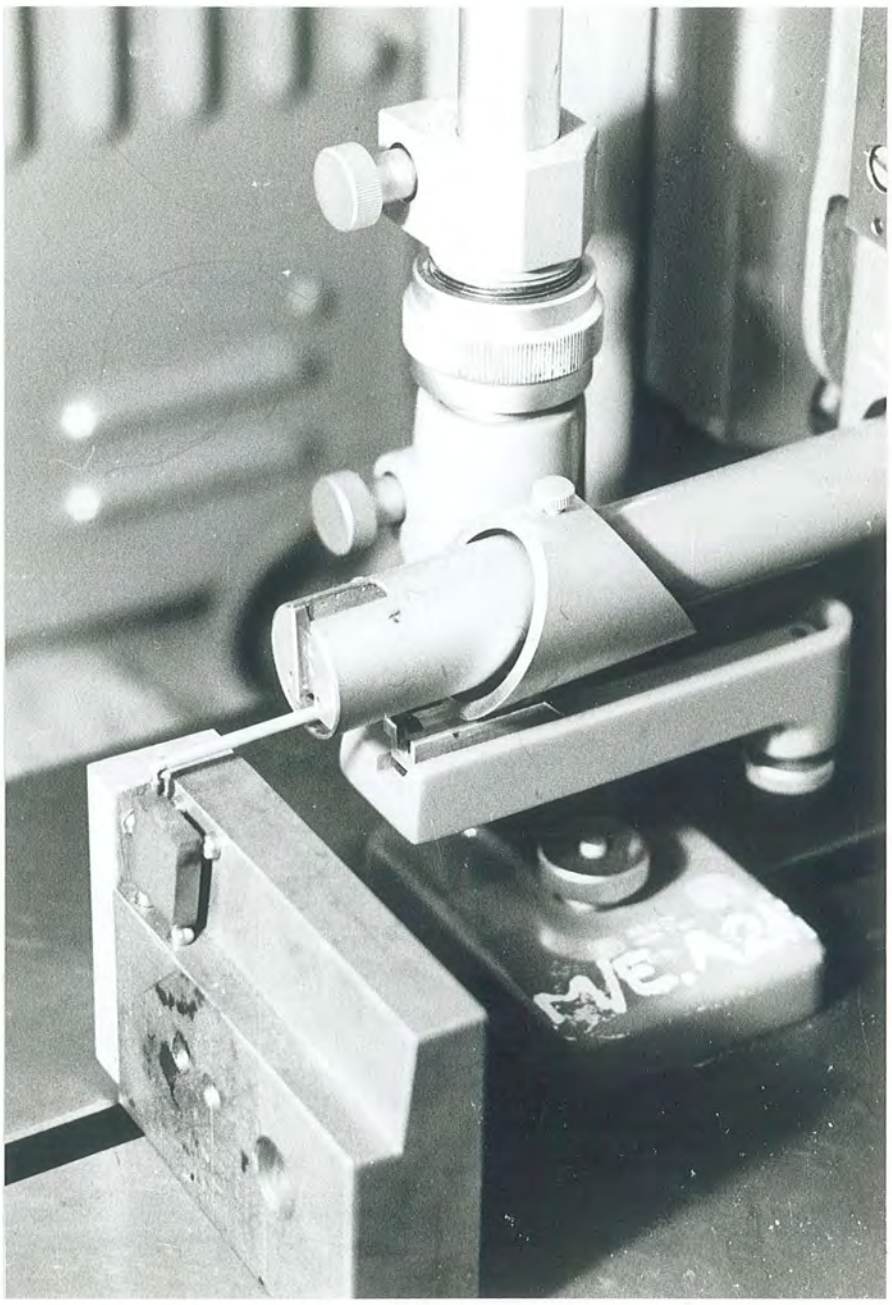

FIGURE 4.1 MEASUREMEMENT OF FLANK FACE BULGING.

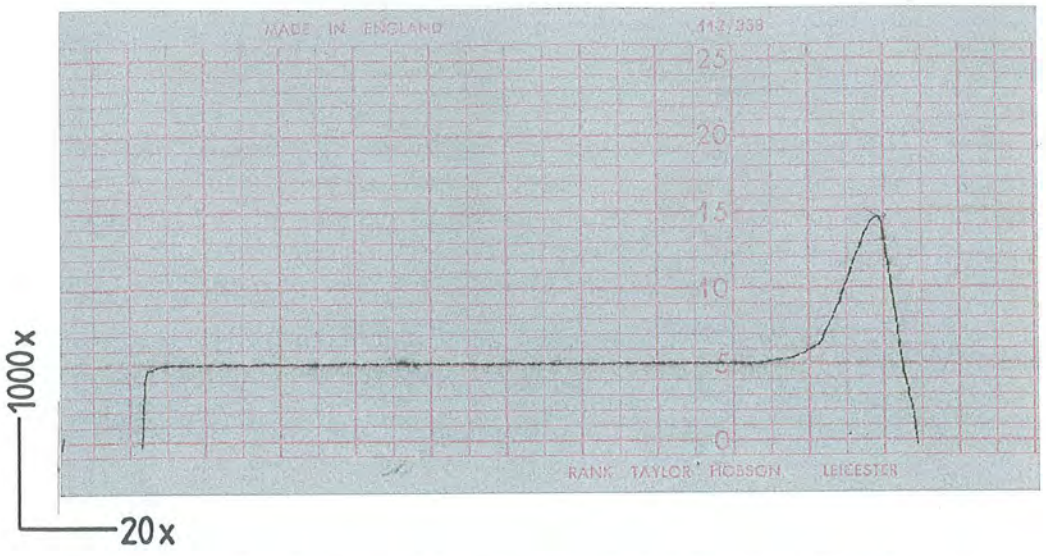

FIGURE 4.2, TOOL WITH DEFORMATION AND WEAR LAND.

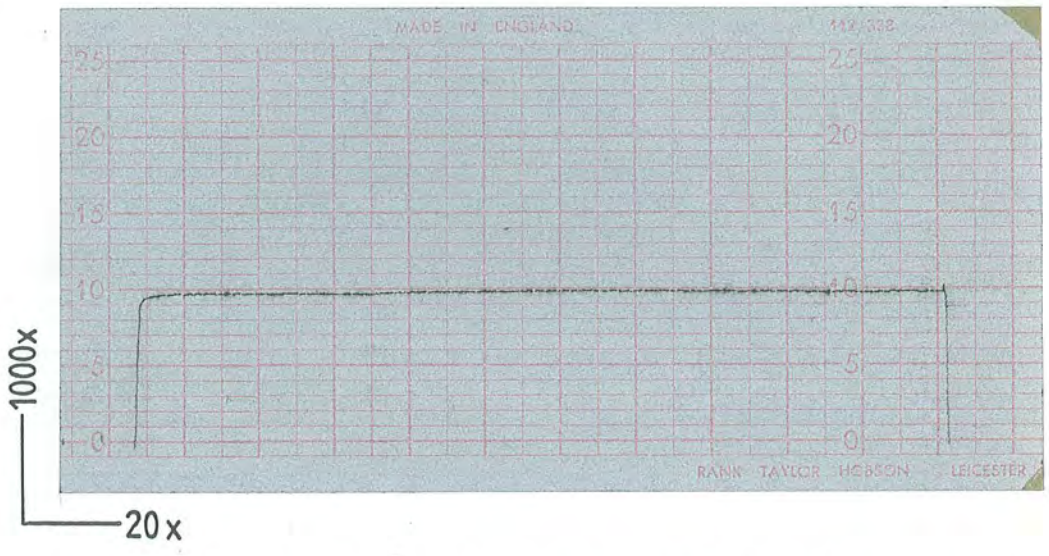

FIGURE 4.3, NEW TOOL WITHOUT DEFORMATION OR WEAR LAND.

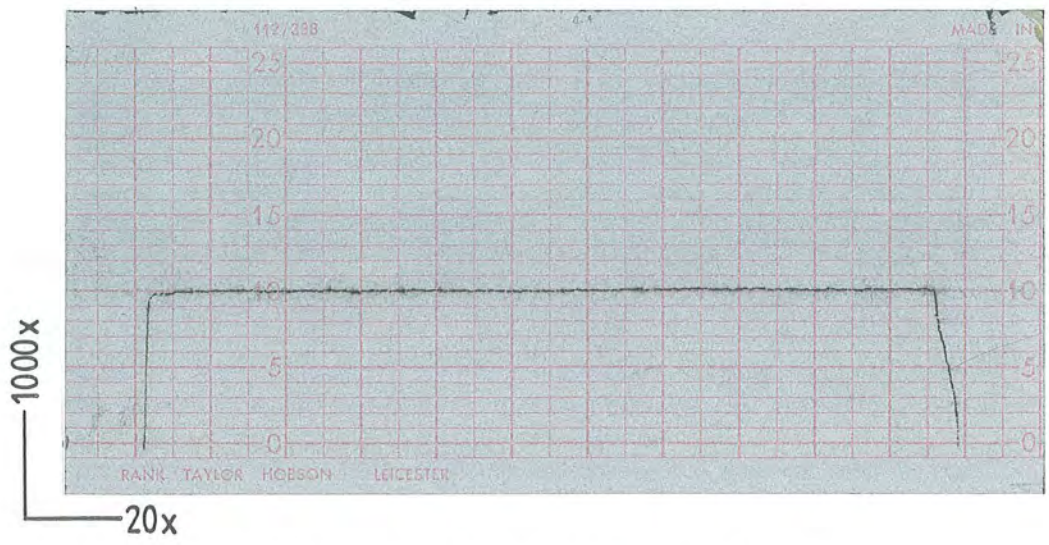

FIGURE 4.4, NEW TOOL WITH PRE-GROUND WEAR LAND.

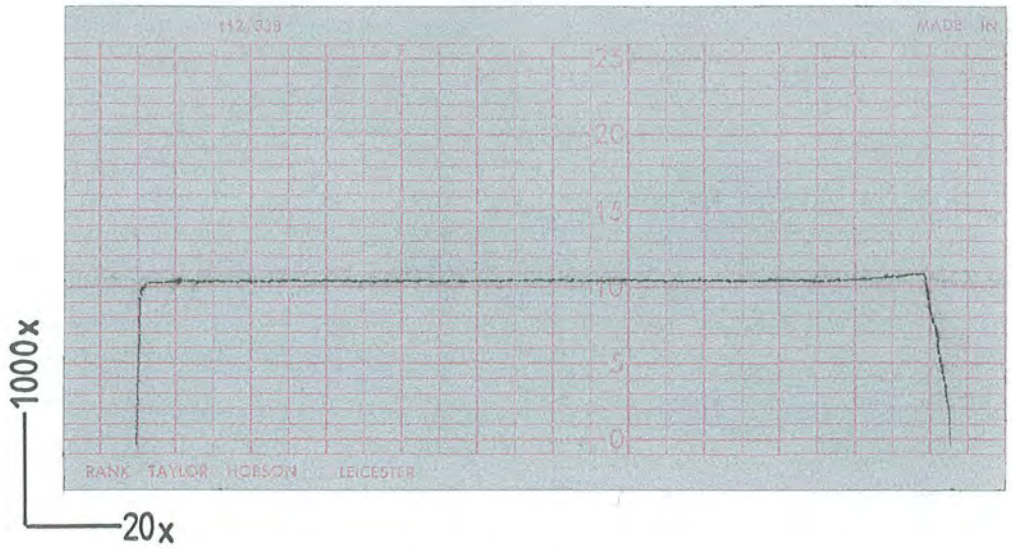

FIGURE 4.5, TOOL WITH A MAXIMUM OF 1.5μm BULGING.

FIGURE 4.6, TOOL WITH A MAXIMUM OF 3μm BULGING.

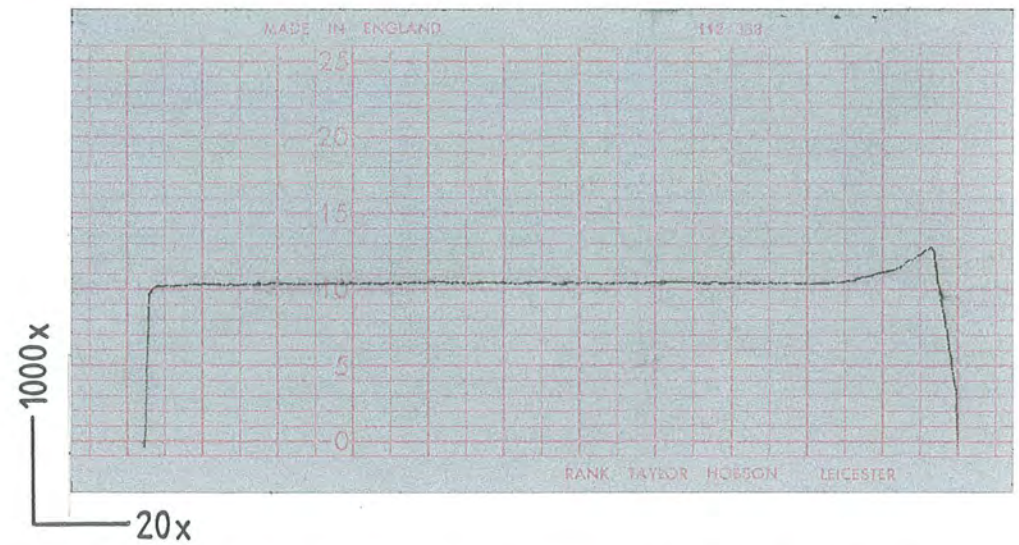

FIGURE 4.7, TOOL WITH A MAXIMUM OF 5μm BULGING.

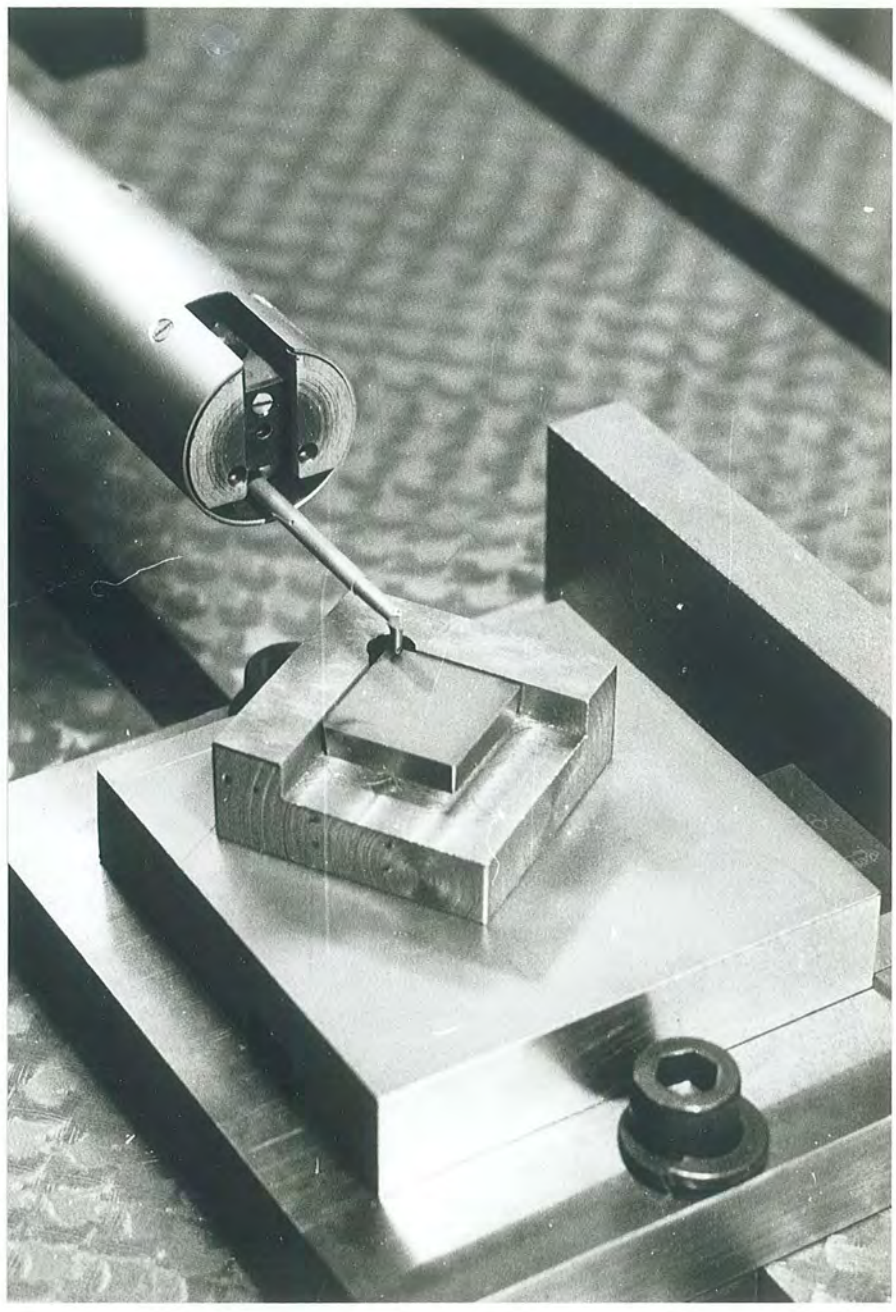

FIGURE 4.8, MEASUREMENT OF EDGE DEPRESSION.

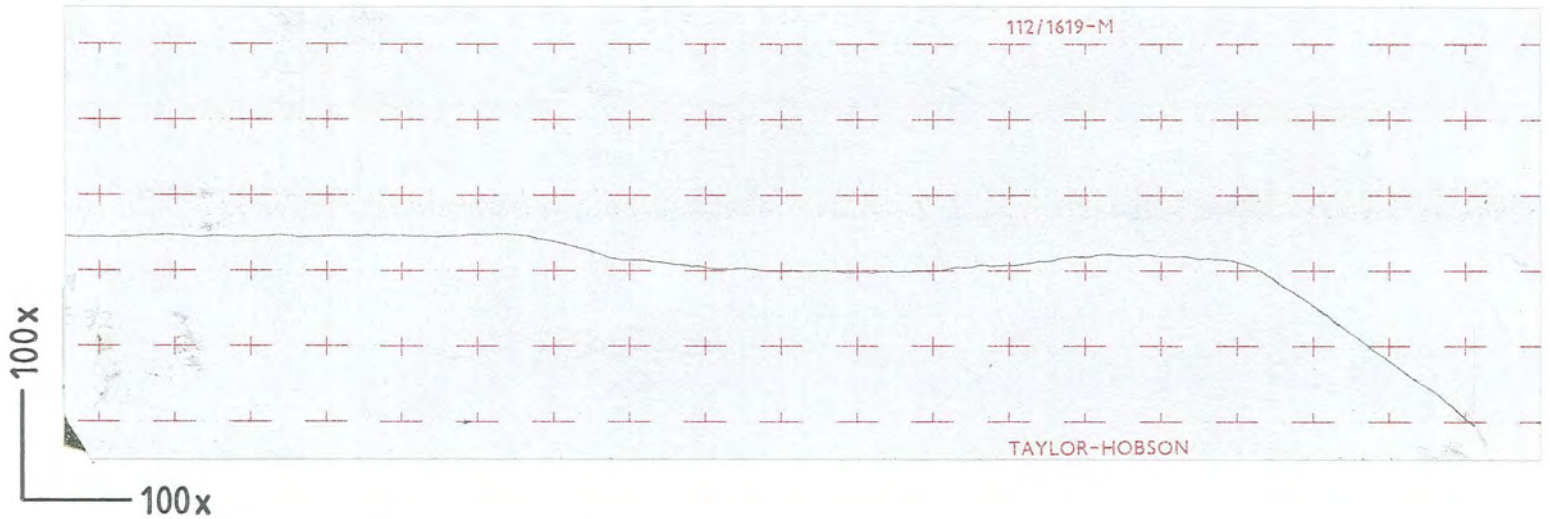

FIGURE 4.9, CRATER WEAR WITH PARALLEL EDGE DEPRESSION.

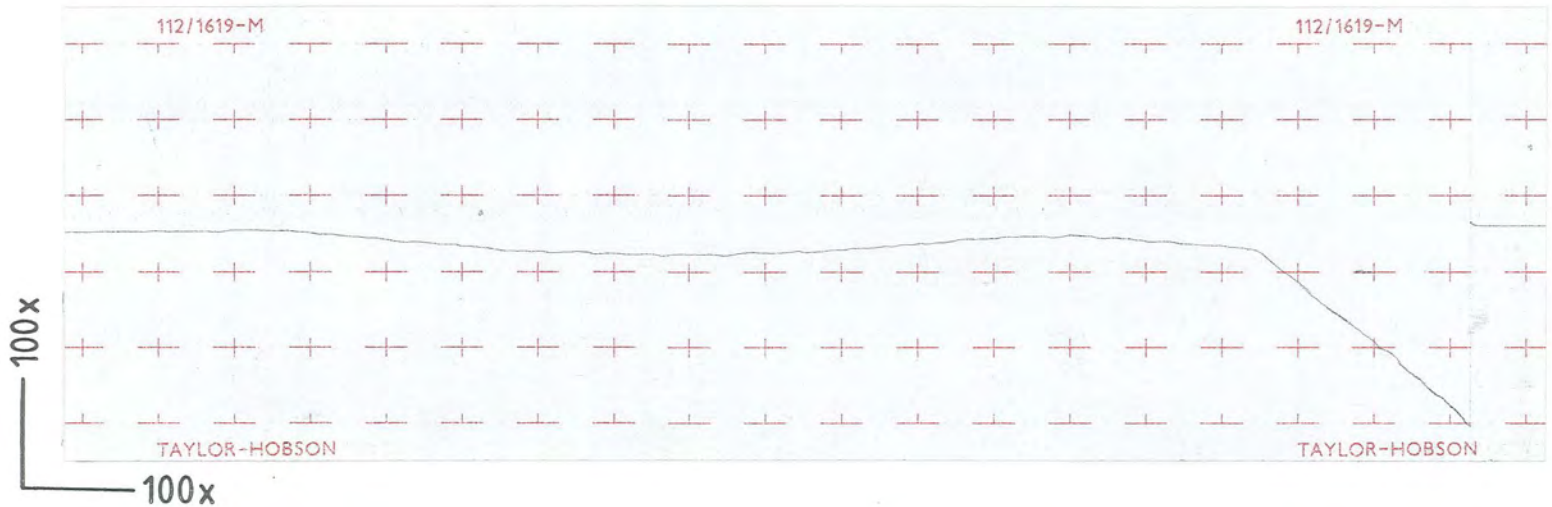

FIGURE 4.10, CRATER WEAR WITH TAPERED EDGE DEPRESSION.

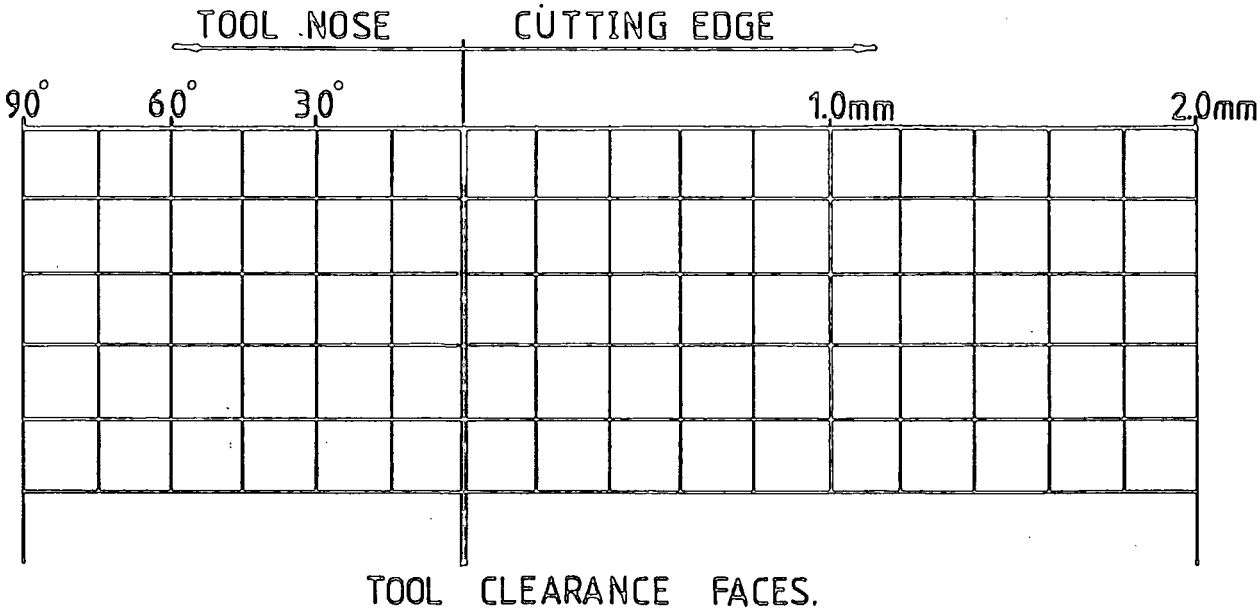

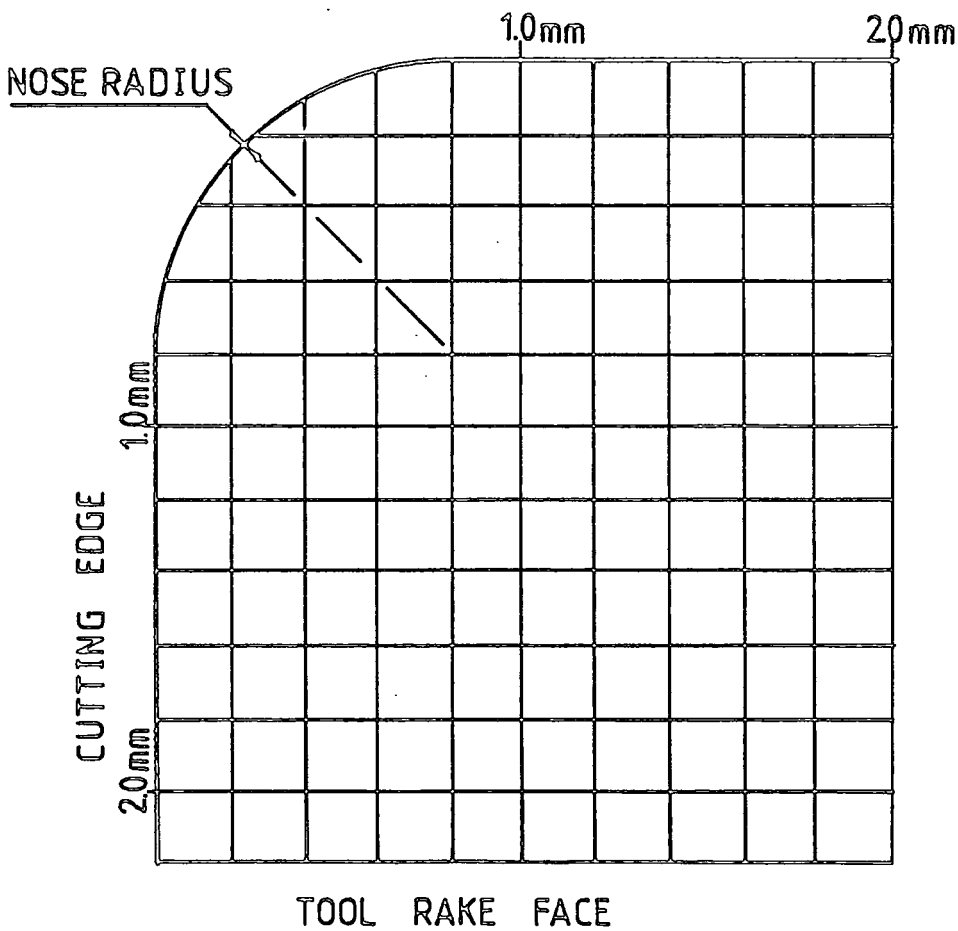

FIGURE 4.11, CHARTS FOR RECORDING FLANK AND CRATER WEAR

FIGURE 4,12. CHIP CROSS-SECTION, FEED RATE = 0.25 mm.

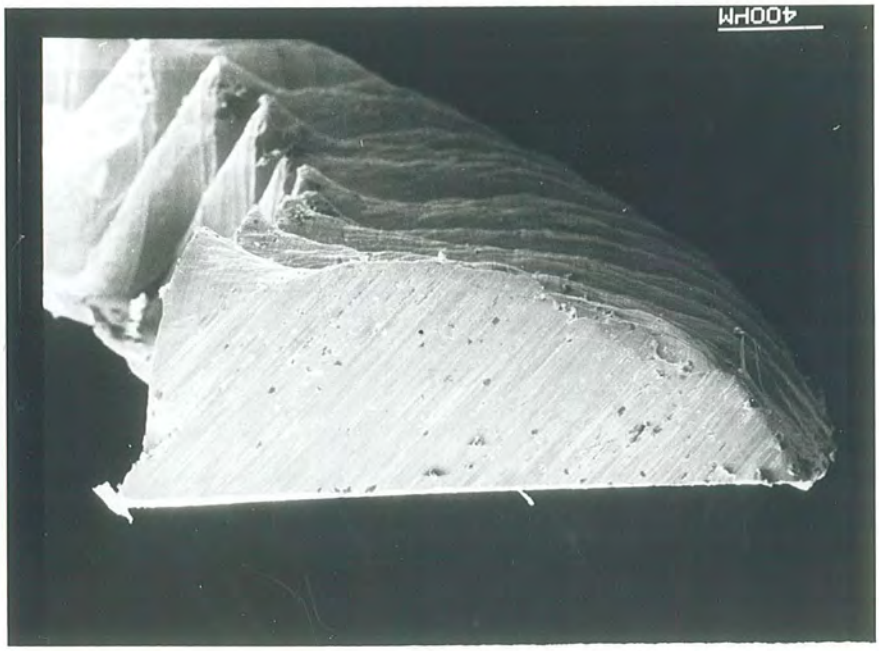

FIGURE 4.13. CHIP CROSS-SECTION, FEED RATE = 0.50 mm.

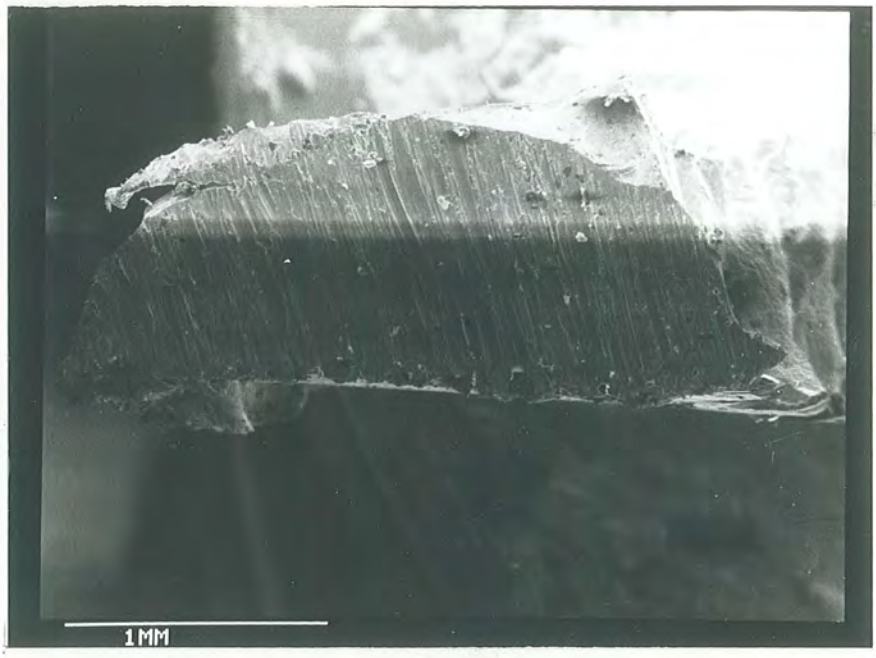

FIGURE 4.14, CHIP CROSS-SECTION, FEED RATE = 0.65 mm.

FIGURE 4.15, TOOL WITH TITANIUM NITRIDE COATING.

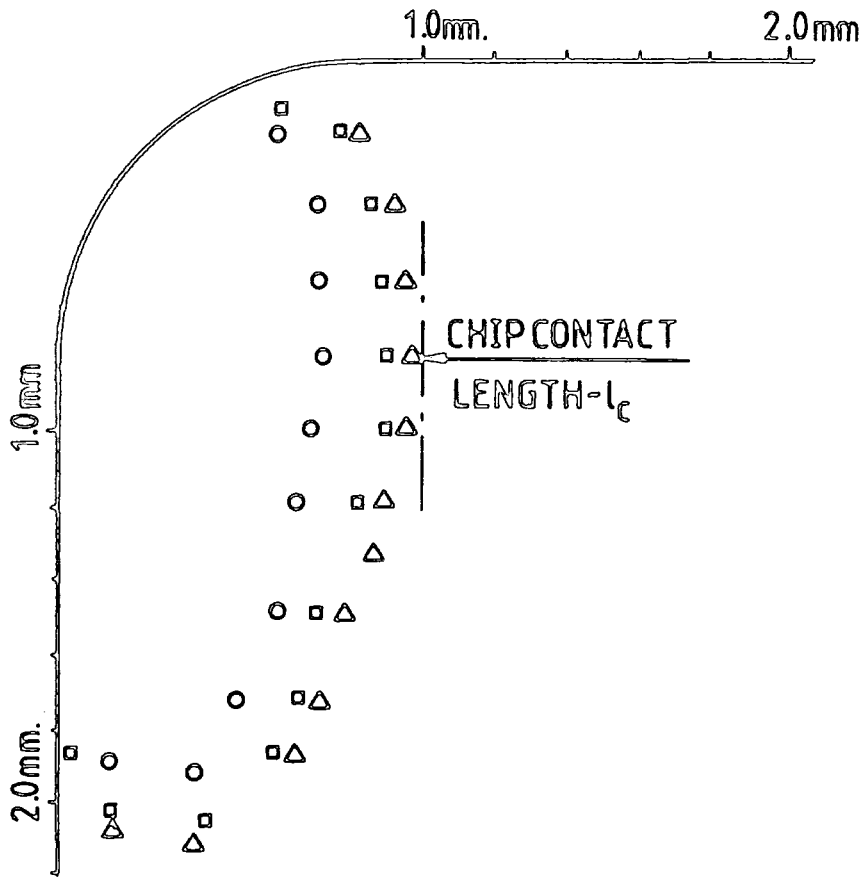

FIGURE 4.16, REMOVAL OF TITANIUM NITRIDE COATING (V=1.25, F=0.40)

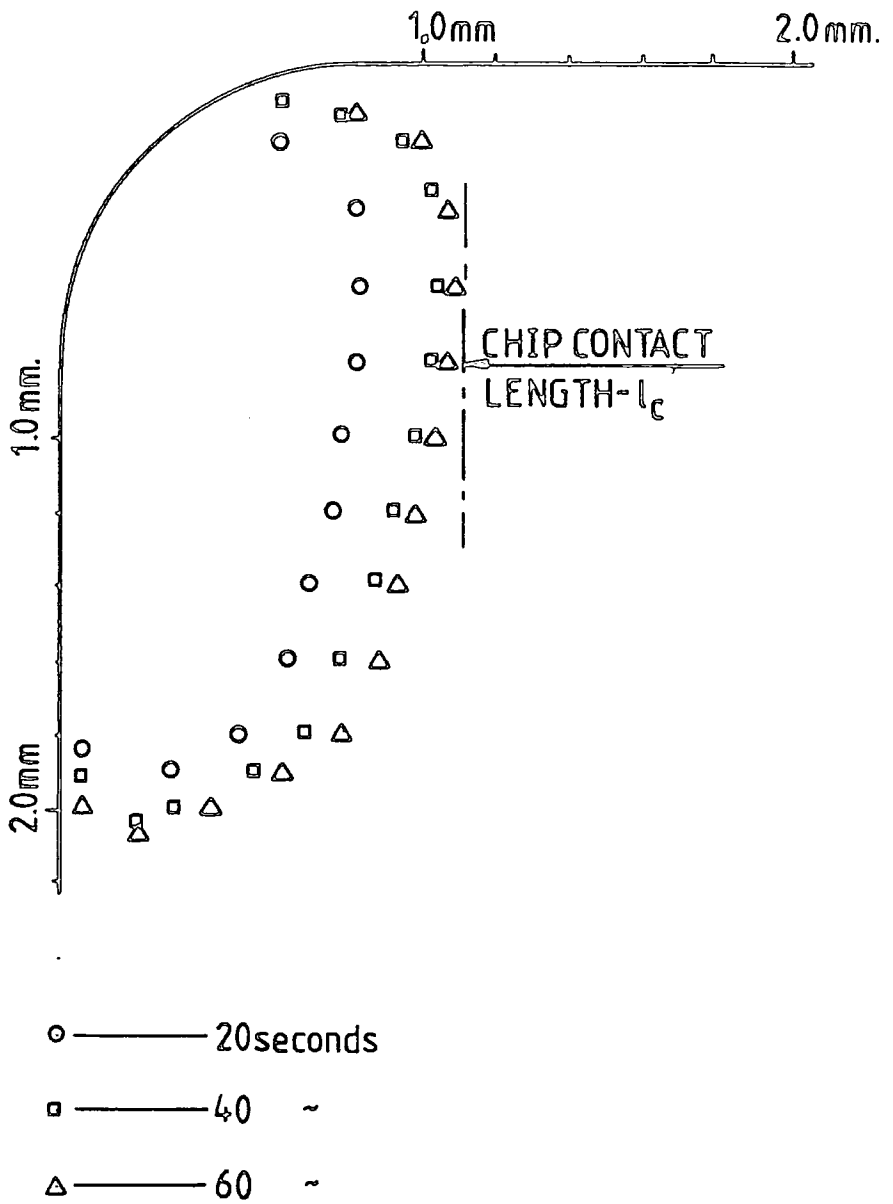

FIGURE 4.17, REMOVAL OF TITANIUM NITRIDE COATING (V=1.25, F=0.50)

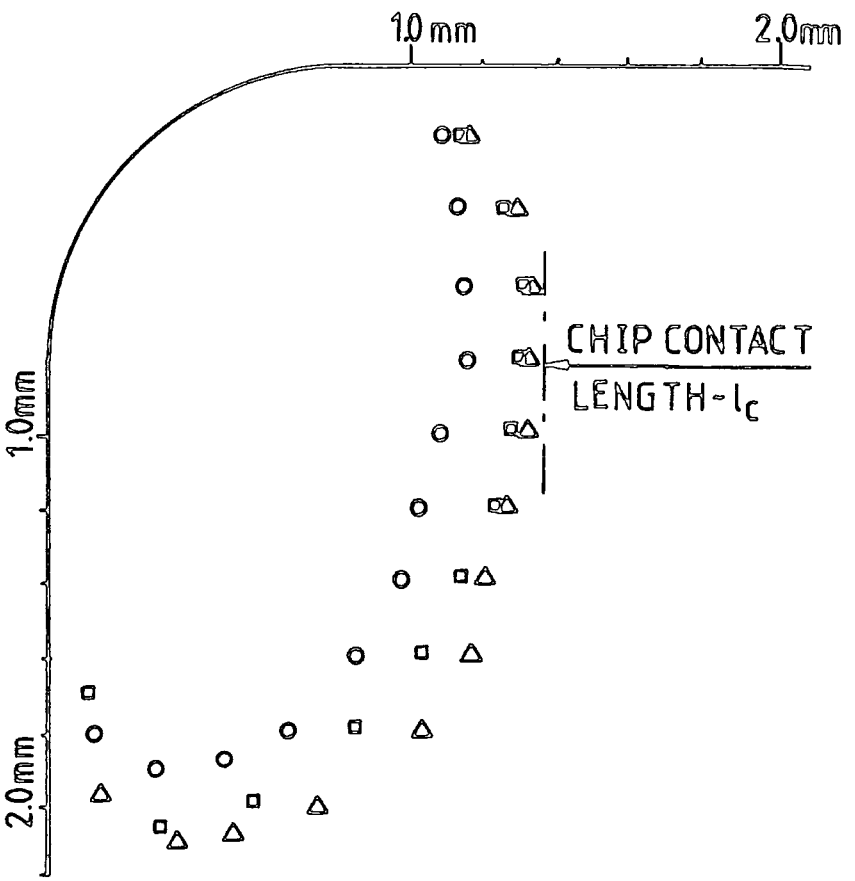

FIGURE 4.18, REMOVAL OF TITANIUM NITRIDE COATING (V=1.25, F=0.80)

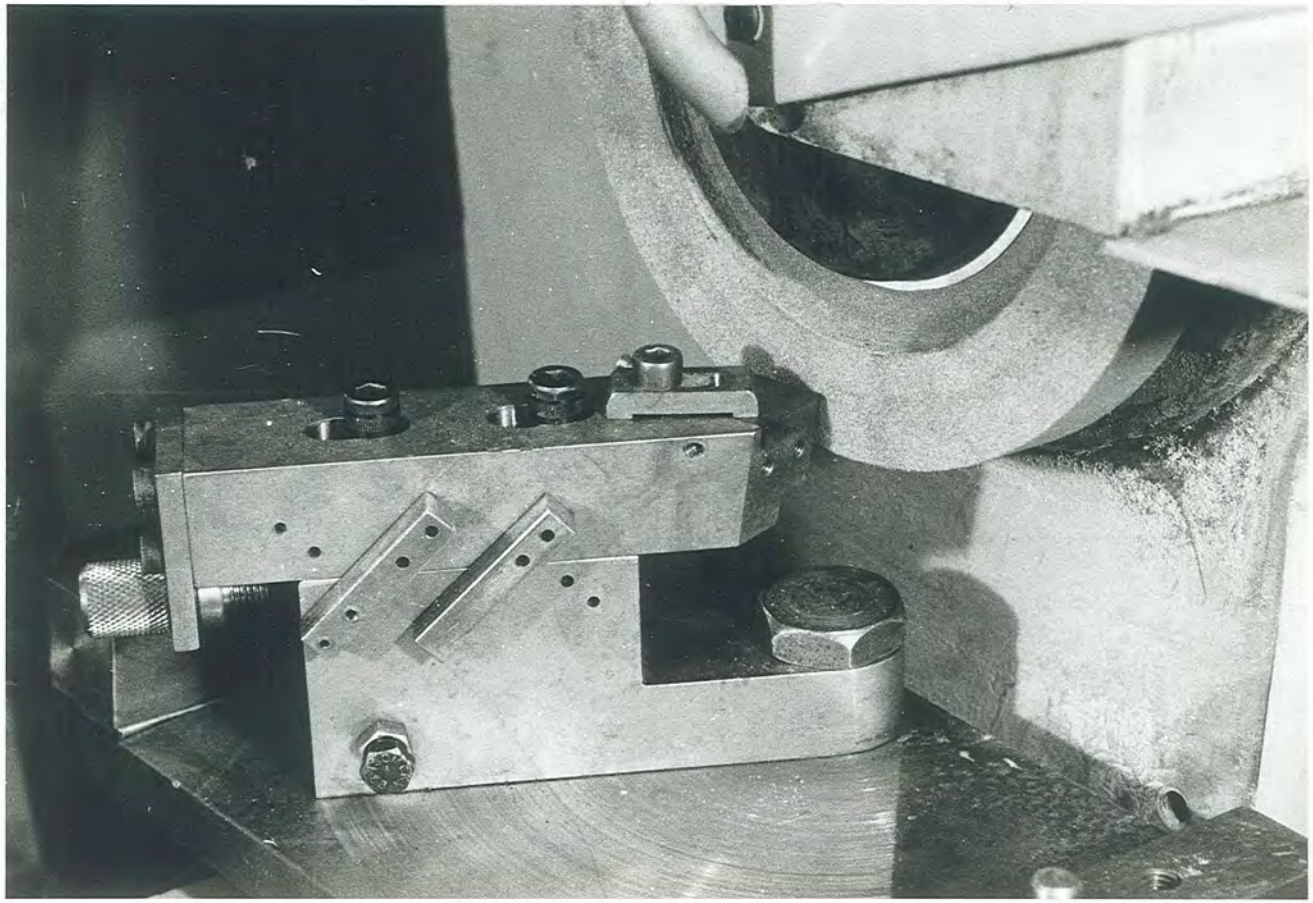

FIGURE 5.1, TOOL NOSE GRINDING ATTACHMENT.

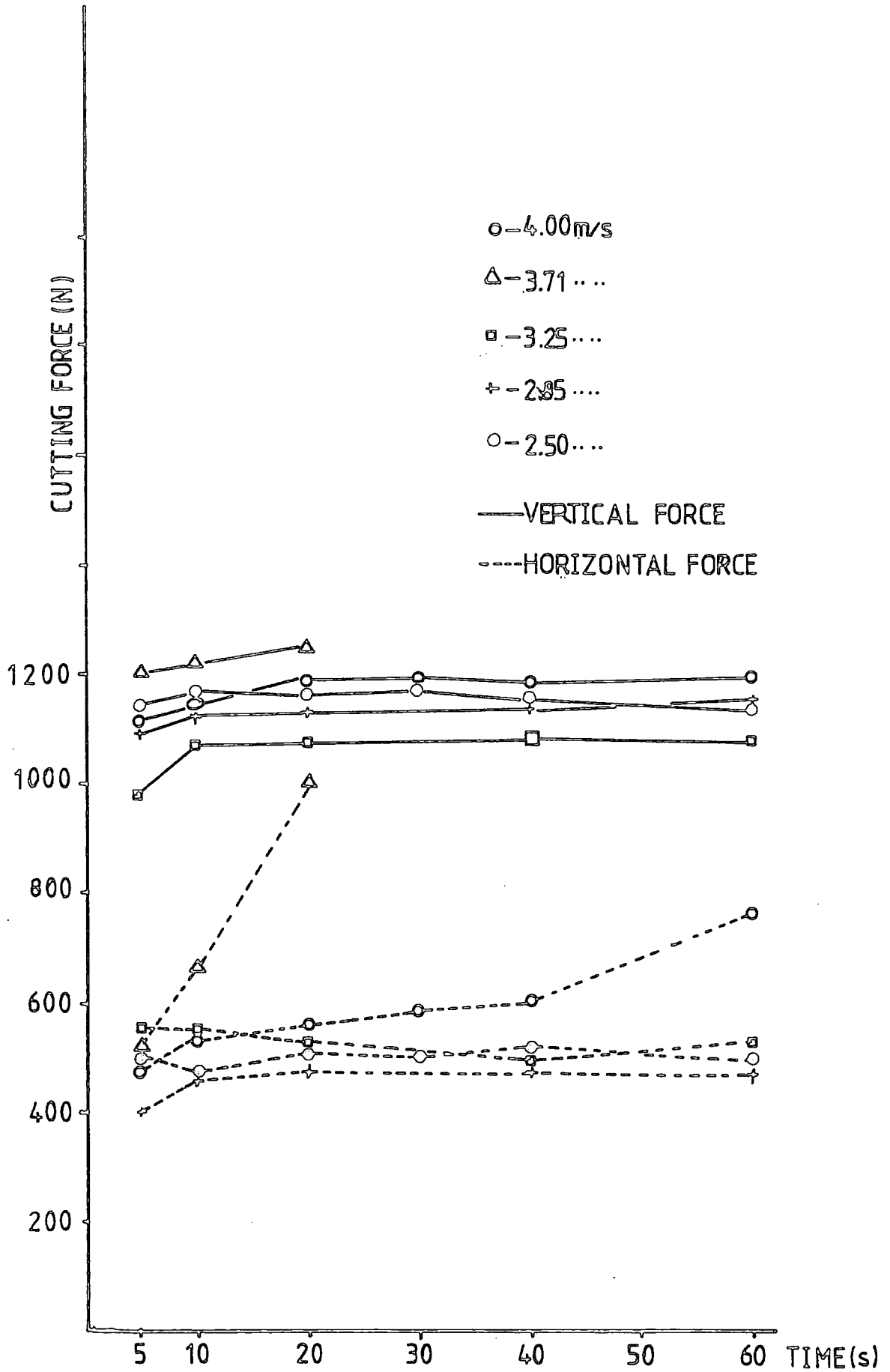

FIGURE 6.1 CUTTING FORCES Vs TIME, GRADE-TE, FEED=0.25mm

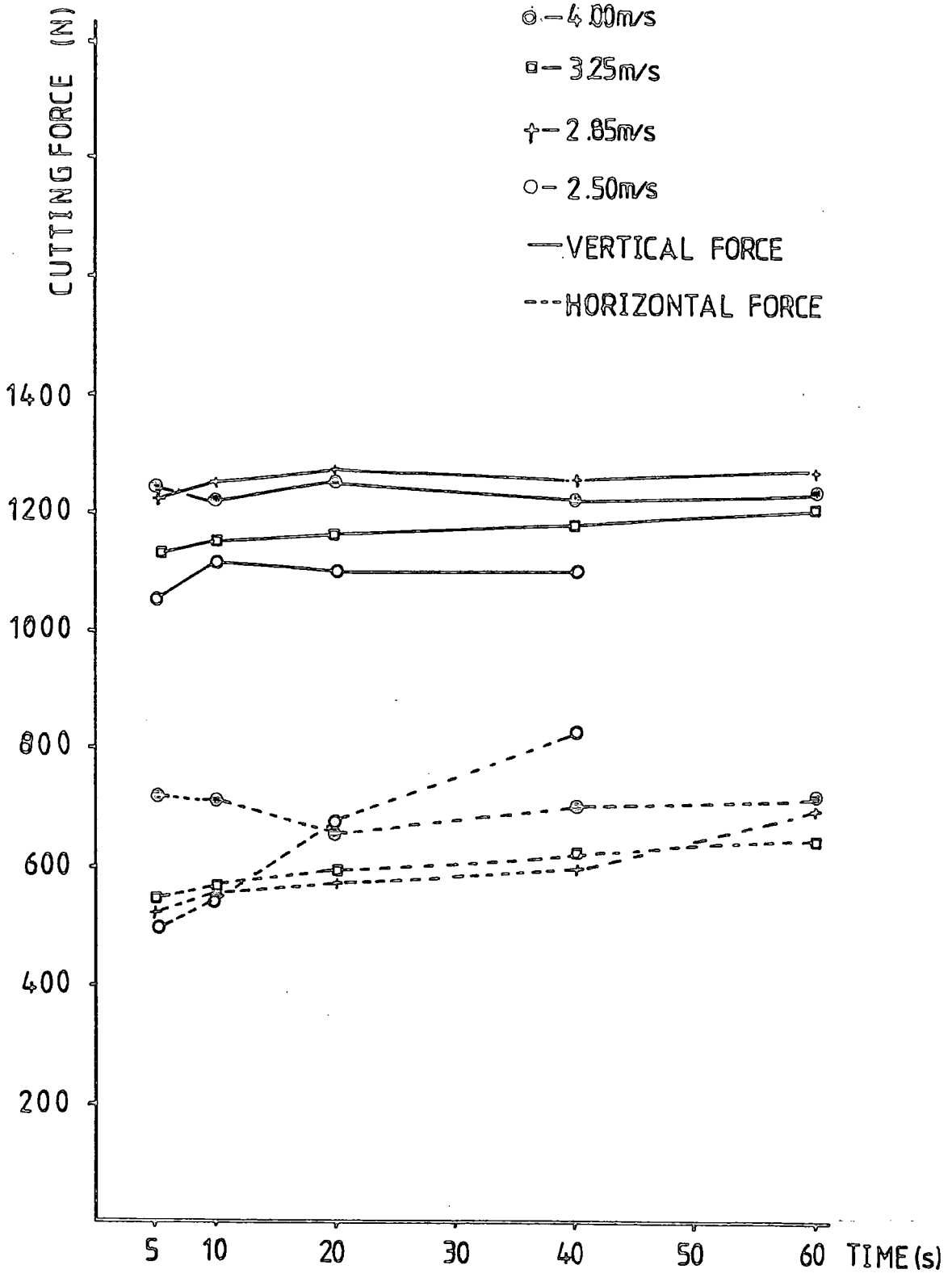

FIGURE 6.2 CUTTING FORCES Vs TIME, GRADE-TE, FEED=0.30mm

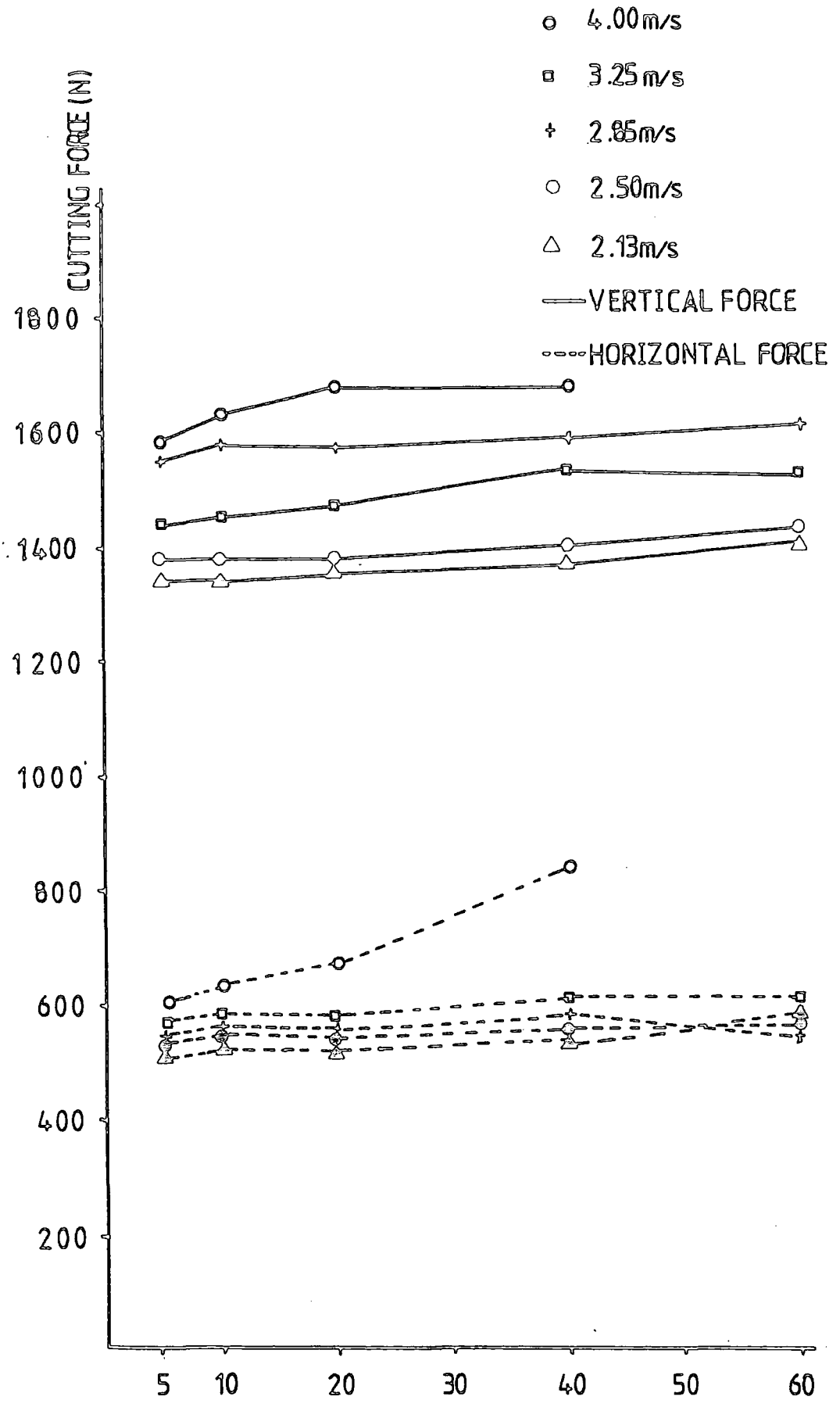

FIGURE 6.3 CUTTING FORCES Vs TIME, GRADE-TE, FEED= 0.35 mm

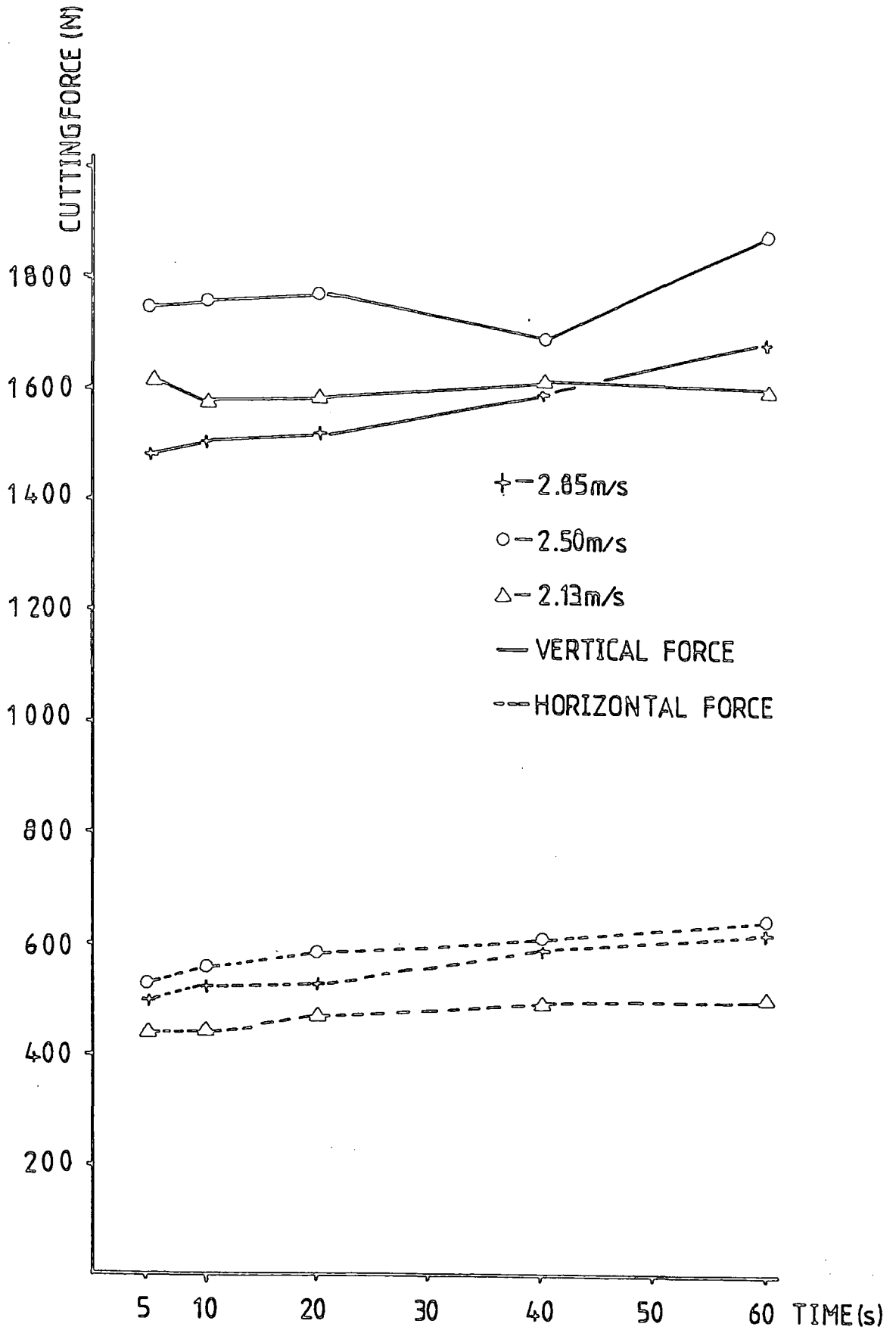

FIGURE 6.4 CUTTING FORCES Vs TIME, GRADE-TE, FEED=0.40mm

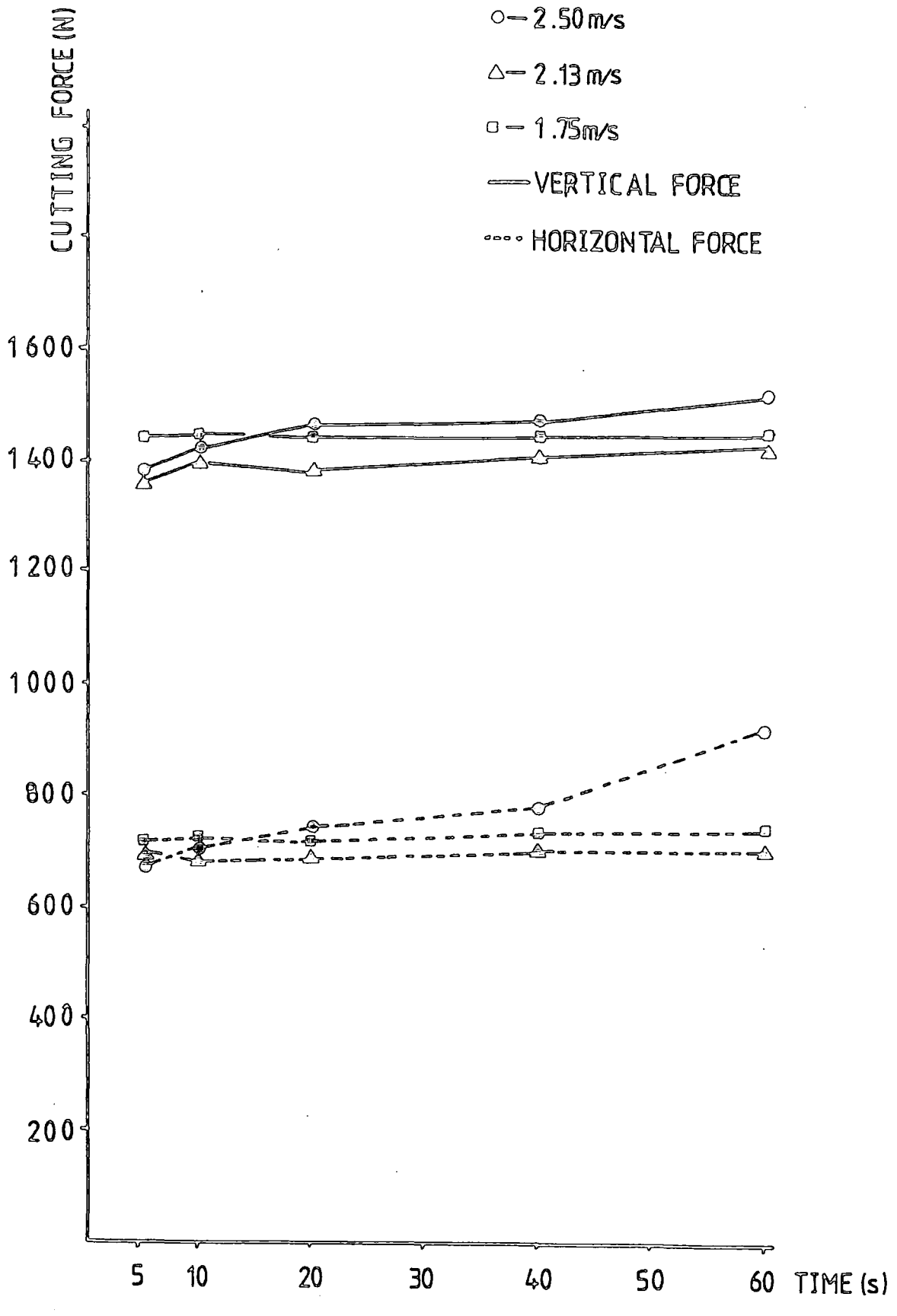

FIGURE 6.5 CUTTING FORCES Vs TIME, GRADE-TTA, FEED=0.35 mm

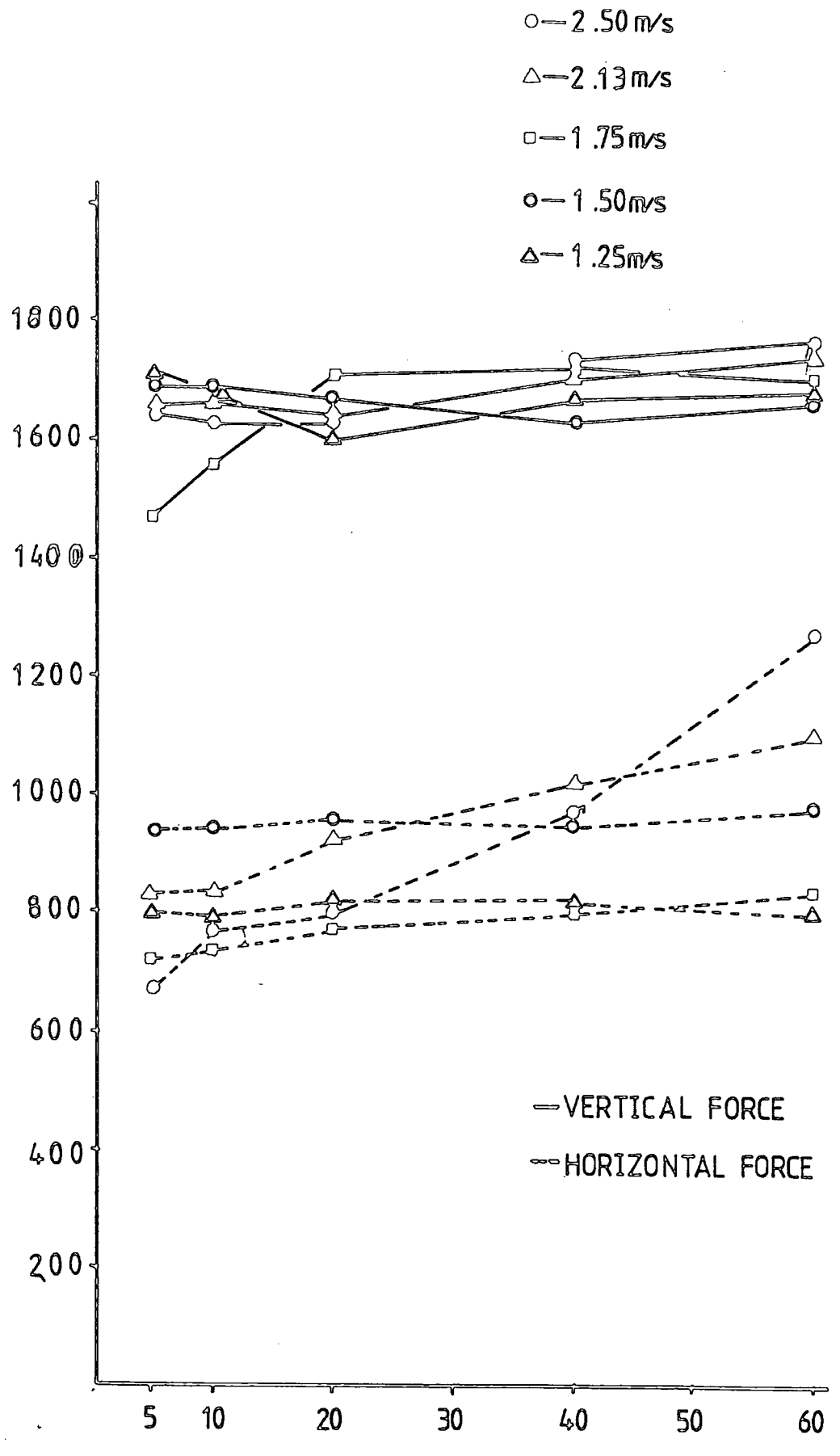

FIGURE 6.6 CUTTING FORCES Vs TIME, GRADE-TTA, FEED=0.40mm

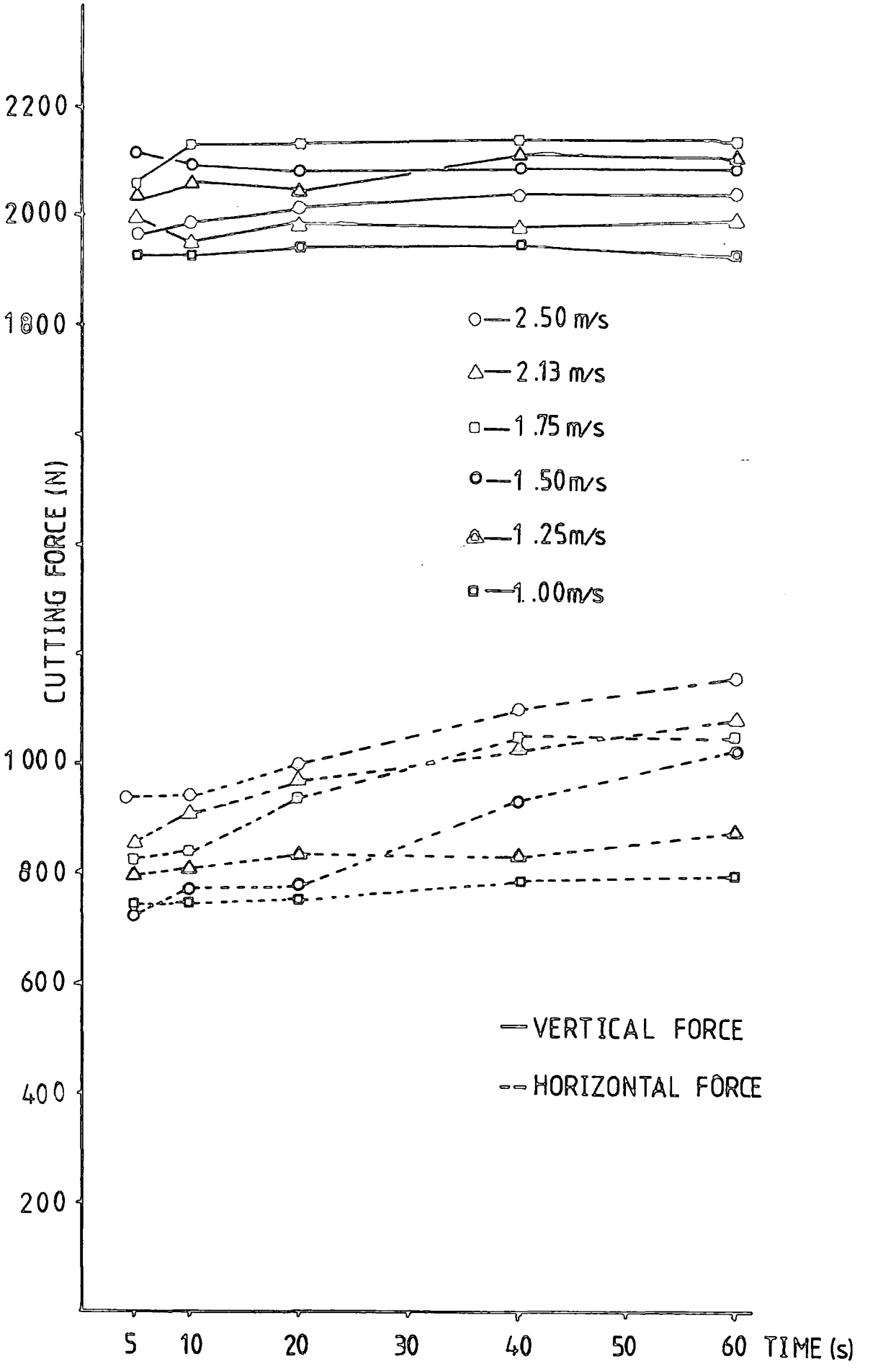

FIGURE 6.7 CUTTING FORCES Vs TIME, GRADE-TTA, FEED=0.5mm

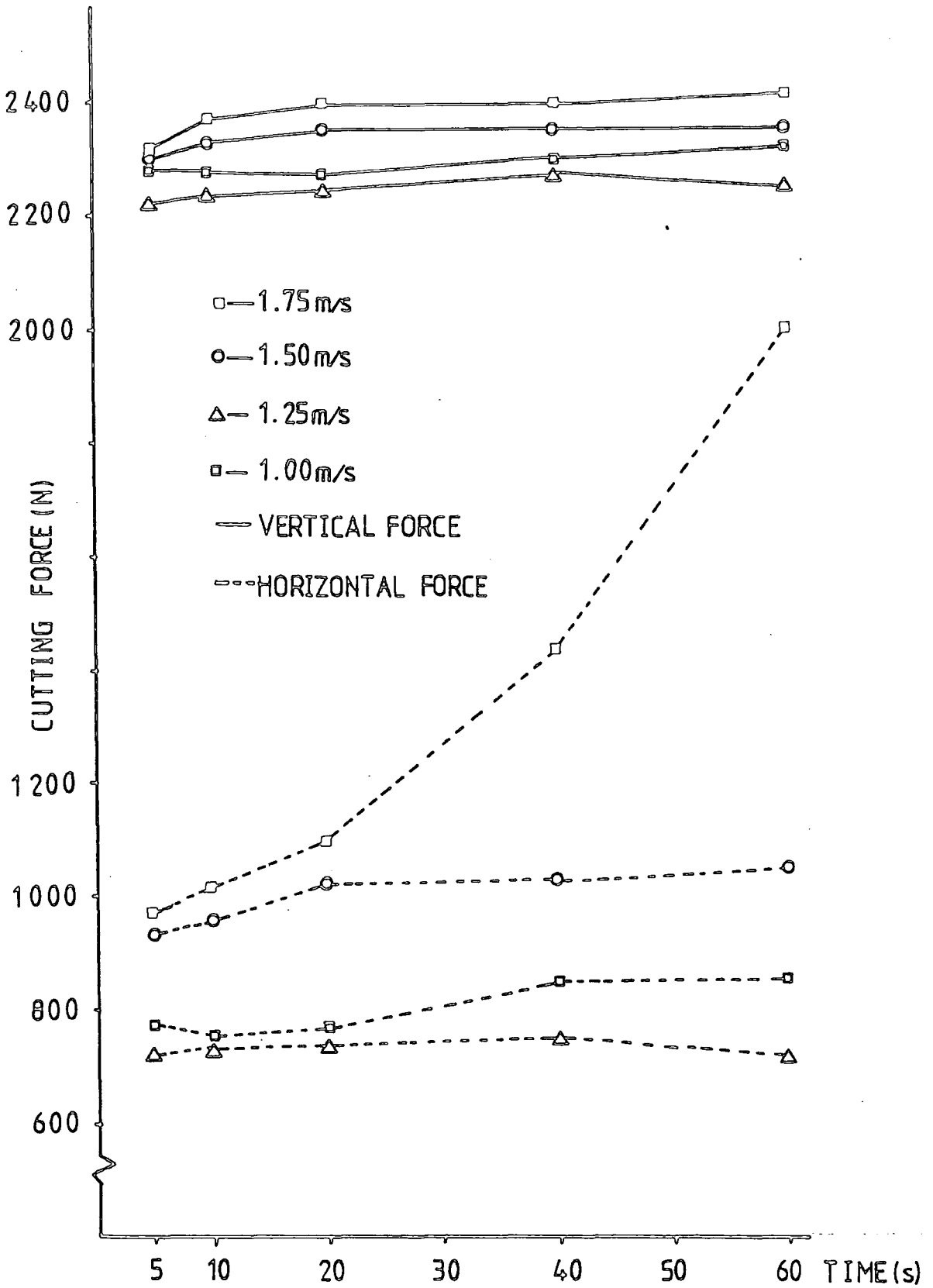

FIGURE 6.8 CUTTING FORCES Vs TIME, GRADE-TTA, FEED=0.65mm

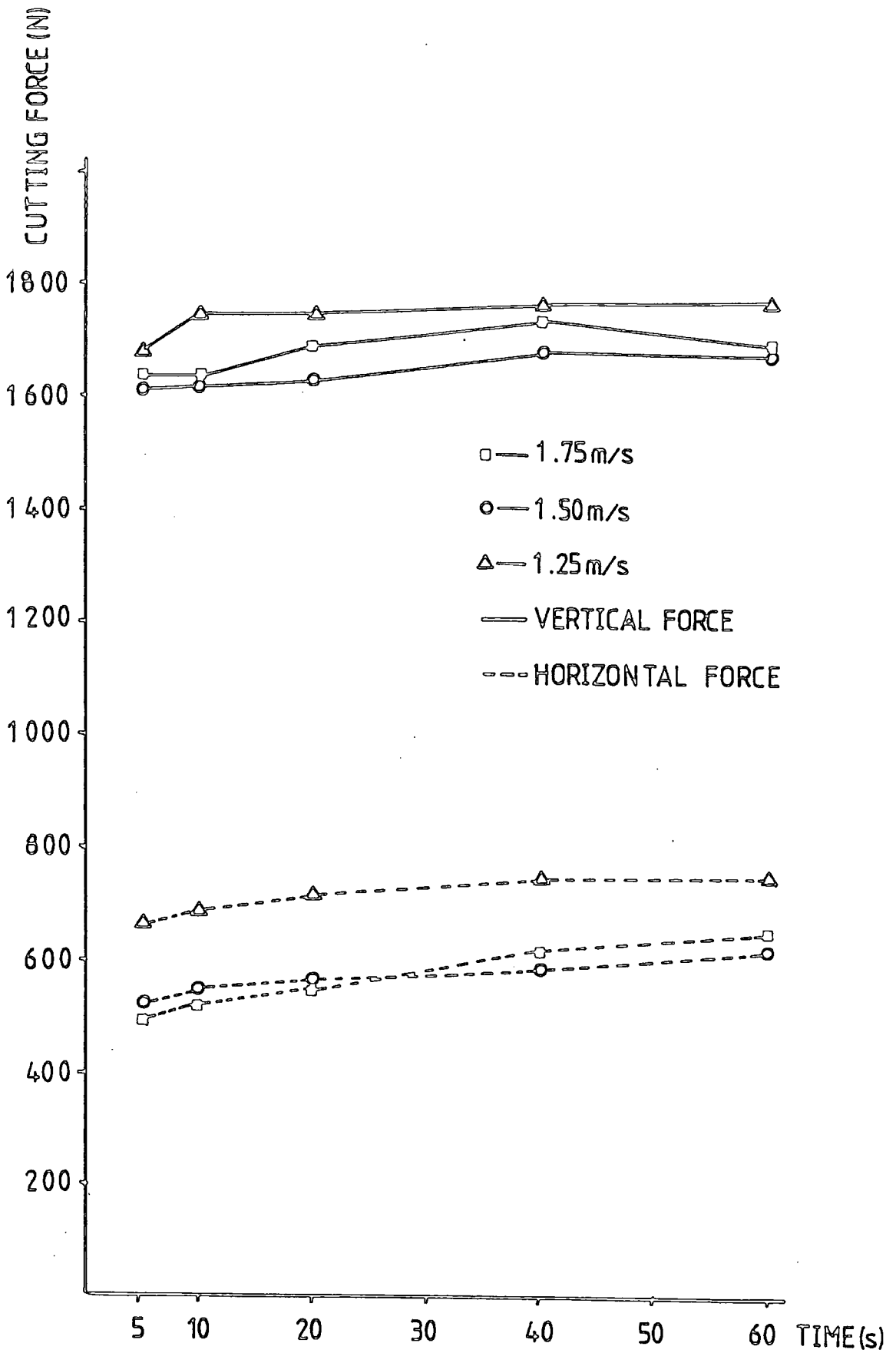

FIGURE 6.9 CUTTING FORCES Vs TIME, GRADE-TA5, FEED=0.40mm

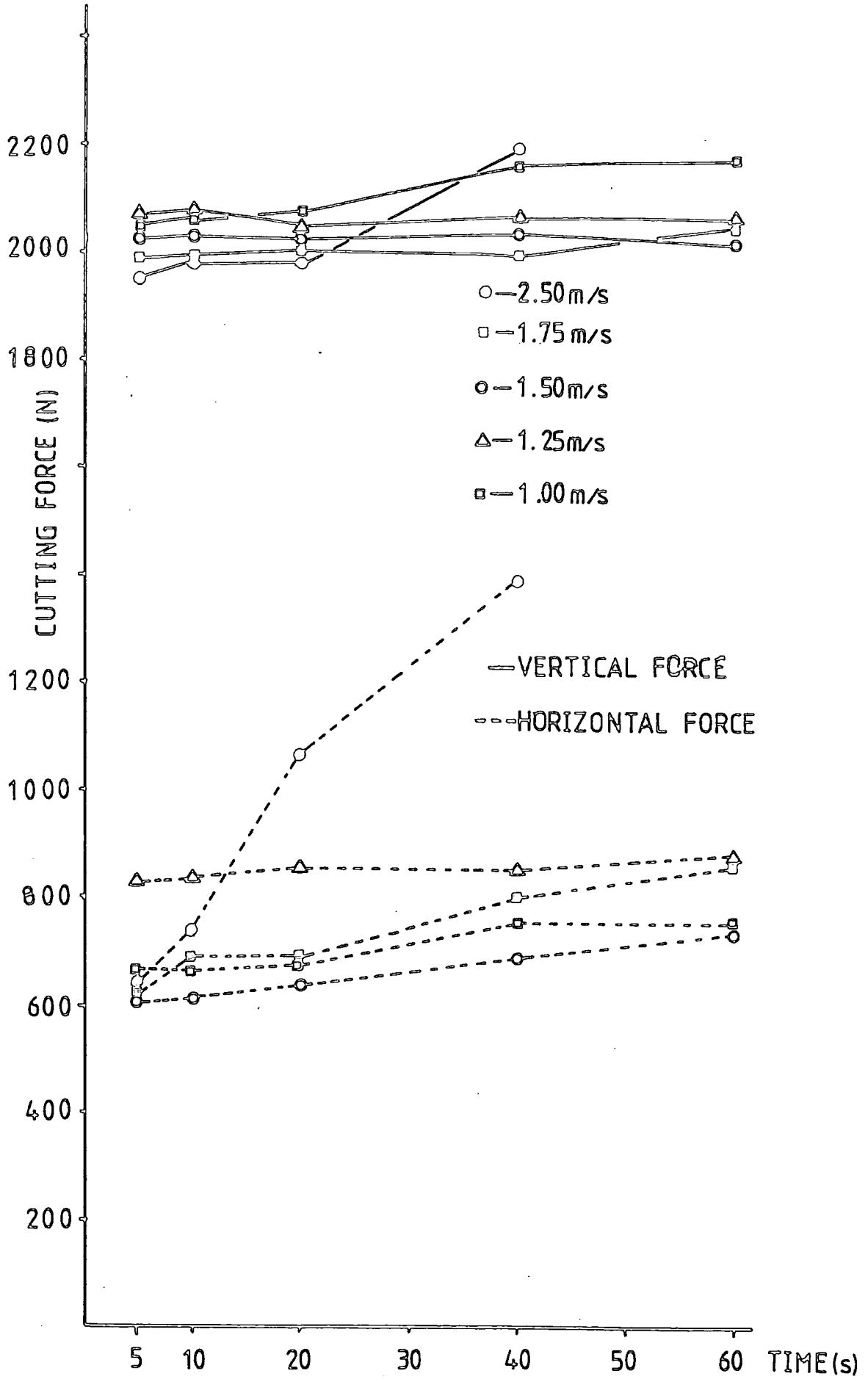

FIGURE 6.10 CUTTING FORCE Vs TIME, GRADE-TA5, FEED=0.50mm

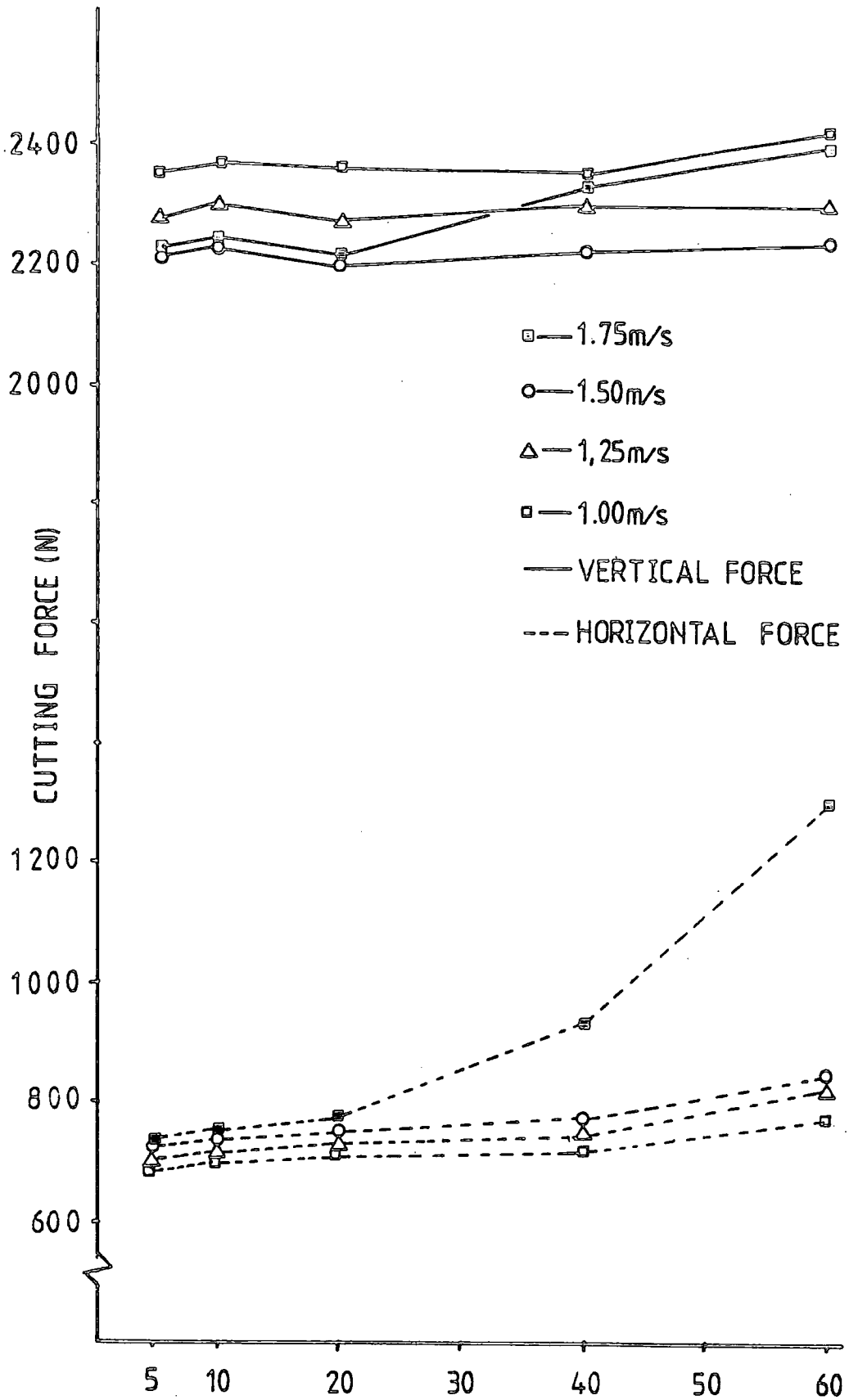

FIGURE 6.11, CUTTING FORCES Vs TIME, GRADE-TA5, FEED=0.65mm

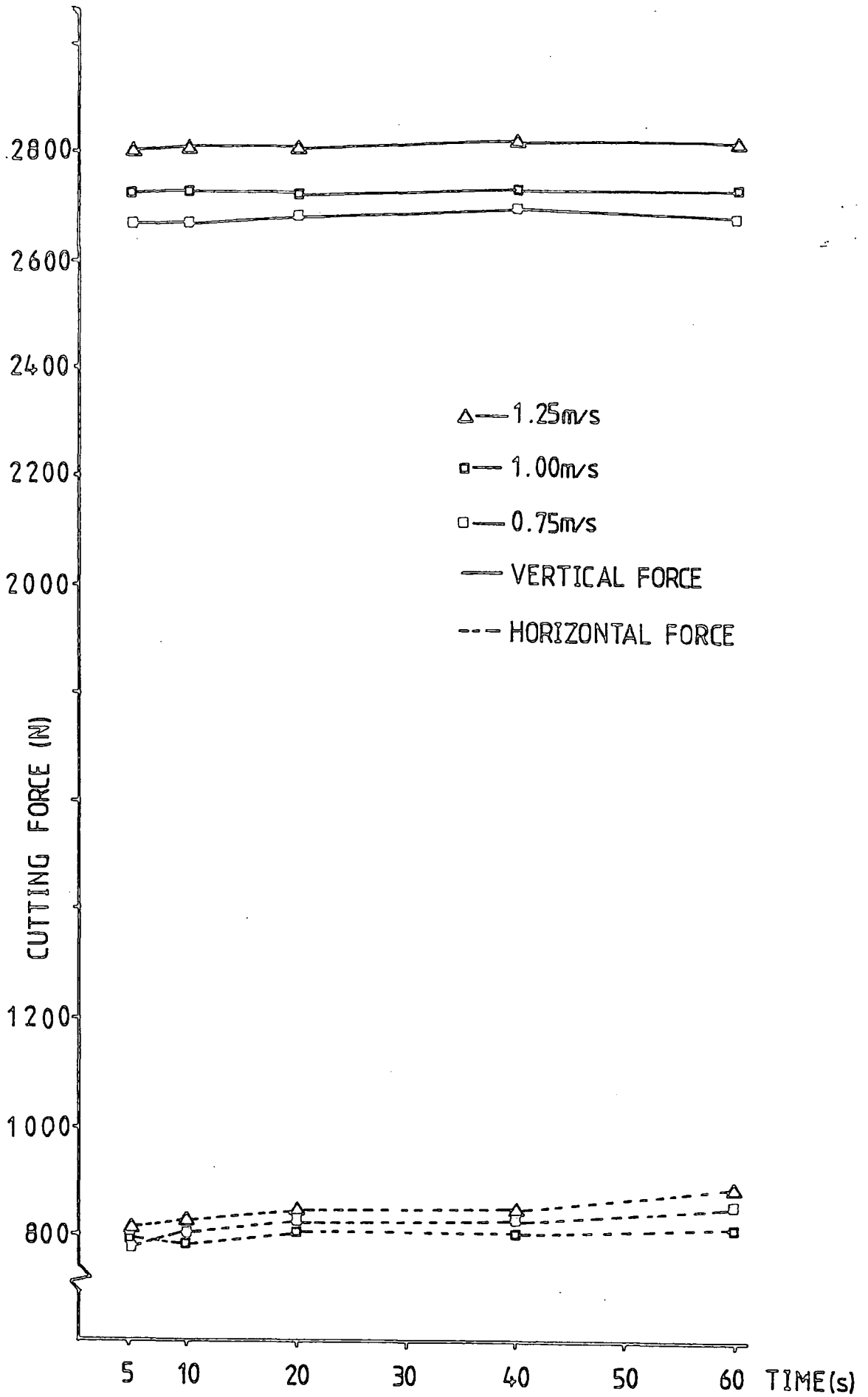

FIGURE 6.12, CUTTING FORCES Vs TIME, GRADE-TA5, FEED=0.80mm

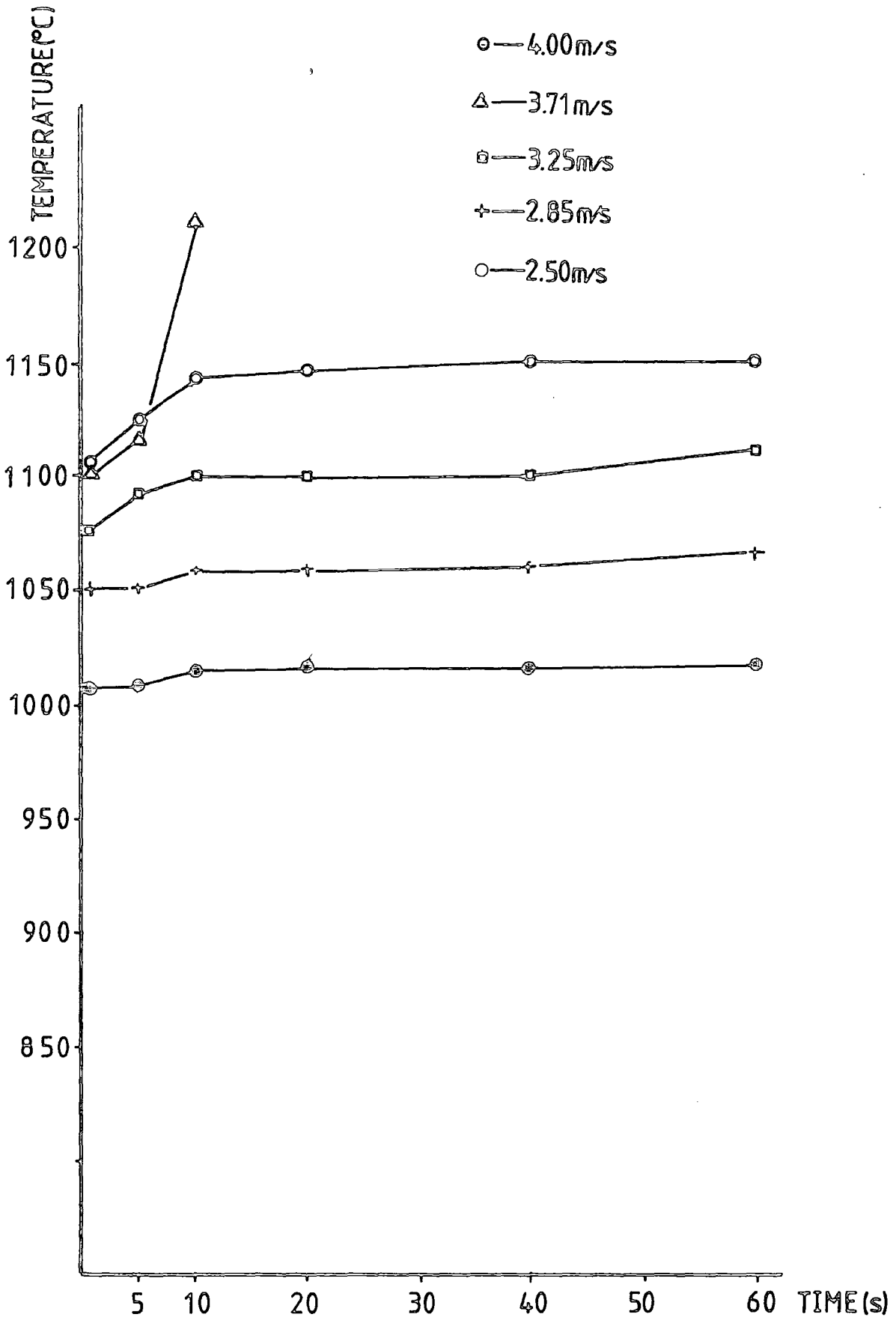

FIGURE 6.13, TEMPERATURE Vs TIME, GRADE-TE, FEED=0.25mm

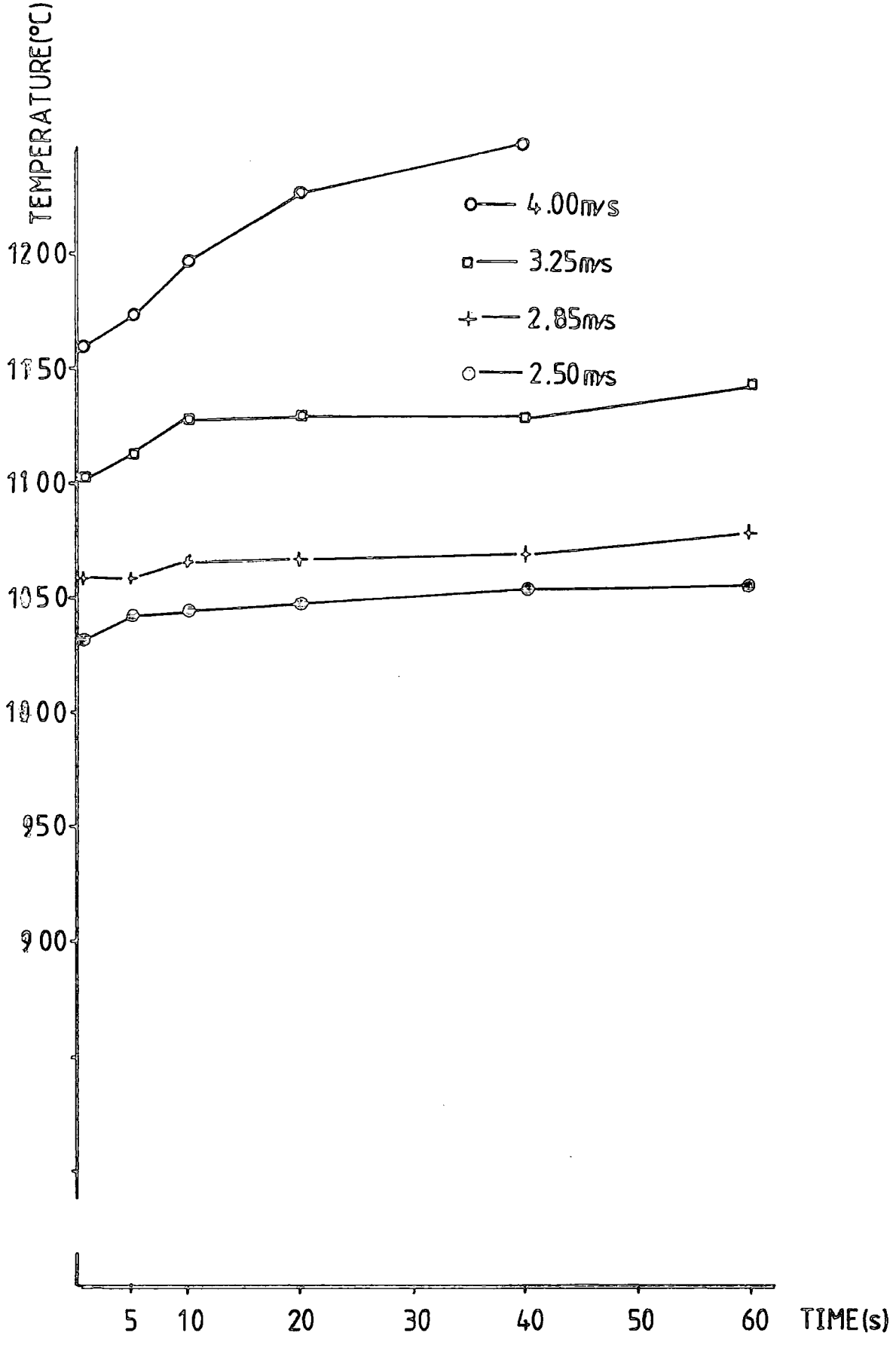

FIGURE 6.14, TEMPERATURE Vs TIME, GRADE-TE, FEED=0,30mm

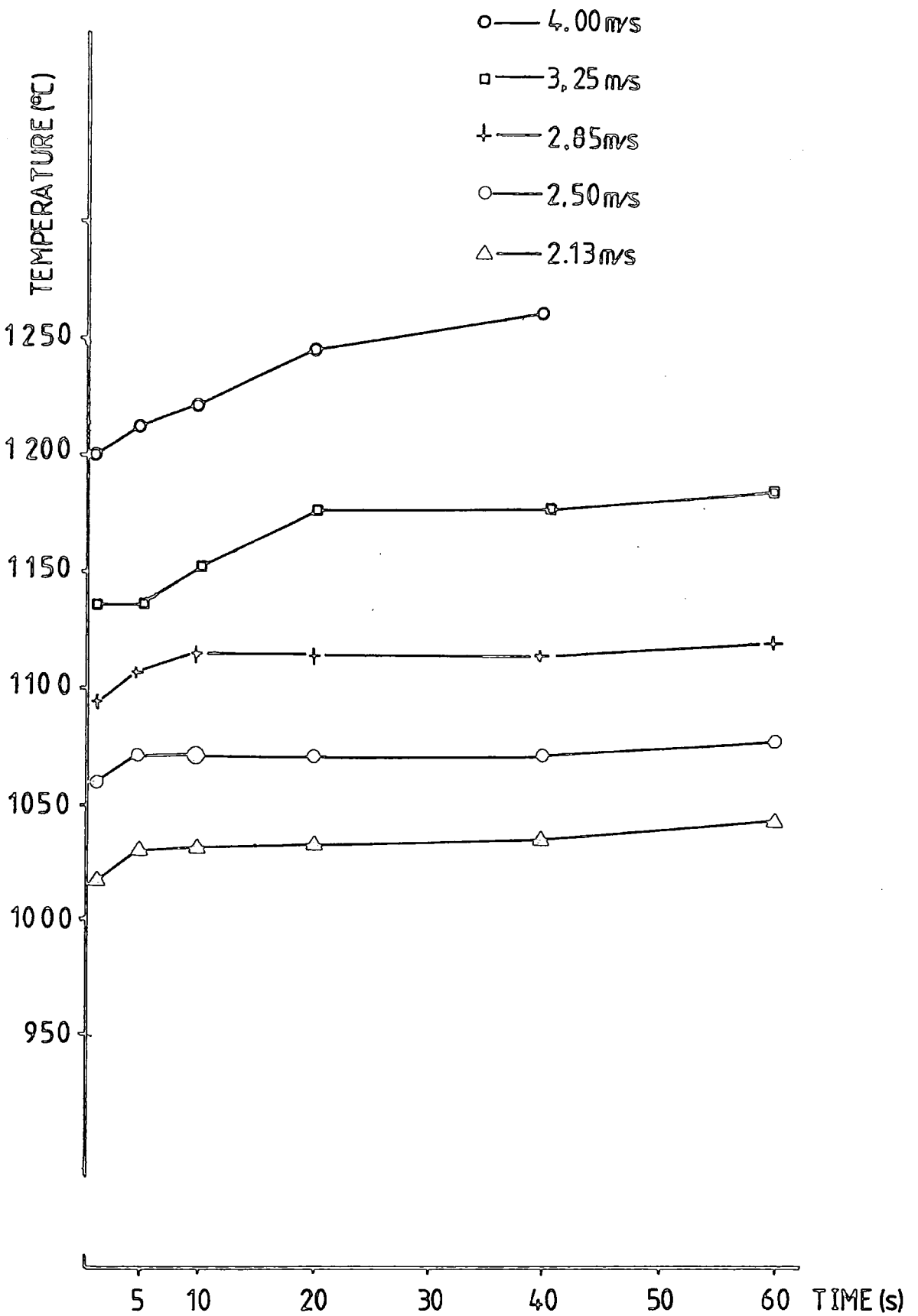

FIGURE 6.15, TEMPERATURE Vs TIME, GRADE-TE, FEED=0.35mm

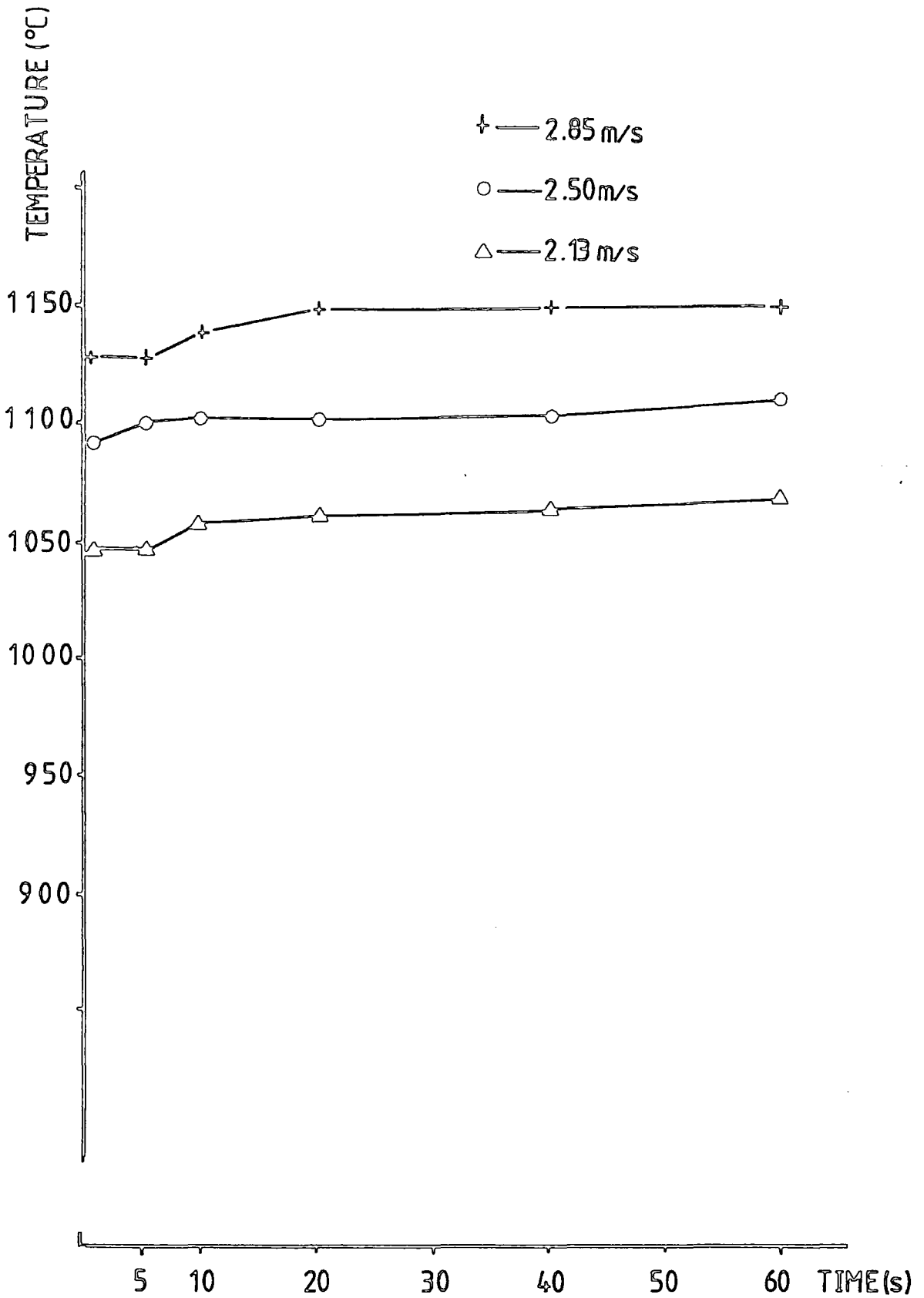

FIGURE 6.16, TEMPERATURE Vs TIME, GRADE-TE, FEED= 0.40mm

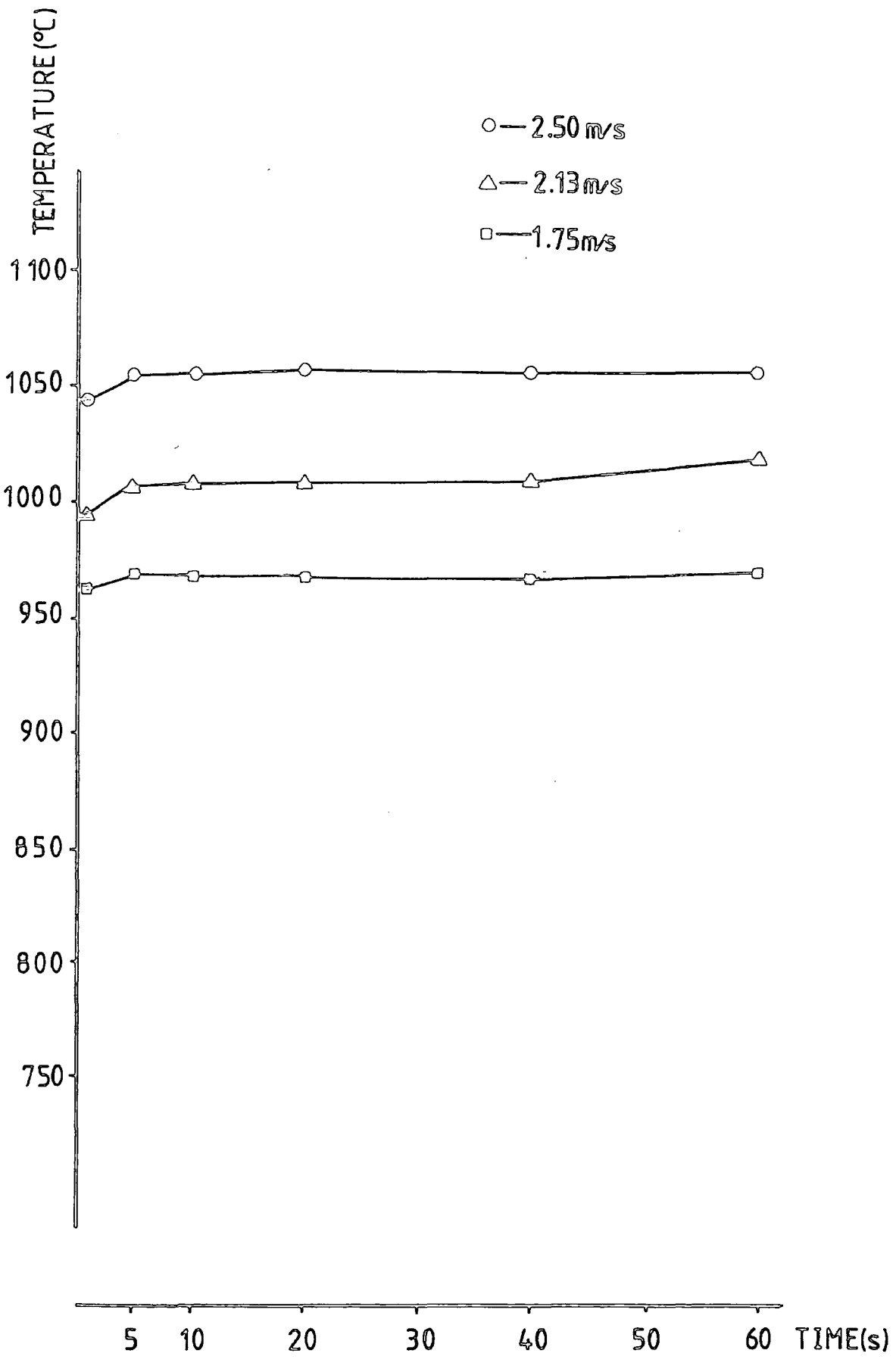

FIGURE 6.17, TEMPERATURE Vs TIME, GRADE-TTA, FEED=0.35 mm

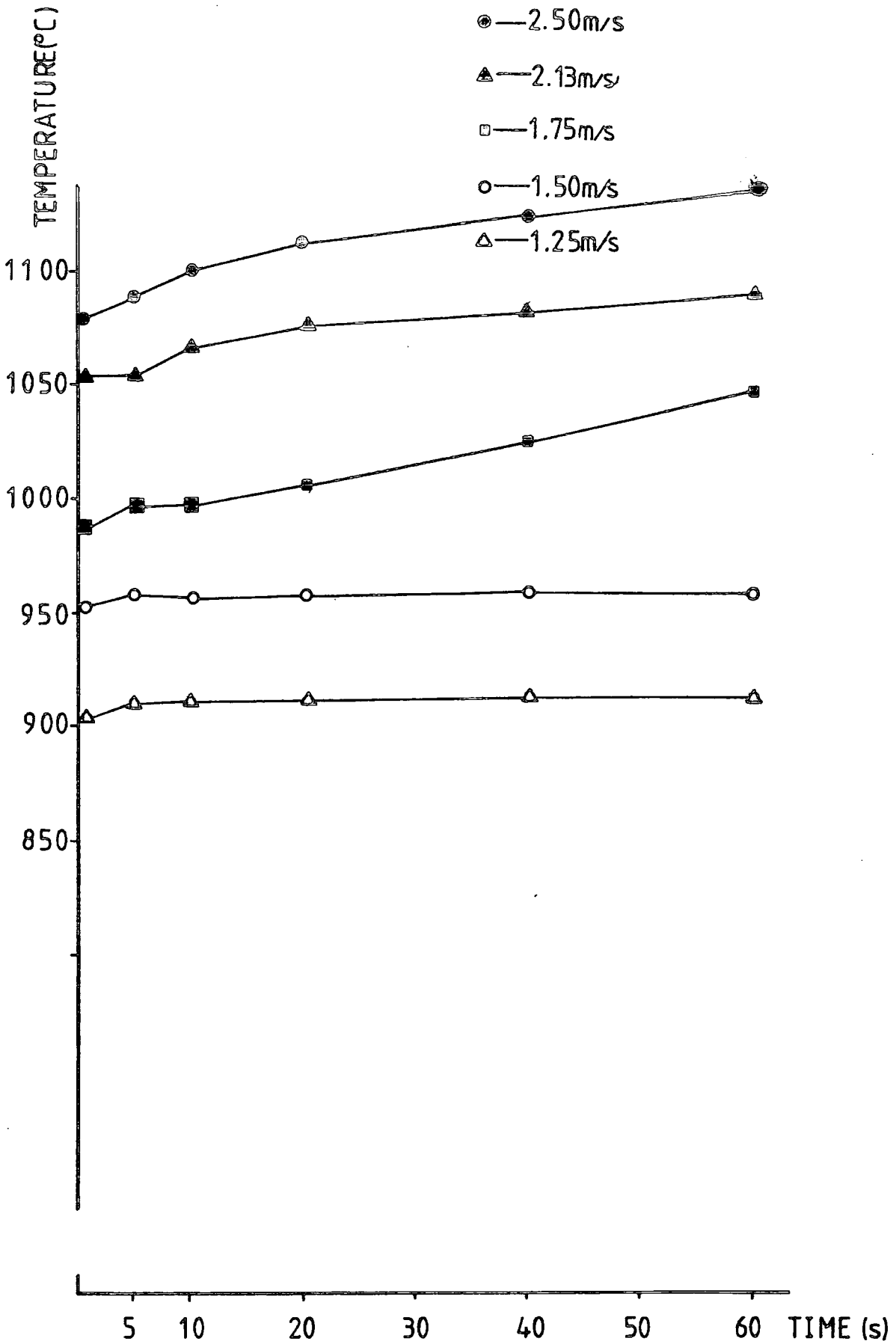

FIGURE 6.18, TIME Vs TEMPERATURE, GRADE -TTA, FEED = 0.40mm

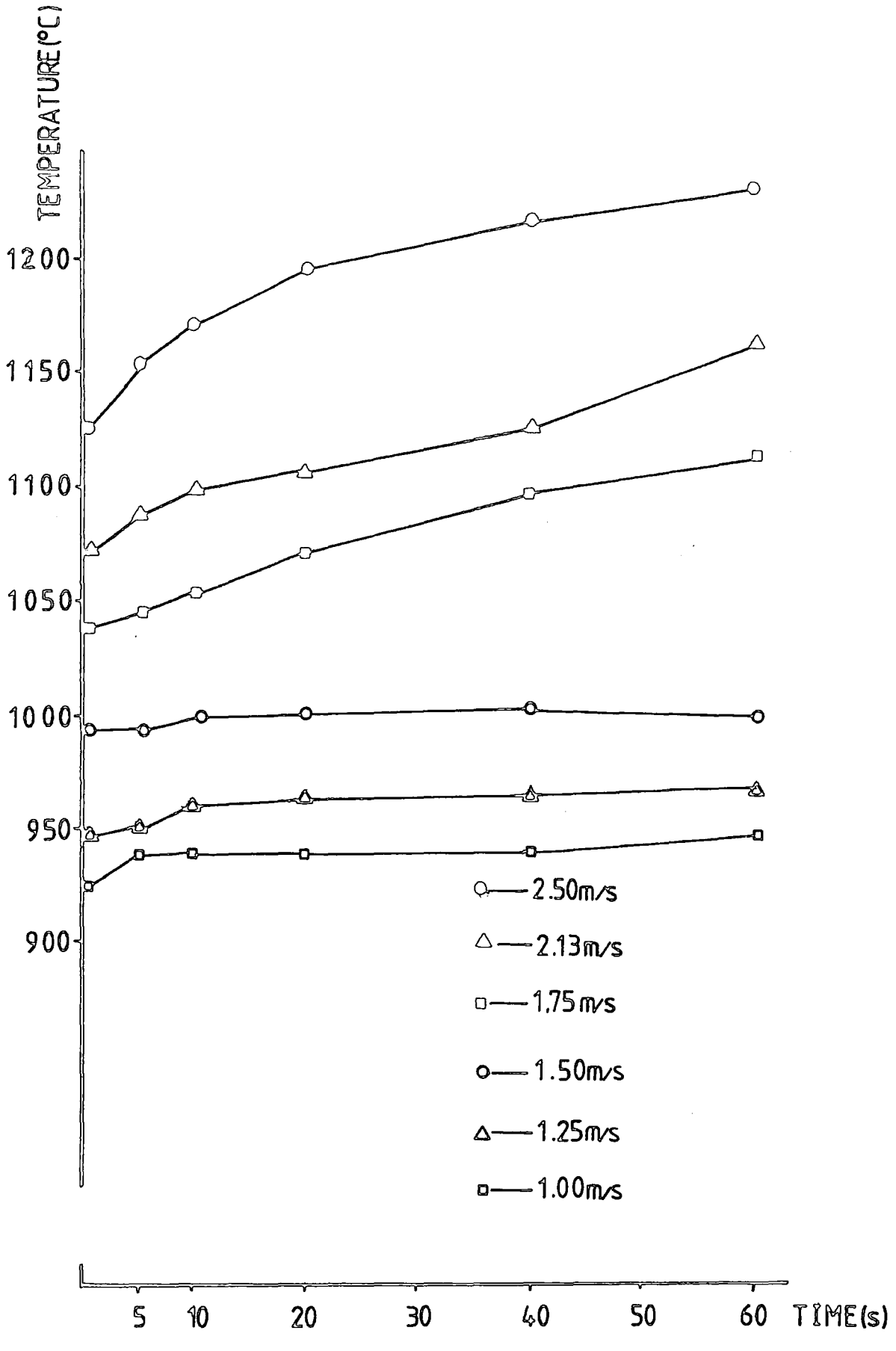

FIGURE 6.19, TEMPERATURE Vs TIME, GRADE-TTA, FEED=0.50mm.

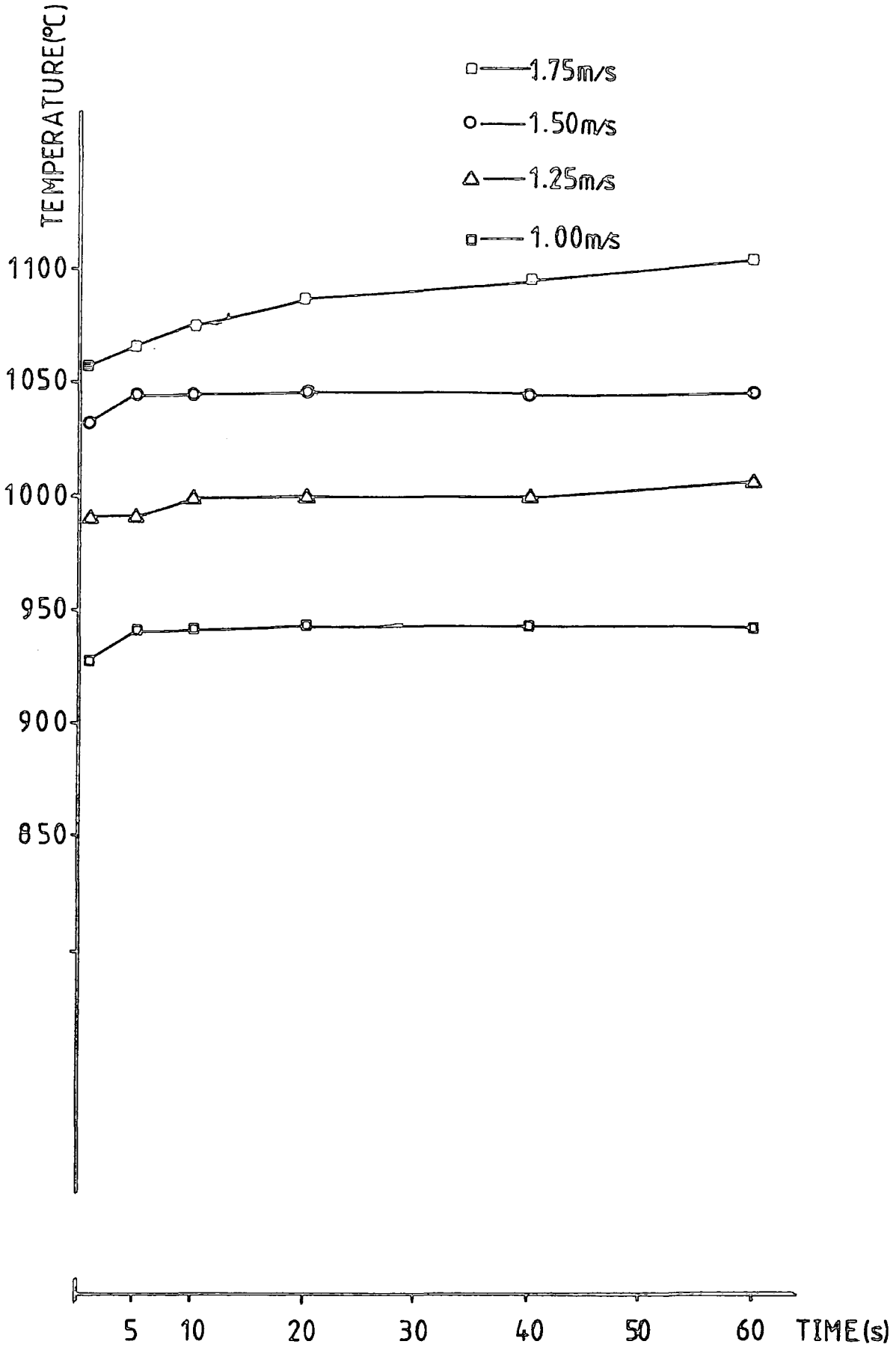

FIGURE 6.20, TEMPERATURE Vs TIME, GRADE-TTA, FEED=0.65mm

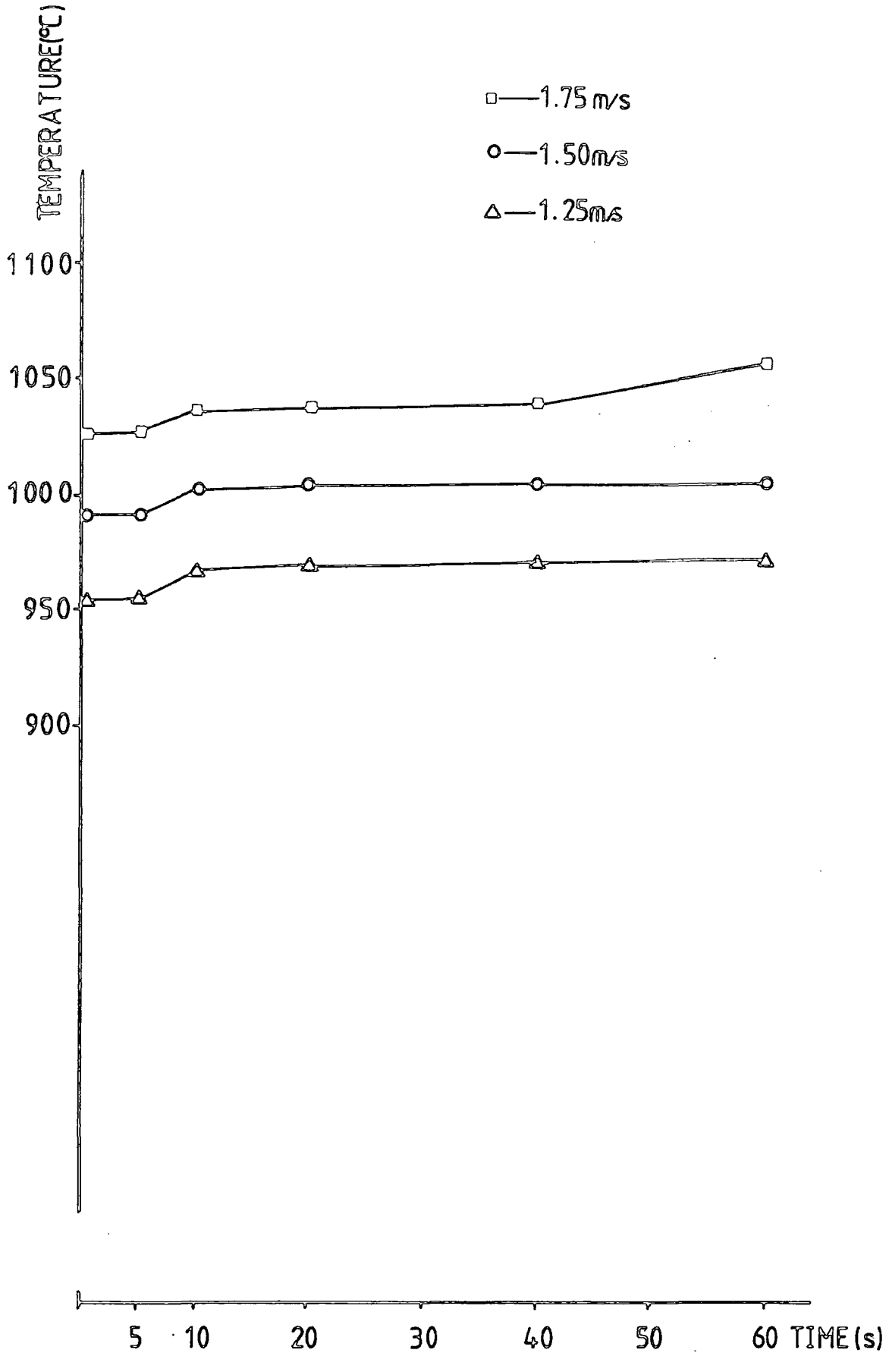

FIGURE 6.21, TEMPERATURE Vs TIME, GRADE -TA5, FEED = 0.40mm

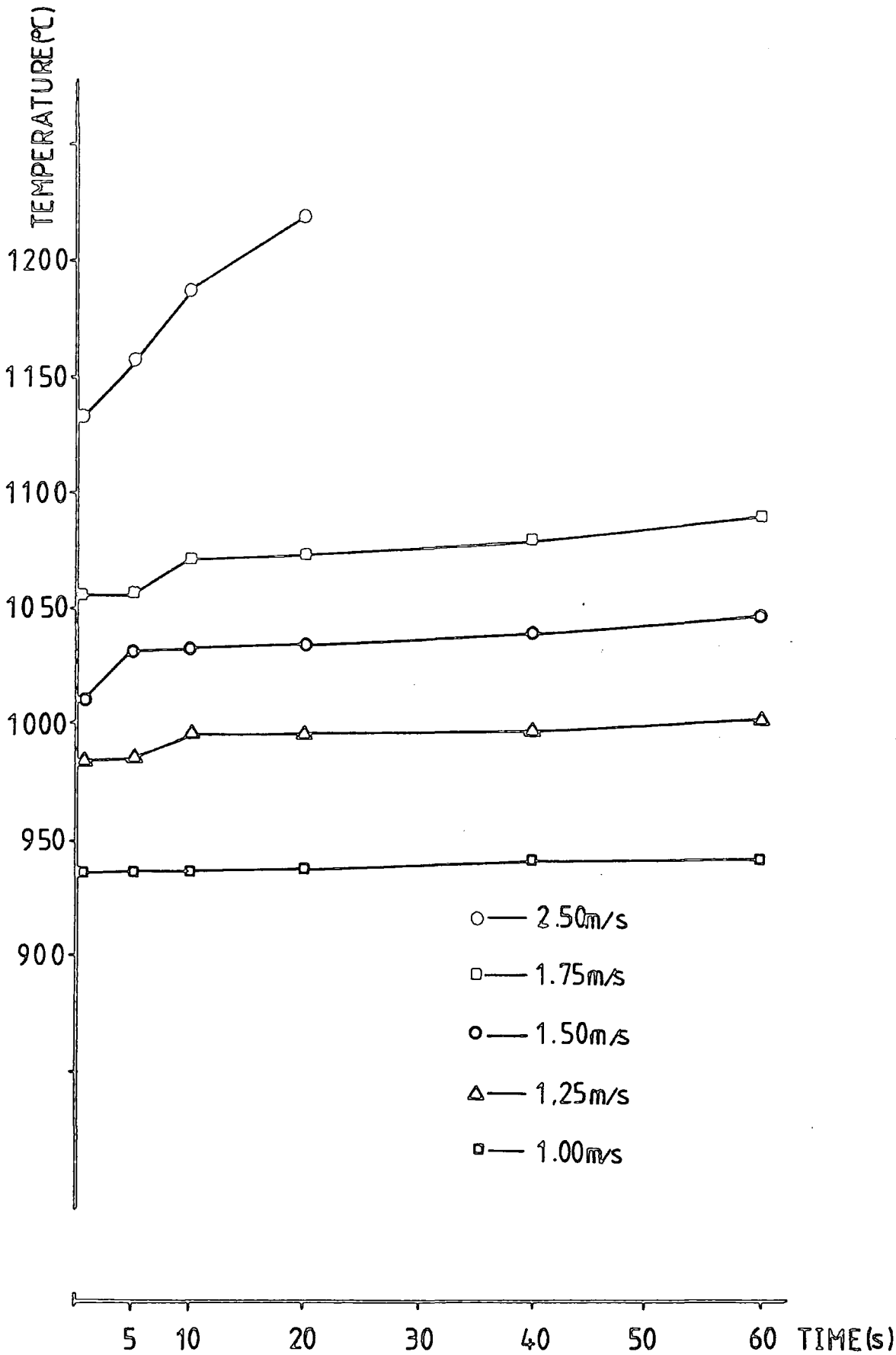

FIGURE 6.22, TEMPERATURE Vs TIME, GRADE-TA5, FEED = 0.50mm

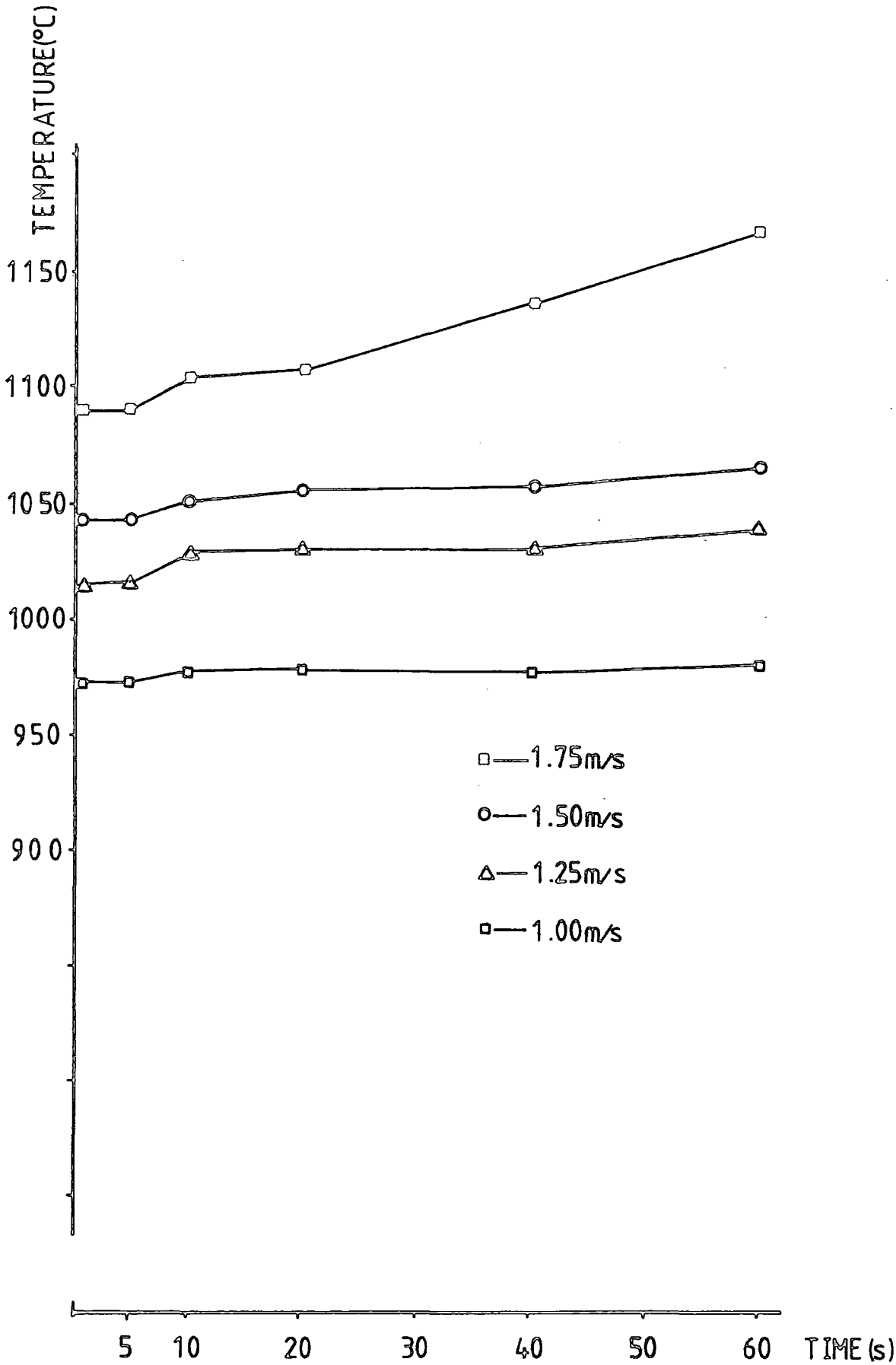

FIGURE 6·23, TEMPERATURE Vs TIME, GRADE-TA5, FEED=0.65mm

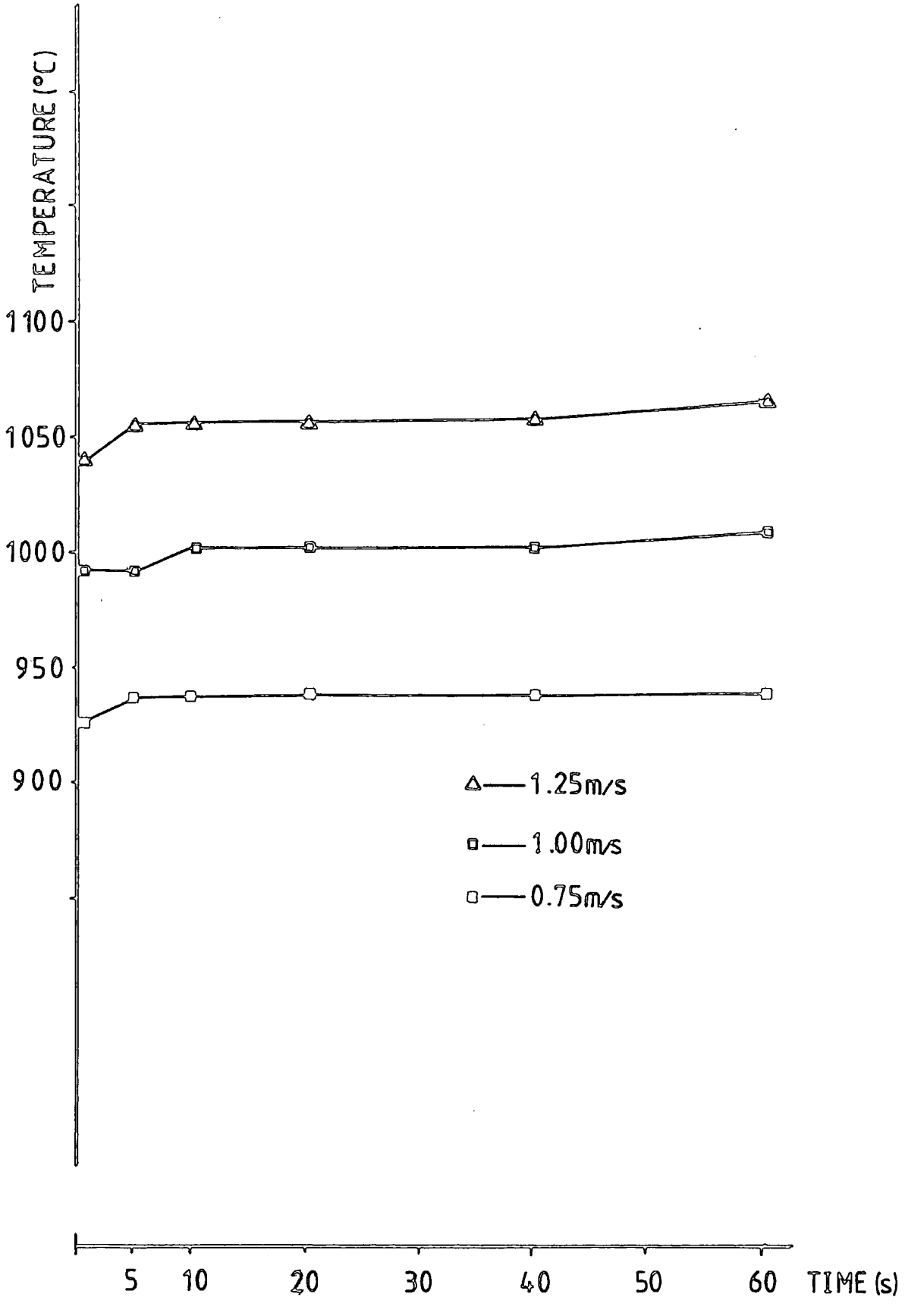

FIGURE 6.24, TEMPERATURE Vs TIME, GRADE-TA5, FEED=0.80mm.

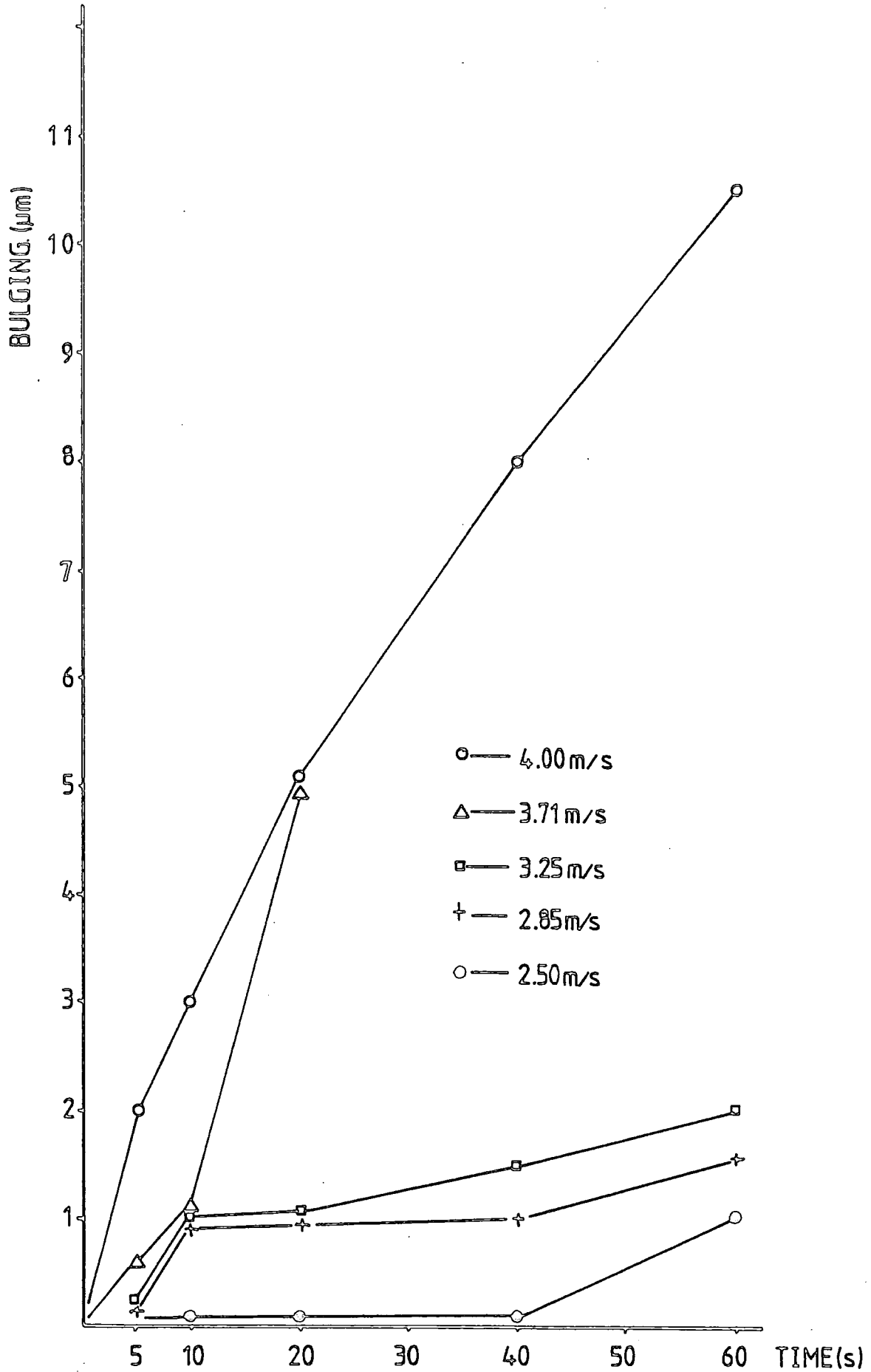

FIGURE 6.25, BULGING Vs TIME, GRADE-TE, FEED = 0.25

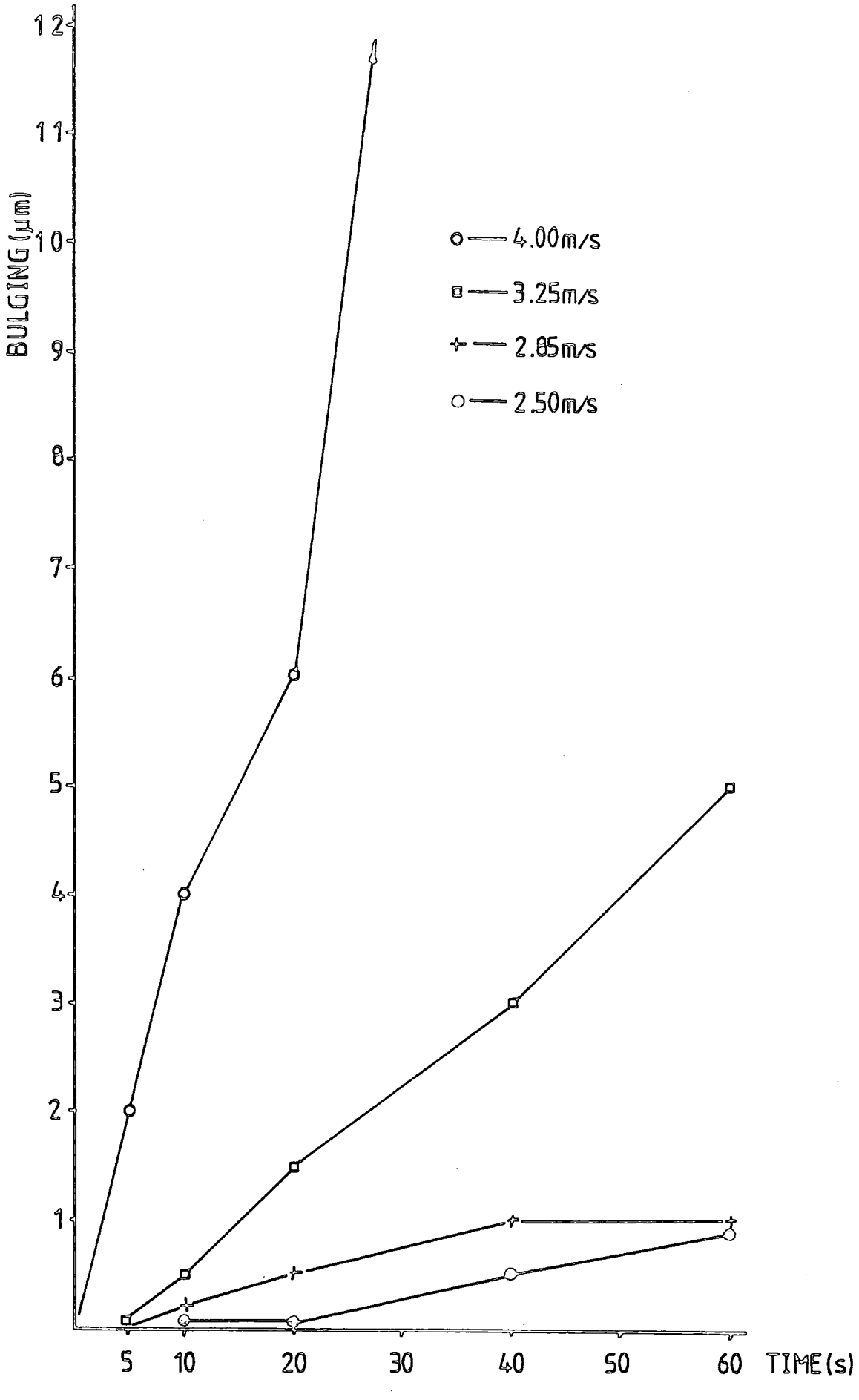

FIGURE 6.26, BULGING Vs TIME, GRADE-TE, FEED=0.30mm

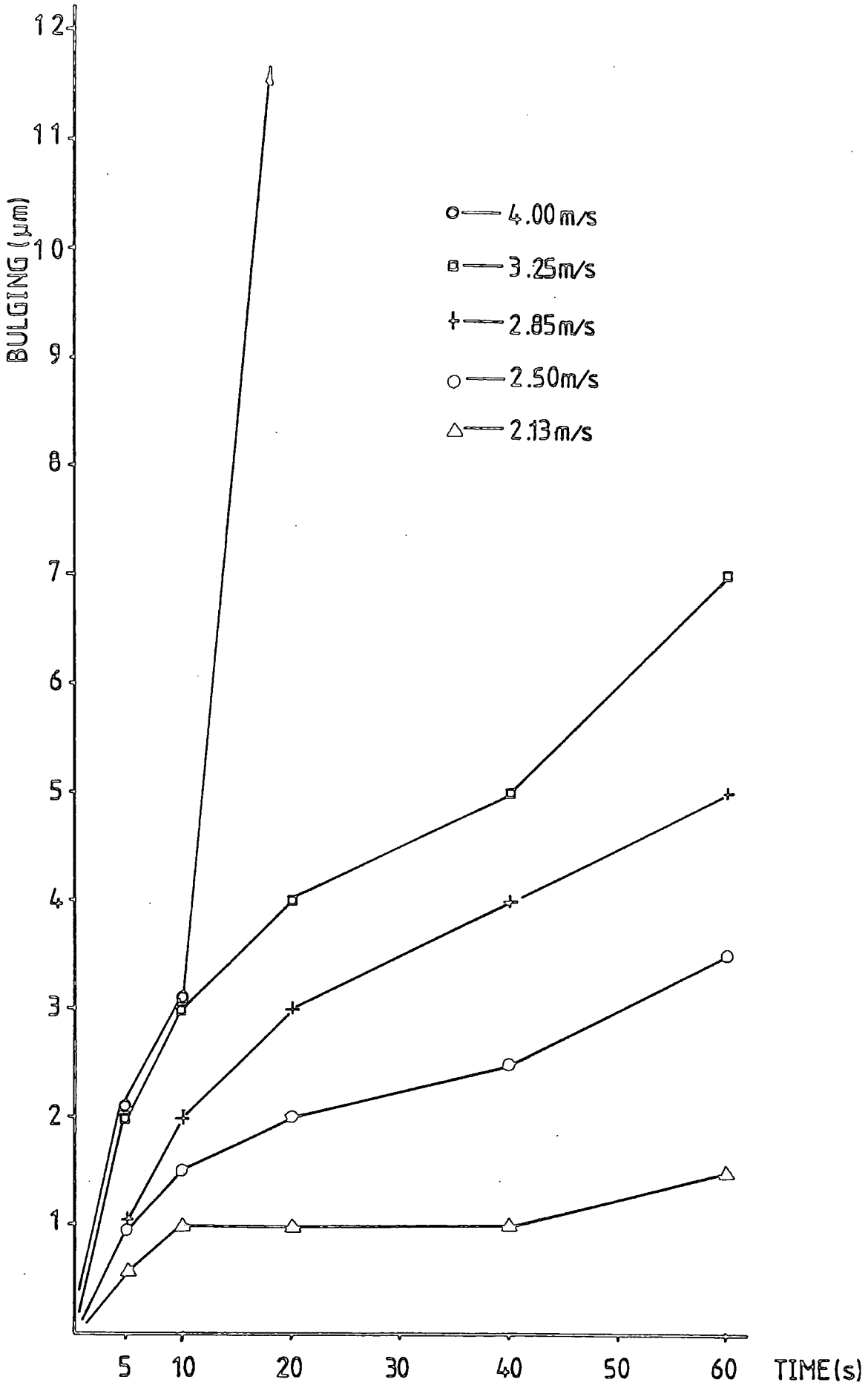

FIGURE 6.27, BULGING Vs TIME, GRADE-TE, FEED = 0.35mm

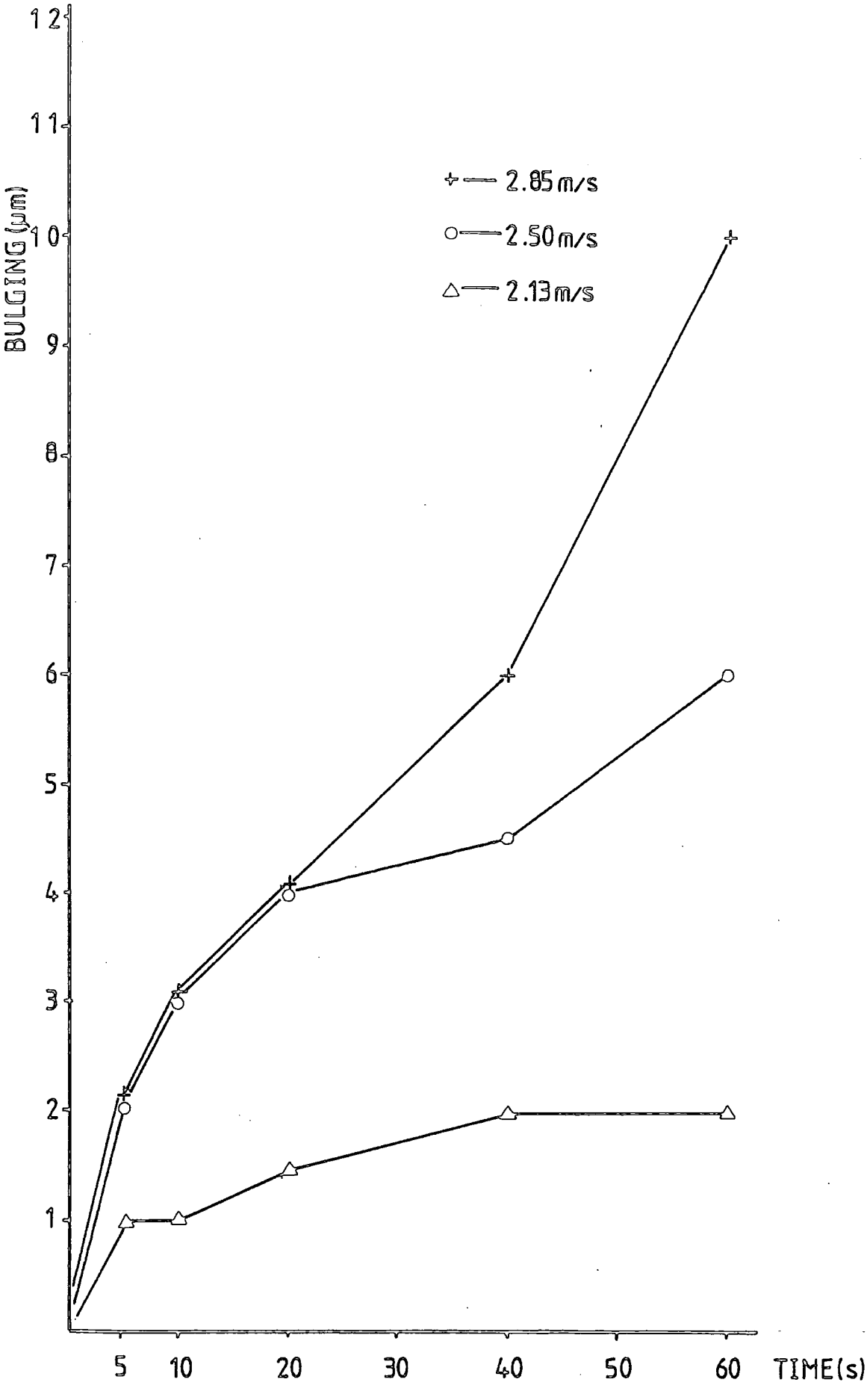

FIGURE 6.28, BULGING Vs TIME, GRADE-TE, FEED=0.40mm

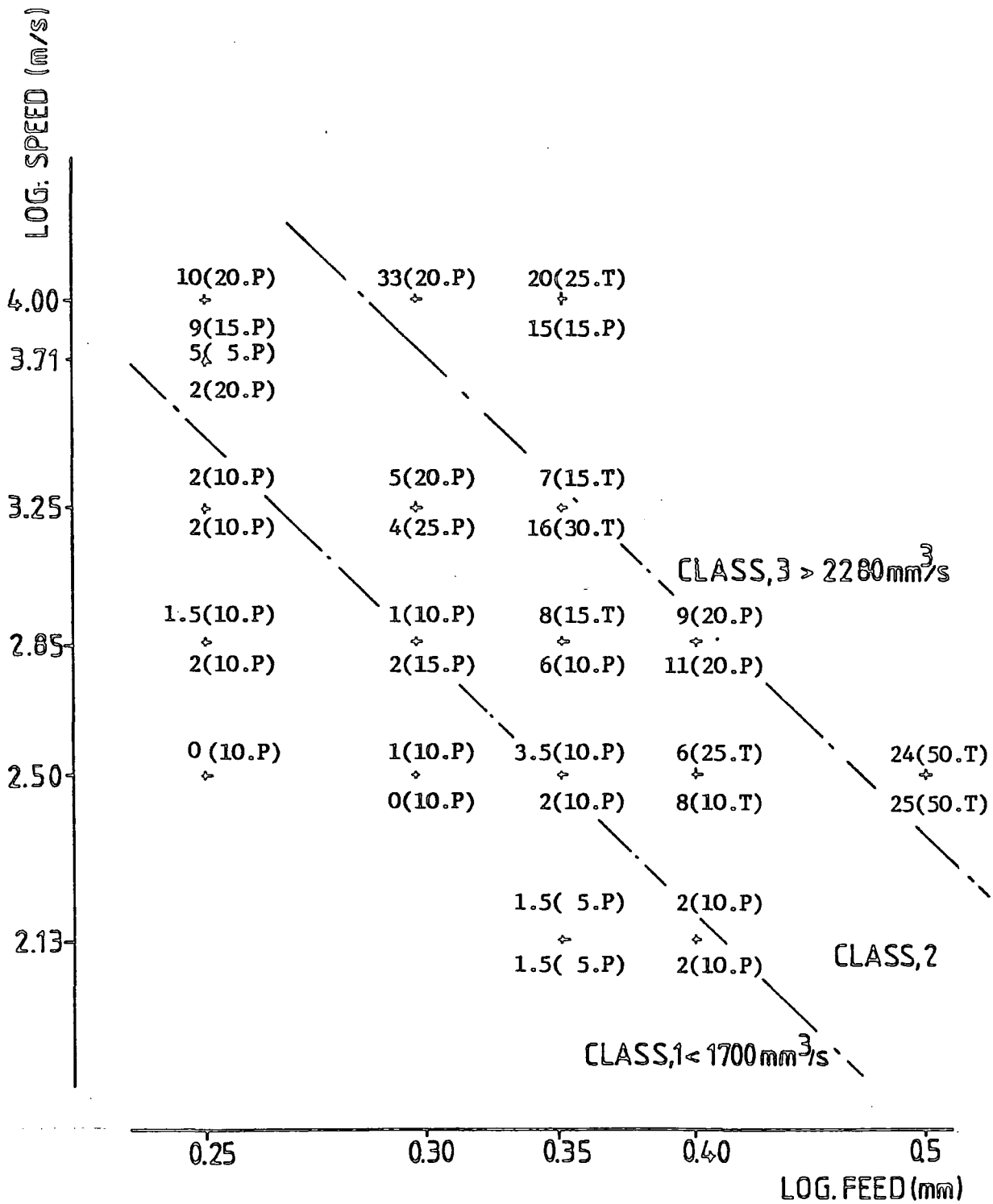

FIGURE 6.29, BULGING AND EDGE DEPRESSION - GRADE - TE

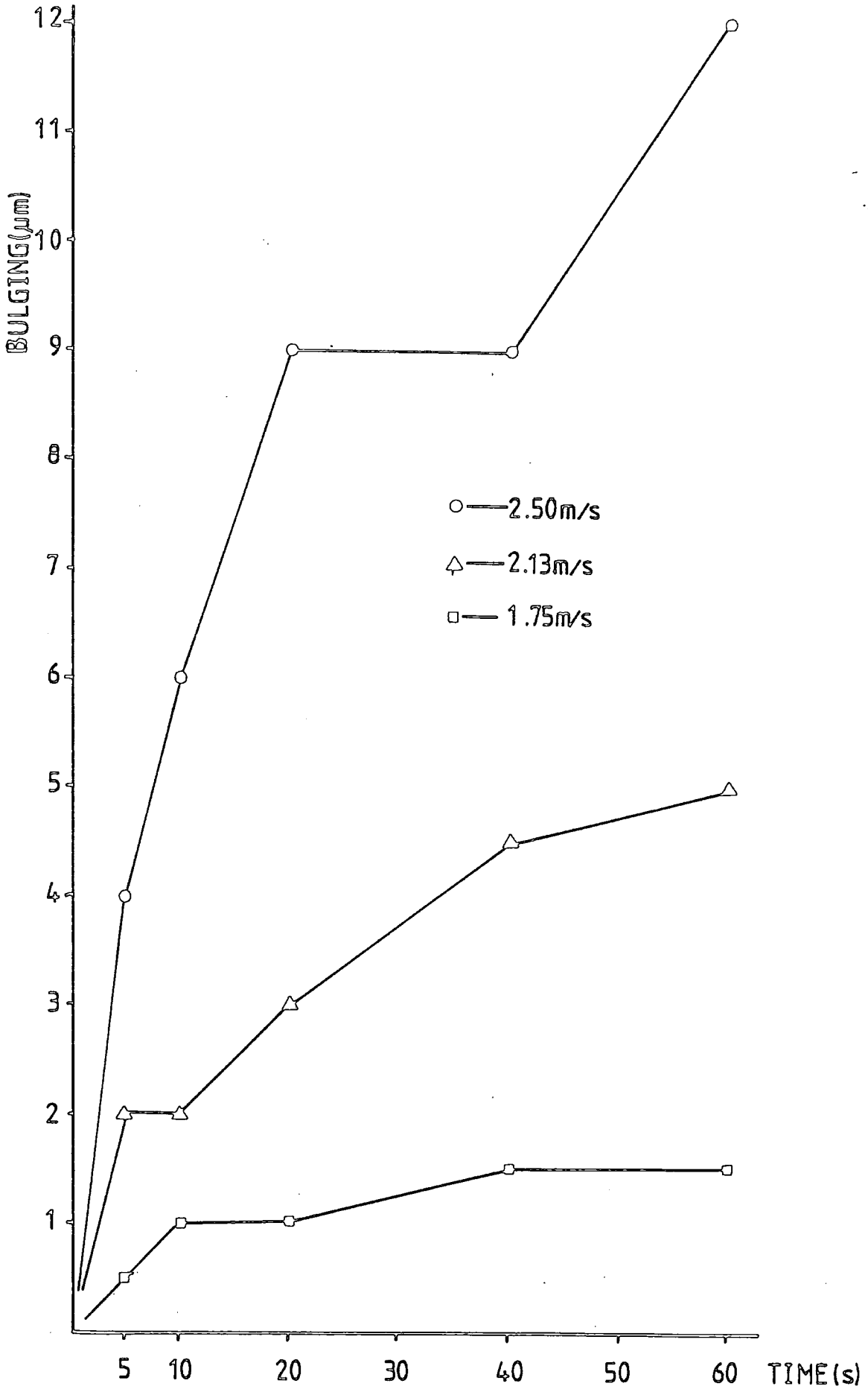

FIGURE 6.30, BULGING Vs TIME, GRADE-TTA, FEED = 0.35mm

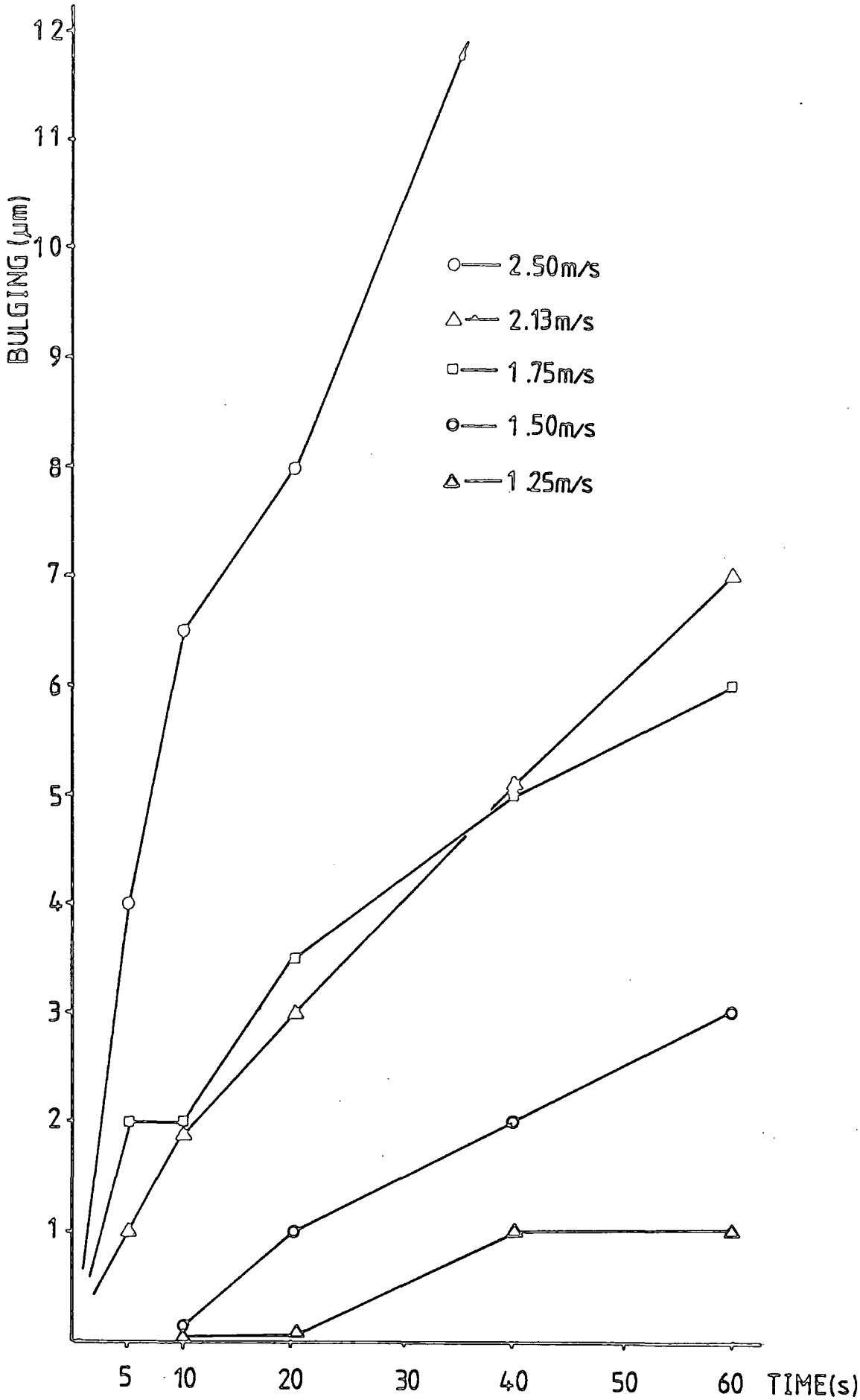

FIGURE 6.31, BULGING Vs TIME, GRADE-TTA, FEED=0.40mm

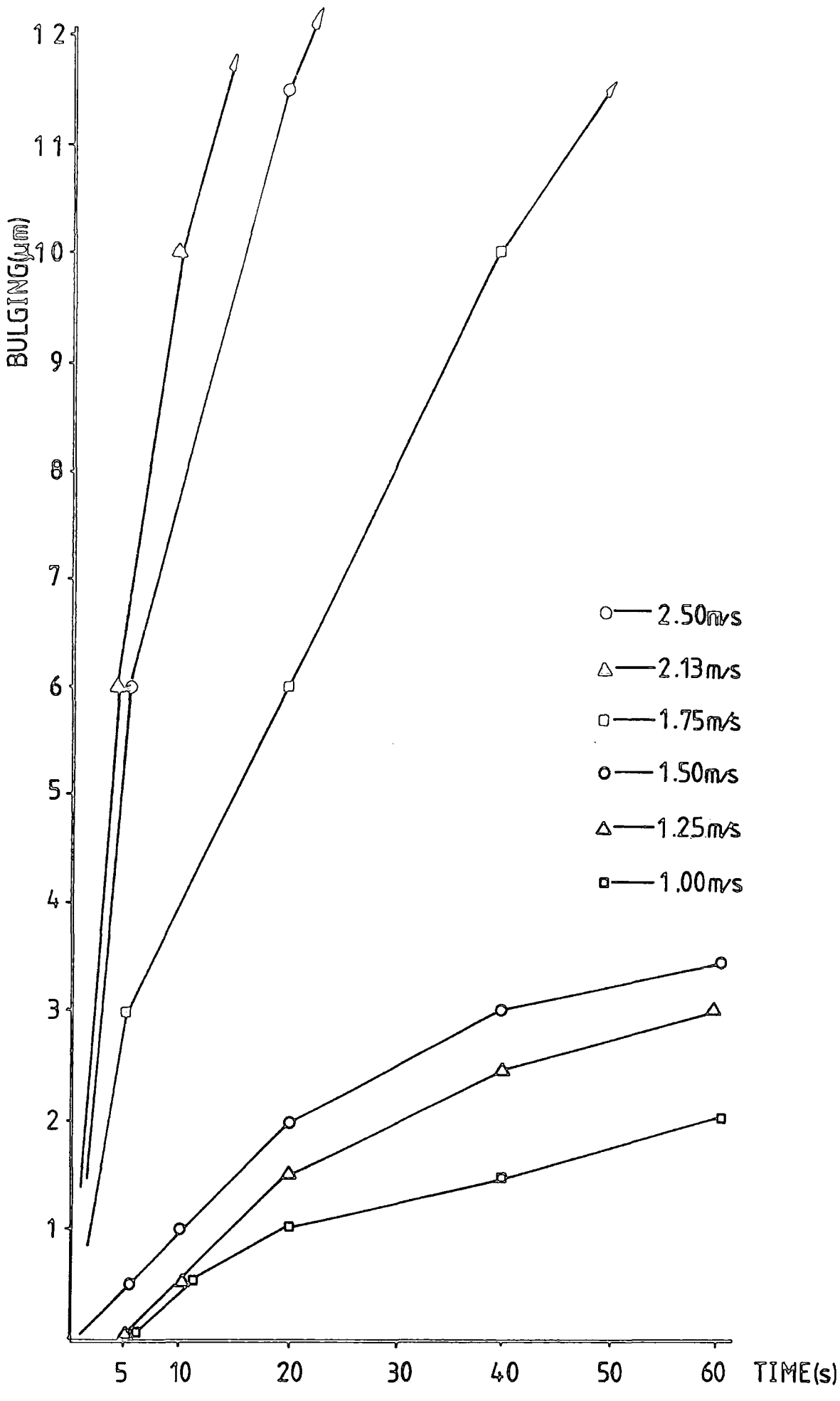

FIGURE 6.32, BULGING Vs TIME, GRADE-TTA, FEED=0.50mm

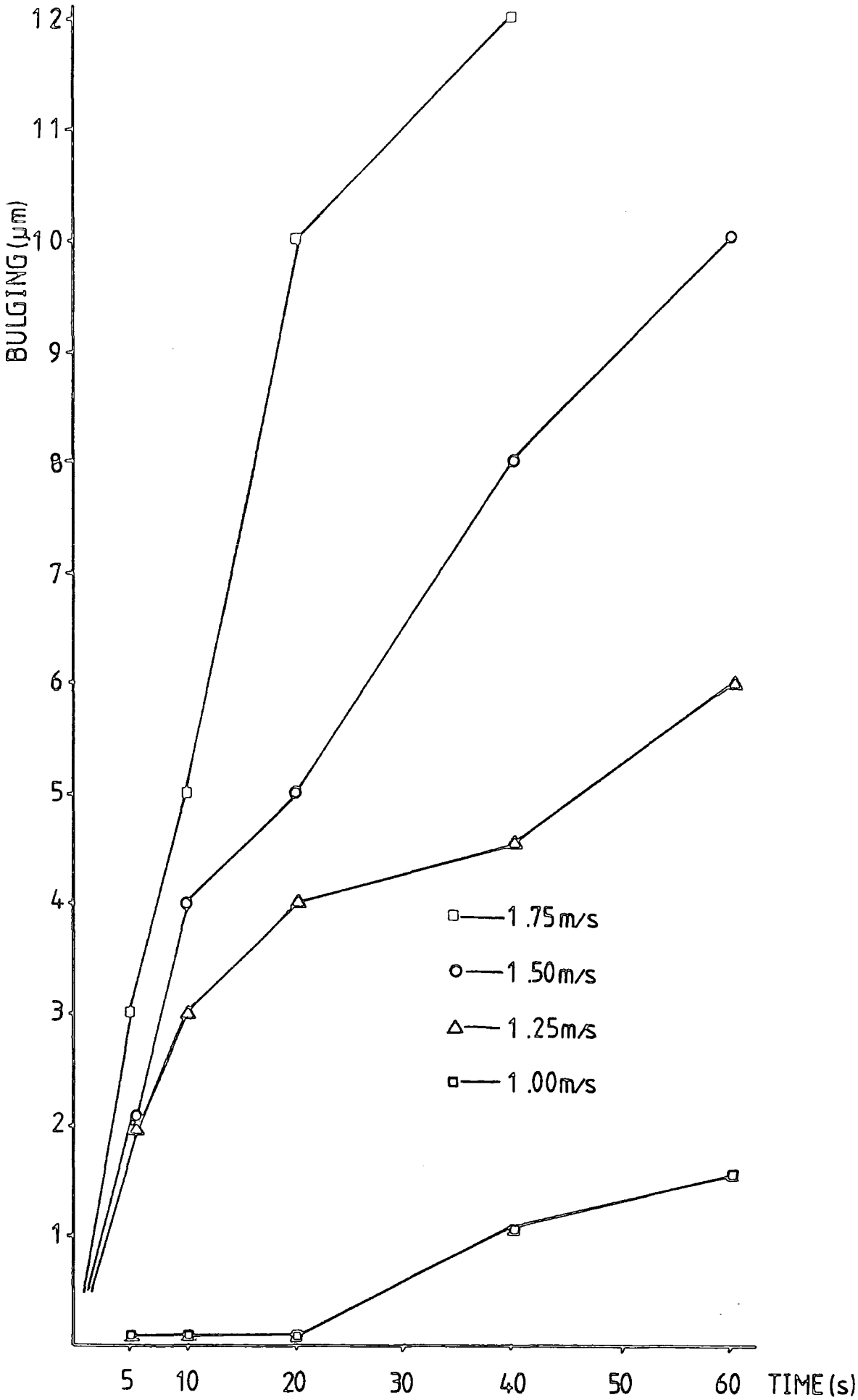

FIGURE 6.33, BULGING Vs TIME, GRADE-TTA, FEED=0.65mm

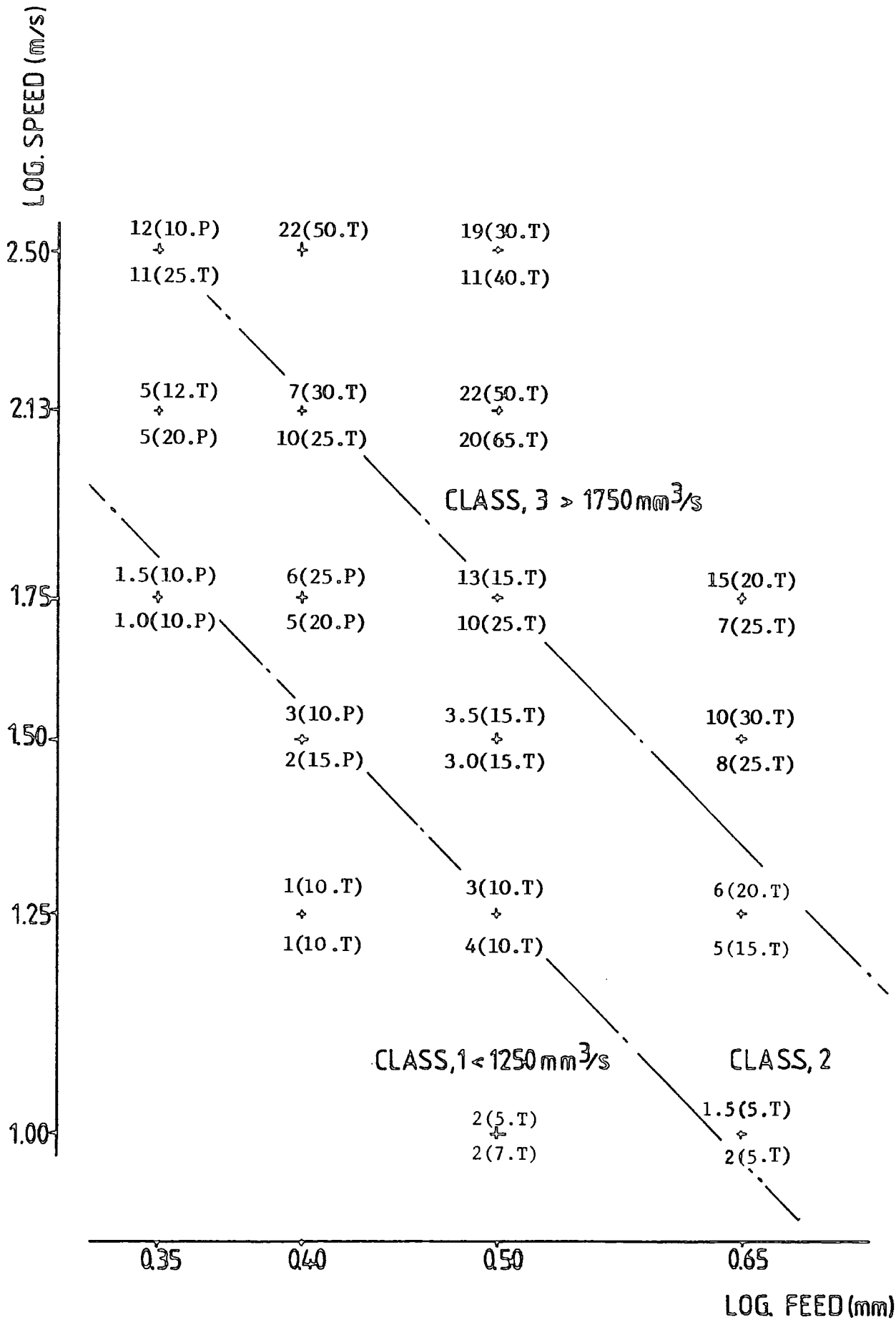

FIGURE 6.34, BULGING AND EDGE DEPRESSION - GRADE - TTA

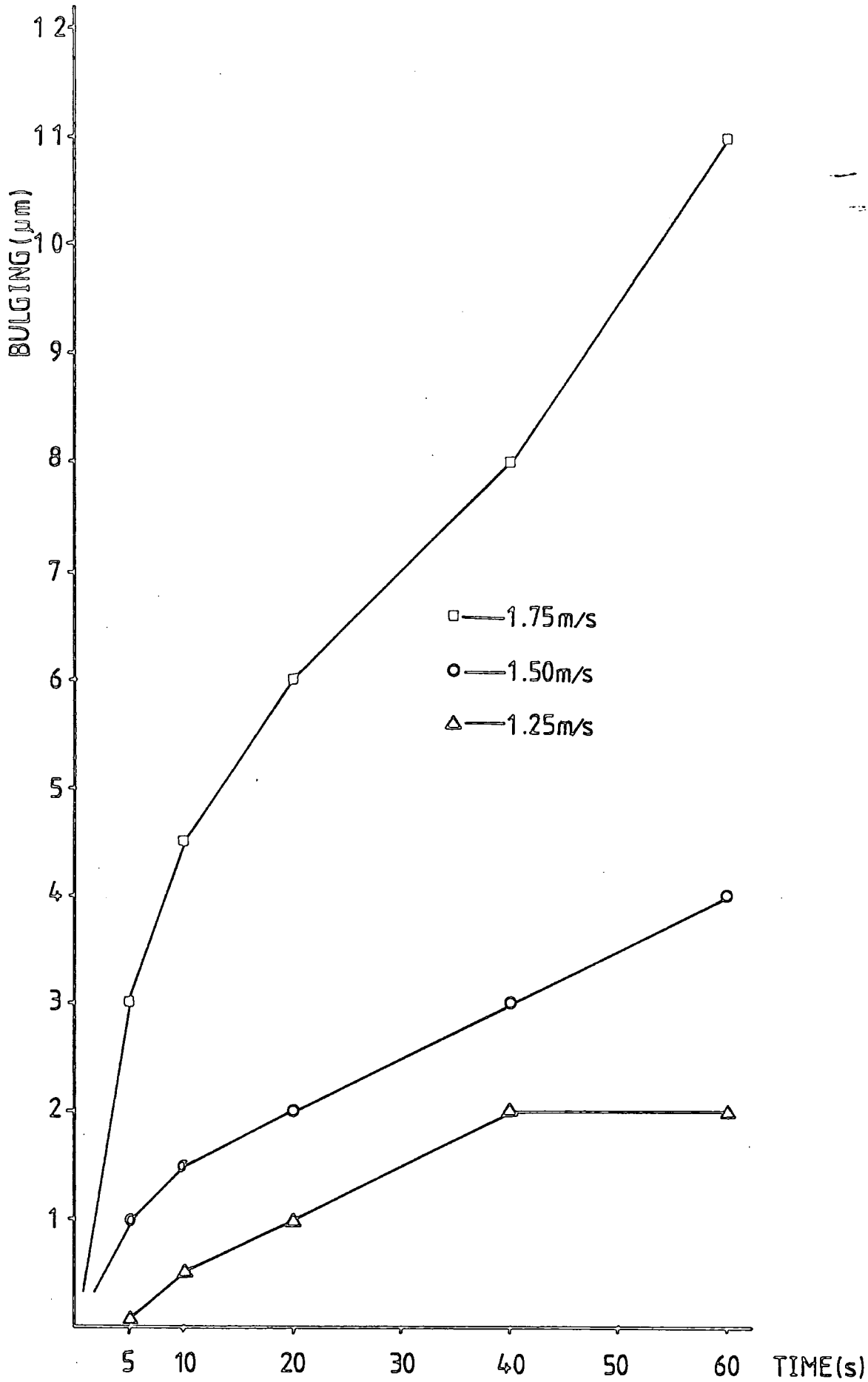

FIGURE 6.35, BULGING Vs TIME, GRADE-TA5, FEED=0.40mm

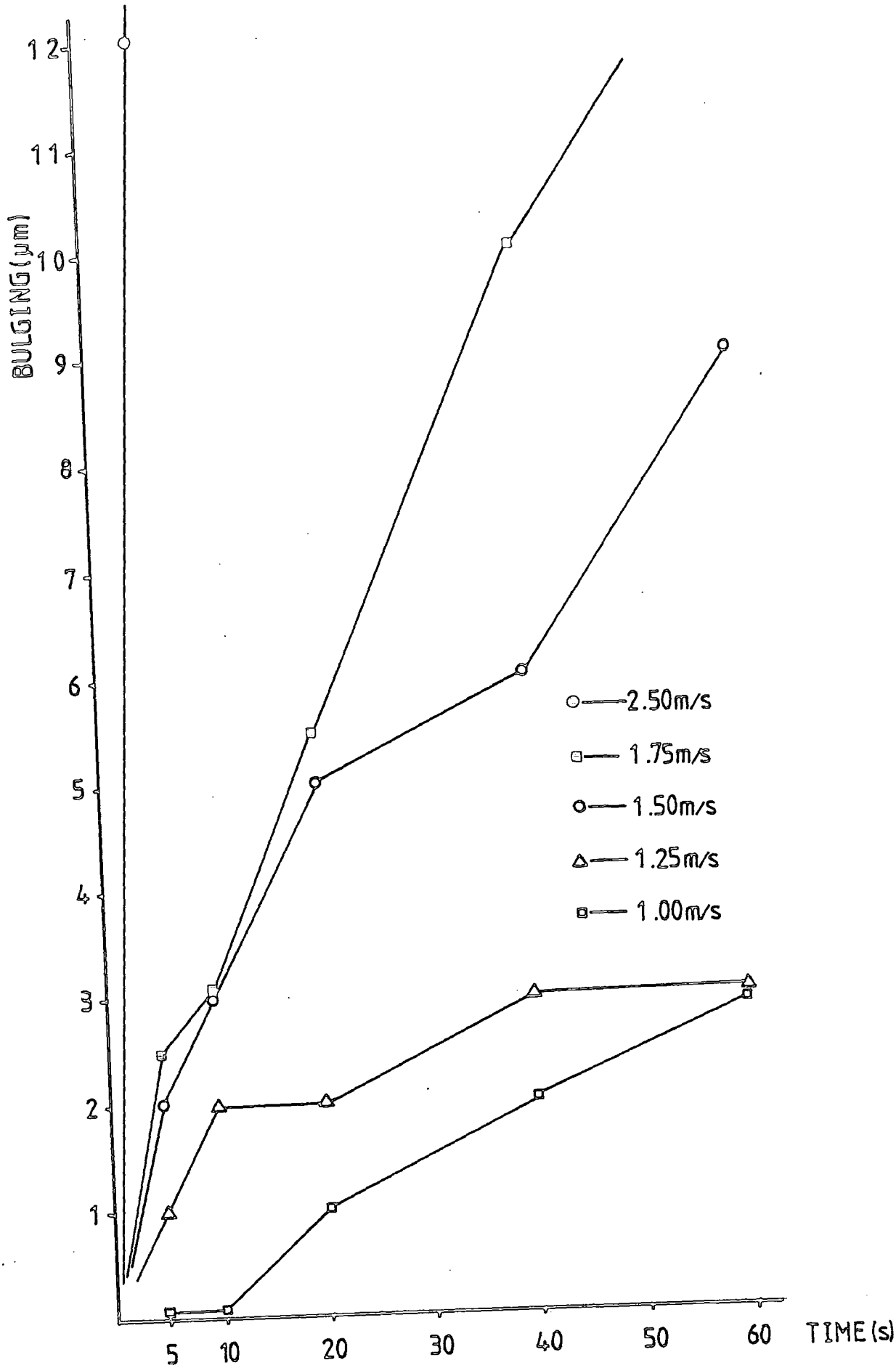

FIGURE 6.36, BULGING Vs TIME, GRADE-TA5, FEED = 0.50mm

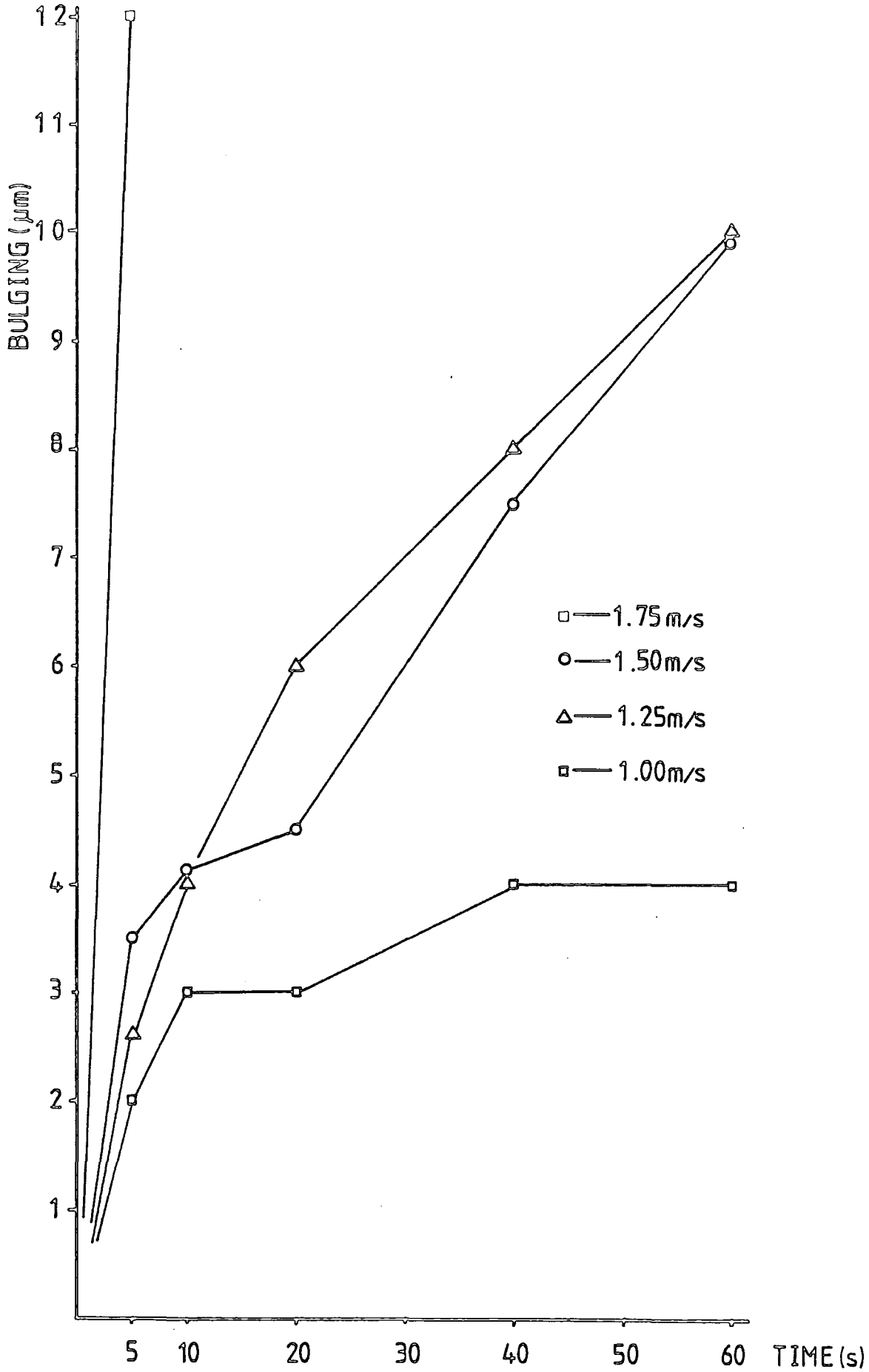

FIGURE 6.37, BULGING Vs TIME, GRADE-TA5, FEED = 0.65mm

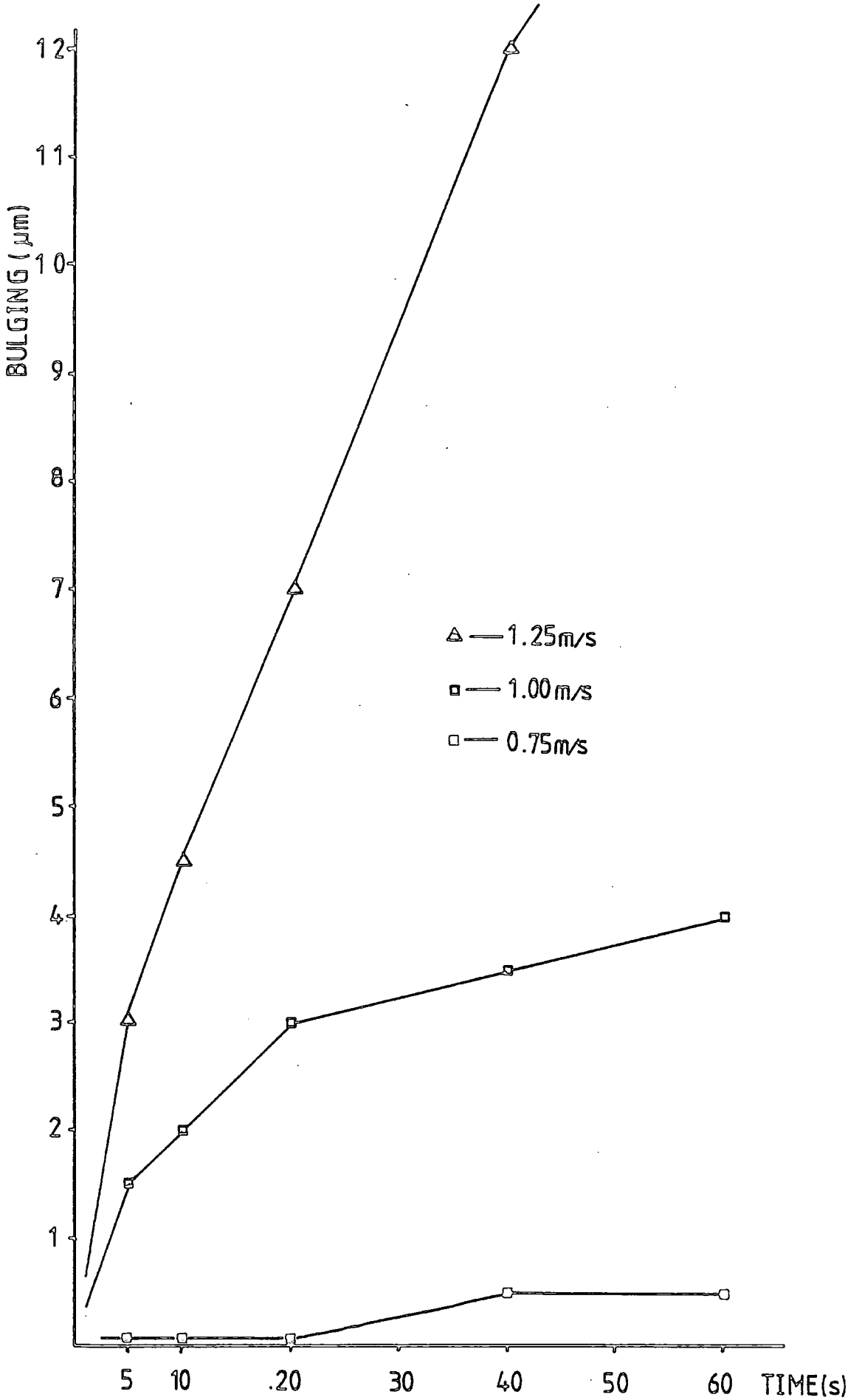

FIGURE 6.38, BULGING Vs TIME, GRADE-TA5, FEED=0.80mm

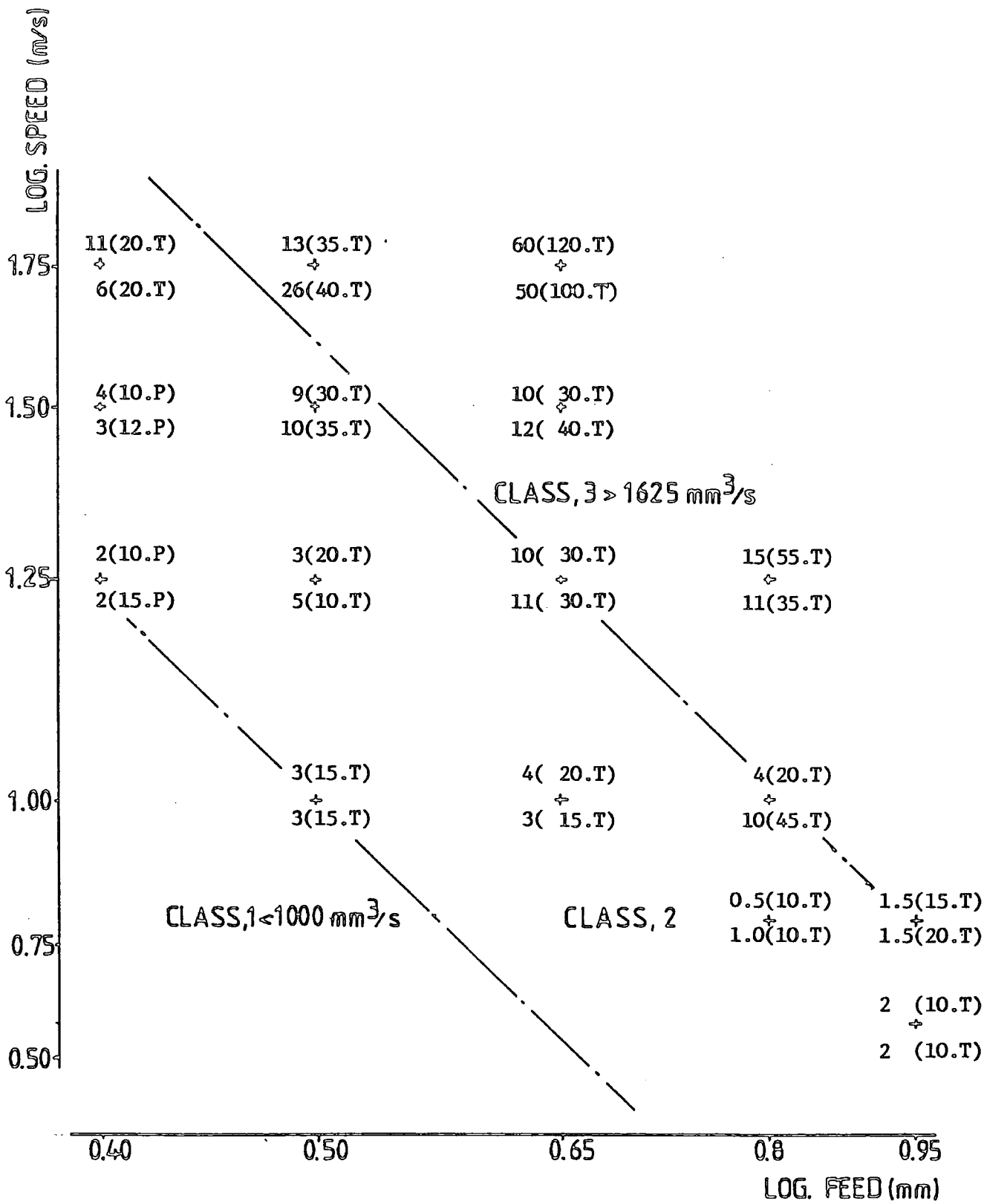

FIGURE 6.39 BULGING AND EDGE DEPRESSION - GRADE - TAS.

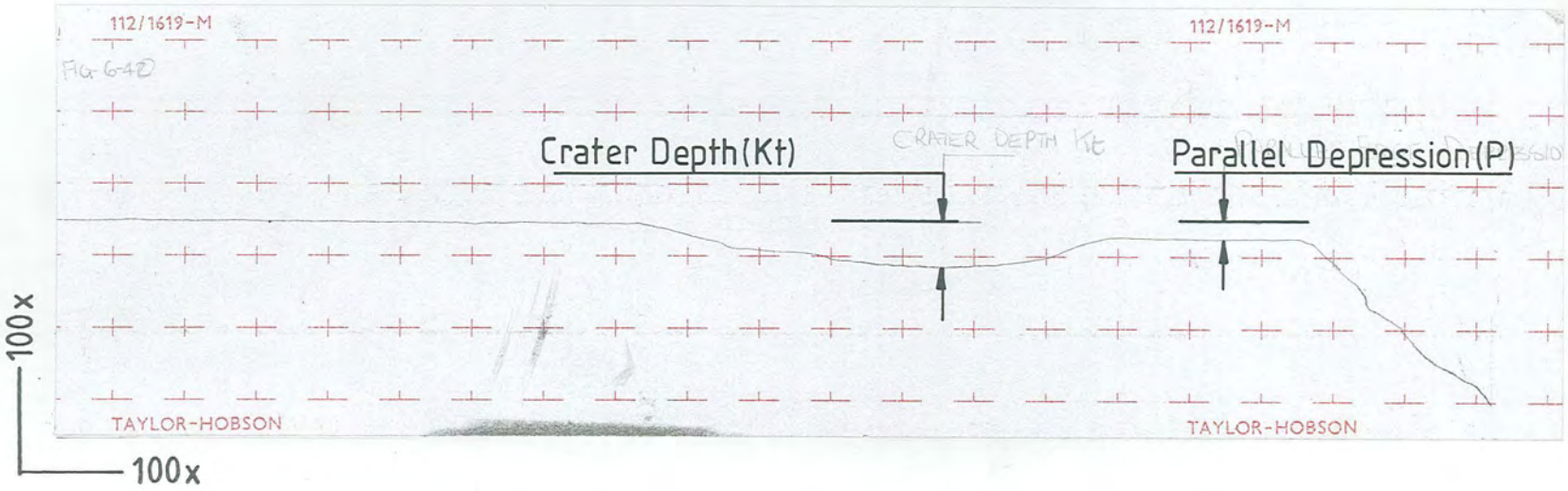

FIGURE 6.40, PARALLEL EDGE DEPRESSION

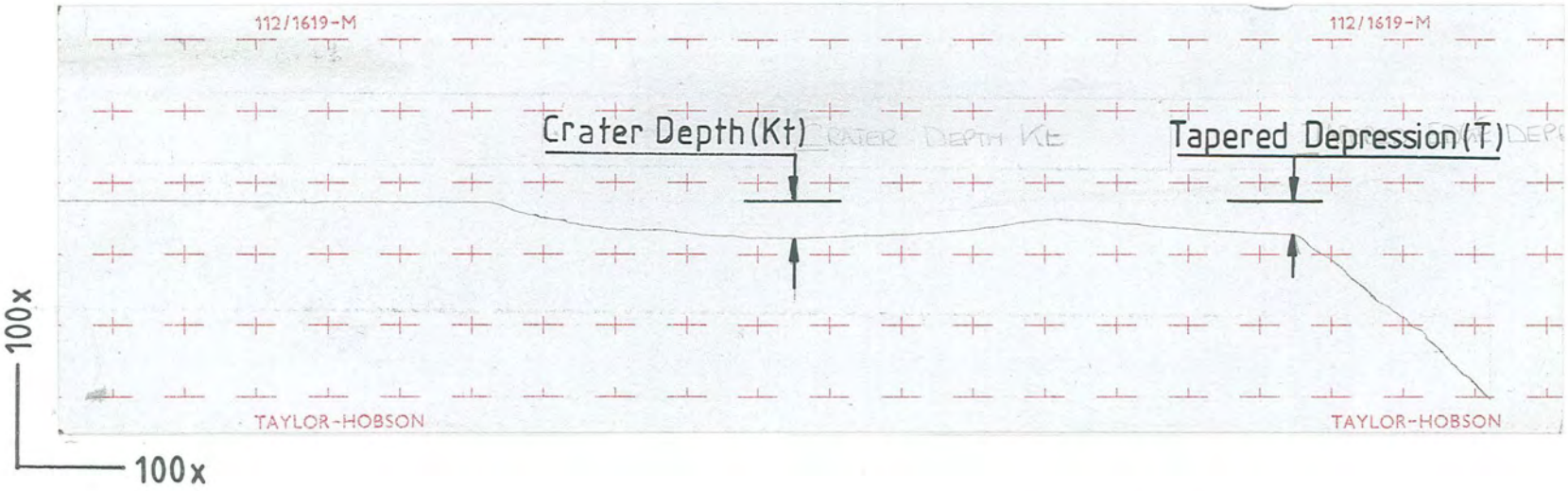

FIGURE 6.41, TAPERED EDGE DEPRESSION

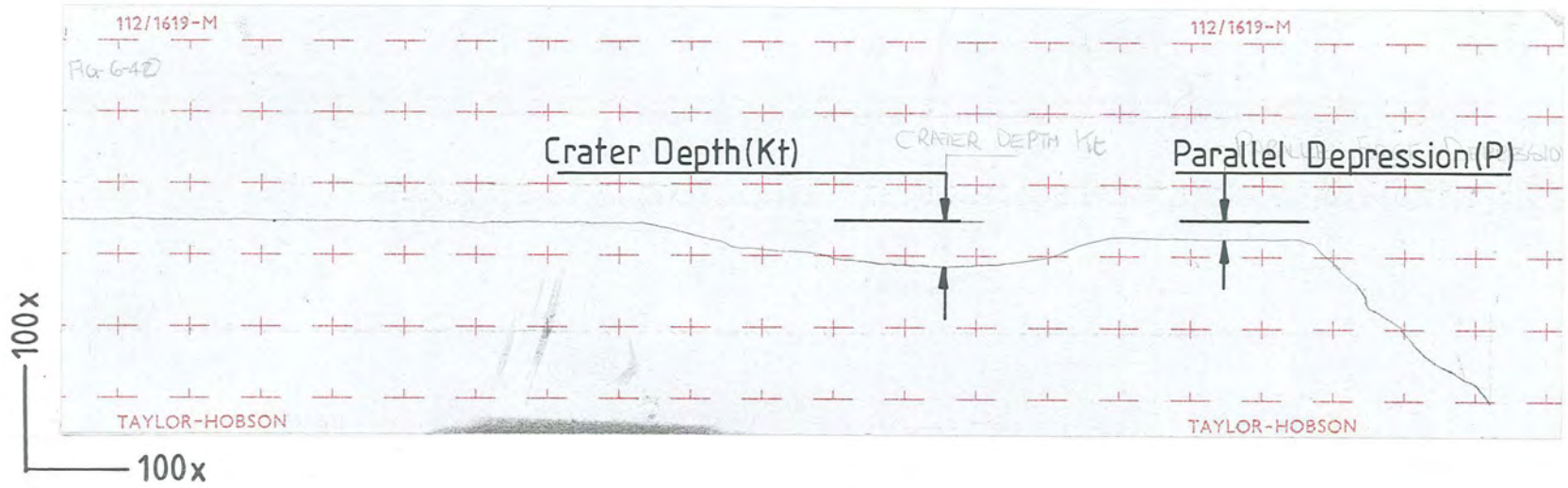

FIGURE 6.40, PARALLEL EDGE DEPRESSION

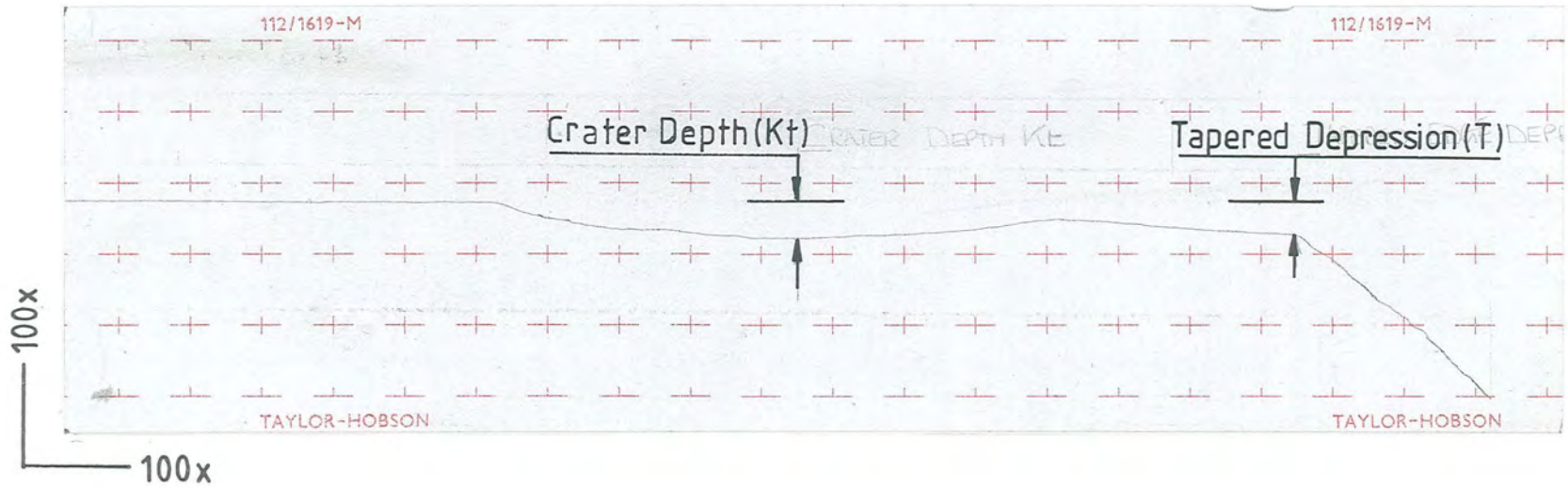

FIGURE 6.41, TAPERED EDGE DEPRESSION

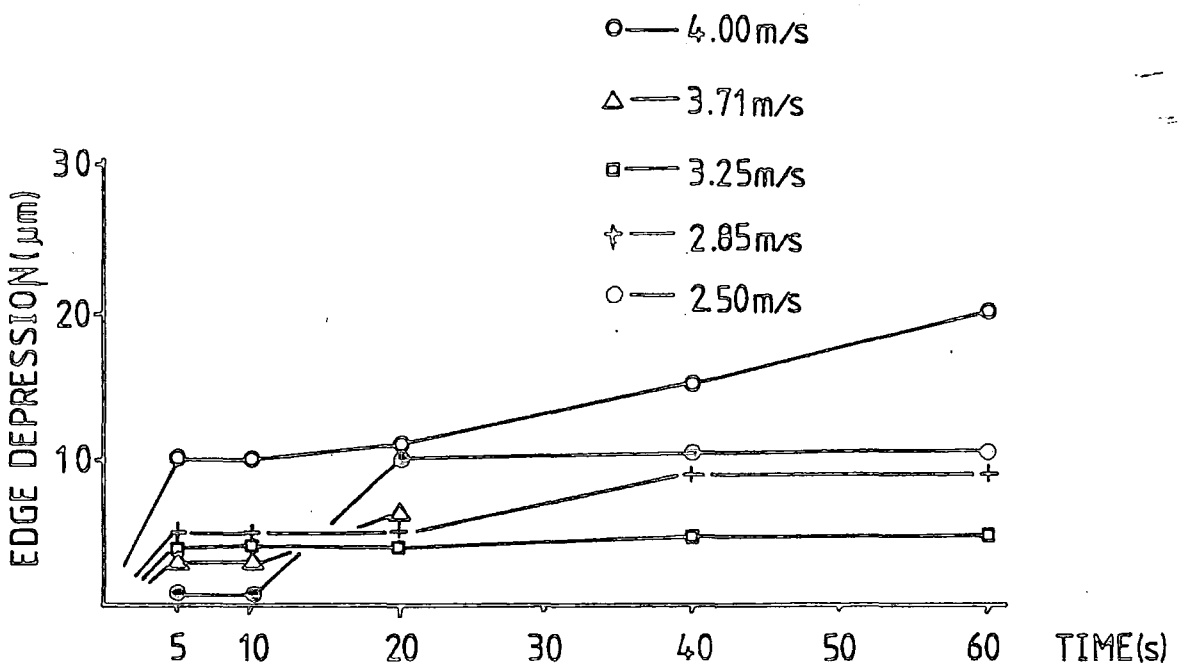

FIGURE 6.42, EDGE DEPRESSION Vs TIME, GRADE-TE, FEED=0.25mm

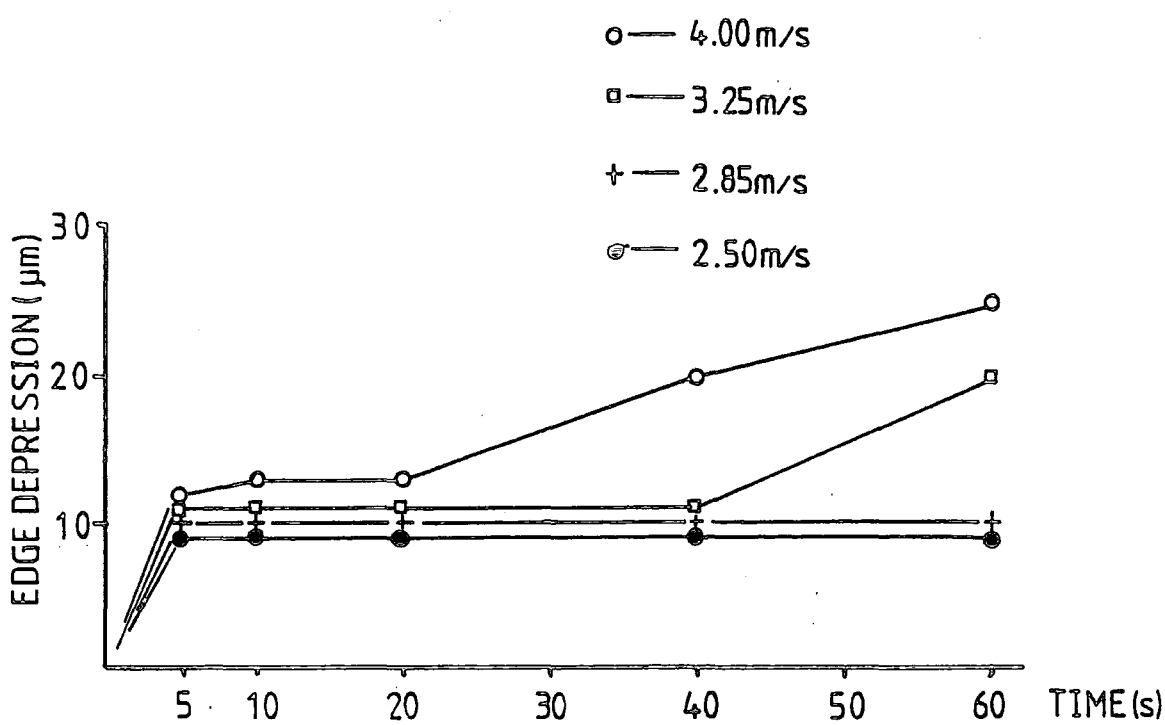

FIGURE 6.43, EDGE DEPRESSION Vs TIME, GRADE-TE, FEED=0.30mm

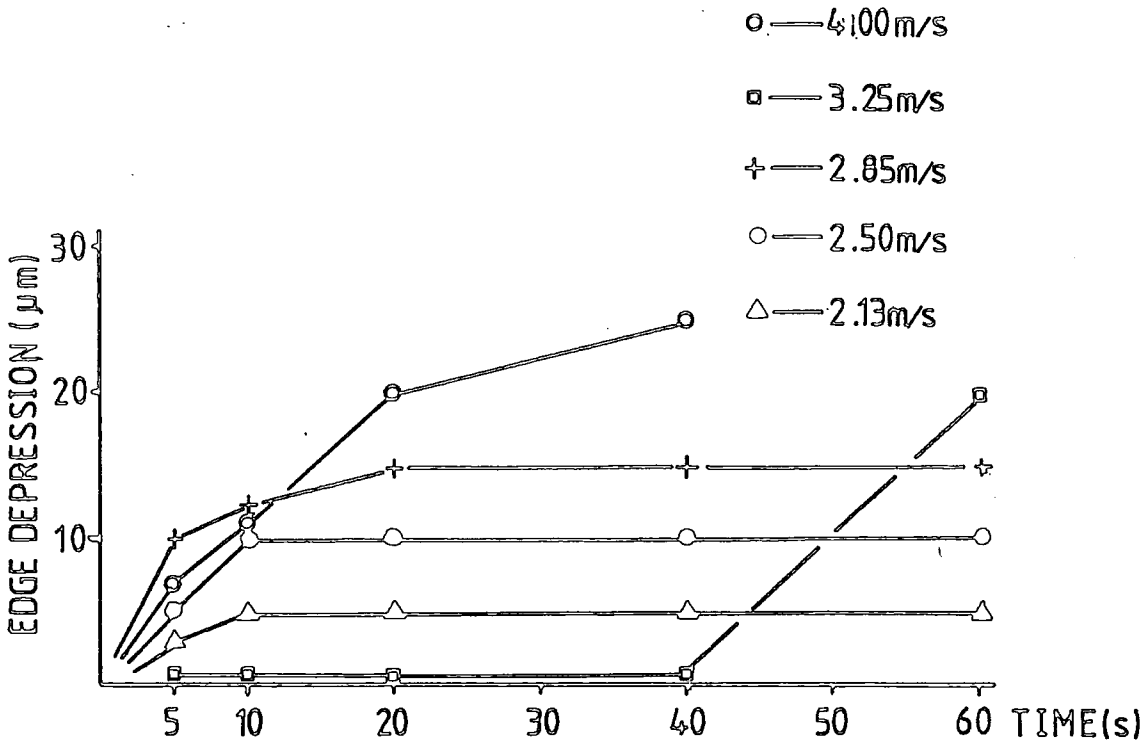

FIGURE 6.44, EDGE DEPRESSION Vs TIME, GRADE-TE, FEED=0.35mm

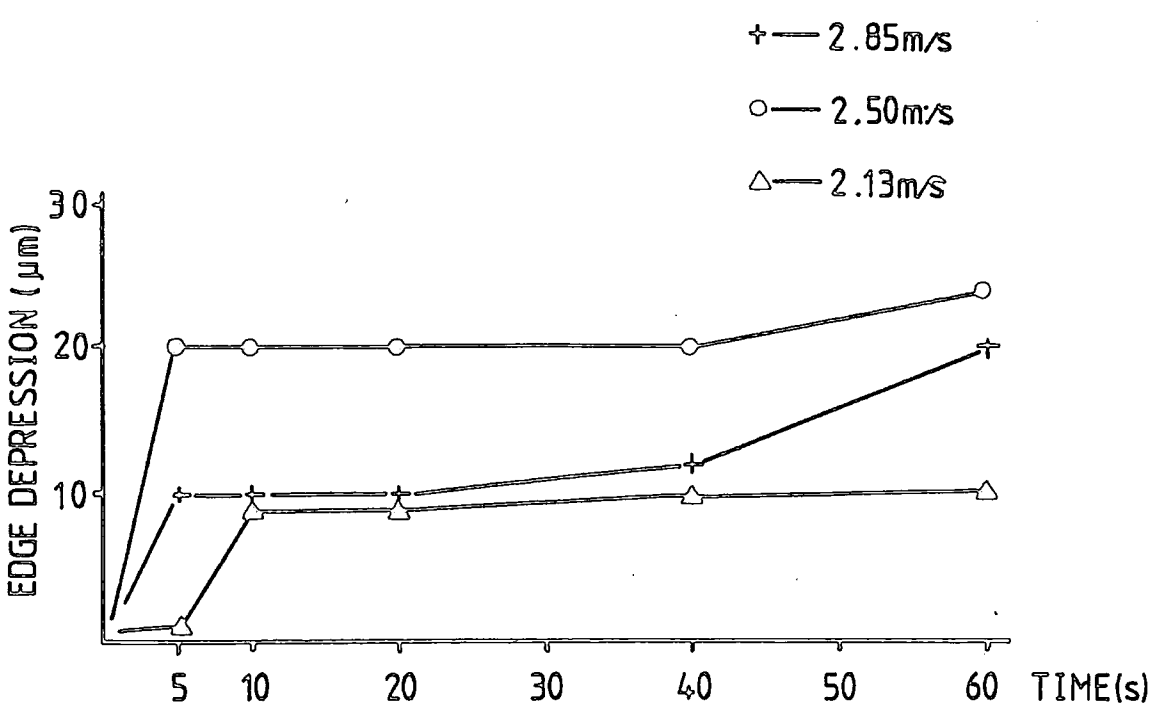

FIGURE 6.45, EDGE DEPRESSION Vs TIME, GRADE-TE, FEED=0.40mm

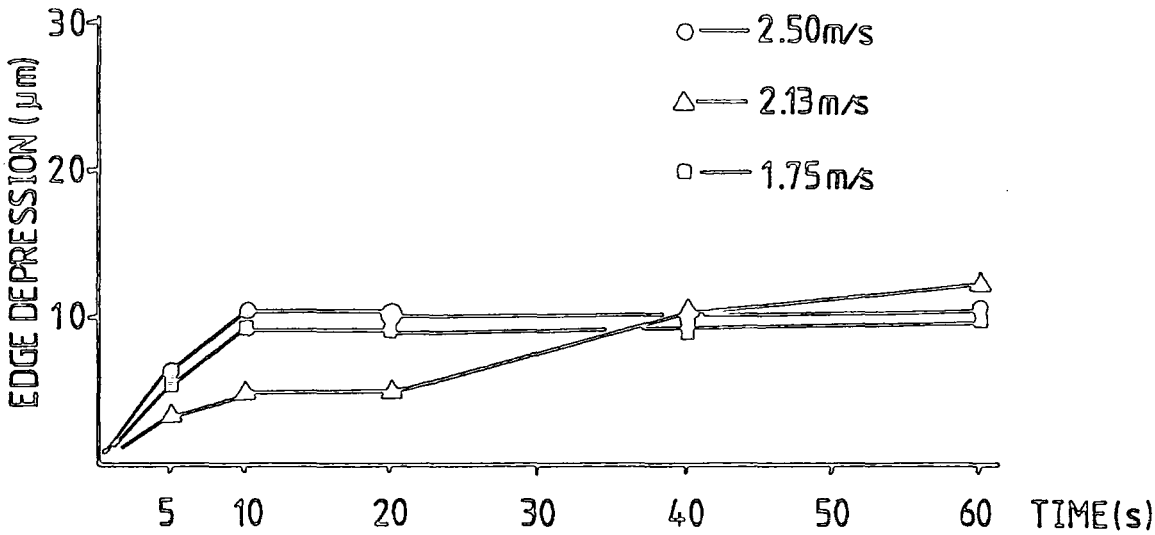

FIGURE 6.46, EDGE DEPRESSION Vs TIME, GRADE-TTA, FEED=0.35mm

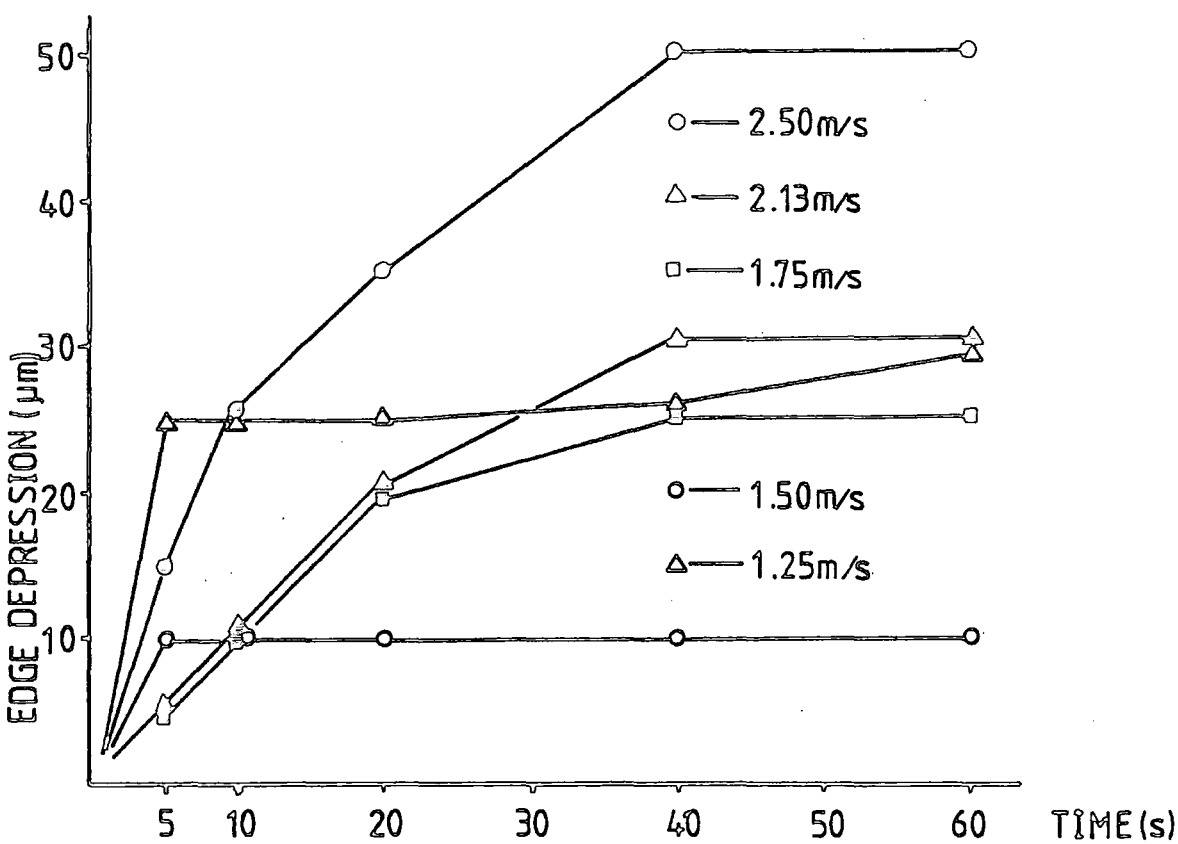

FIGURE 6.47, EDGE DEPRESSION Vs TIME, GRADE-TTA, FEED=0.40mm

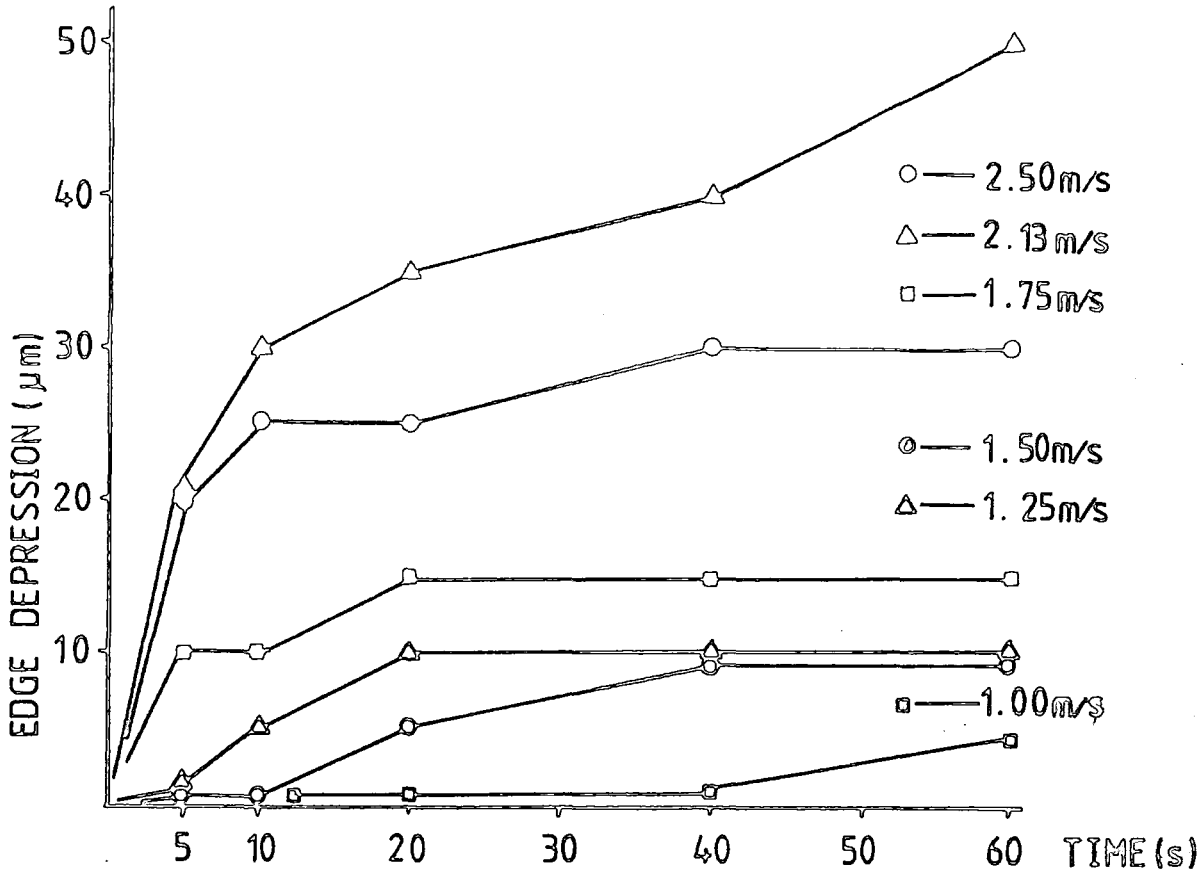

FIGURE 6.48, EDGE DEPRESSION Vs TIME, GRADE-TTA, FEED=0.50mm

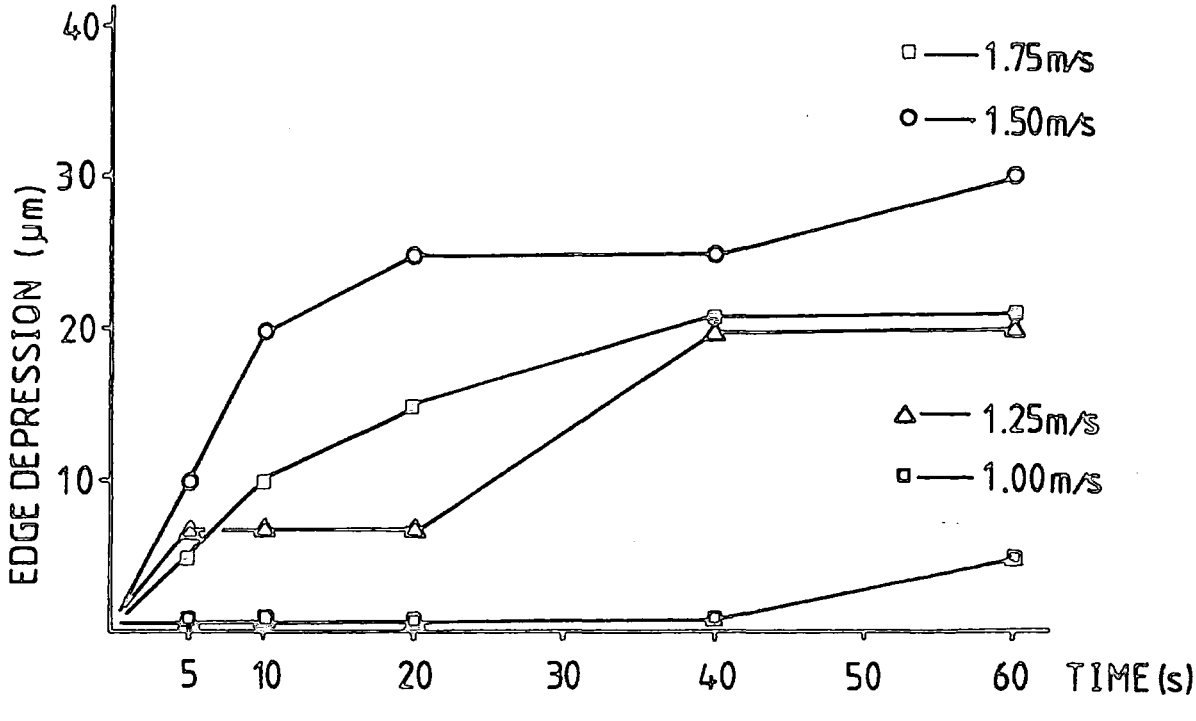

FIGURE 6.49, EDGE DEPRESSION Vs TIME, GRADE-TTA, FEED=0.65mm

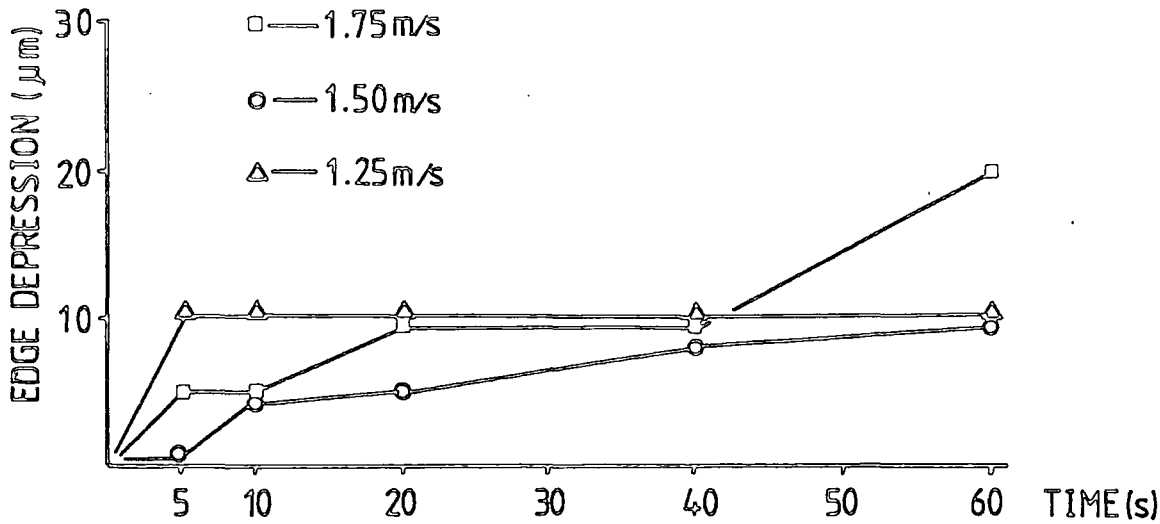

FIGURE 6.50, EDGE DEPRESSION Vs TIME, GRADE-TA5, FEED=0.40mm

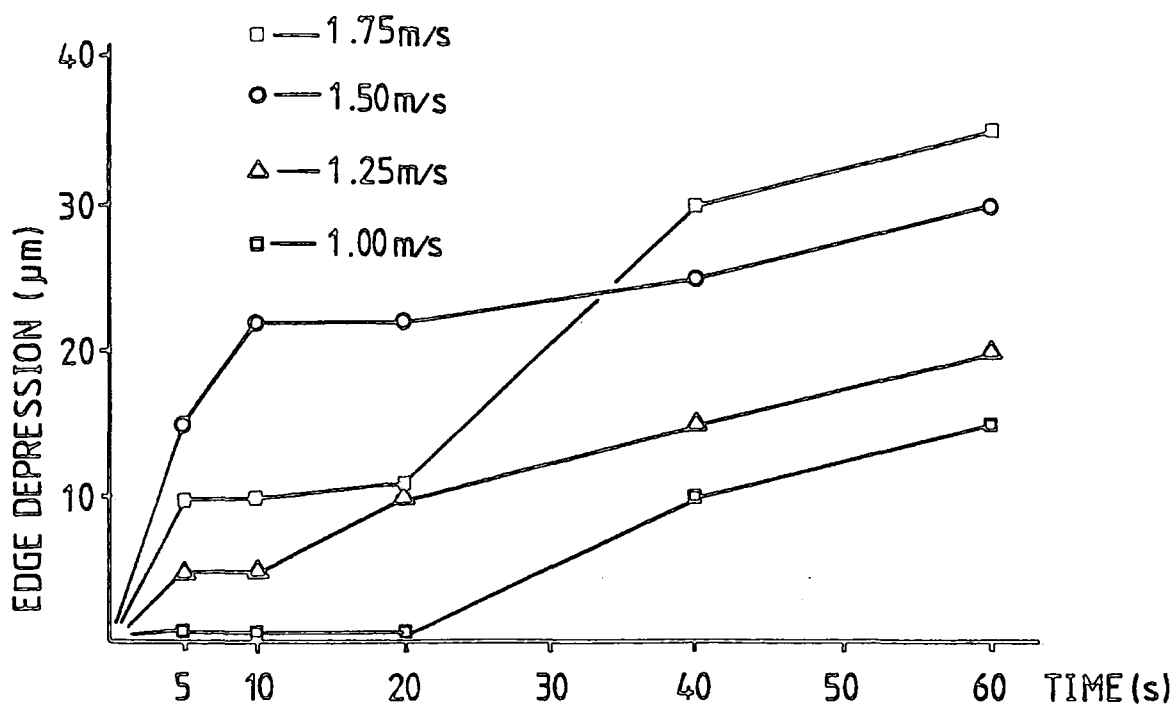

FIGURE 6.51, EDGE DEPRESSION Vs TIME, GRADE-TA5, FEED=0.50mm

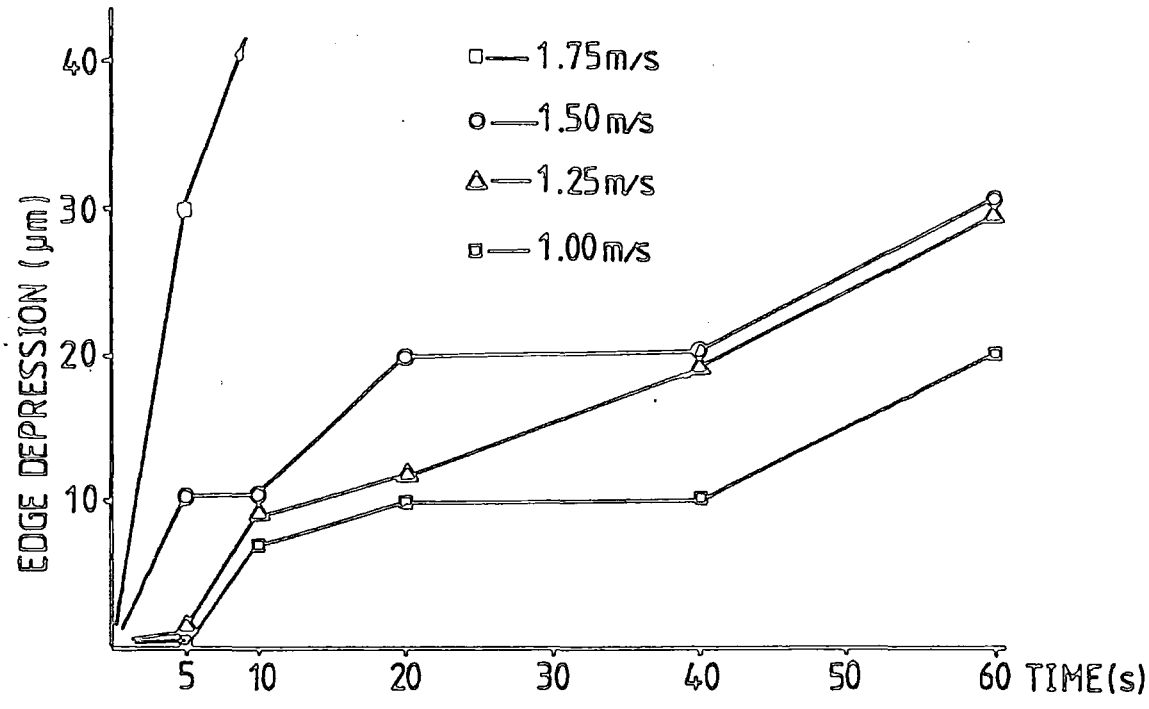

FIGURE 6.52, EDGE DEPRESSION Vs TIME, GRADE-TA5, FEED=0.65mm

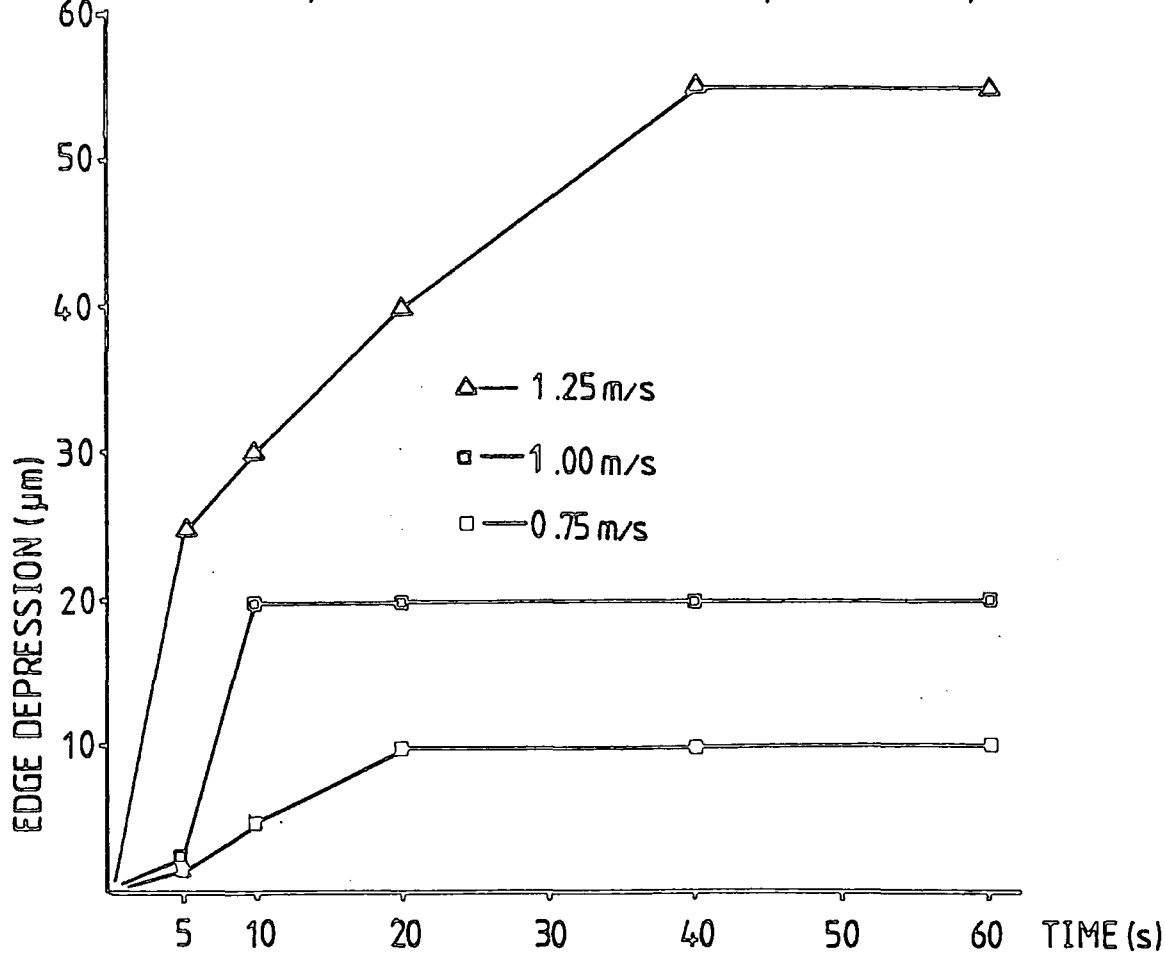

FIGURE 6.53, EDGE DEPRESSION Vs TIME, GRADE-TA5, FEED=0.80mm

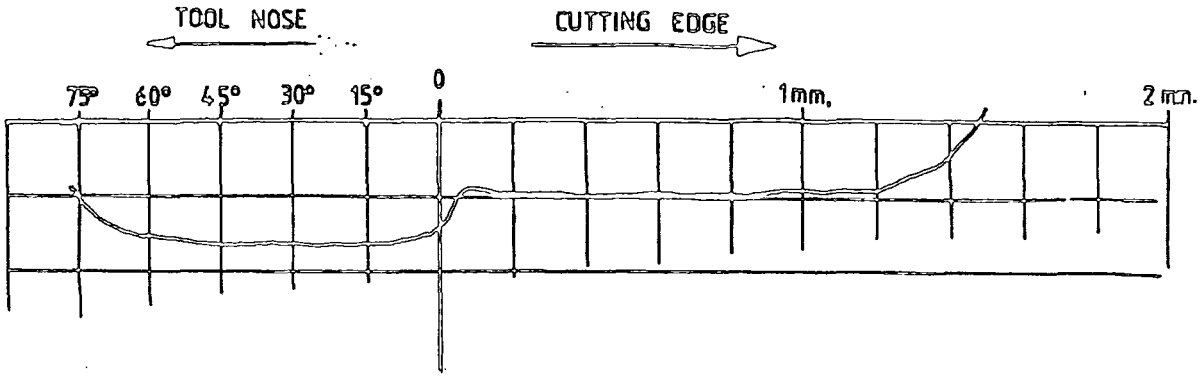

TOOL NOSE (No)

WEAR TYPE "E" BELOW TOOL NOSE

TOOL FLANK (F?)

WEAR TYPE "E" BELOW CUTTING EDGE

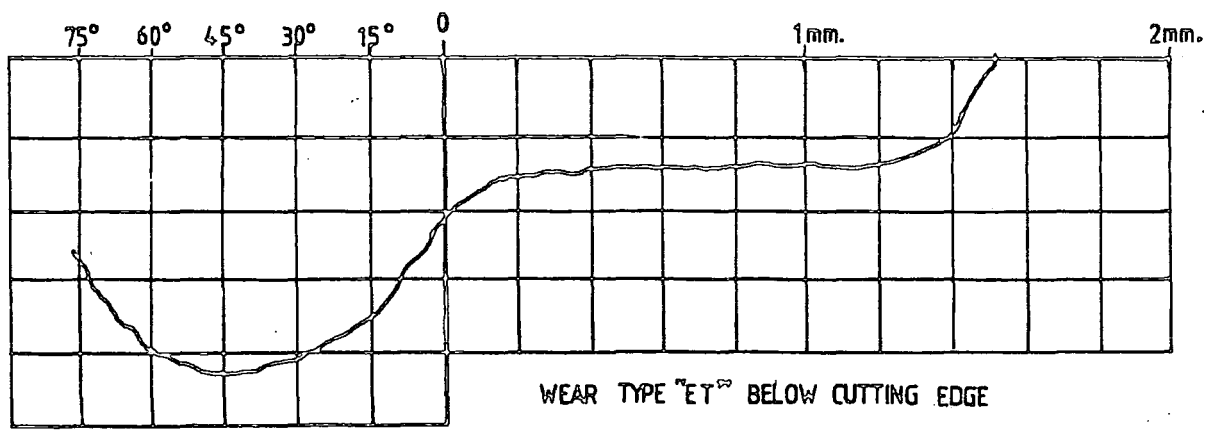

WEAR TYPE "ET" BELOW CUTTING EDGE

WEAR TYPE "45°" BELOW TOOL NOSE

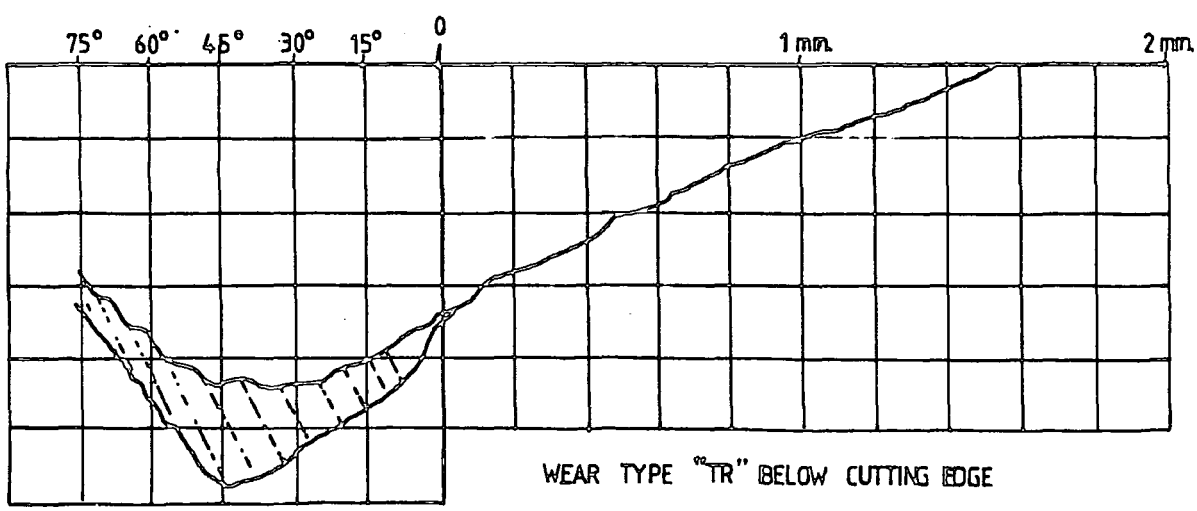

WEAR TYPE "TR" BELOW CUTTING EDGE

WEAR TYPE "R" BELOW NOSE

FIGURE 6.54, WEAR PATTERNS ON CLEARANCE FACES.

FIGURE 6.55, WEAR TYPE "2" BELOW NOSE.

FIGURE 6.56, WEAR TYPE "E" BELOW NOSE AND EDGE.

FIGURE 6.57, WEAR TYPE "E" BELOW NOSE ONLY.

FIGURE 6.58, WEAR TYPES "45" AND "TR".

FIGURE 6.59, WEAR TYPE "E" BELOW NOSE AND EDGE.

FIGURE 6.60, WEAR TYPE "E" BELOW NOSE ONLY.

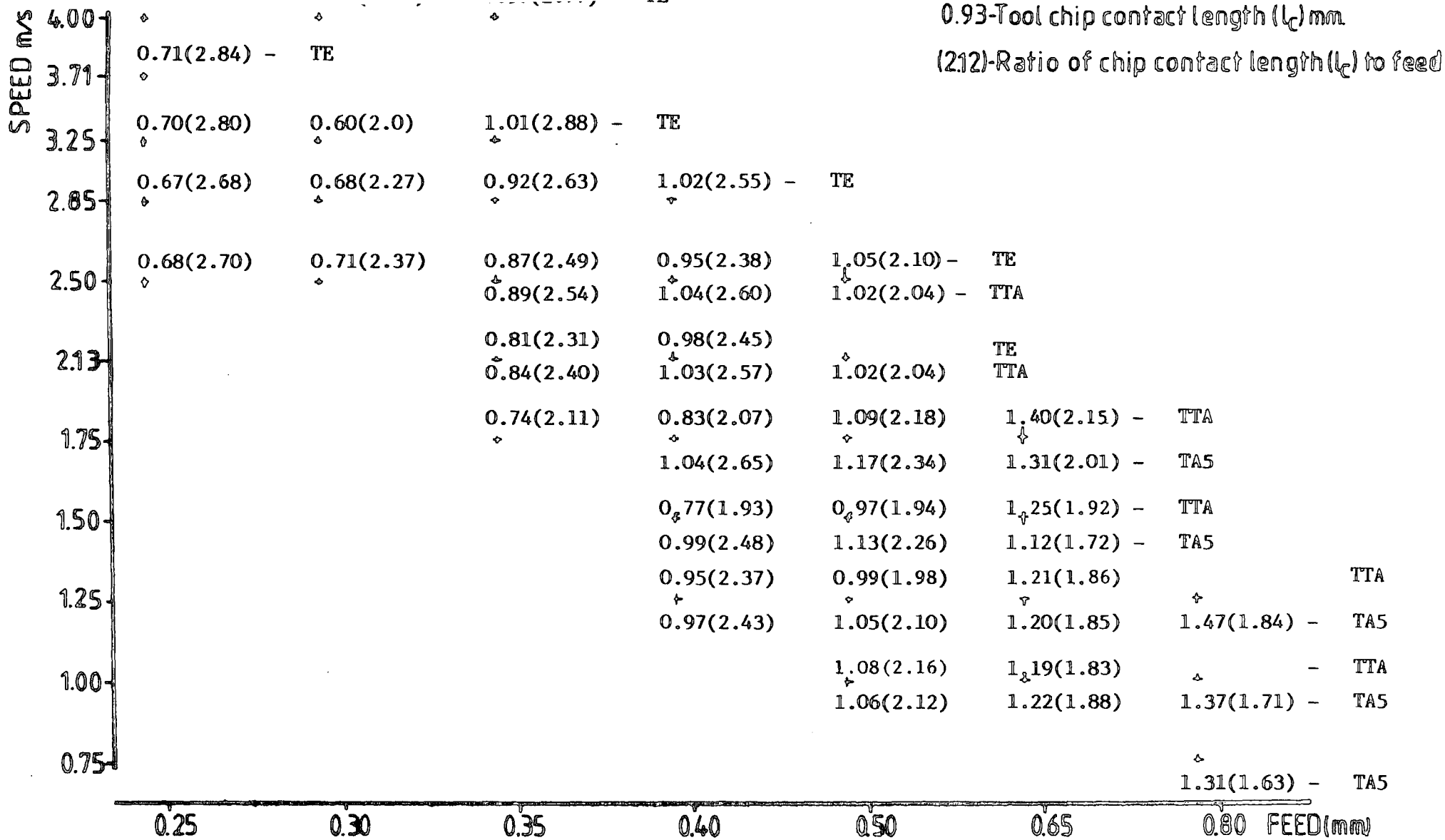

FIGURE 6.61, TOOL/CHIP CONTACT LENGTHS FOR DIFFERENT GRADES, SPEEDS AND FEEDS.

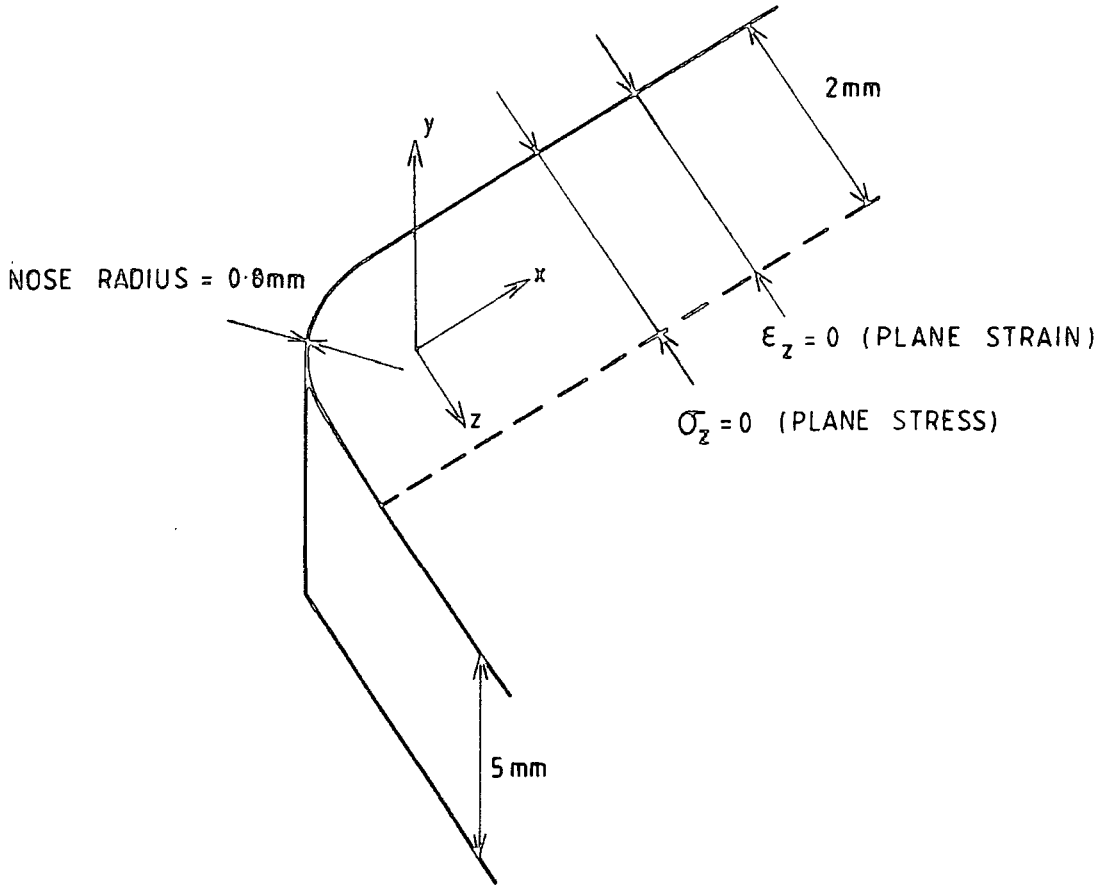

(a) CO-ORDINATE AXES

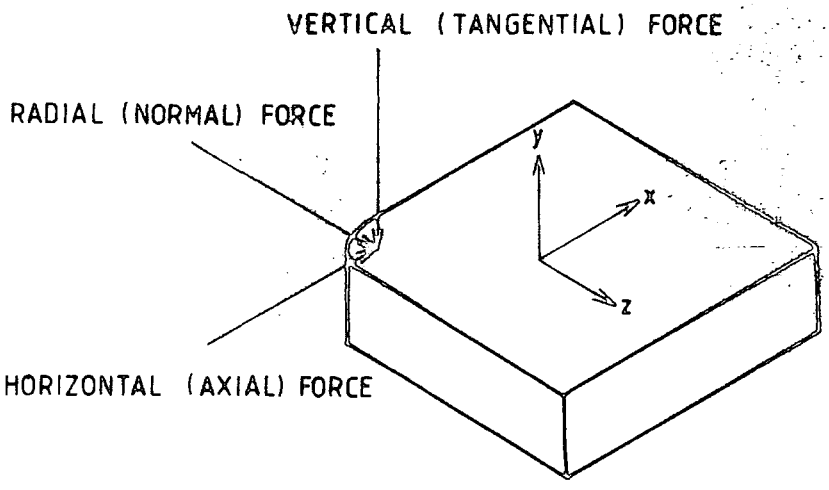

(b) FORCES ON TOOL

FIGURE 7·1 3-D VIEW OF CUTTING TOOL

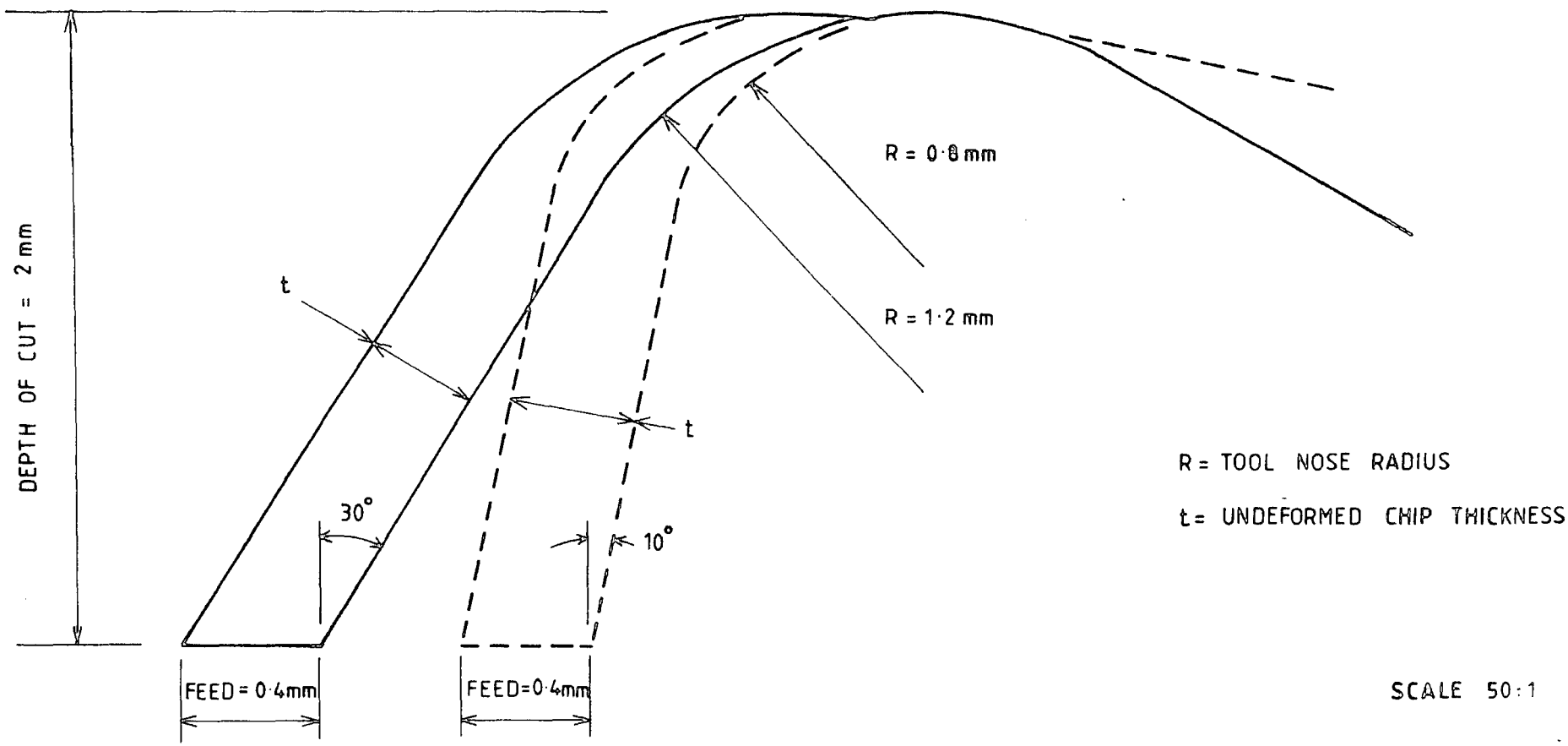

FIGURE 7·2 INFLUENCE OF NOSE RADIUS AND PLAN APPROACH ANGLE ON UNDEFORMED CHIP THICKNESS

TITLE TEMPERATURE MODEL TYPE 1 PAFBLOCK TRANTEMP3A TRANIA

PAFEC

VIEW FROM X = 0.0000
Y = 0.0000
Z = 1.000

X

Z TOWARDS VIEWER

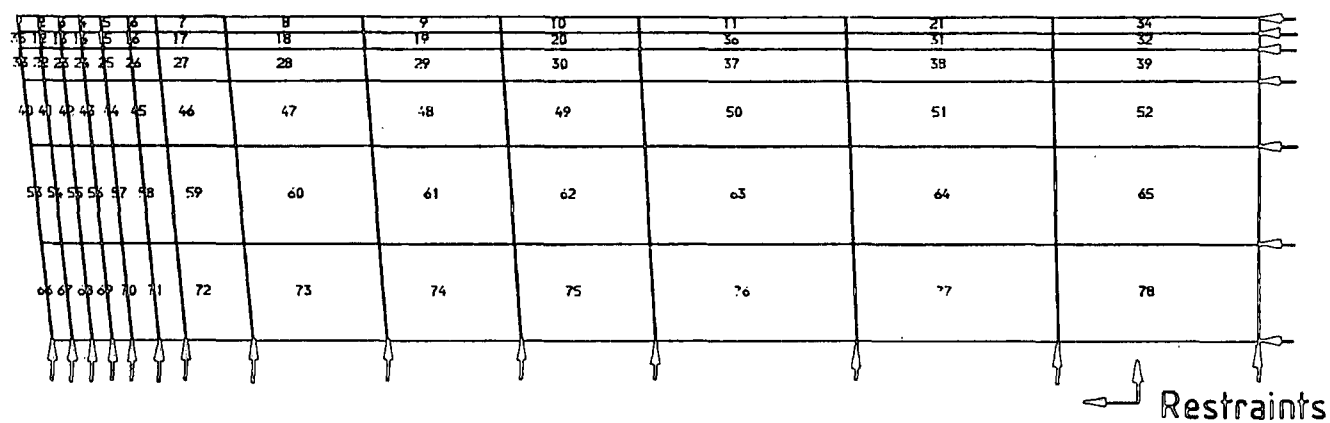

FIGURE 7.3, F.E. MODEL OF CUTTING TOOL.

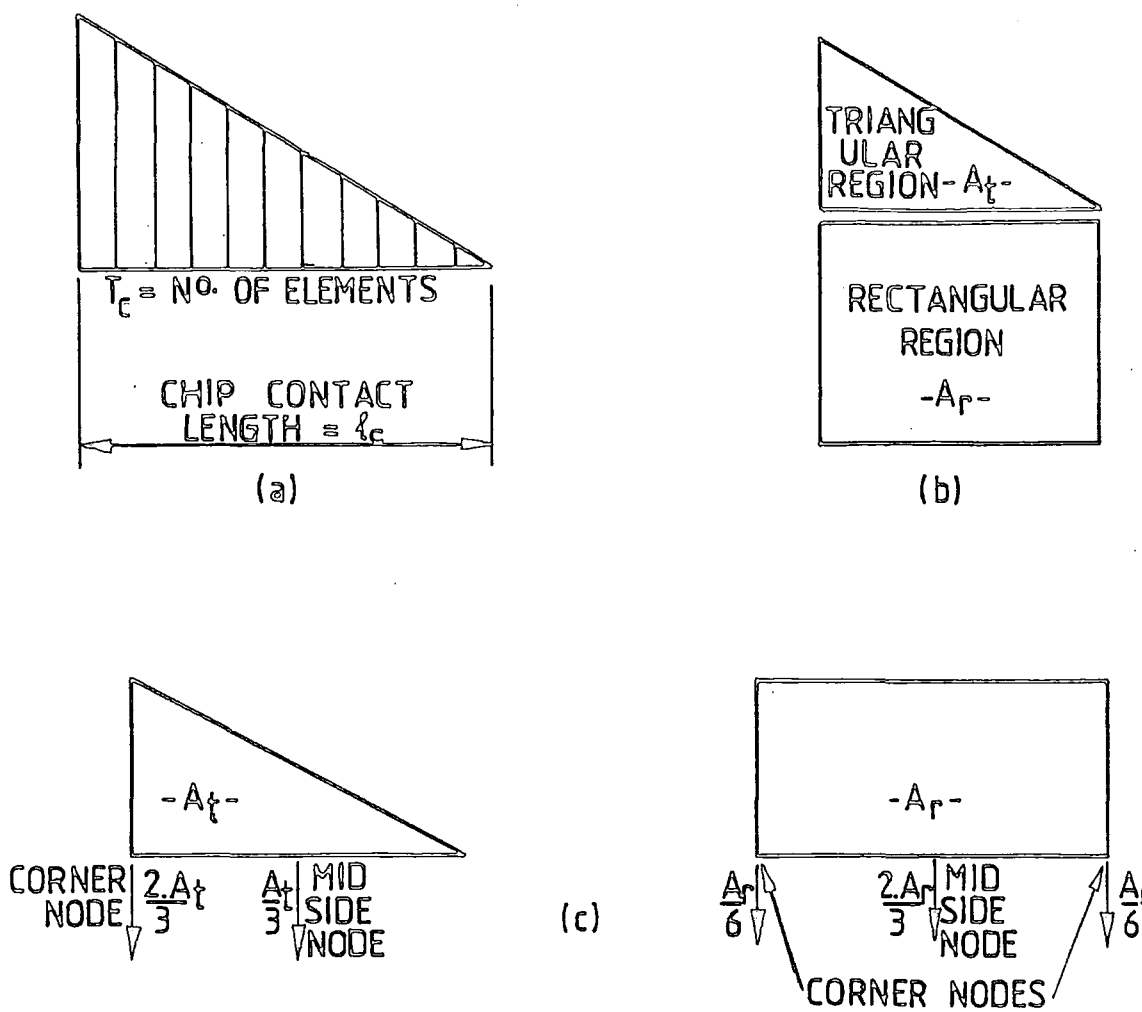

FIGURE 7.4, LINEARLY DECREASING FORCE DISTRIBUTION.

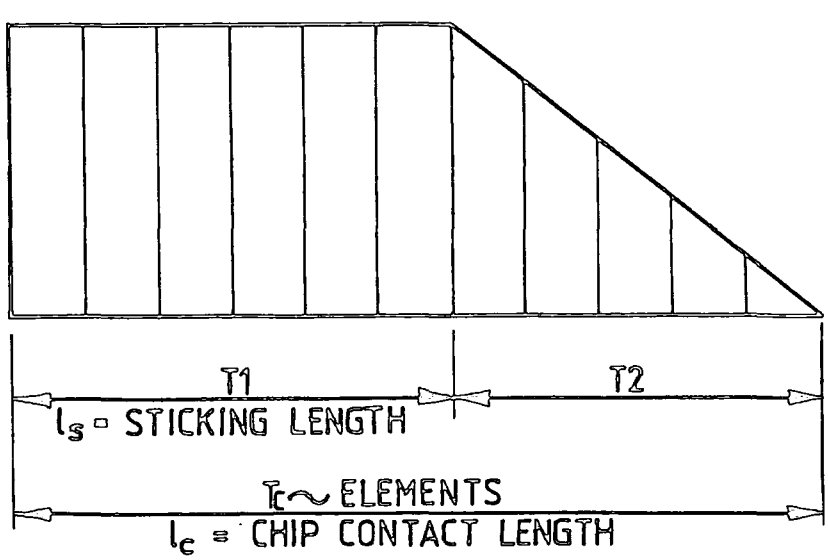

FIGURE 7.5, AXIAL FORCE DISTRIBUTION.

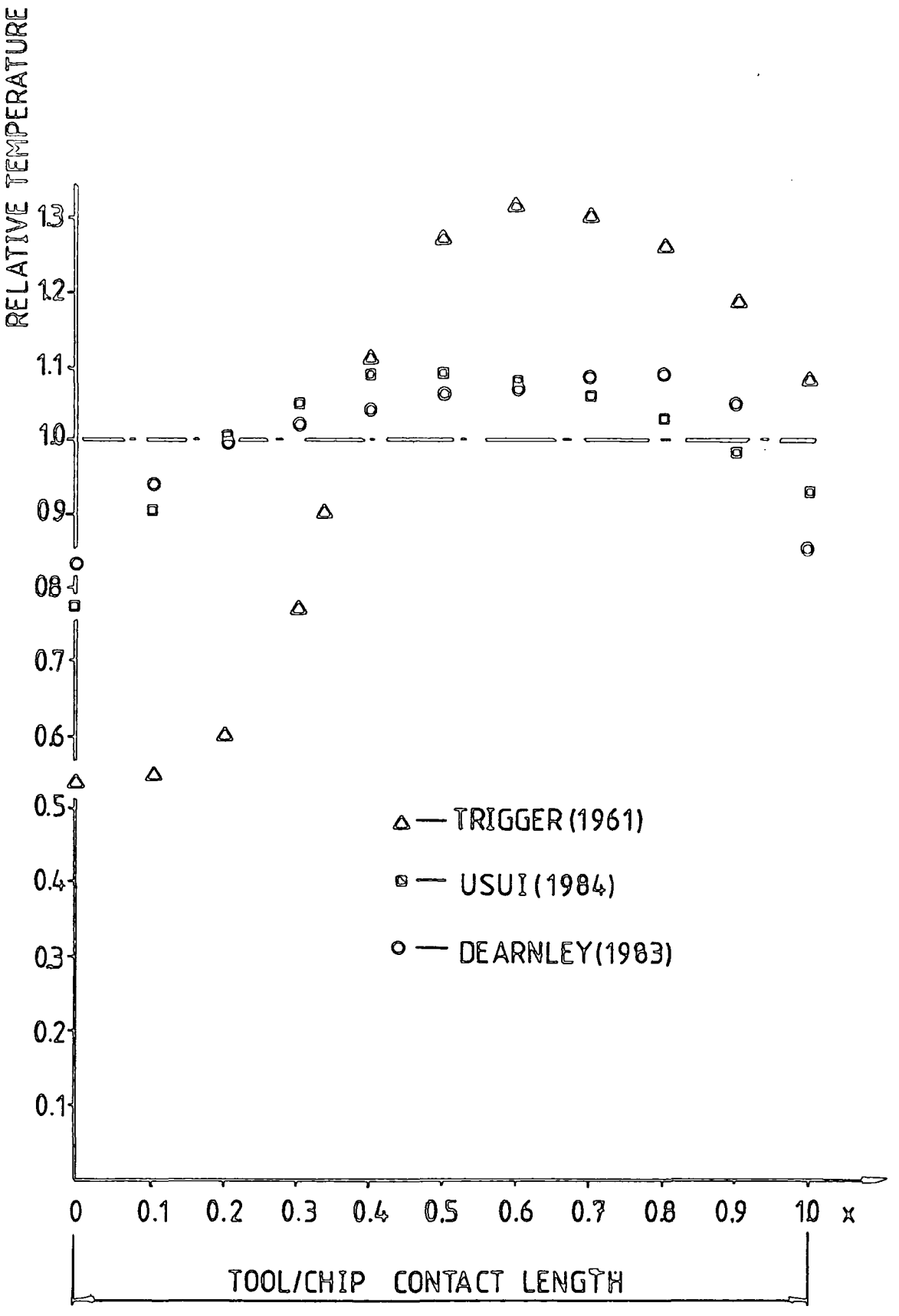

FIGURE 7.6, RELATIVE TOOL/CHIP TEMPERATURE DISTRIBUTIONS.

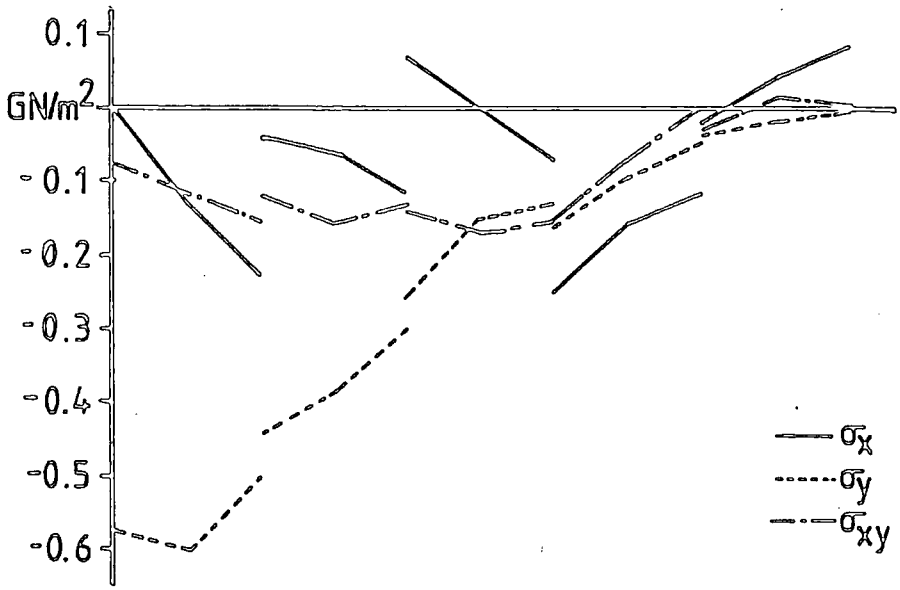

FIGURE 7.7, MECHANICAL STRESSES ON THE RAKE FACE.

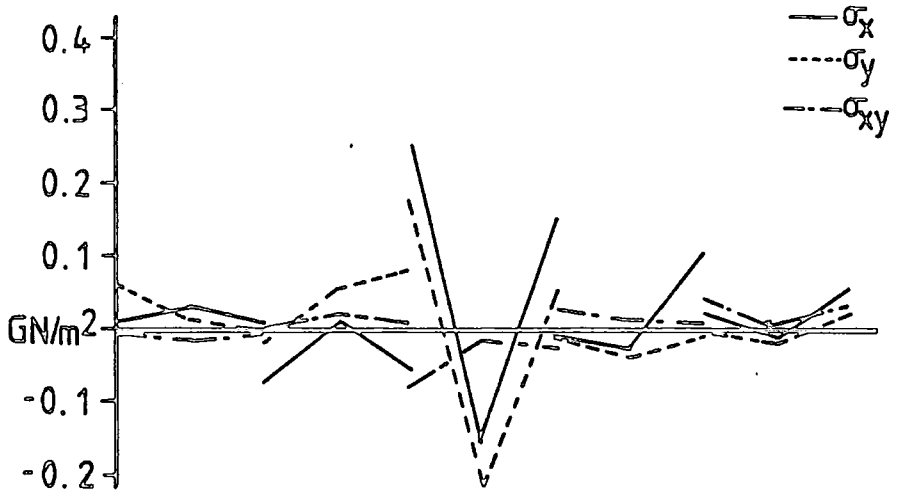

FIGURE.7.8, THERMAL STRESSES ON THE RAKE FACE.

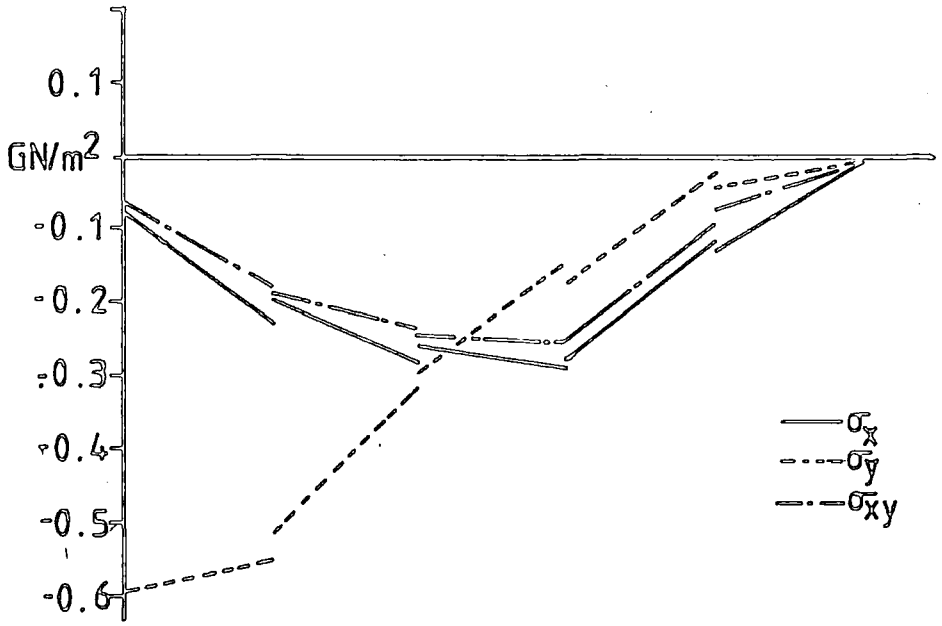

FIGURE 7.9, MECHANICAL STRESSES AFTER SMOOTHING.

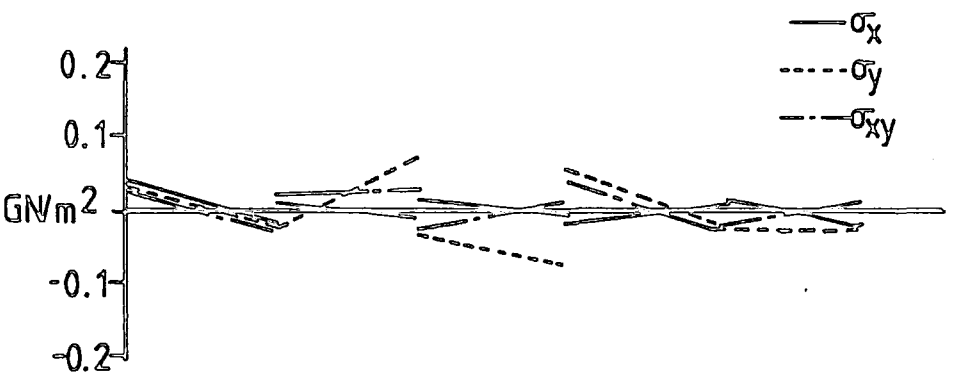

FIGURE 7.10, THERMAL STRESSES AFTER SMOOTHING.

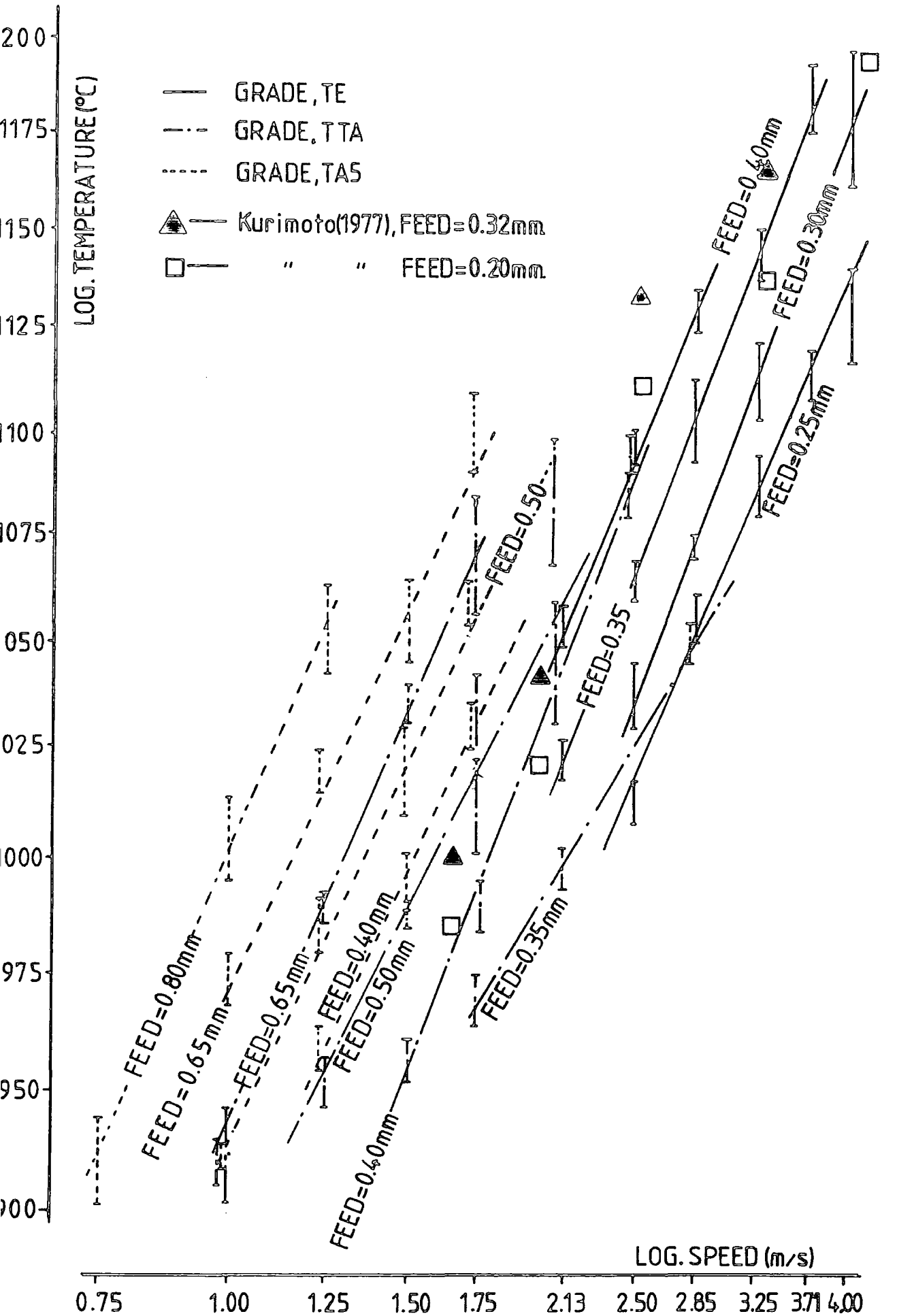

FIGURE 8.1, COMPARISON OF AVERAGE CUTTING TEMPERATURES.

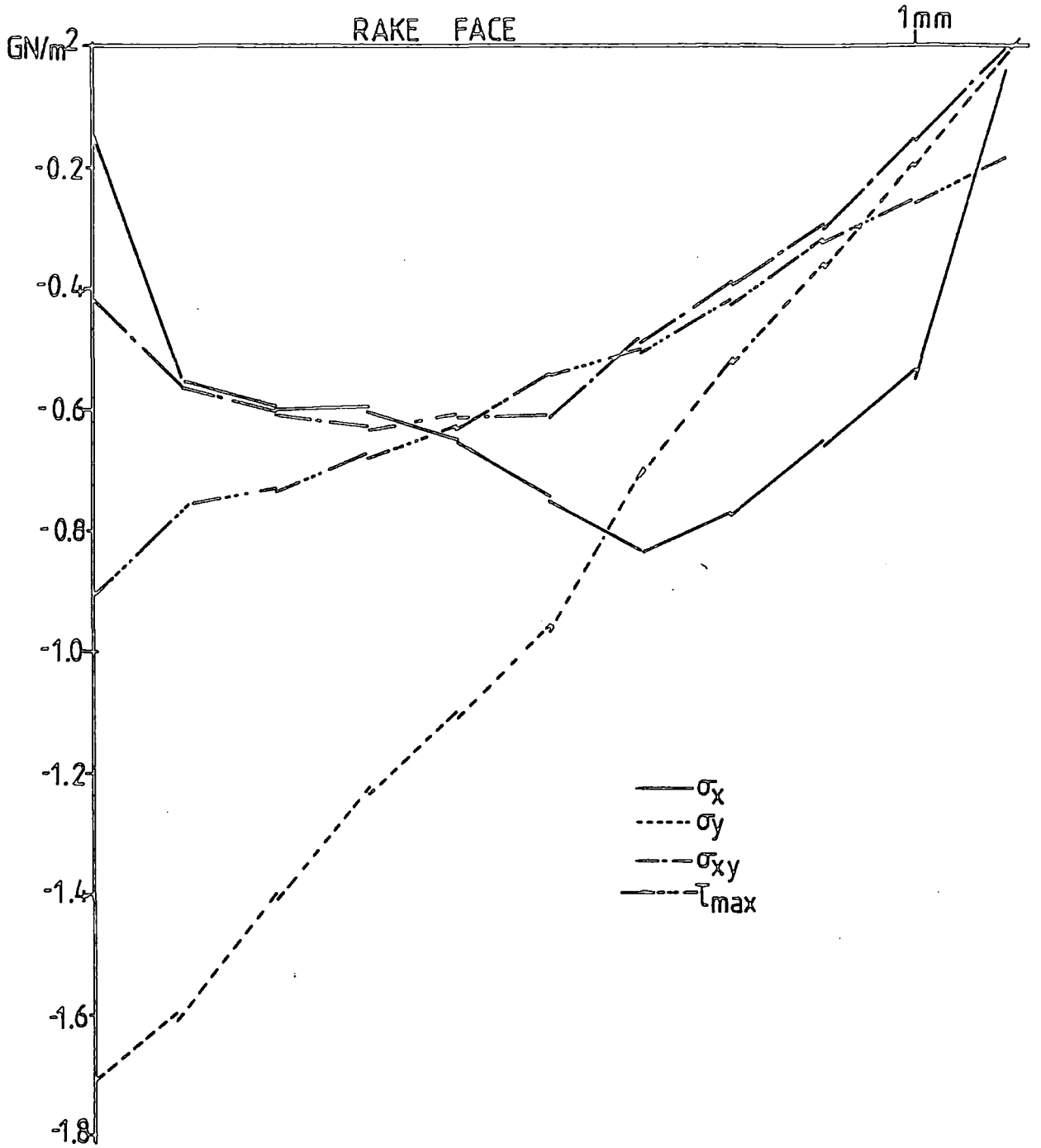

FIGURE 8.2, STRESS ON RAKE FACE (CHAN AND BRAIDEN, 1981)

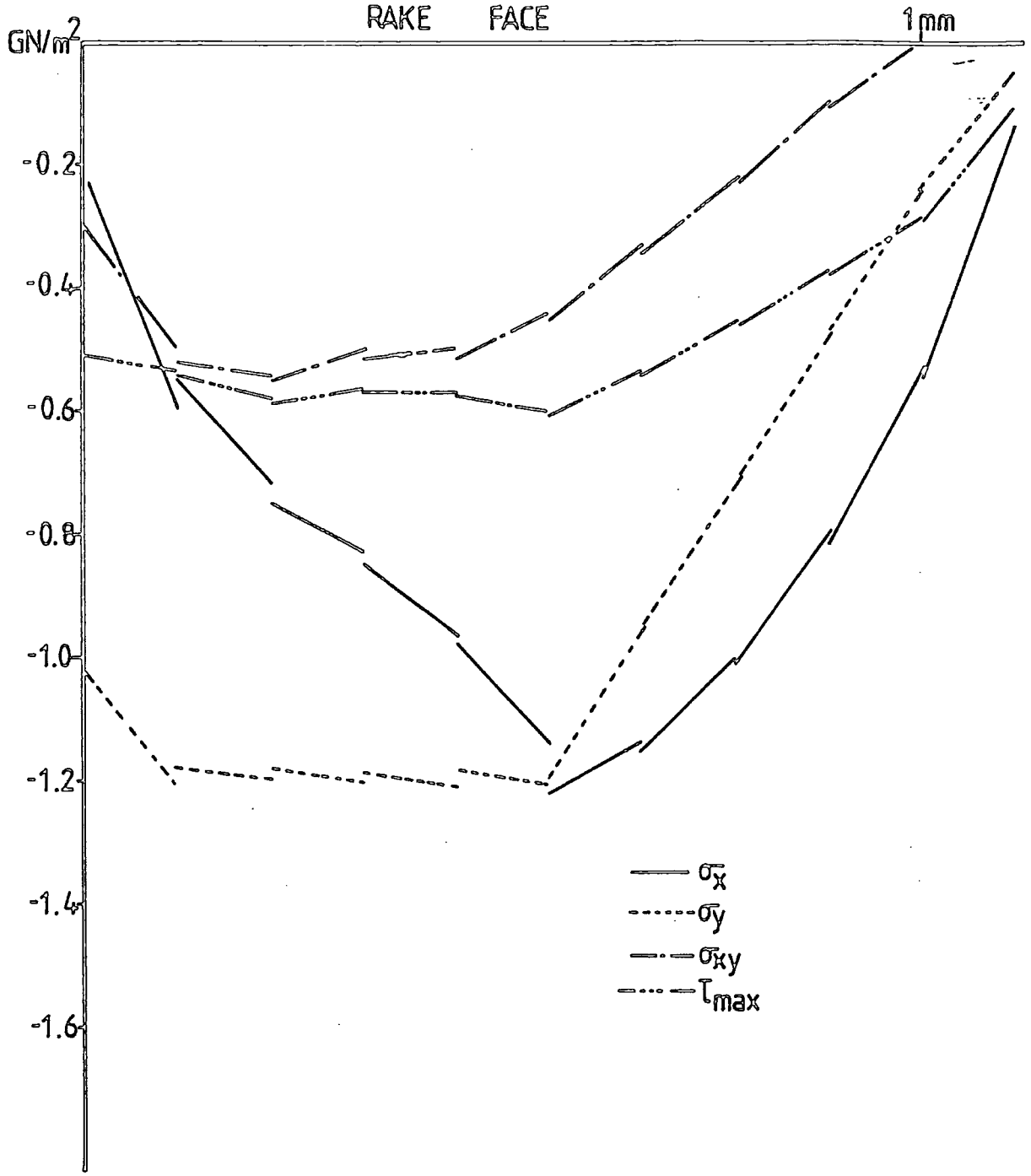

FIGURE 8.3, STRESSES ON RAKE FACE. (BARROW, 1982)

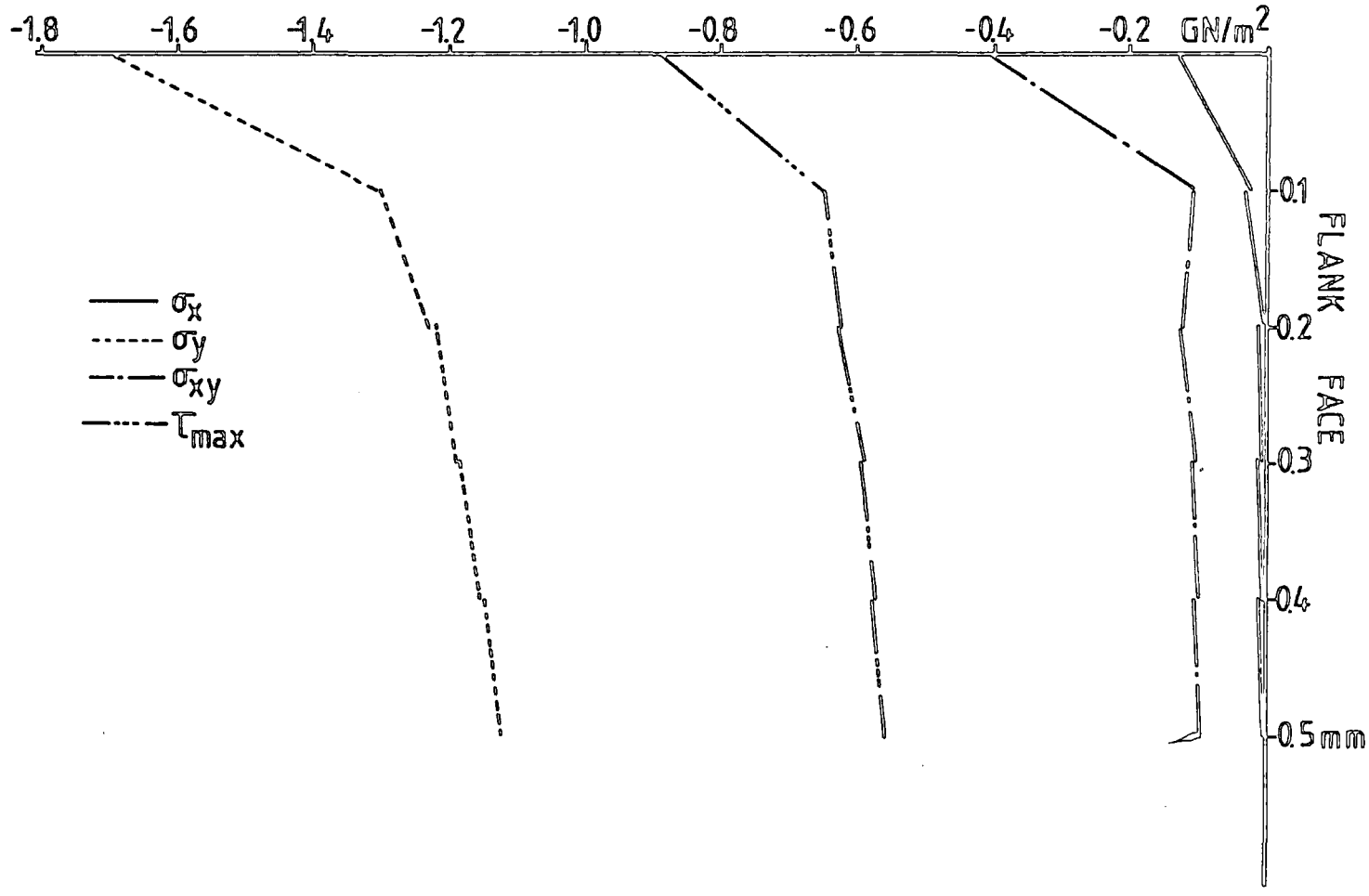

FIGURE 8.4, STRESSES ON FLANK FACE (CHAN AND BRAIDEN, 1981)

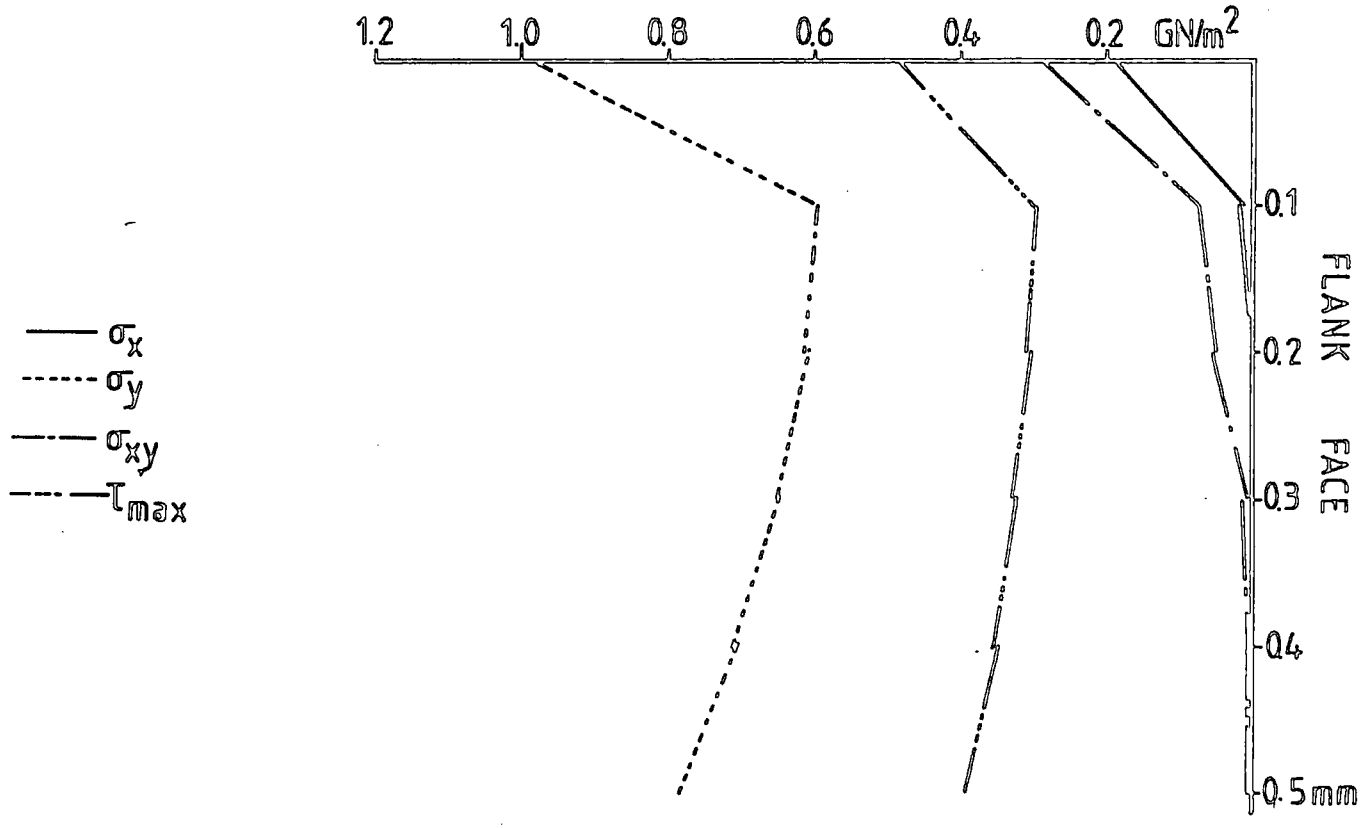

FIGURE 8.5, STRESSES ON FLANK FACE (BARROW, 1982)

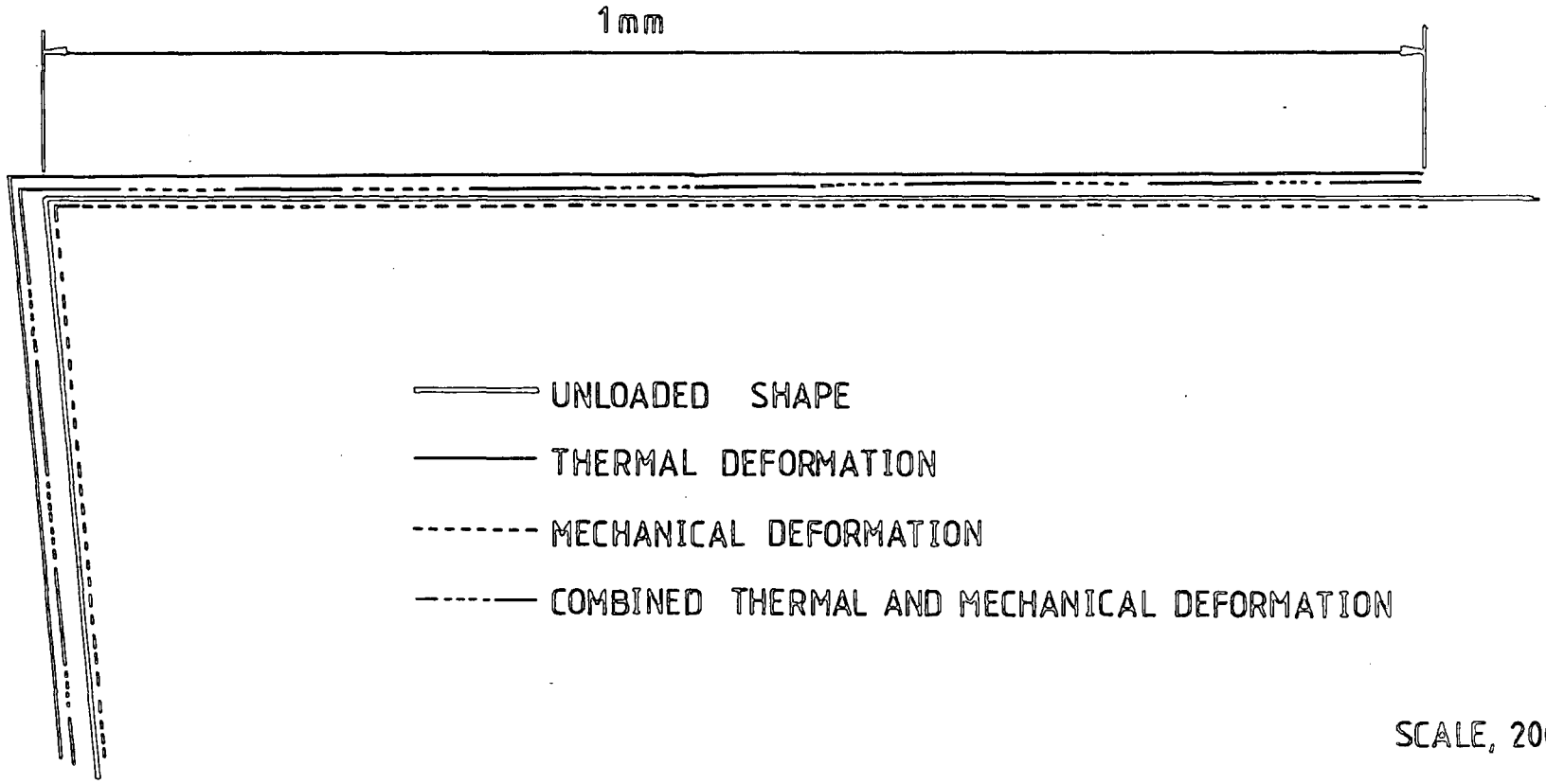

FIGURE 8.6, ELASTICALLY DEFORMED CUTTING TOOL.

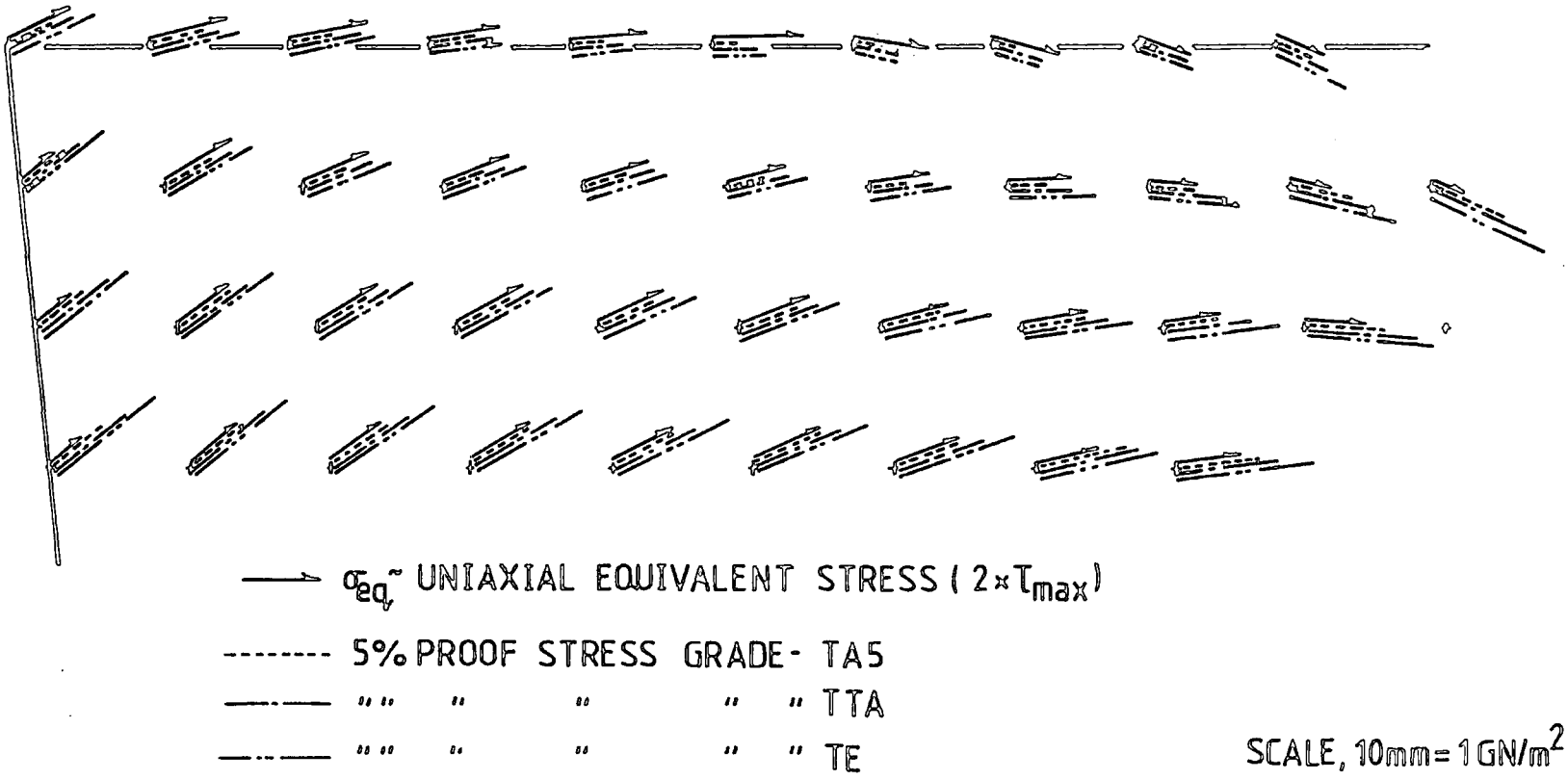

FIGURE 8.7, DISTRIBUTION OF UNIAXIAL EQUIVALENT STRESS.

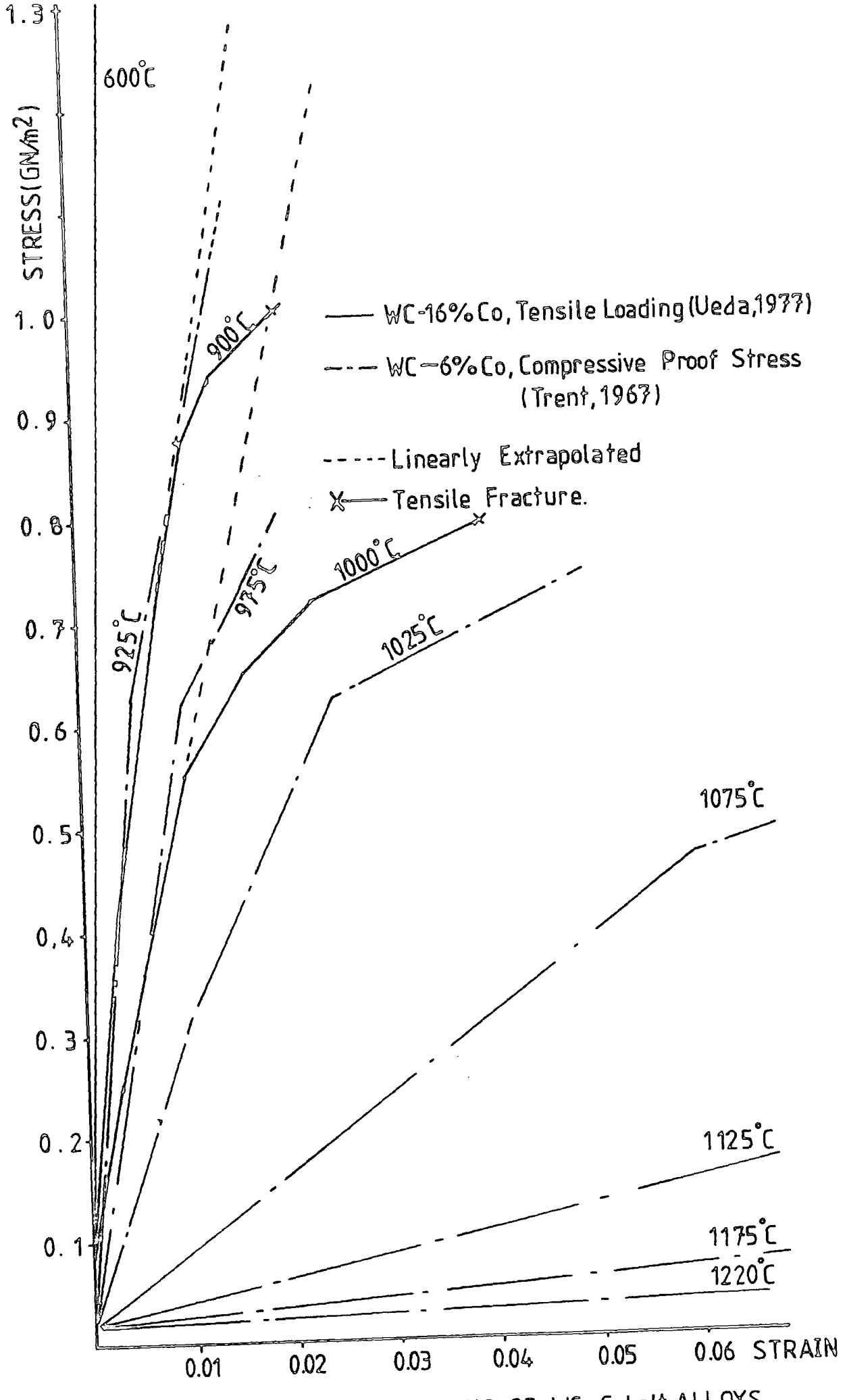

FIGURE 8.8, STRESS/STRAIN RELATIONS OF WC-Cobalt ALLOYS.

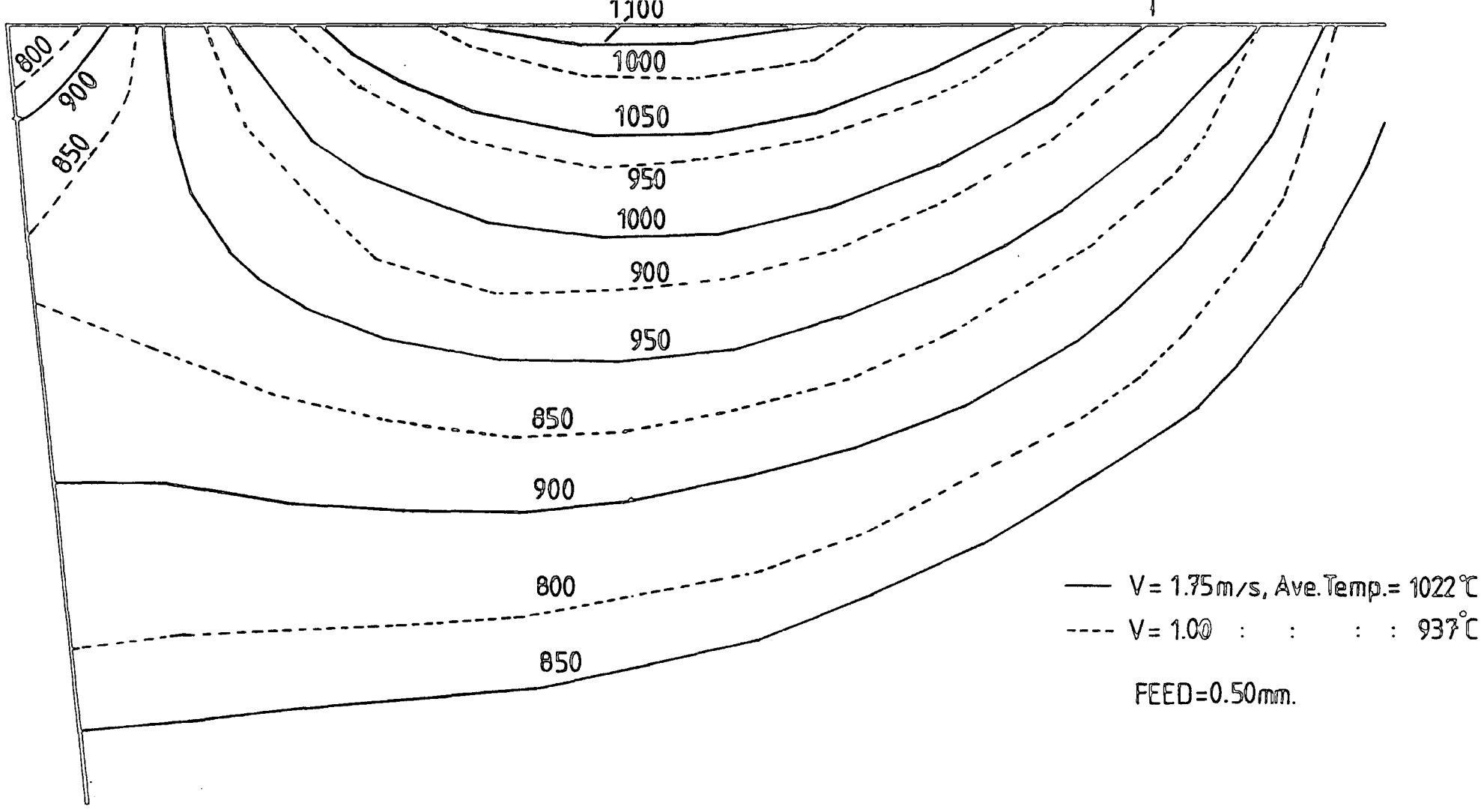

FIGURE 8.9, INFLUENCE OF CUTTING SPEED ON CALCULATED TEMPERATURE DISTRIBUTIONS.

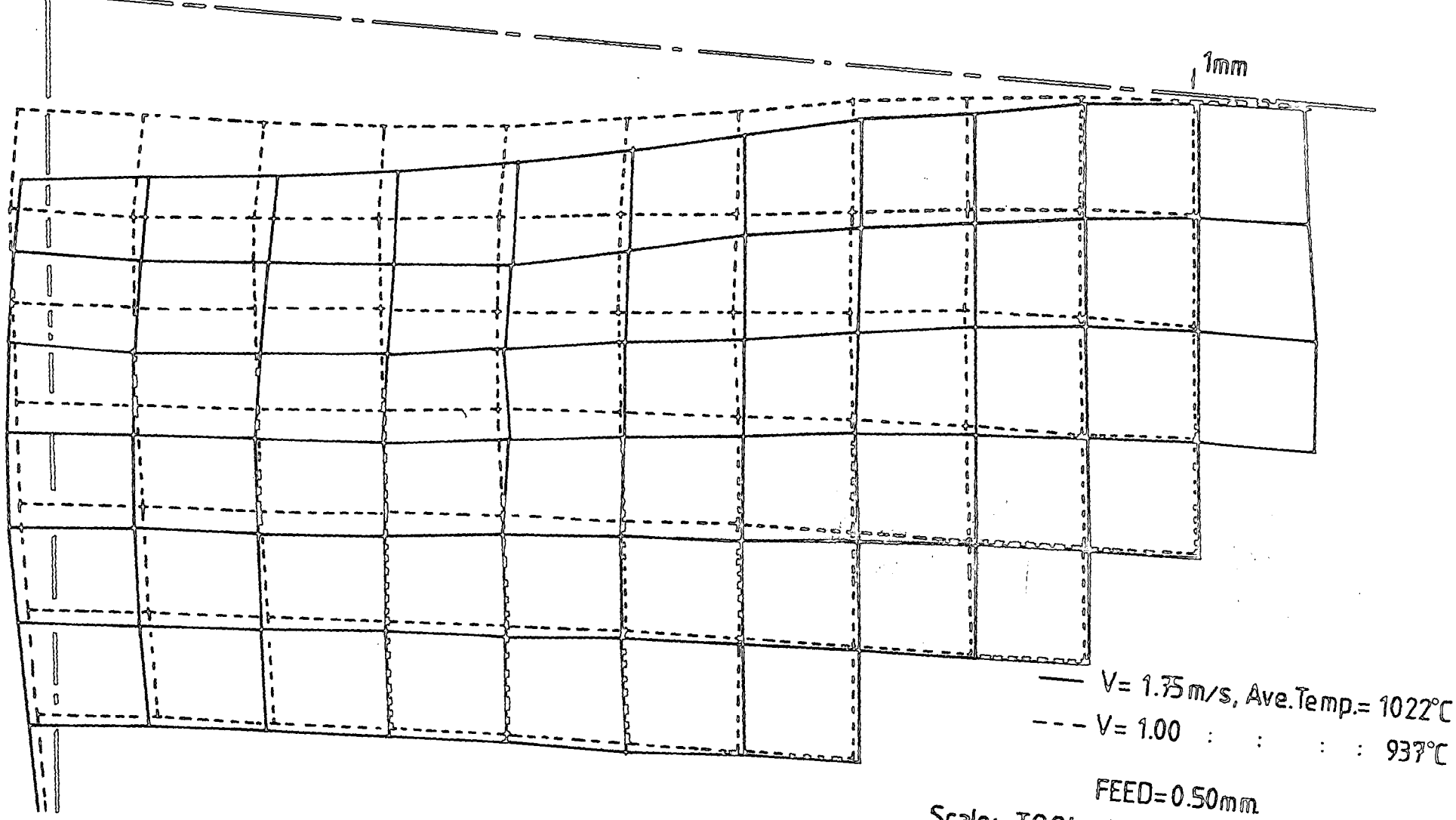

FIGURE 8.10, INFLUENCE OF CUTTING SPEED ON PREDICTED PERMANENT DEFORMATION.

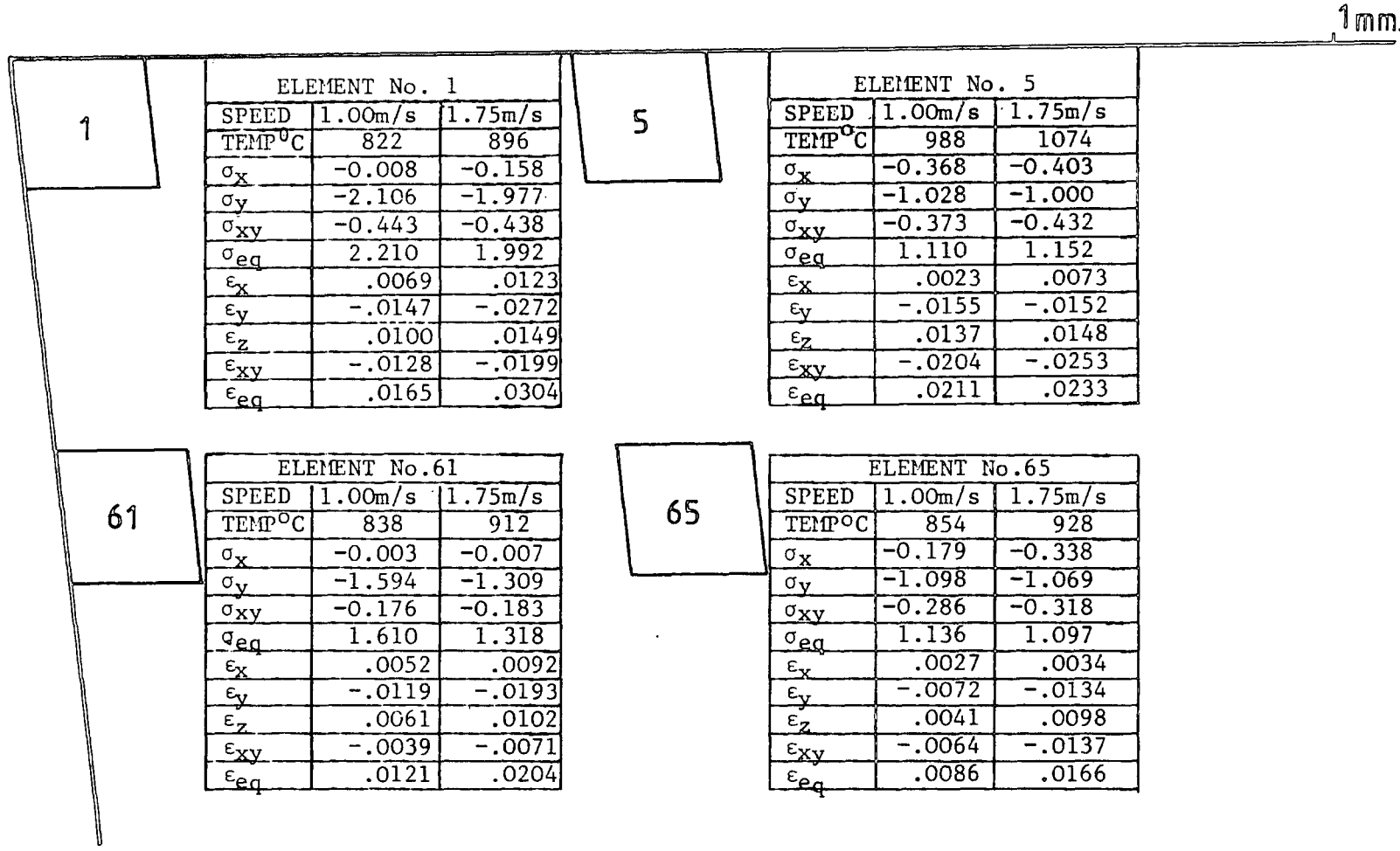

ELEMENT No. 1		
SPEED	1.00m/s	1.75m/s
TEMP°C	822	896
σ_x	-0.008	-0.158
σ_y	-2.106	-1.977
σ_{xy}	-0.443	-0.438
σ_{eq}	2.210	1.992
ε_x	.0069	.0123
ε_y	-.0147	-.0272
ε_z	.0100	.0149
ε_{xy}	-.0128	-.0199
ε_{eq}	.0165	.0304

ELEMENT No. 5		
SPEED	1.00m/s	1.75m/s
TEMP°C	988	1074
σ_x	-0.368	-0.403
σ_y	-1.028	-1.000
σ_{xy}	-0.373	-0.432
σ_{eq}	1.110	1.152
ε_x	.0023	.0073
ε_y	-.0155	-.0152
ε_z	.0137	.0148
ε_{xy}	-.0204	-.0253
ε_{eq}	.0211	.0233

ELEMENT No.61		
SPEED	1.00m/s	1.75m/s
TEMP°C	838	912
σ_x	-0.003	-0.007
σ_y	-1.594	-1.309
σ_{xy}	-0.176	-0.183
σ_{eq}	1.610	1.318
ε_x	.0052	.0092
ε_y	-.0119	-.0193
ε_z	.0061	.0102
ε_{xy}	-.0039	-.0071
ε_{eq}	.0121	.0204

ELEMENT No.65		
SPEED	1.00m/s	1.75m/s
TEMP°C	854	928
σ_x	-0.179	-0.338
σ_y	-1.098	-1.069
σ_{xy}	-0.286	-0.318
σ_{eq}	1.136	1.097
ε_x	.0027	.0034
ε_y	-.0072	-.0134
ε_z	.0041	.0098
ε_{xy}	-.0064	-.0137
ε_{eq}	.0086	.0166

FEED RATE =0.50mm.

FIGURE 8.11, INFLUENCE OF CUTTING SPEED ON CALCULATED STRAINS AND STRESSES.

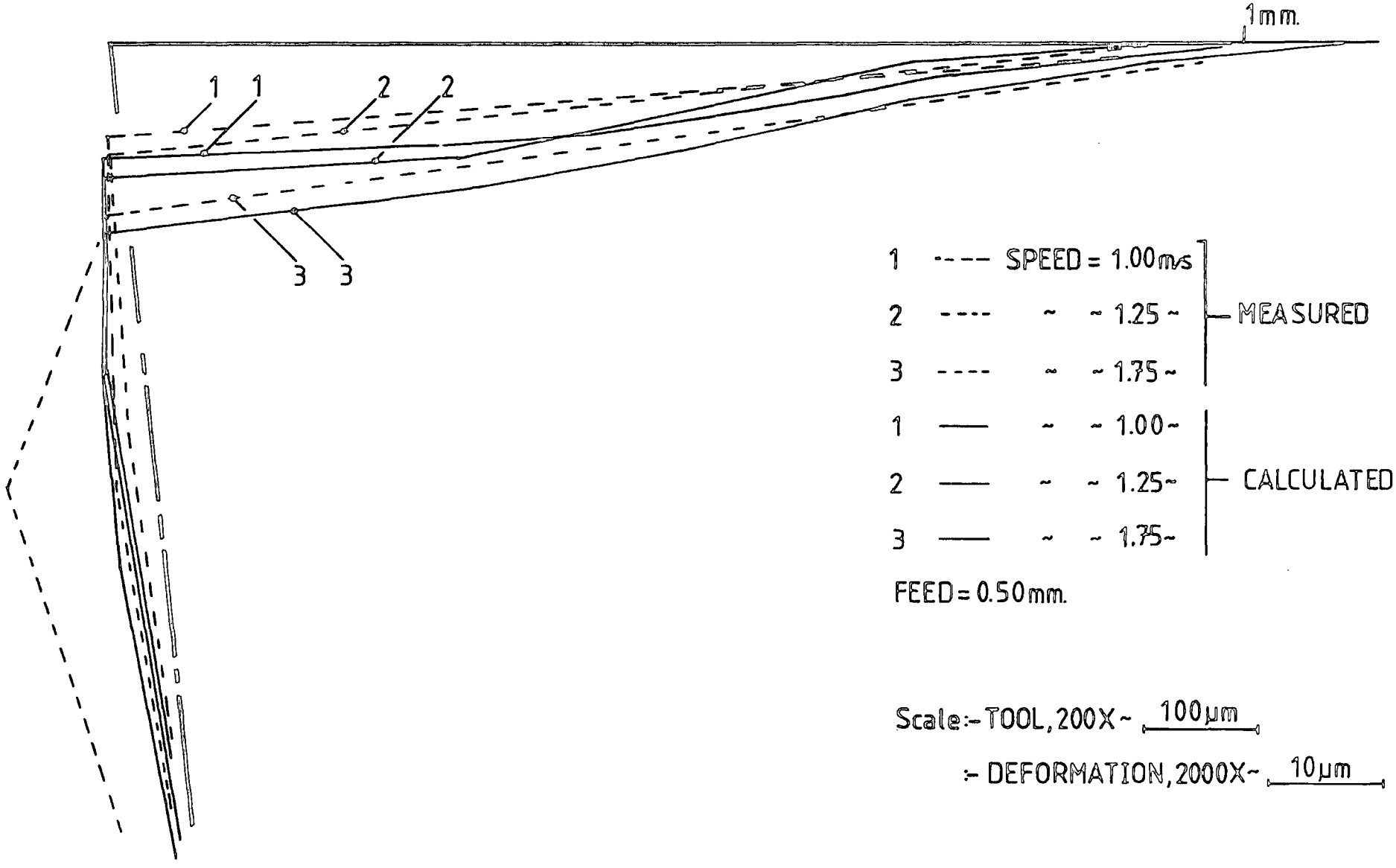

FIGURE 8.12, COMPARISON OF MEASURED AND CALCULATED DEFORMATION FOR VARIABLE SPEED.

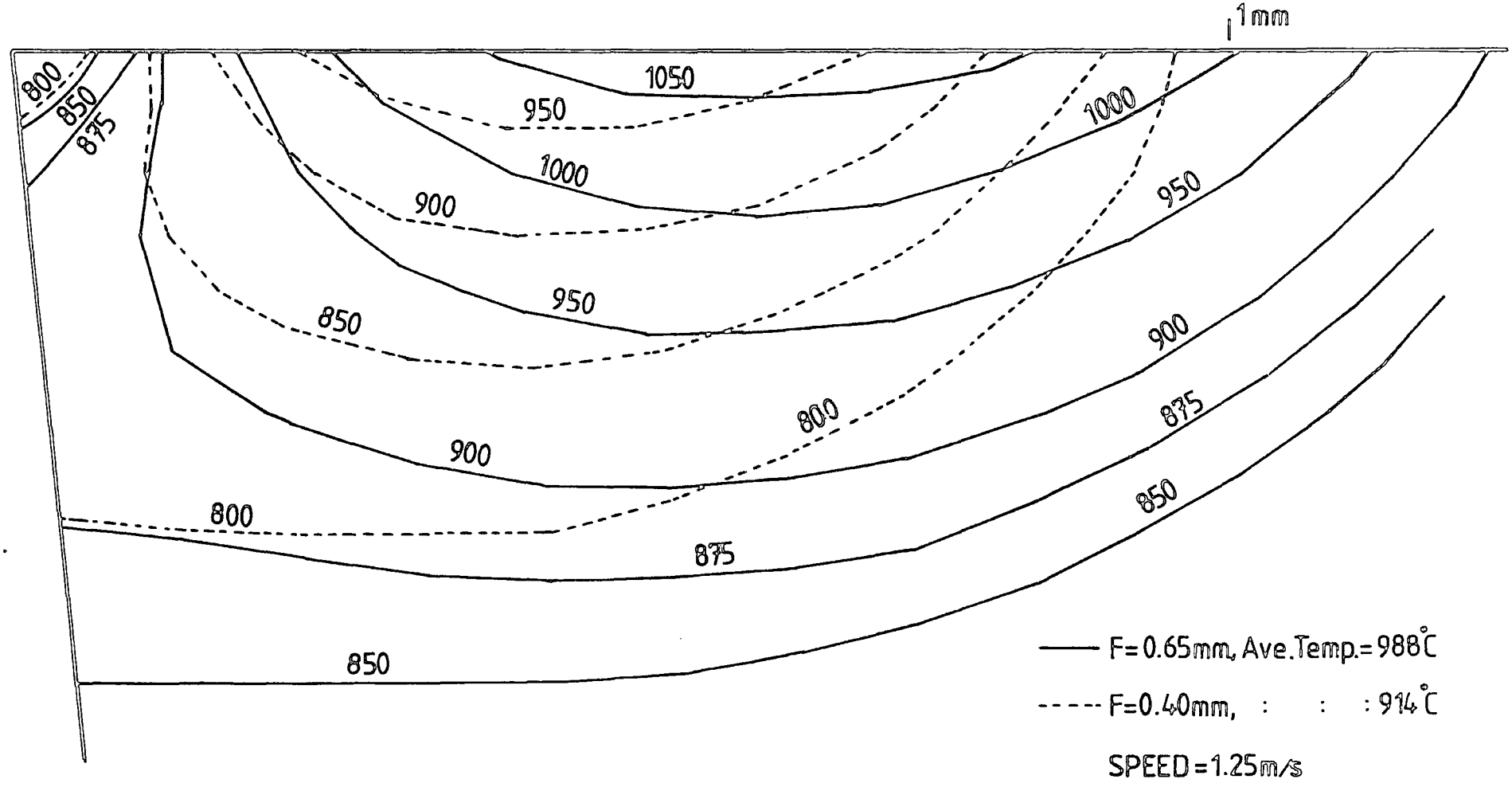

FIGURE 8.13, INFLUENCE OF FEED RATE ON CALCULATED TEMPERATURE DISTRIBUTIONS.

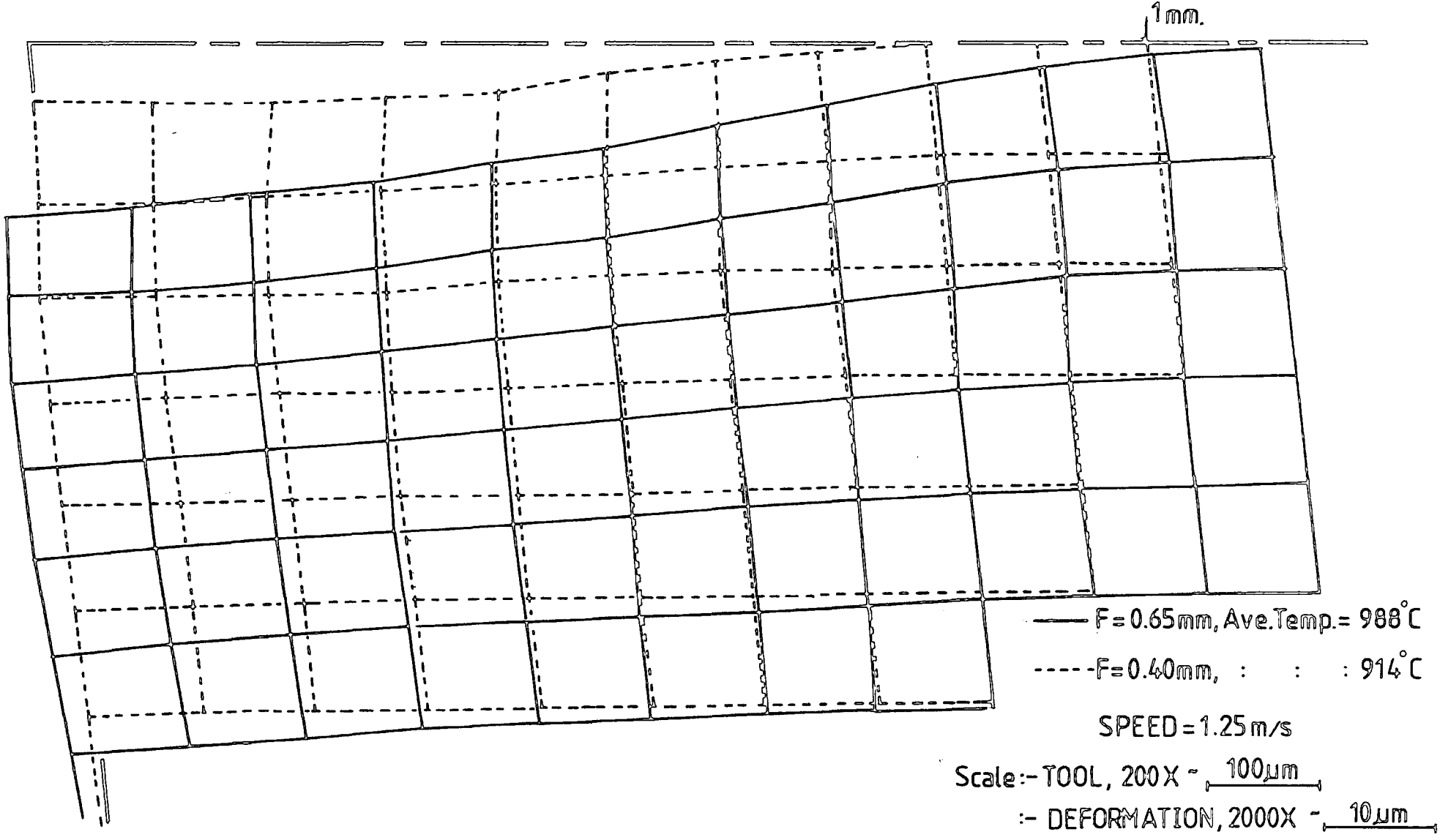

FIGURE 8.14, INFLUENCE OF FEED RATE ON PREDICTED PERMANENT DEFORMATION.

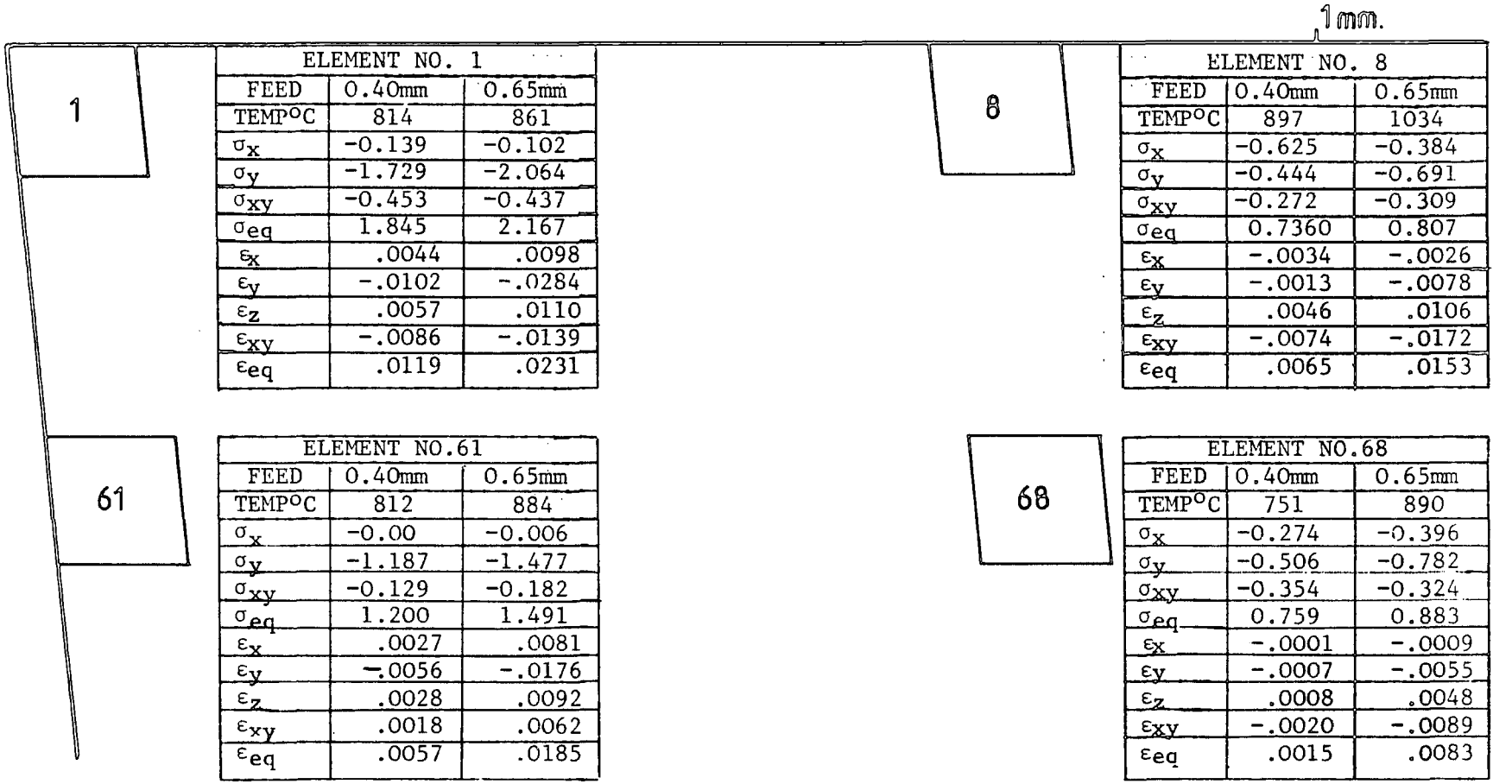

ELEMENT NO. 1		
FEED	0.40mm	0.65mm
TEMP°C	814	861
σ_x	-0.139	-0.102
σ_y	-1.729	-2.064
σ_{xy}	-0.453	-0.437
σ_{eq}	1.845	2.167
ε_x	.0044	.0098
ε_y	-.0102	-.0284
ε_z	.0057	.0110
ε_{xy}	-.0086	-.0139
ε_{eq}	.0119	.0231

ELEMENT NO. 8		
FEED	0.40mm	0.65mm
TEMP°C	897	1034
σ_x	-0.625	-0.384
σ_y	-0.444	-0.691
σ_{xy}	-0.272	-0.309
σ_{eq}	0.7360	0.807
ε_x	-.0034	-.0026
ε_y	-.0013	-.0078
ε_z	.0046	.0106
ε_{xy}	-.0074	-.0172
ε_{eq}	.0065	.0153

ELEMENT NO.61		
FEED	0.40mm	0.65mm
TEMP°C	812	884
σ_x	-0.00	-0.006
σ_y	-1.187	-1.477
σ_{xy}	-0.129	-0.182
σ_{eq}	1.200	1.491
ε_x	.0027	.0081
ε_y	-.0056	-.0176
ε_z	.0028	.0092
ε_{xy}	.0018	.0062
ε_{eq}	.0057	.0185

ELEMENT NO.68		
FEED	0.40mm	0.65mm
TEMP°C	751	890
σ_x	-0.274	-0.396
σ_y	-0.506	-0.782
σ_{xy}	-0.354	-0.324
σ_{eq}	0.759	0.883
ε_x	-.0001	-.0009
ε_y	-.0007	-.0055
ε_z	.0008	.0048
ε_{xy}	-.0020	-.0089
ε_{eq}	.0015	.0083

CUTTING SPEED = 1.25m/s.

FIGURE 8.15, INFLUENCE OF FEED RATE ON CALCULATED STRAINS AND STRESSES.

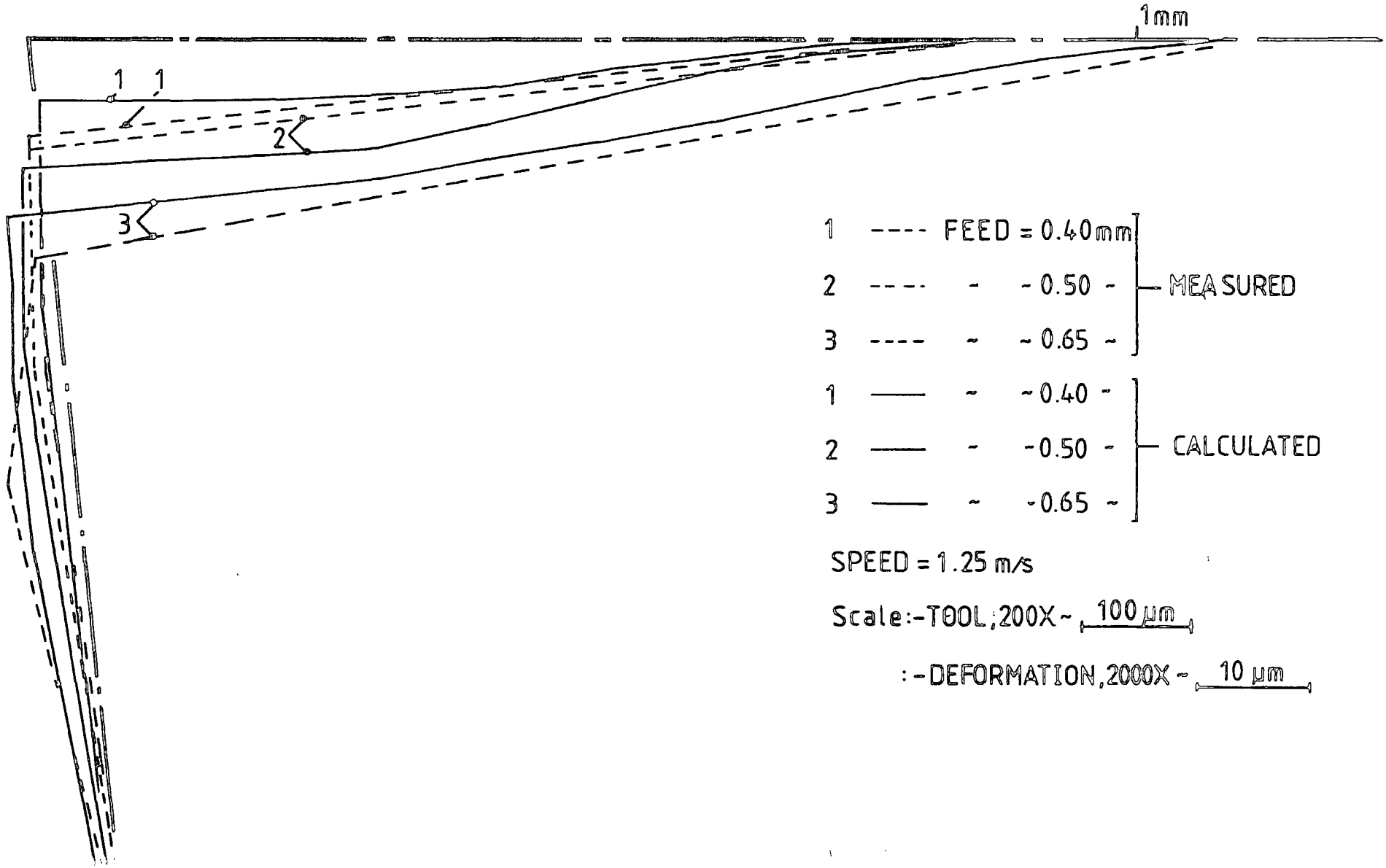

FIGURE 8.16, COMPARISON OF MEASURED AND CALCULATED DEFORMATION FOR VARIABLE FEED.

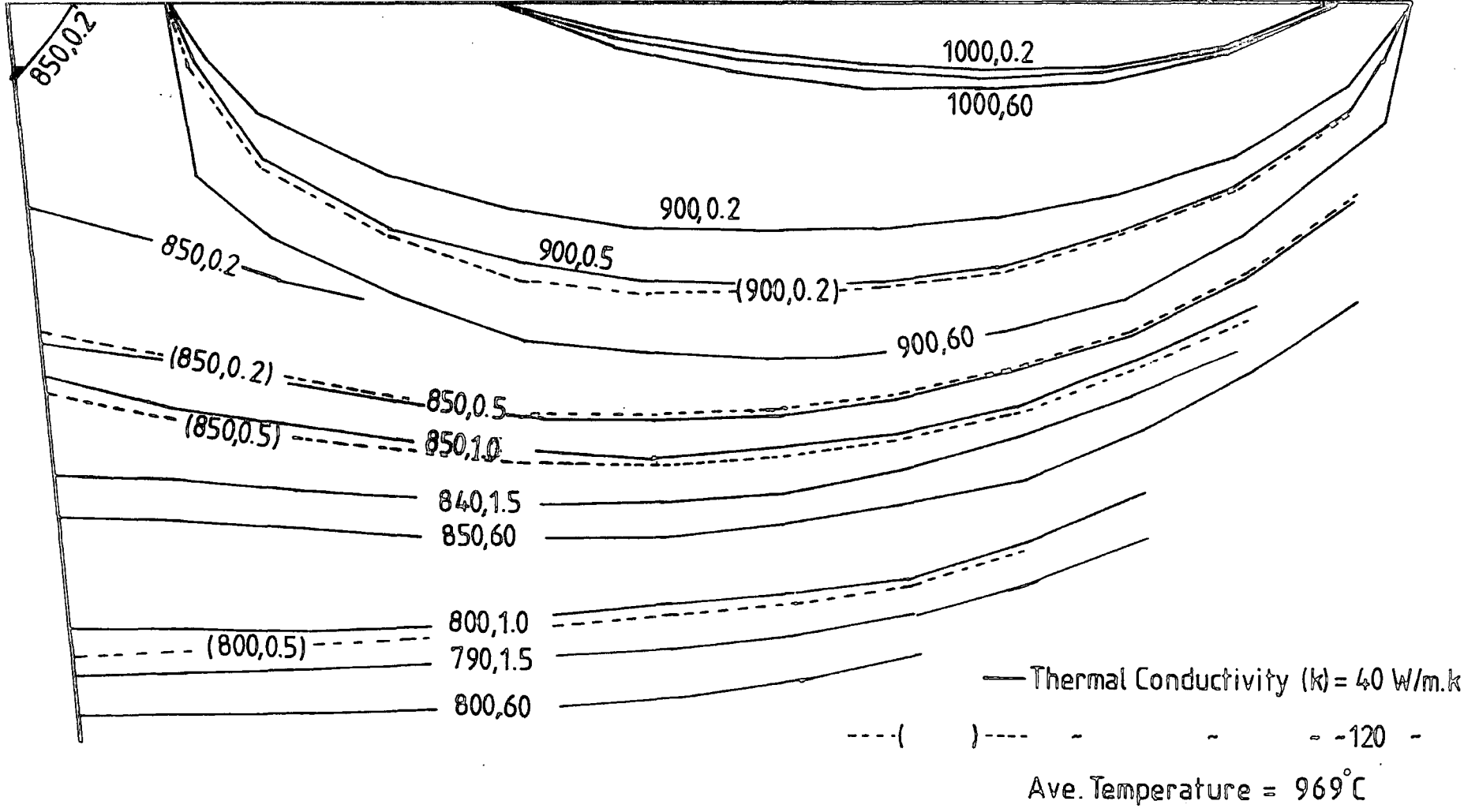

FIGURE 8.17, CALCULATED TRANSIENT TEMPERATURE DISTRIBUTIONS WITHIN THE TOOL.

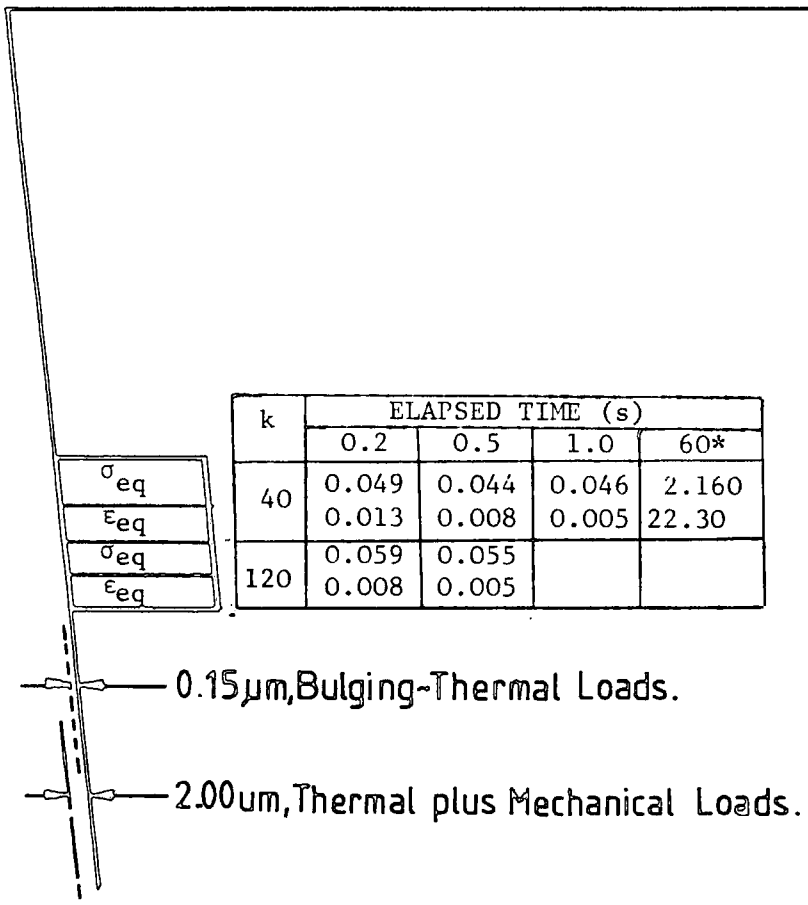

	k	ELAPSED TIME (s)			
		0.2	0.5	1.0	60*
σ_{eq}	40	0.049	0.044	0.046	2.160
ε_{eq}		0.013	0.008	0.005	22.30
σ_{eq}	120	0.059	0.055		
ε_{eq}		0.008	0.005		

	k	ELAPSED TIME (s)			
		0.2	0.5	1.0	60*
σ_{eq}	40	0.054	0.044	0.042	1.070
ε_{eq}		0.042	0.007	0.001	21.00
σ_{eq}	120	0.054	0.053		
ε_{eq}		0.007	0.001		
σ_{eq}	40	0.101	0.088	0.085	1.060
ε_{eq}		0.258	0.160	0.131	19.10
σ_{eq}	120	0.088	0.084		
ε_{eq}		0.161	0.127		
σ_{eq}	40	0.156	0.119	0.110	1.050
ε_{eq}		0.414	0.336	0.302	16.20
σ_{eq}	120	0.119	0.109		
ε_{eq}		0.337	0.296		
σ_{eq}	40	0.246	0.177	0.158	1.040
ε_{eq}		0.474	0.432	0.409	13.50
σ_{eq}	120	0.178	0.155		
ε_{eq}		0.433	0.407		

Notes: 1) k - Thermal conductivity of tool material W/mk.

2) 60* - Addition of Mechanical Loads.

3) σ_{eq} - Von-Mises Equivalent Stress (GN/m^2).

4) ε_{eq} - Equivalent Strain x 10^{-3} (i.e. milli-strain).

FIGURE 8.18, TRANSIENT THERMAL STRAINS AND STRESSES.

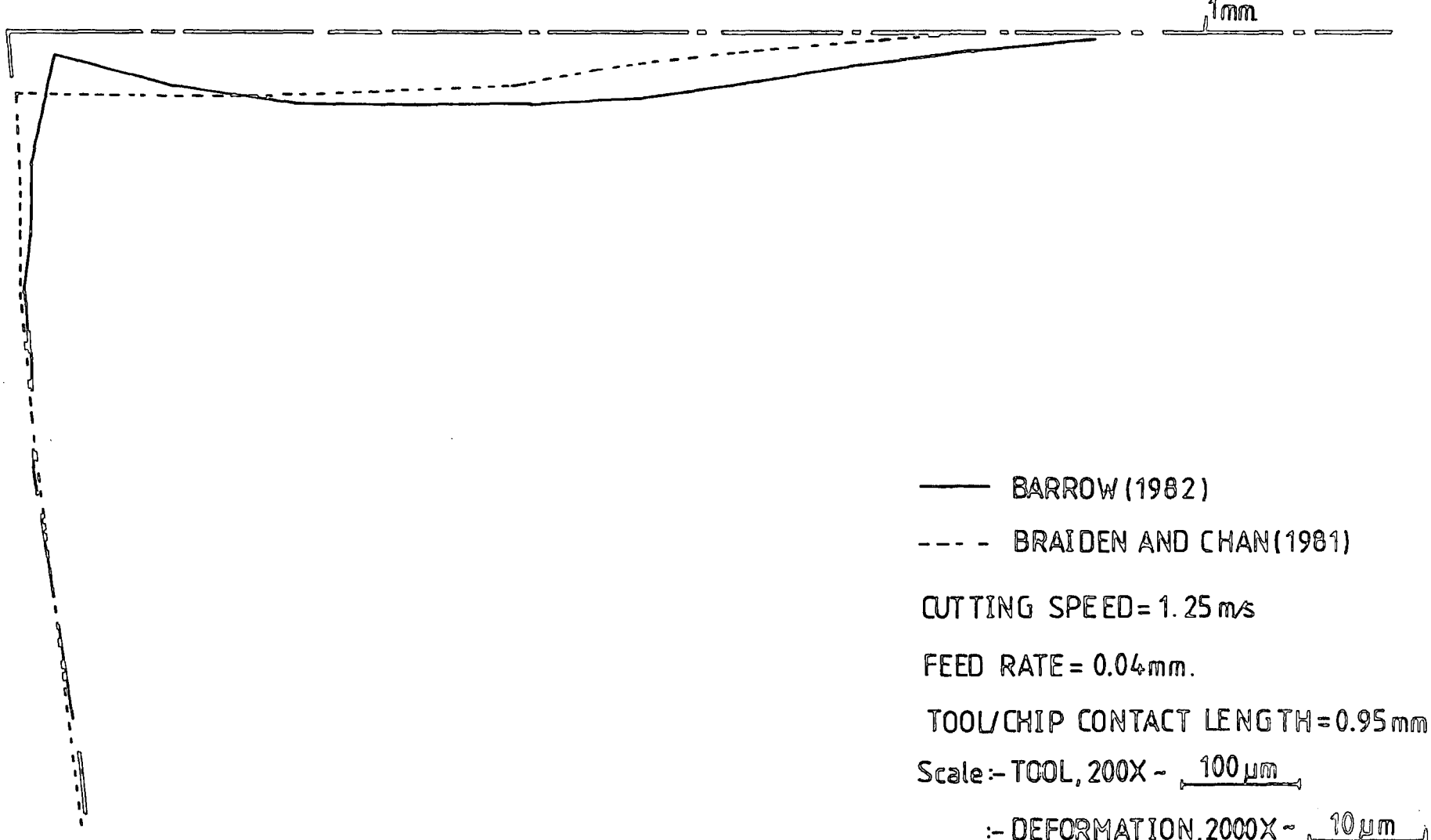

FIGURE 8.19 COMPARISON OF DIFFERENT TOOL/CHIP STRESS DISTRIBUTIONS ON DEFORMATION.

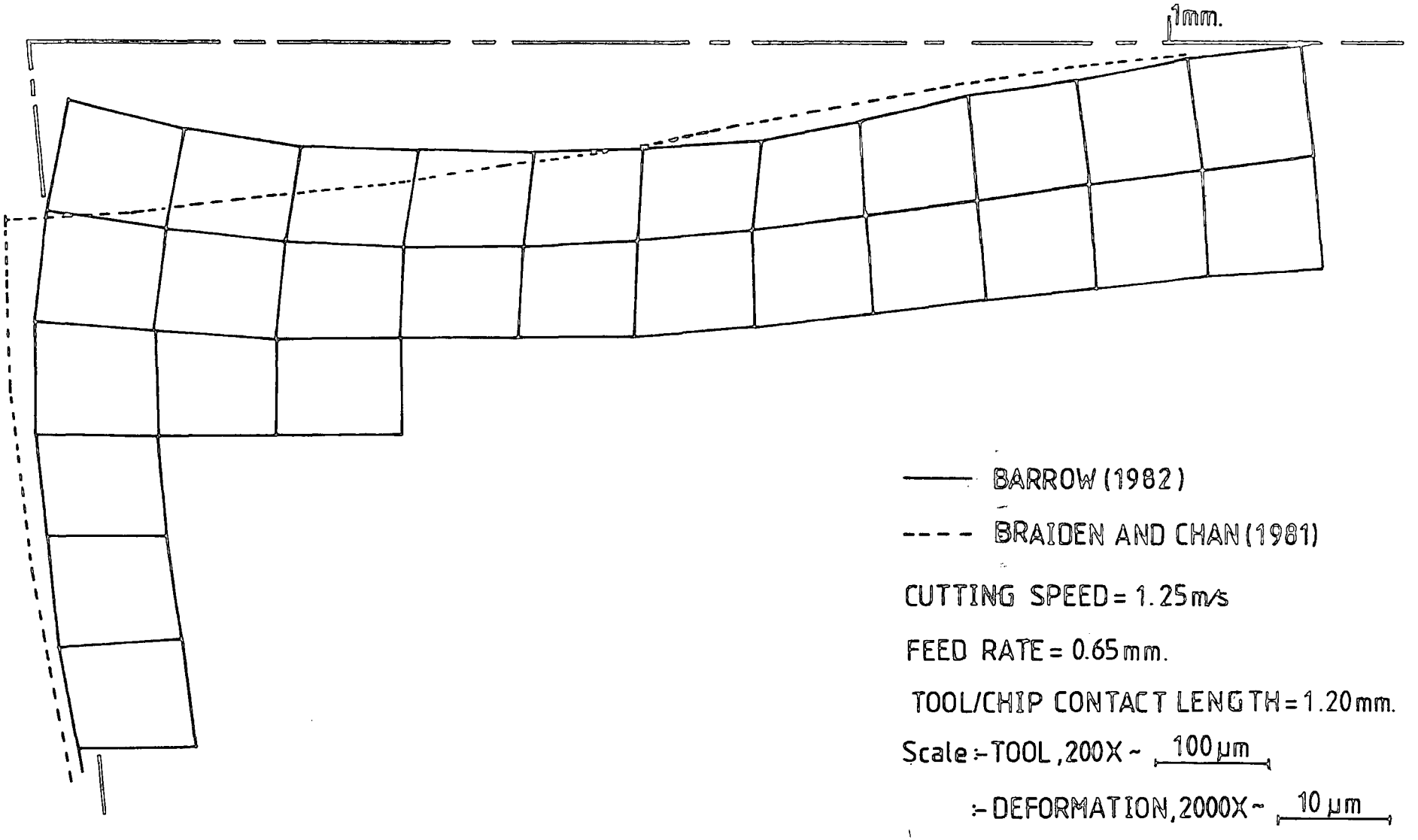

FIGURE 8.20, COMPARISON OF DIFFERENT TOOL/CHIP STRESS DISTRIBUTIONS ON DEFORMATION

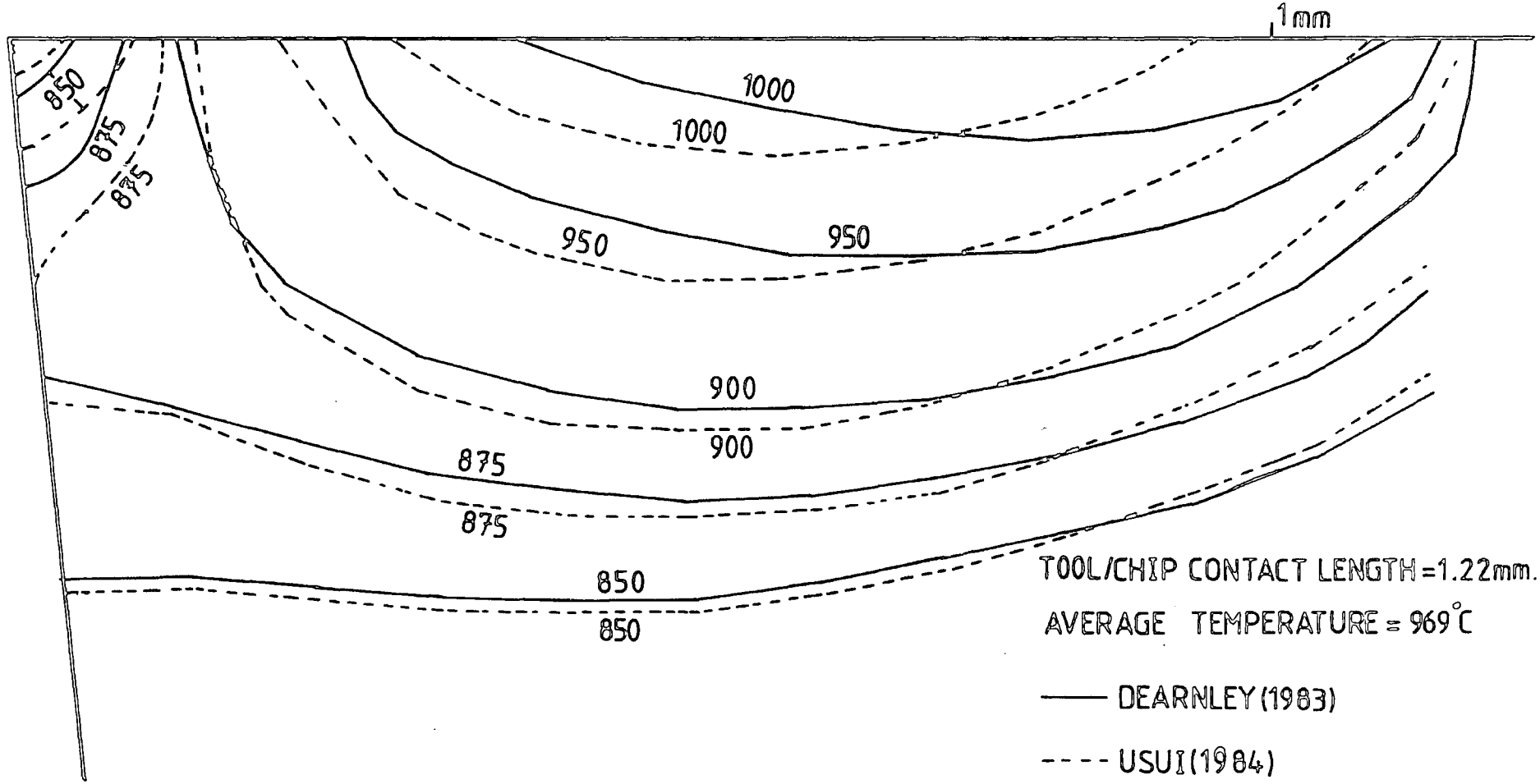

FIGURE 8.21, INFLUENCE OF THE TEMPERATURE DISTRIBUTION AT THE TOOL/CHIP INTERFACE.

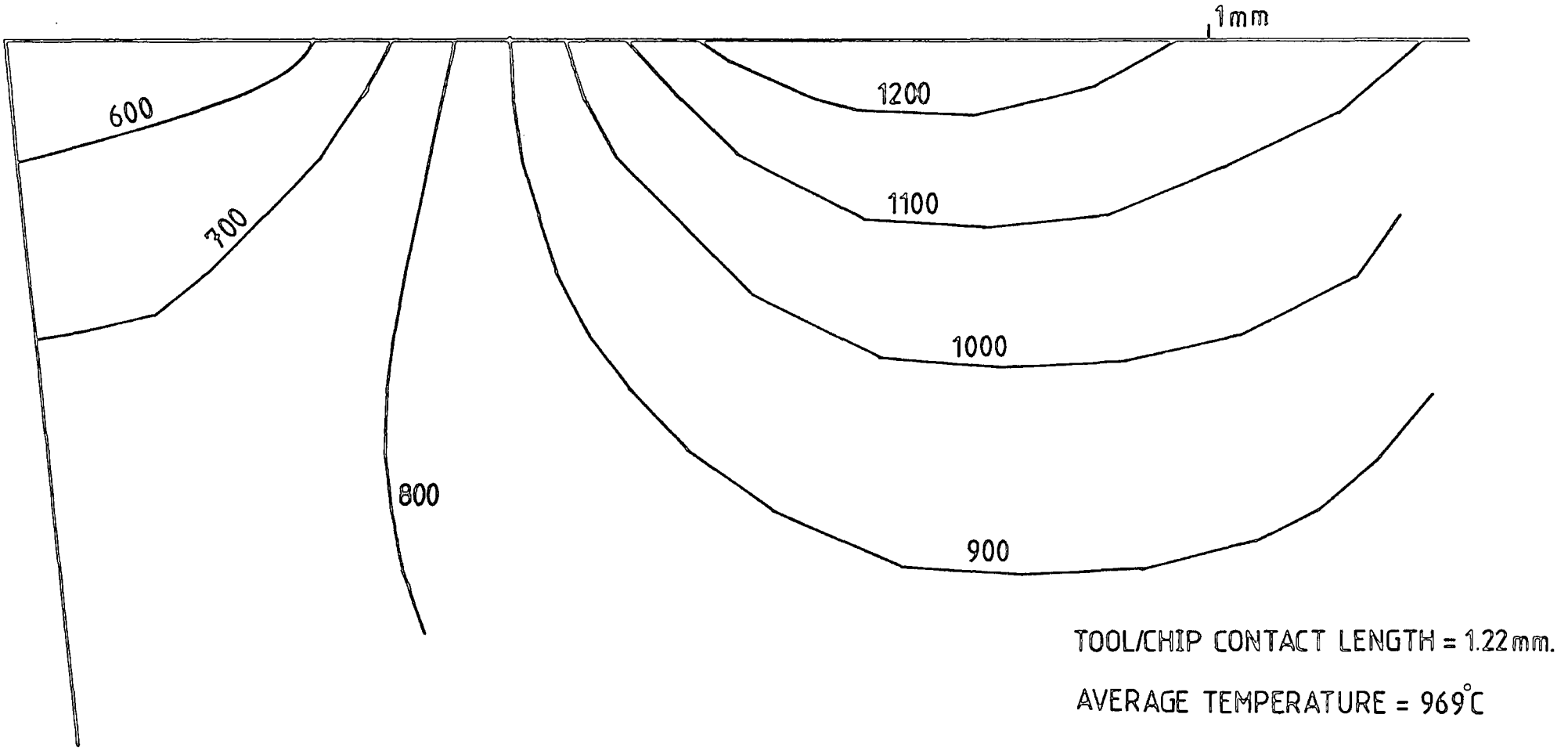

FIGURE 8.22, CALCULATED TEMPERATURE CONTOURS FOR THE TOOL/CHIP INTERFACE DISTRIBUTION BY TRIGGER (1961)

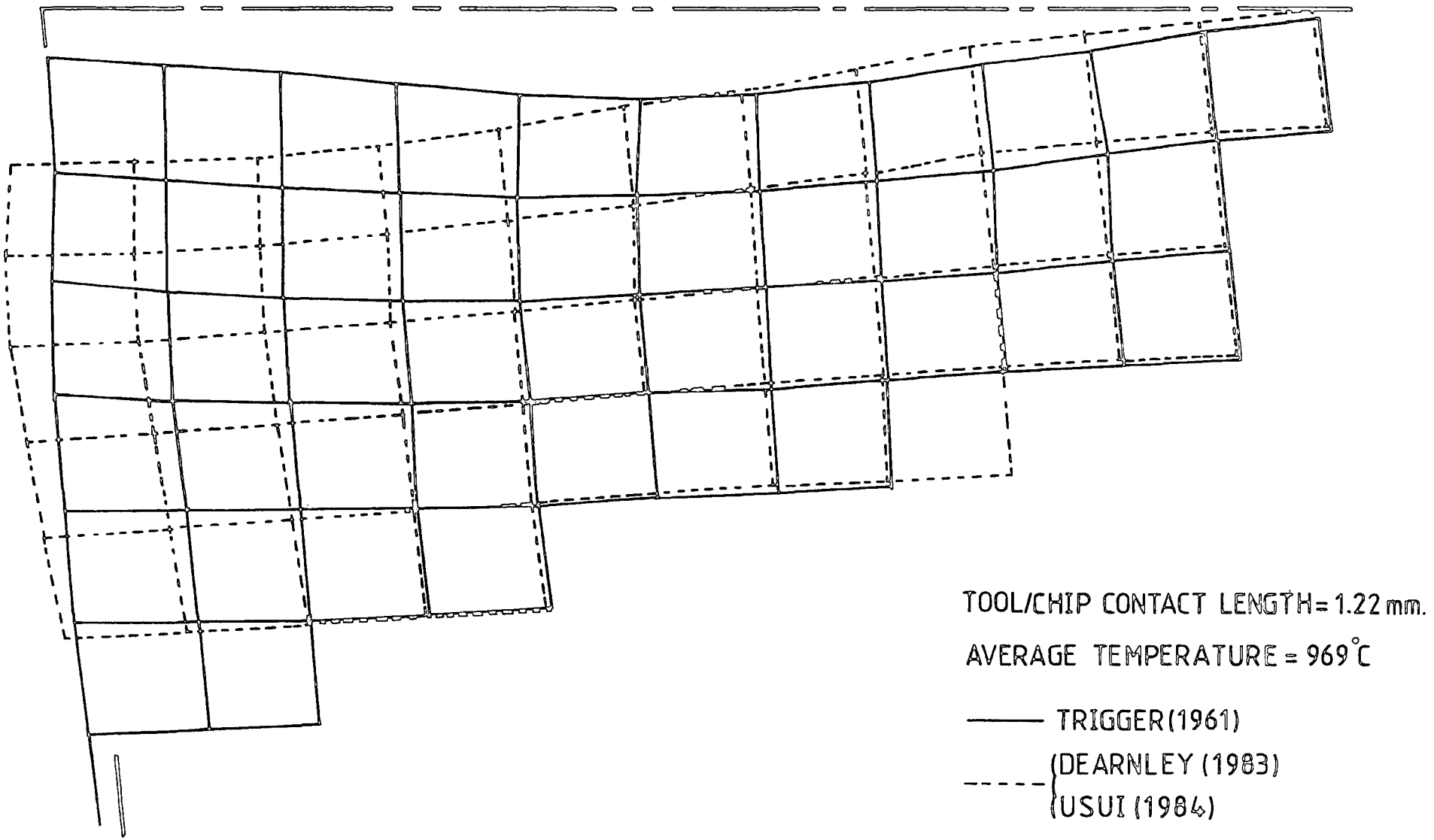

FIGURE 8.23. INFLUENCE OF TEMPERATURE DISTRIBUTION ON PREDICTED PERMANENT DEFORMATION.

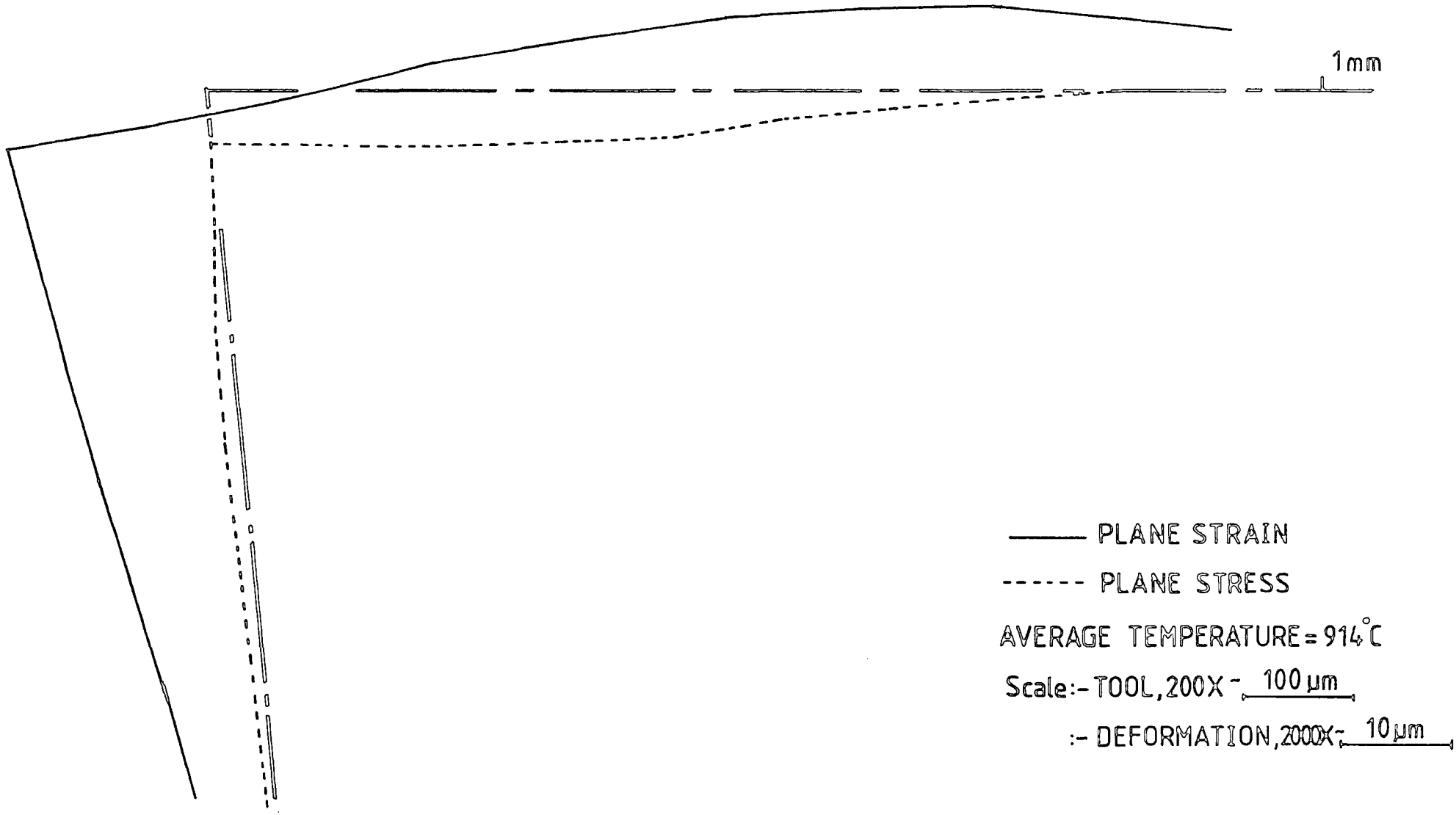

FIGURE 8.24, COMPARISON OF PLANE STRAIN AND PLANE STRESS F.E. MODELS (V=1.25m/s, F=0.40mm).

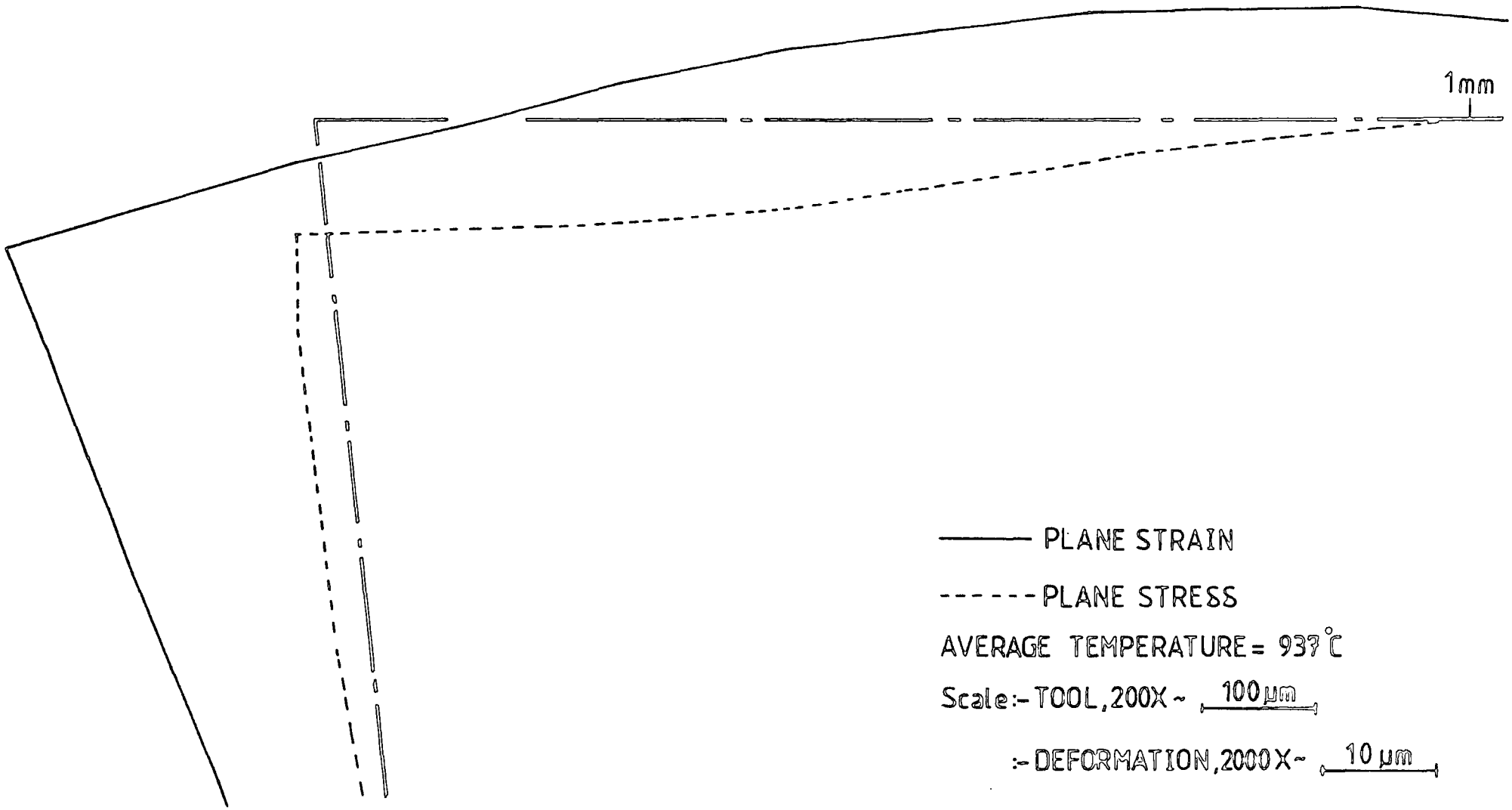

FIGURE 8.25, COMPARISON OF PLANE STRAIN AND PLANE STRESS F.E. MODELS (V=1.00m/s, F=0.50mm).

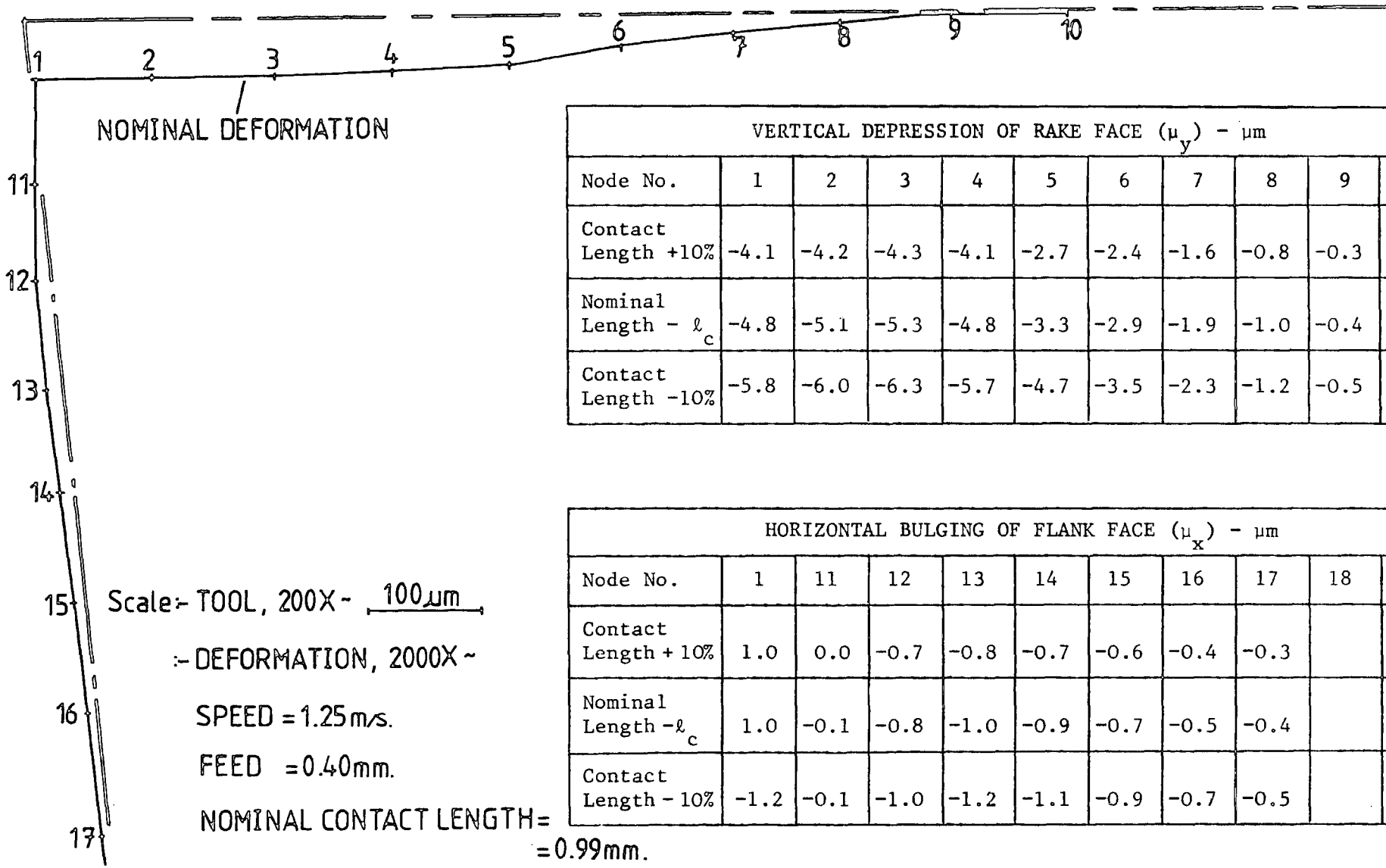

VERTICAL DEPRESSION OF RAKE FACE (μ_y) - µm										
Node No.	1	2	3	4	5	6	7	8	9	10
Contact Length +10%	-4.1	-4.2	-4.3	-4.1	-2.7	-2.4	-1.6	-0.8	-0.3	-0.1
Nominal Length - ℓ_c	-4.8	-5.1	-5.3	-4.8	-3.3	-2.9	-1.9	-1.0	-0.4	-0.1
Contact Length -10%	-5.8	-6.0	-6.3	-5.7	-4.7	-3.5	-2.3	-1.2	-0.5	-0.1

HORIZONTAL BULGING OF FLANK FACE (μ_x) - µm										
Node No.	1	11	12	13	14	15	16	17	18	19
Contact Length + 10%	1.0	0.0	-0.7	-0.8	-0.7	-0.6	-0.4	-0.3		
Nominal Length - ℓ_c	1.0	-0.1	-0.8	-1.0	-0.9	-0.7	-0.5	-0.4		
Contact Length - 10%	-1.2	-0.1	-1.0	-1.2	-1.1	-0.9	-0.7	-0.5		

FIGURE 8.26, INFLUENCE OF VARIATIONS IN TOOL/CHIP CONTACT LENGTH ON PREDICTED DEFORMATION.

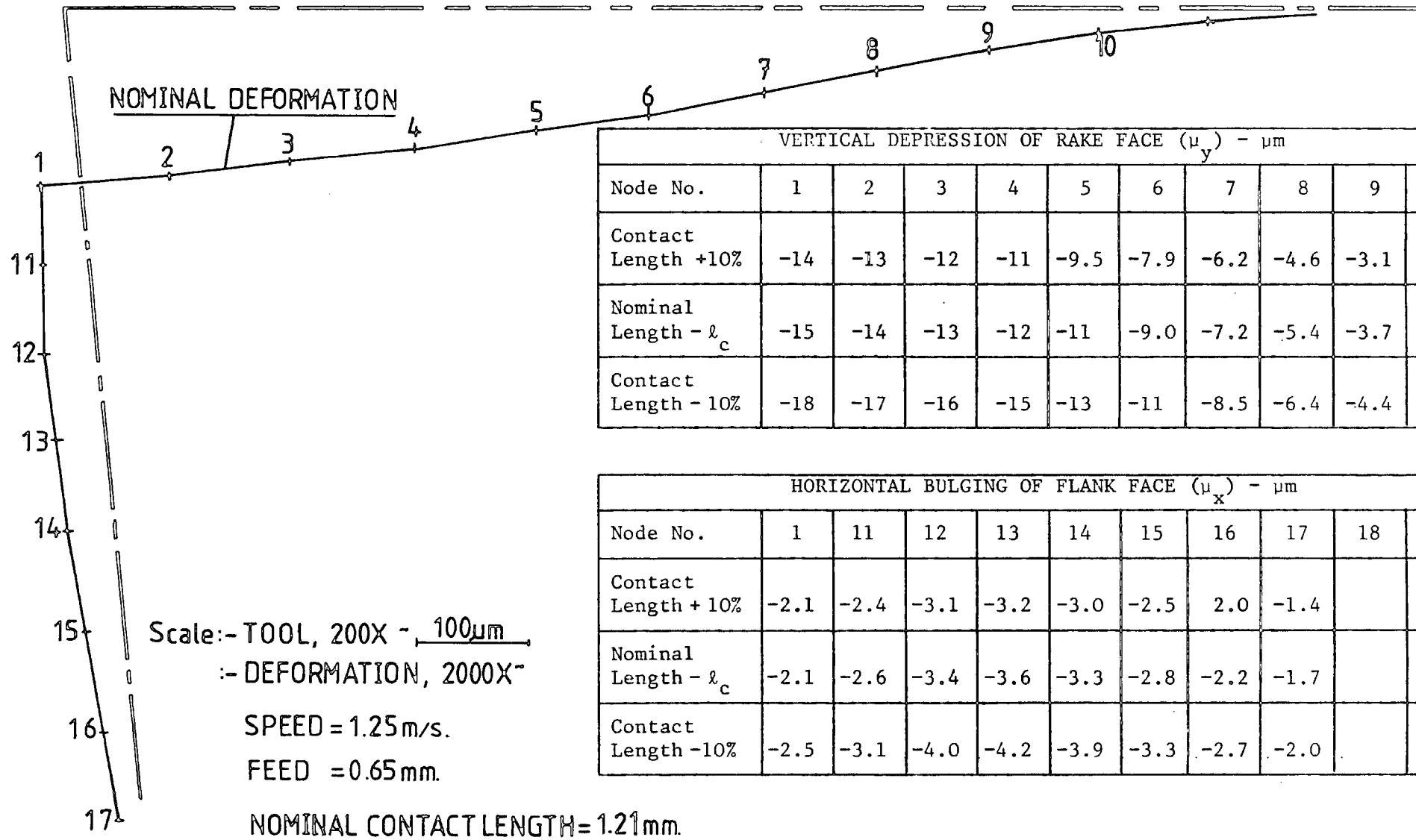

VERTICAL DEPRESSION OF RAKE FACE (μ_y) - µm										
Node No.	1	2	3	4	5	6	7	8	9	10
Contact Length +10%	-14	-13	-12	-11	-9.5	-7.9	-6.2	-4.6	-3.1	-1.9
Nominal Length - ℓ_c	-15	-14	-13	-12	-11	-9.0	-7.2	-5.4	-3.7	-2.2
Contact Length - 10%	-18	-17	-16	-15	-13	-11	-8.5	-6.4	-4.4	-2.7

HORIZONTAL BULGING OF FLANK FACE (μ_x) - µm										
Node No.	1	11	12	13	14	15	16	17	18	19
Contact Length + 10%	-2.1	-2.4	-3.1	-3.2	-3.0	-2.5	2.0	-1.4		
Nominal Length - ℓ_c	-2.1	-2.6	-3.4	-3.6	-3.3	-2.8	-2.2	-1.7		
Contact Length -10%	-2.5	-3.1	-4.0	-4.2	-3.9	-3.3	-2.7	-2.0		

FIGURE 8.27. INFLUENCE OF VARIATION IN TOOL/CHIP CONTACT LENGTH ON PREDICTED DEFORMATION.

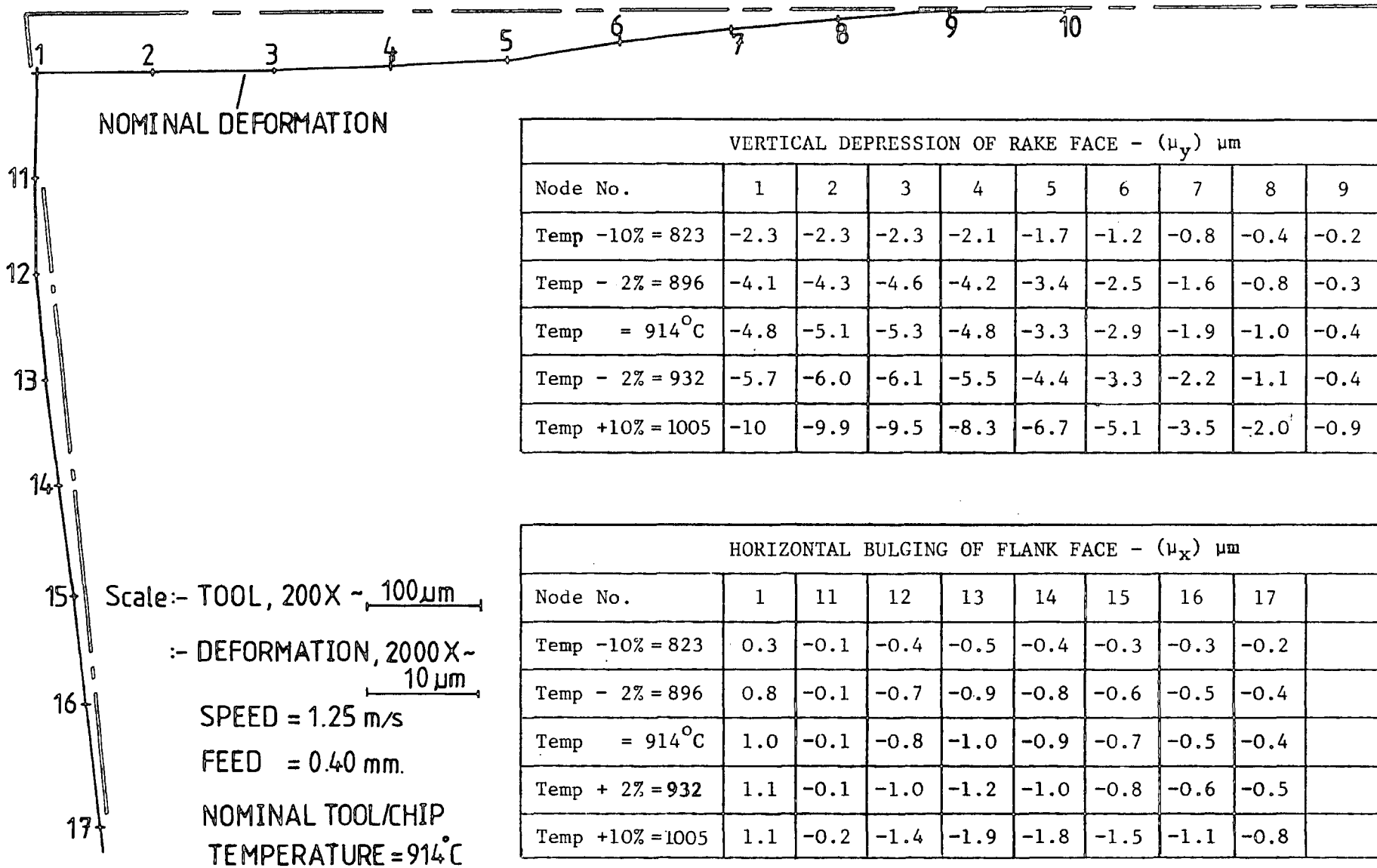

VERTICAL DEPRESSION OF RAKE FACE - (μ_y) µm										
Node No.	1	2	3	4	5	6	7	8	9	10
Temp -10% = 823	-2.3	-2.3	-2.3	-2.1	-1.7	-1.2	-0.8	-0.4	-0.2	-0.1
Temp - 2% = 896	-4.1	-4.3	-4.6	-4.2	-3.4	-2.5	-1.6	-0.8	-0.3	-0.1
Temp = 914°C	-4.8	-5.1	-5.3	-4.8	-3.3	-2.9	-1.9	-1.0	-0.4	-0.1
Temp - 2% = 932	-5.7	-6.0	-6.1	-5.5	-4.4	-3.3	-2.2	-1.1	-0.4	-0.1
Temp +10% = 1005	-10	-9.9	-9.5	-8.3	-6.7	-5.1	-3.5	-2.0	-0.9	-0.2

HORIZONTAL BULGING OF FLANK FACE - (μ_x) µm										
Node No.	1	11	12	13	14	15	16	17		
Temp -10% = 823	0.3	-0.1	-0.4	-0.5	-0.4	-0.3	-0.3	-0.2		
Temp - 2% = 896	0.8	-0.1	-0.7	-0.9	-0.8	-0.6	-0.5	-0.4		
Temp = 914°C	1.0	-0.1	-0.8	-1.0	-0.9	-0.7	-0.5	-0.4		
Temp + 2% = 932	1.1	-0.1	-1.0	-1.2	-1.0	-0.8	-0.6	-0.5		
Temp +10% = 1005	1.1	-0.2	-1.4	-1.9	-1.8	-1.5	-1.1	-0.8		

FIGURE 8.28, INFLUENCE OF VARIATIONS IN TOOL/CHIP TEMPERATURE ON PREDICTED DEFORMATION.

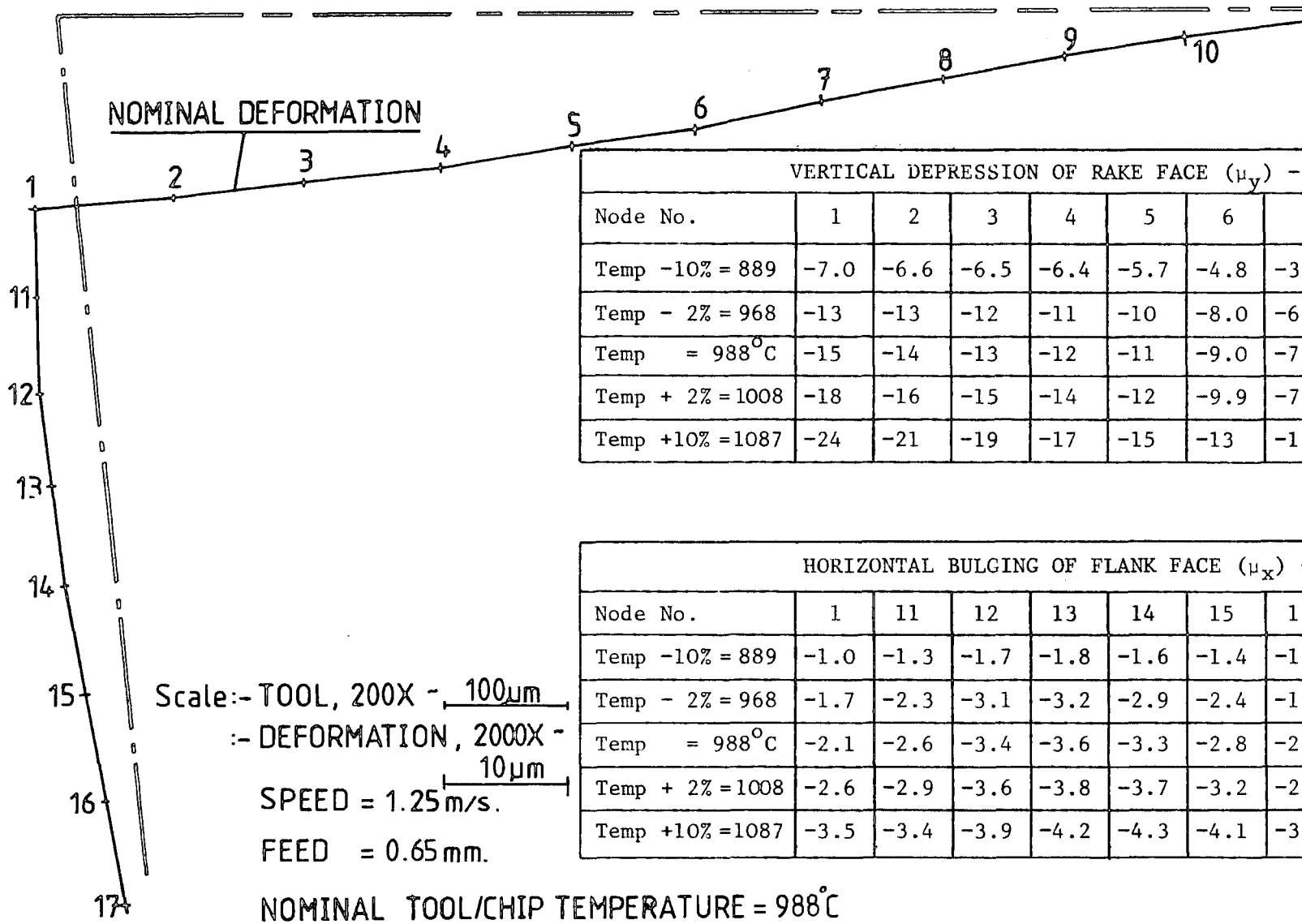

VERTICAL DEPRESSION OF RAKE FACE (μ_y) - µm										
Node No.	1	2	3	4	5	6	7	8	9	10
Temp -10% = 889	-7.0	-6.6	-6.5	-6.4	-5.7	-4.8	-3.7	-2.7	-1.7	-1.0
Temp - 2% = 968	-13	-13	-12	-11	-10	-8.0	-6.4	-4.8	-3.2	-2.0
Temp = 988°C	-15	-14	-13	-12	-11	-9.0	-7.2	-5.4	-3.7	-2.2
Temp + 2% = 1008	-18	-16	-15	-14	-12	-9.9	-7.9	-6.0	-4.2	-2.6
Temp +10% = 1087	-24	-21	-19	-17	-15	-13	-11	-8.4	-6.2	-4.1

HORIZONTAL BULGING OF FLANK FACE (μ_x) - µm										
Node No.	1	11	12	13	14	15	16	17	18	19
Temp -10% = 889	-1.0	-1.3	-1.7	-1.8	-1.6	-1.4	-1.1	-0.8		
Temp - 2% = 968	-1.7	-2.3	-3.1	-3.2	-2.9	-2.4	-1.9	-1.5		
Temp = 988°C	-2.1	-2.6	-3.4	-3.6	-3.3	-2.8	-2.2	-1.7		
Temp + 2% = 1008	-2.6	-2.9	-3.6	-3.8	-3.7	-3.2	-2.5	-1.9		
Temp +10% = 1087	-3.5	-3.4	-3.9	-4.2	-4.3	-4.1	-3.6	-2.8		

FIGURE 8.29, INFLUENCE OF VARIATIONS IN TOOL/CHIP TEMPERATURE ON PREDICTED DEFORMATION.

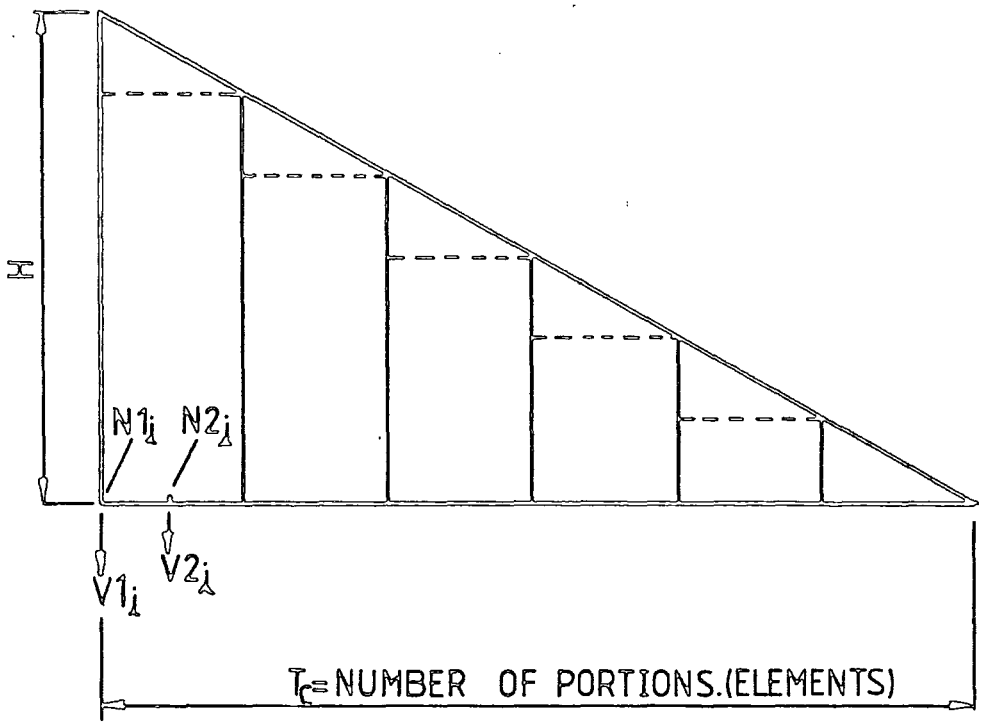

FIGURE A2.1

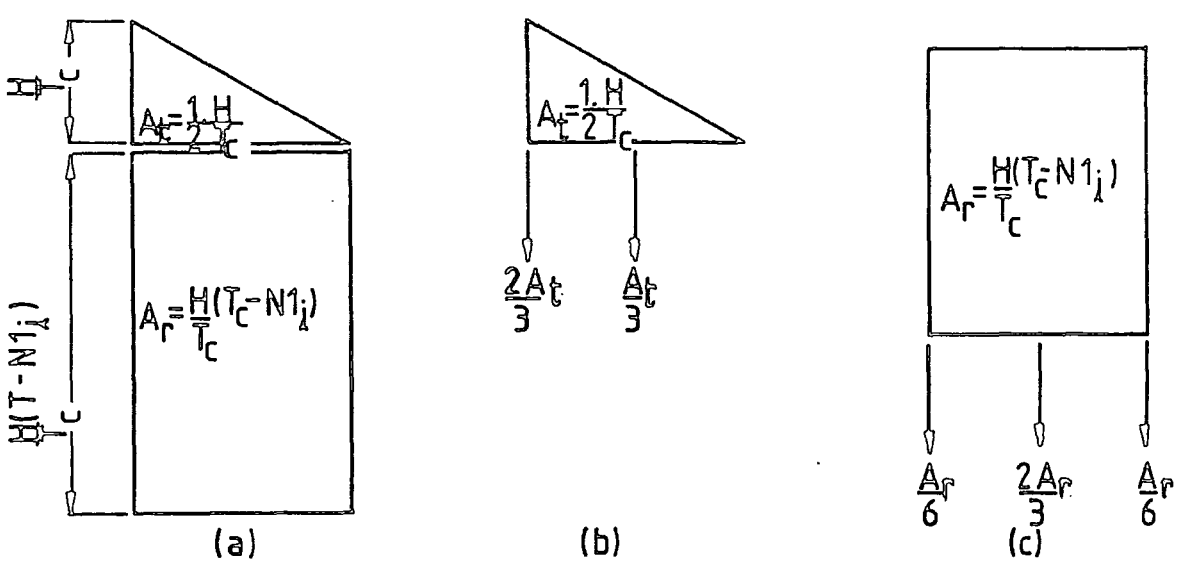

FIGURE A2.2

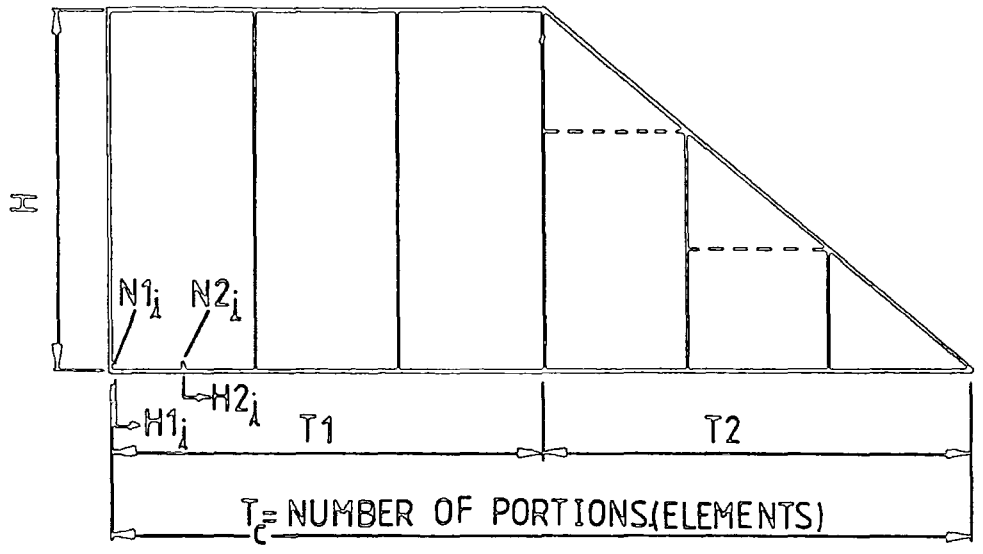

FIGURE A 2.3

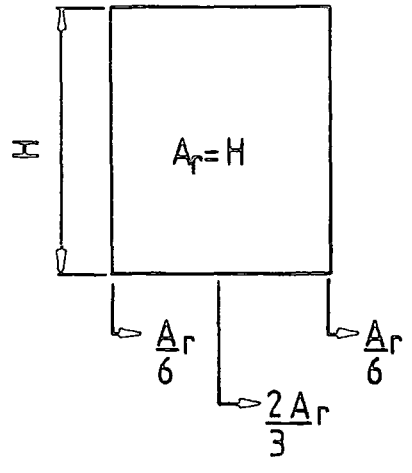

FIGURE A2.4(a)

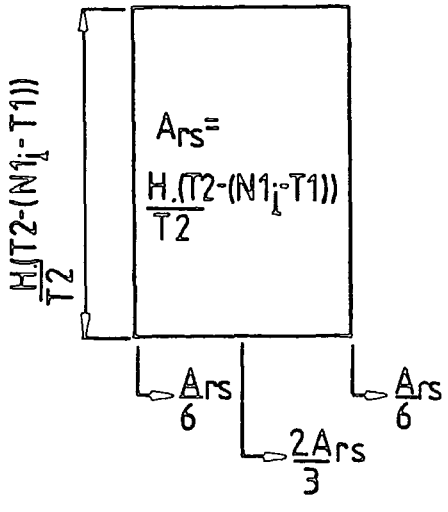

FIGURE A 2.4(b)

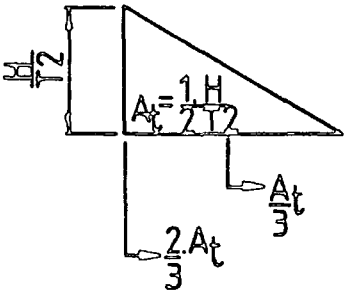

FIGURE A 2.4(c)

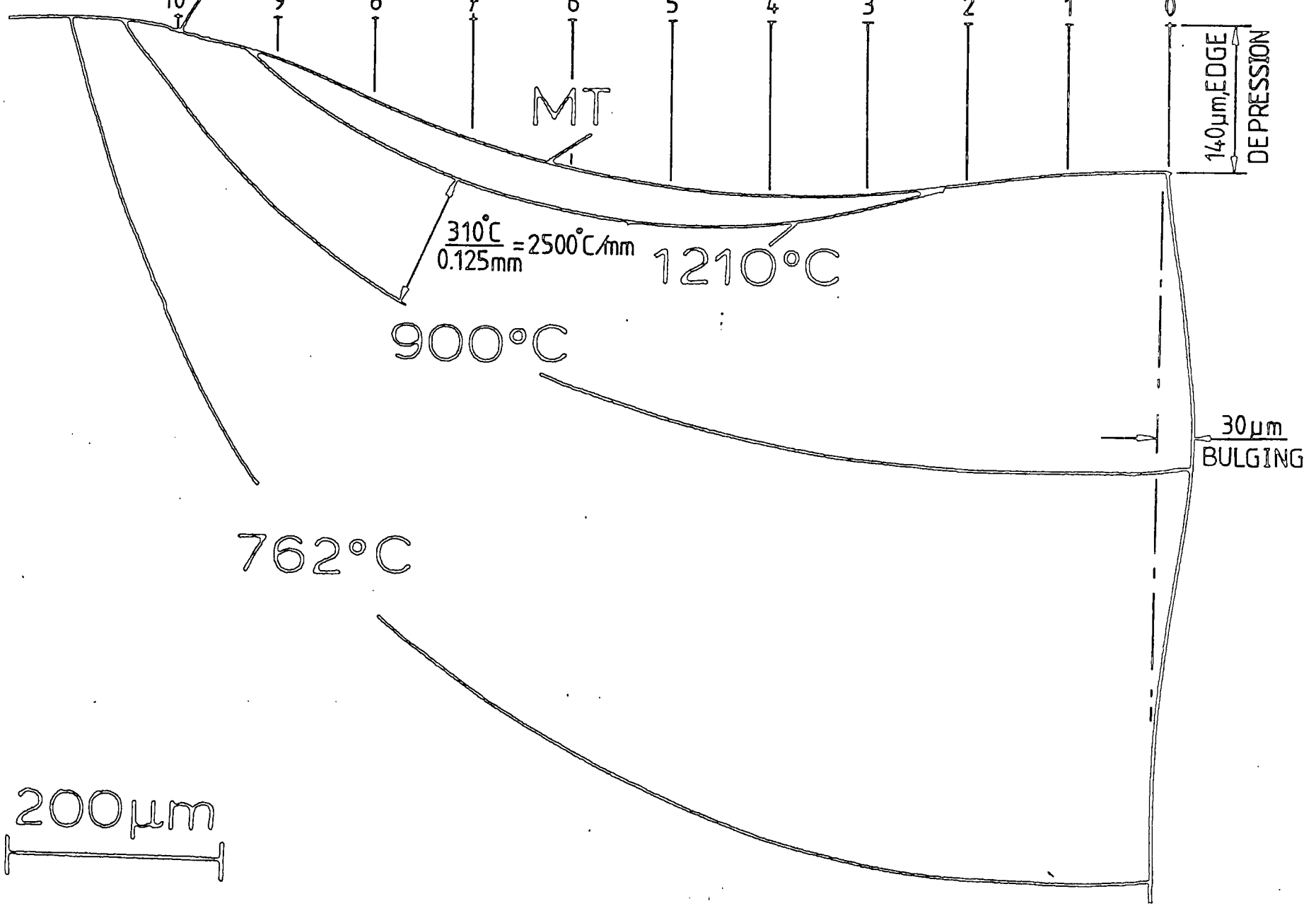

FIGURE A3.1 TOOL TEMPERATURE DISTRIBUTION PROPOSED BY DEARNLEY (1983)

Position on rake face	Method of Temperature Calculation	Distance and Temp. of Contours mm ∿ °C	Calculated Temperature (T) ∿ °C	Relative Temperature T/T_{ave}
0	Perpendicular extrapolation	$\sim \frac{134}{78}$ (900 - 762) + 762	= 999	0.829
1	Average value of positions 0 and 2		= 1100	0.913
2	Horizontal extrapolation	$\sim 1223 - \frac{18.6}{11}$ (1223-1210)	= 1201	0.997
3	Perpendicular extrapolation	$\sim \frac{50}{48}$ (1210 - 900) + 900	= 1223	1.015
4	" "	$\sim \frac{47}{41}$ (1210 - 900) + 900	= 1255	1.042
5	" "	$\sim \frac{44}{36}$ (1210 - 900) + 900	= 1279	1.062
6	" "	$\sim \frac{39}{31}$ (1210 - 900) + 900	= 1290	1.071
7	" "	$\sim \frac{34}{36}$ (1210 - 900) + 900	= 1305	1.083
8	" "	$\sim \frac{29}{22}$ (1210 - 900) + 900	= 1308	1.086
9	Horizontal extrapolation = 1273, Perpendicular extrapolation = 1256		∿ Average = 1264	1.049
10	Horizontal interpolation	$\sim \frac{10}{24}$ (1210 - 900) + 900	= 1029	0.854

Average temperature $T_{ave} = 1205^{\circ}C$

Figure A3.2 Quantification of Temperature Distribution Proposed by Dearnley (1983)